RAISING EFFICIENCY IN PHOTOVOLTAIC SYSTEMS: HIGH RESOLUTION MONITORING AND PERFORMANCE ANALYSIS

S. K. FIRTH

The Institute of Energy and Sustainable Development

De Montfort University

A thesis submitted in partial fulfilment of the requirements of De Montfort University for the degree of Doctor of Philosophy

October 2006

Abstract

Many countries are installing photovoltaic (PV) systems as part of a shift towards a low carbon economy. This thesis describes the development of new PV system monitoring techniques to improve understanding in PV system performance. One hundred and nine domestic PV systems are studied and their energy performance is revealed through high resolution monitored data.

The PV systems studied were installed from 2002 to 2004 as part of the UK Government's PV Domestic Field Trial. Located in five clusters throughout the UK, the sites are a combination of new build and retrofit projects. Each house has a separate grid-connected PV system and the 109 systems cover a variety of orientations, PV array sizes, PV module types and inverter sizes. The monitored performance data includes measurements of in-plane solar irradiance, PV module temperature, and DC and AC energy outputs. Data is recorded as five minutely average values for periods of up to two years. Data loggers store and provide access to the data through the public telephone network.

New techniques have been developed to analyse the five minutely monitored data from each house directly without averaging or aggregating the values. Data quality and plausibility checks are undertaken to ensure the reliability of the measurements and the monitoring techniques are developed using data from fifty four of the PV systems. Plots of five minutely irradiance versus efficiency values show clouds of points which represent 'normal operation'. A statistical method is developed to detect faults and to separate them from the normal operation. Six types of normal operation energy losses and four types of faults are identified and these are investigated through original techniques including a method of constructing 'efficiency curves' for the different stages of normal operation and a method to detect shading based on the position of the sun. The reduction in overall annual performance caused by each type of loss and fault is calculated and the opportunities to minimise the losses and faults are investigated.

This approach demonstrates a new strategy for monitoring PV systems, based on directly analysing high resolution monitored data. The method provides detailed insight into PV system performance and the results can be used to make recommendations for raising the efficiency of existing and future PV systems.

Acknowledgements

First of all I would like to thank Kevin Lomas and Simon Rees for their excellent supervision and support at every stage of this project. Further thanks are due to Paul Ruyssevelt at ESD who provided the opportunity for me to carry out this research. I would also like to thank Paul Evans and Sarah Greenwood at the INREB Faraday partnership for their support of this project.

Many people have helped me along the way. In particular thanks are due to: John Malone, Nick Neal, Steffie Broer and all at ESD; Ralph Gottschalg, Tom Betts and Anton Simmons at CREST; Oliver Miles; Harry Edwards; Neil Shankland; Chris Martin at EMC; and Anne Smith, Paul Cropper, John Mardaljevic, Graeme Stuart, Rob Wall and all the staff at IESD. I am indebted to my family for their continual encouragement and support, in particular my father John and my mother Joanna. I would also like to express my gratitude to Allan and Rita White.

Finally, special thanks to Allison for her patience and her love.

This work is dedicated to my late grandmother Joyce Tyldesley, whose sense of humour and love of life I'll never forget.

Contents

List of Figures

List of Tables

Nomenclature

Nomenclature for Chapter 6

Symbol	Definition
α_t	Temperature coefficient of power (%/K)
A	Area of the PV array (m^2)
E_G	Annual total energy generated by the PV system as output from the inverter (kWh)
G_i	In-plane solar irradiation energy at irradiance i (kWh/m^2)
G_I	Annual total in-plane solar irradiation (kWh/m^2)
i	In-plane solar irradiance (W/m^2)
I_{PV}	DC current of the PV array (A)
n	Number of PV modules in the PV array
$\eta_{array,25°C}$	Equivalent array efficiency at 25 °C
$\eta_{array,t}$	Array efficiency at temperature t
η_i	System efficiency at irradiance i
$\hat{\eta}_i$	Upper limit of system efficiency
η_{STC}	Rated efficiency of the PV modules
$P_{DC,ARRAY}$	DC power output from the PV array (W)
$P_{DC,INV}$	DC power input to the inverter (W)
$P_{DC,LOSS}$	Power loss in the DC cables due to DC cable resistance (W)
$\hat{P}_{INV}$	Power rating of the inverter (W)
PR	Annual performance ratio
R	Resistance of the DC cables connecting the PV array to the inverter (Ω)
t	Temperature of the PV module (°C)
V_{MPP}	Maximum power point voltage of PV module at STC (V)

Nomenclature for Chapter 7

Symbol	Definition
α	Solar azimuth (°)
α_0	Solar azimuth of the fault (°)
$\Delta\alpha$	Solar azimuth width of sun position region (°)
A	Area of the PV array (m^2)
β	Solar elevation (°)
β_0	Solar elevation of the fault (°)
$\Delta\beta$	Solar elevation height of the sun position region (°)
e_F	Energy loss due to an individual fault (kWh)
E_F	Annual energy lost due to a type of fault (kWh)
F	Number of faults within the sun position region
$FC_{\alpha_0 \beta_0}$	Fault concentration about sun position α_0 β_0
G_i	In-plane solar irradiation energy at irradiance i (kWh/m^2)
G_I	Annual total in-plane solar irradiation (kWh/m^2)
i	In-plane solar irradiance at which the fault occurred (W/m^2)
η_F	System efficiency of the fault
$\eta_{NO,i}$	System efficiency of normal operation at irradiance i
η_{STC}	Rated efficiency of the PV modules
n	Total number of faults of a certain type in the annual data
PR_{loss}	Loss in annual performance ratio due to the type of fault
S	Number of five minute sun positions within the sun position region

1. Introduction

Solar photovoltaic (PV) systems offer a solution in the search for low carbon, non-fossil fuel electricity generation. Sunlight, captured and converted by semiconductor solar cells, can provide a supply of electricity for the world's energy needs. An energy source with low carbon emissions, no reliance on fossil fuels, massive potential for developing countries and well suited to distributed, embedded generation, solar PV is considered as a medium and long term energy prospect (DTI, 2001). This thesis examines PV systems installed on UK domestic buildings and their energy performance as revealed through high resolution monitored data.

1.1. Building integrated PV

The world is using increasing amounts of energy, as economies grow and the developing world industrialises. The International Energy Agency's (IEA) World Energy Outlook 2004 stated that 'the world primary energy demand ... is projected to expand by almost 60% between 2002 and 2030' (IEA, 2005a). Energy consumption is often linked to economic development and increasing consumption is seen as a necessity of the industrialising developing world, currently demonstrated by China and India. This presents a dilemma for the world's governments: where will this energy come from and how will it be provided without producing adverse consequences.

The most high profile adverse consequence of energy generation at present is climate change, the change in weather patterns and temperatures due to emissions of carbon dioxide and other 'greenhouse gases'. In its latest report, the Intergovernmental Panel on Climate Change (IPCC), a large body of scientists from across the world formed by the United Nations to provide information and advice on climate change, concluded that 'most of the observed warming over the last 50 years [is] likely due to increases in greenhouse gas concentrations due to human activities' (IPCC, 2001). Future climate change is predicted by the IPCC to 'have both beneficial and adverse effects on both environmental and social-economic systems'. However 'the larger the changes and the rate of change in climate, the more the adverse effects predominate' and 'the adverse impacts of climate change are expected to fall disproportionately upon developing countries and the poor persons within countries'.

The subject of climate change has climbed to the top of the international political agenda and has brought about the Kyoto Protocol (UNFCCC, 2005), an international emissions treaty, and high level negotiations and discussion. It was one of the two main topics at the 2005 G8 summit in the UK. However such actions are widely seen as only the first steps of what is required. The Royal Commission on Environmental Pollution (RCEP, 2000), a UK policy unit, recommends a target of a 60% cut in greenhouse gas emissions by 2050. This view, taken seriously by the UK Government, was echoed as an ambition in the 2002 White Paper 'Our Energy Future – Creating a Low Carbon Economy' (DTI, 2002).

The vast majority of greenhouse gas emissions come from the use of fossil fuels (coal, oil and gas) in our electricity generation, heating, transport and industrial processes. An essential part of climate change mitigation is the conversion of these systems to low carbon processes. A low carbon process is a generic term for processes and methods with low greenhouse gas emissions. The methods and technologies currently being promoted to create a low carbon economy are energy efficiency practices, carbon sinks (e.g. storing carbon underground), low carbon industrial processes and low carbon energy generation.

The generation of electricity through low carbon processes is an important part of this approach. Electricity generation is a major source of greenhouse gas emissions which accounted for 37.5% of worldwide carbon emissions in 1995 (IPCC, 2001). Current practice using generation from coal, oil and gas fired power stations accounts for these high emission figures. There are three low carbon alternatives to the use of traditional fossil fuel power stations: 'clean' fossil fuel technologies which reduce or store the carbon emissions; nuclear power which, although it has other economic, environmental and safety issues, has low greenhouse gas emissions; and renewable forms of electricity generation.

Renewable electricity generation methods (renewables) comprise of a range of technologies which almost all utilise energy from the sun, either directly or indirectly. They generate electricity with low emissions of greenhouse gases. The technologies include wind power, solar photovoltaics, hydro power, wave power, tidal power[1] and biomass[2]. Renewables are capital intensive generation sources, requiring a high initial investment relative to the energy yield (compared with conventional generation based on fossil fuels), but operation costs and fuel costs are generally low. Through the issues of climate change mitigation, security of energy supply, and the increasing price of conventional fossil fuel energy, the use of renewables has steadily increased in recent years. Renewables produced 3.6% of the total electricity in the UK in 2004, compared with less than 2.5% in 1997 (DTI, 2005a). A target of 15.4% renewable generation by 2015/6 has recently been announced by the UK government (DTI, 2005b).

This thesis examines one of the forms of renewable electricity generation: solar photovoltaics (PV), the direct conversion of sunlight to electricity. A solar PV cell, most commonly a semi-conductor p-n junction, absorbs sunlight and generates an electric current. PV is a low carbon electricity generation technology with several unique characteristics. It has no moving parts, creates no noise during operation and has low maintenance requirements. There are no fuel costs as it is powered by sunlight and operating costs (such as maintenance costs) are negligible. Solar PV systems are modular and suited to both small scale and large scale applications, from pocket calculators to buildings to large power stations located in deserts. The only emissions generated throughout their lifetime are during manufacture of the photovoltaic components. During operation solar PV systems have no emissions and create zero pollution. Carbon dioxide emissions from solar PV systems are approximately 3% to 4% of those from coal fired power plants when the complete life cycle (construction, operation and decommissioning) is considered (Alsema, 2005).

Solar PV can be integrated into the built environment and is installed as part of the roof, walls or facades of buildings (DTI, 2000). Thus the building becomes a generator of electricity and can supply some or all of its own electricity needs. As the electricity is generated at the point of demand (the building), distribution losses are avoided. A typical building integrated PV application for a small domestic

[1] Tidal power derives its energy predominantly from the moon rather than the sun

[2] Generation of electricity from biomass sources (using the heat from combustion of plants) does emit greenhouse gases. However the process is carbon neutral provided the harvested biomass is replanted.

system in the UK is shown in Figure 1-1. This PV system, installed in 2003, consists of nine PV modules[3] in a PV array[4] mounted on a south facing roof and is one of the PV systems being studied in this work.

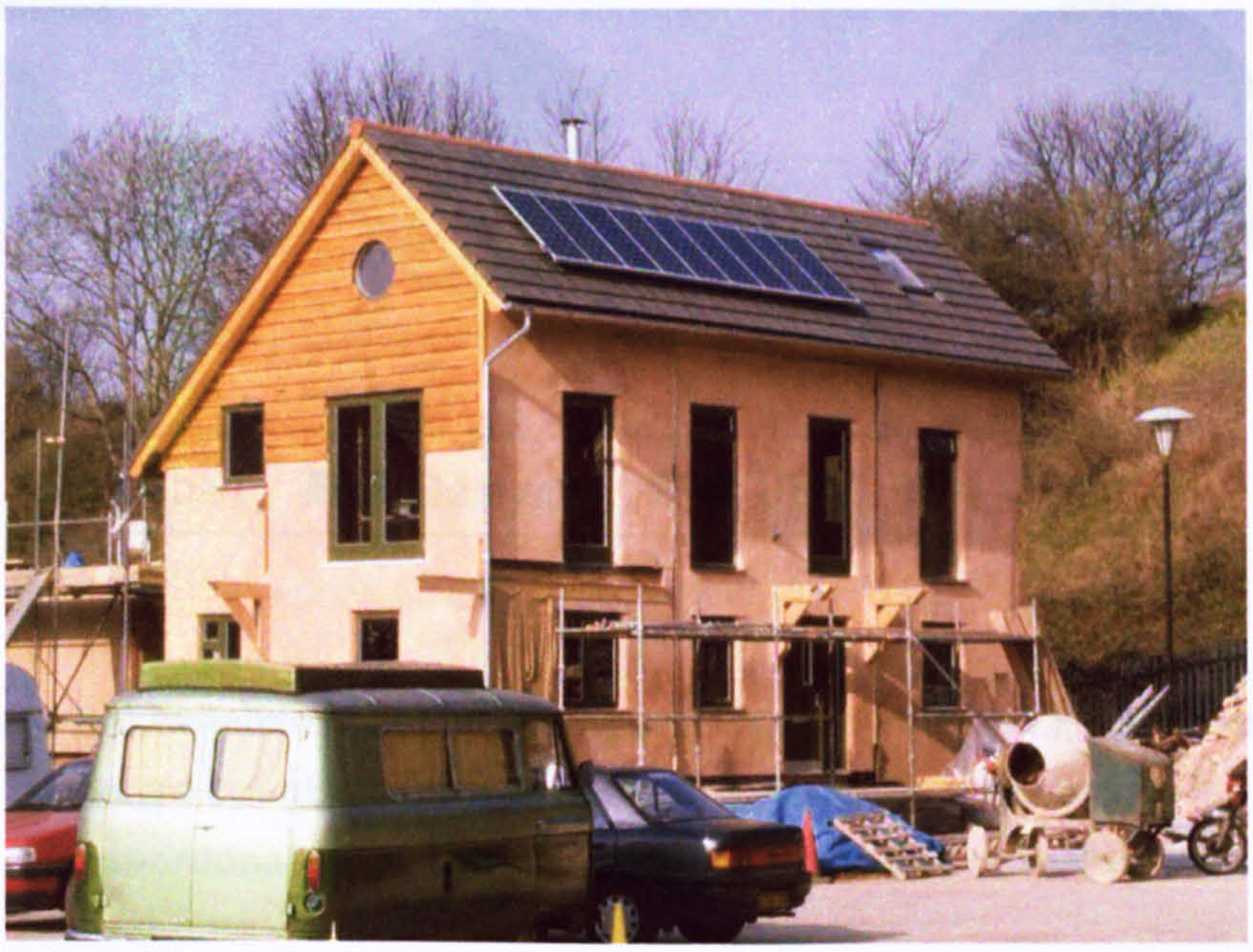

Figure 1-1: A recent UK domestic PV system (installed under the UK Government's Domestic Field Trial)

Building integrated PV has become the dominant type of PV application in recent years. A yearly survey by the International Energy Agency (IEA) in 2004 estimated that worldwide grid-connected[5] dispersed PV systems (almost all of which are building integrated) represented around 75% of all PV applications (IEA, 2005b). The total installed capacity of grid-connected dispersed systems was 2,060 MWp[6] at the end of 2004, an increase of about 50% from the previous year (IEA, 2005b). The IEA also provides a breakdown of the PV capacity of twenty countries from 2002 to 2004 (IEA, 2003, IEA, 2004a and IEA, 2005b). Japan, Germany and the

---

[3] A PV module is the component in a PV system which convert sunlight into DC electricity. Modules are flat panels of dimensions typically around 0.5 by 1 metre and contain a number of PV solar cells.

[4] A PV array is a group of PV modules

[5] A grid-connected PV system is connected to the mains electricity grid and exports excess electricity to the grid

[6] Wp (watt peak) is the measure used to describe the size of a PV system. A 1 kWp system will generate 1 kW of electric power under bright sunny conditions known as Standard Test Conditions, which are defined in Section 2.1.1.

USA have the majority of the world's PV installations (Figure 1-2).

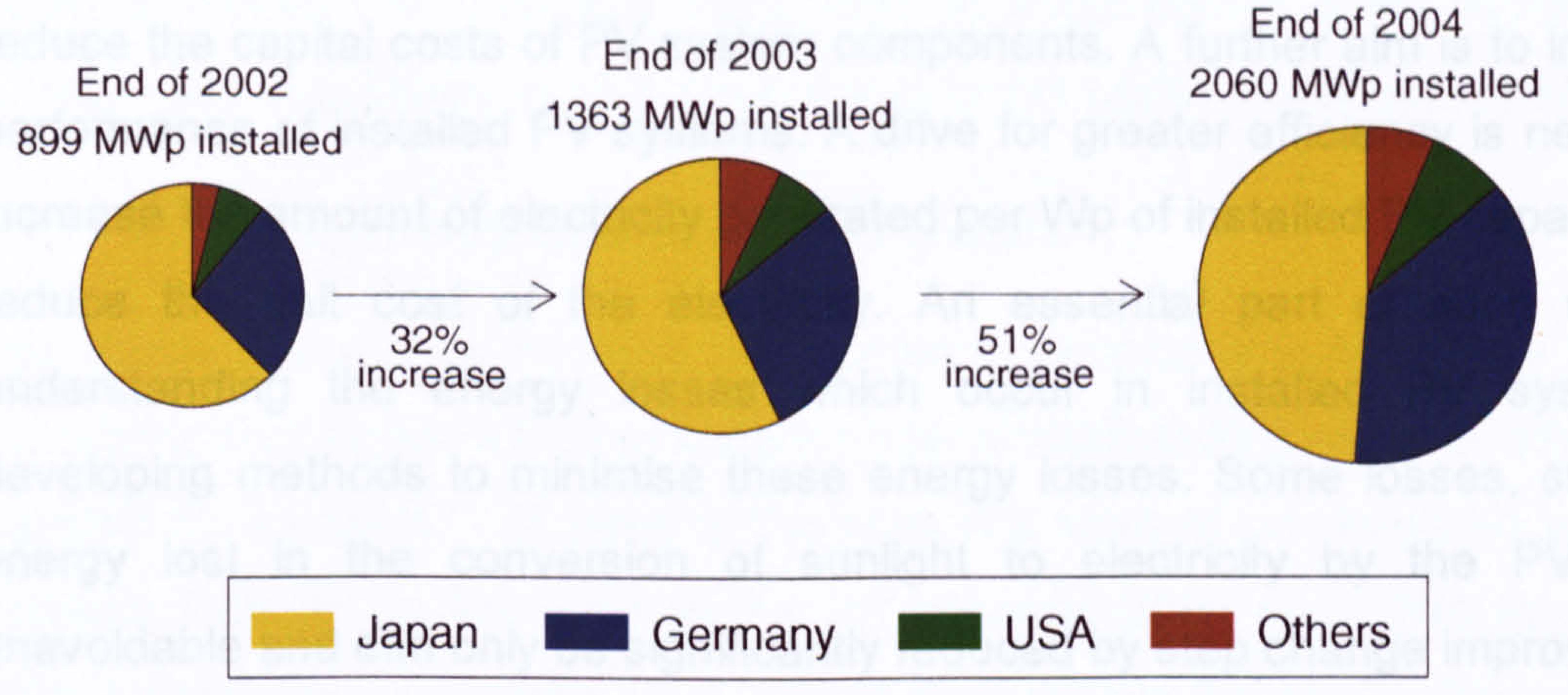

Figure 1-2: Installed capacity of dispersed grid connected PV systems in selected countries from 2002 to 2004. The size of the charts is proportional to the total PV installed at the end of that year.

The UK had 7.4 MWp of dispersed grid connected PV systems at the end of 2004, 0.4% of the worldwide total (IEA, 2005b). Governments in Japan, Germany and other countries have encouraged the growth of PV through the use of subsidies, guaranteed "feed-in" tariffs[7] and other market stimulation mechanisms (IEA, 2004a). The current target of the Japanese government is an installed capacity of 4.8 GWp of PV by 2010, double the 2004 world capacity and four times the Japanese capacity of 2004 (IEA, 2004b).

In 2002, the UK Government introduced its own subsidy programme to stimulate the UK PV industry and increase capacity. The Major Demonstration Programme (MDP) provided 50% of the costs for domestic PV systems, and 40% to 60% for larger commercial or public building installations (IEA, 2004c). Funded by the Department of Trade and Industry (DTI), the MDP resulted in the installation of PV systems on 172 domestic and 16 non-domestic buildings in 2003 (IEA, 2004c).

[7] A feed-in tariff is an agreed price for the sale of excess PV electricity

1.2. Efficiency improvements and monitoring

The main aim of researchers and industry in the building integrated PV sector is to reduce the capital costs of PV system components. A further aim is to improve the performance of installed PV systems. A drive for greater efficiency is necessary to increase the amount of electricity generated per Wp of installed PV capacity and so reduce the unit cost of the electricity. An essential part of such work is in understanding the energy losses which occur in installed PV systems and developing methods to minimise these energy losses. Some losses, such as the energy lost in the conversion of sunlight to electricity by the PV cell, are unavoidable and can only be significantly reduced by step change improvements in the technology of PV system components. Other energy losses, such as shading, are related to the installation of the PV systems and can be minimised through careful planning, design and operation.

Energy losses in installed PV systems can be detected by monitoring the operational performance and analysing the recorded data. Monitoring of PV systems has been used to develop guides and benchmarks for PV system performance (IEA, 2000). Demonstration PV systems (usually among the first PV systems to be installed in a country) and systems with unique characteristics (such as new cell technologies or novel construction techniques) often have their performance monitored in detail (e.g. IEA, 2000; Roaf and Fuentes, 1999; Kiefer et al., 1995). These monitoring studies record the performance of PV systems, analyse the energy losses and provide recommendations to improve the design of future systems. This becomes an iterative process when the next generation of PV systems incorporating the design improvements are themselves monitored and used to develop further recommendations to raise efficiency.

This process can be seen in the history of PV system installations in Germany, In the early 1990s Germany introduced a major subsidy programme for building integrated PV and many of the initial systems were monitored (Erge et al. 2001). Studies of the performance of these early systems showed that the reliability of the inverters[8], the length of time taken to repair any faults, and shading were reducing

[8] The inverter is an electronic device which converts DC electricity to AC electricity, often used so that the PV generated electricity can be used by household appliances and exported to the mains electricity grid

the system efficiency (Kiefer et al., 1995; Erge et al., 2001). These observations were used to improve future PV installations and, as a result, a recent study of PV systems installed in Germany from 1991 to 2002 shows a 4% increase in the energy yield of systems installed in the later years (Jahn and Nasse, 2004).

1.3. Aims and objectives of this thesis

This thesis documents the work undertaken to develop a suite of new PV system monitoring techniques which provide a better understanding of the energy losses in installed PV systems. The basis of this work is a study of one hundred and nine PV systems installed at five sites in the UK between 2002 and 2004 as part of the DTI's Photovoltaic Domestic Field Trial (a precursor to the MDP). Each of the sites has twelve to thirty grid-connected domestic PV systems and the performance of each system is monitored. Preliminary work for this thesis, undertaken by the author, involved: the commissioning of the monitoring systems at the five sites; installing a monitoring system at one site; conducting several construction and commissioning inspection visits; and setting up data collection and processing procedures.

The performance of the PV systems is monitored every five minutes. Little previous work has been carried out using recorded data at a resolution of five minutes or less (Pearsall and Hynes, 2003; Kiefer et al., 1995). The relevant British Standard for PV system monitoring, BS EN 61724 (BSI, 1998), is based on hourly recorded data which is typical for PV monitoring. Hourly data can be studied directly (for example Oozeki et al., 2003) or analysed using monthly or annual totals (IEA, 2000). The new approach to PV system monitoring developed in this work is based on the high resolution (short time interval) five minutely data available from the monitored PV systems.

The aims of this study are:

- to demonstrate how high resolution monitoring can improve our understanding of PV system performance; and
- to demonstrate how such monitoring can be used to raise the efficiency of current and future PV installations.

The following six objectives were identified to meet these aims:

1. a literature review of current and past PV monitoring and a critique of the analysis techniques

2. a report on the data collection process and the characteristics of the monitored data for the PV systems under study

3. the development of new techniques to investigate the energy losses in PV systems based on high resolution monitored data

4. the development of new techniques to detect faults in PV systems based on high resolution monitored data

5. a study providing insight into the performance of the monitored PV systems and the problems encountered during operation

6. a list of recommendations, based on the findings of this work, to raise the efficiency of the monitored PV systems and future UK domestic PV systems

Objective 1 sets out the need for new PV monitoring techniques and provides the justification for this study. Objective 2 develops confidence in the quality of the monitored data on which the techniques are based. Objectives 3 to 4 form the original aspect of this work and document the development of the new techniques for PV system monitoring. Objective 5 applies the techniques to the monitored PV systems and demonstrated how they improve understanding of the energy losses. Objective 6 gives the practical lessons learnt from this study and recommendations for future PV installations. The chapters within this thesis are structured to meet the six objectives (Figure 1-3).

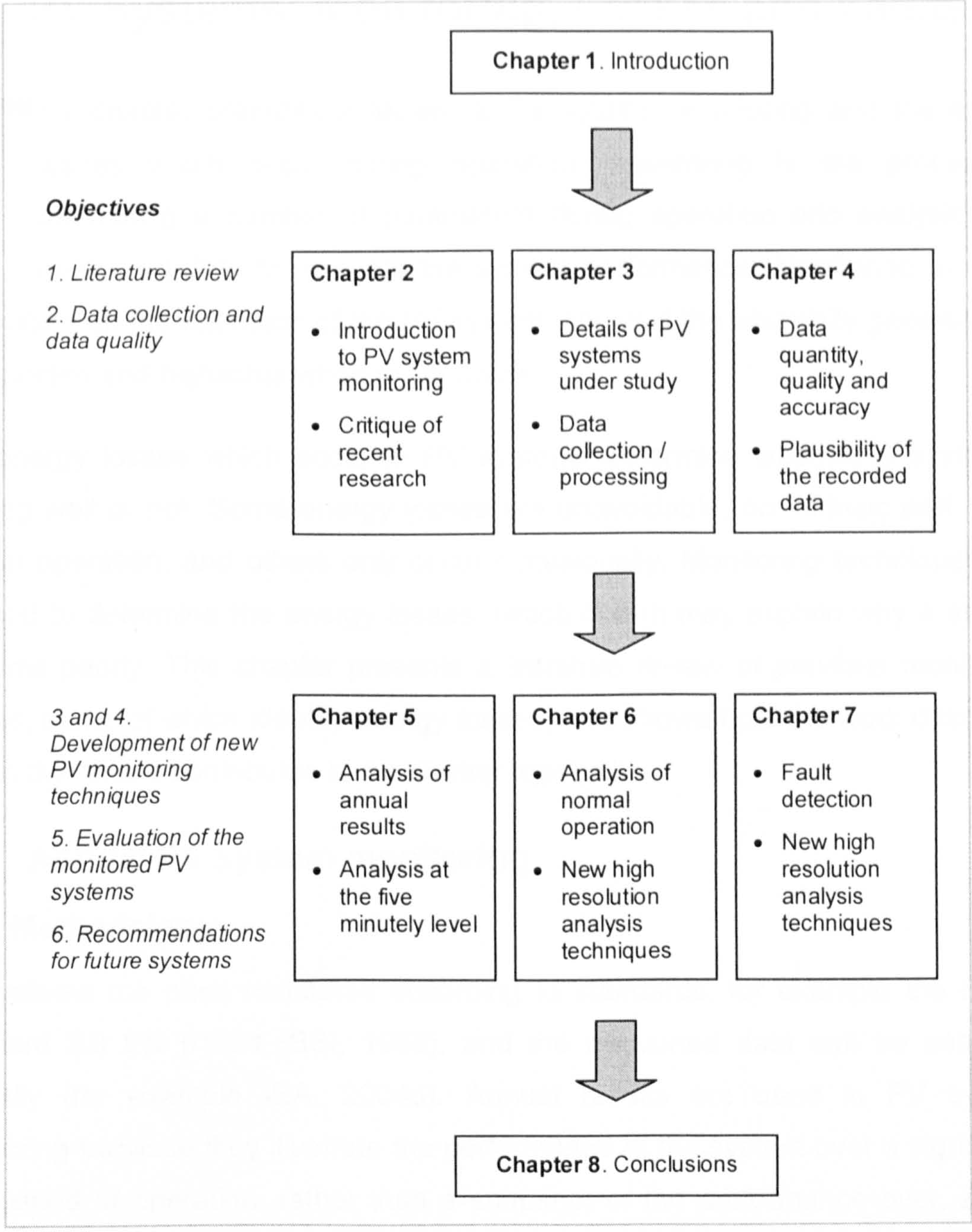

Figure 1-3: Organisational structure of this thesis and the relationship of chapters to objectives

2. PV Systems: Monitoring, Losses and Faults

This chapter presents a review of PV system monitoring and the energy losses which occur during operation. *Monitoring* is the process of measuring a number of parameters during operation and analysing the measured data to evaluate the system performance. Monitoring provides information on the operation of the PV system, shows if the electricity generation is as expected and highlights when faults occur.

The energy losses which occur in PV systems determine whether a system is working well or not. Some energy losses are unavoidable, an intrinsic part of PV system operation, and others only occur occasionally. Monitoring techniques can be used to determine the energy losses, which in turn may explain why a system performs poorly. This chapter presents a literature review of previous monitoring studies, some of which identify energy losses, and shows how the work described later in this thesis contributes to monitoring research.

2.1. Annual PV system monitoring

2.1.1 Methodology

PV systems are often monitored according to standards, for example the British Standard BS EN 61724 (BSI, 1998), and the measured data can be analysed annually (for example IEA, 2004d). Annual results are used in PV system monitoring because they illustrate the performance of the system over a significant time period of operation, rather than a snapshot of the performance over, say, a single day. They are constructed using data throughout the year to account for the effect of seasonal variation. Due to different solar radiation and temperature levels, PV systems operate at their best at certain times of year. The annual results can be compared with benchmark values to assess the system performance.

A simple performance monitoring system of an energy generator measures the energy input and the energy output and uses these values to assess how well the generator works. The ratio of energy output to energy input is the on-site efficiency, a measure of the ability of the generator to convert the input energy into useful energy. In PV systems the energy input is the solar radiation received by the PV array and the energy output is the AC energy output from the inverter (Figure 2-1).

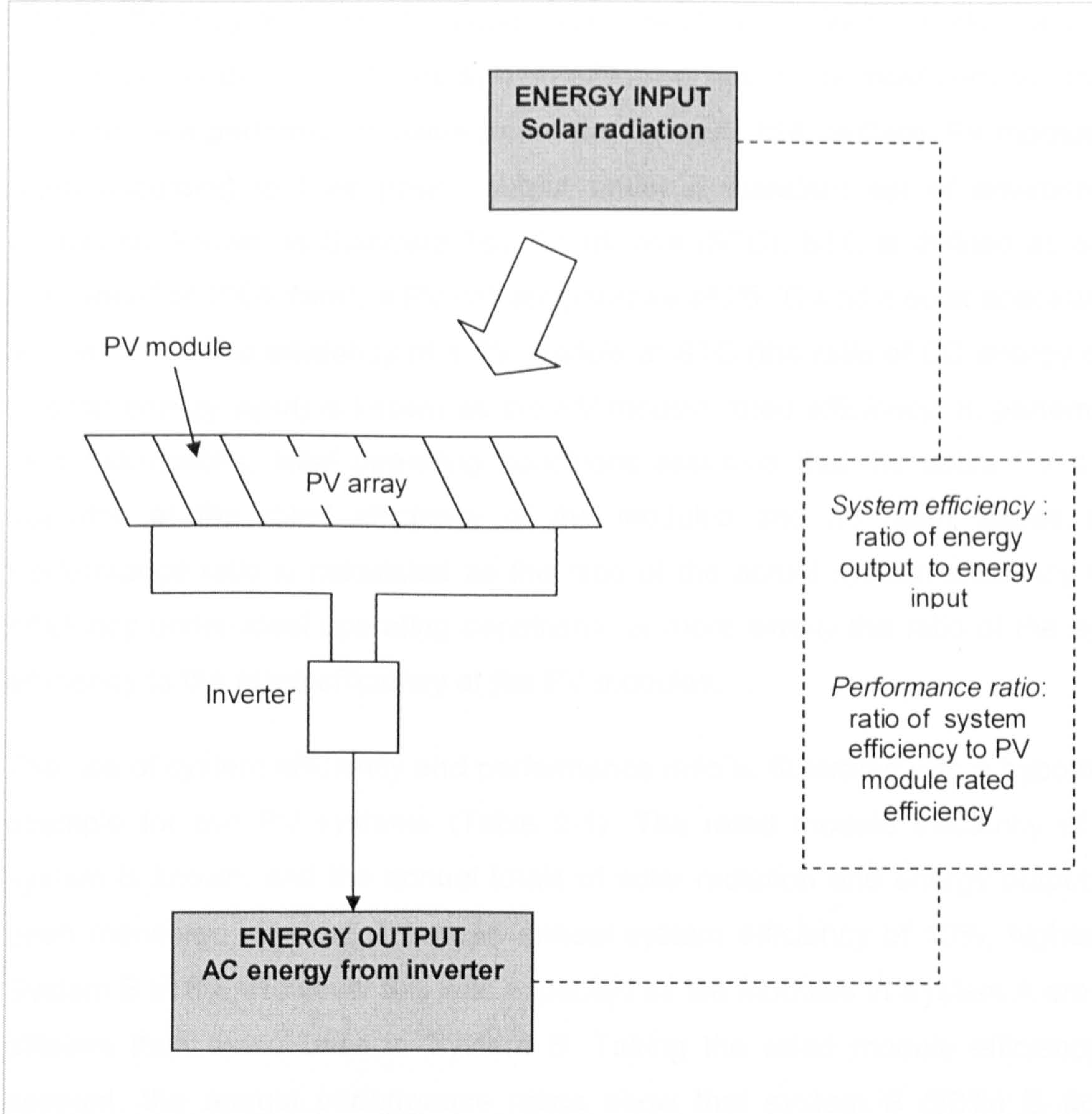

Figure 2-1: Energy input and output in a PV system

BS EN 61724 defines the *overall system efficiency* of a PV system as the ratio of energy output to energy input (BSI, 1998). In this work, this parameter is referred to more simply as the *system efficiency*. System efficiency provides an evaluation of the overall sunlight to AC electricity conversion process and, as the parameter is largely independent of the size of the PV system and the amount of annual solar radiation received, it can be used for all types of systems. However system efficiency does not take into account the expected performance of the PV system (which depends on the choice of PV modules and other components) and thus it is does not provide information on whether the system is operating well or poorly.

The *performance ratio* does provide this information by considering the expected (rated) efficiency of the system under ideal operating conditions. Performance ratio is a parameter derived from the system efficiency and is the most common method of PV system performance assessment (for example IEA, 2004d). PV modules are rated according to their power output under a standard set of environmental conditions, known as Standard Test Conditions (STC). STC is defined as a solar irradiance[9] of 1000 W/m^2, a PV cell temperature of 25 °C and a solar spectrum[10] of air mass 1.5. The efficiency of a PV module at STC (the ratio of DC energy output to solar energy input) is known as the *PV module rated efficiency*. In performance ratio calculations, ideal operating conditions assumes that the entire PV system operates at the rated efficiency of the modules and no other losses occur. Performance ratio is calculated as the ratio of the actual system efficiency to the efficiency under ideal operating conditions, or more simply the ratio of the system efficiency to the rated efficiency of the PV modules.

The use of system efficiency and performance ratio is illustrated with a hypothetical example for two PV systems (Table 2-1). The rated module efficiency of each system is known, and the annual totals of solar radiation and energy output have been monitored. System A has an annual system efficiency of 10%, higher than System B at 8%. However this was expected as the modules in System A are more efficient than those used in System B. Taking the rated module efficiency into account, the annual performance ratios show that system B (80%) is actually performing slightly better than System A (77%).

Table 2-1: An example of system efficiency and performance ratio calculations

System	Rated module efficiency (%)	PV array area (m^2)	Annual solar radiation received (kWh)	Annual energy output from the PV system (kWh)	Annual system efficiency (%)	Annual performance ratio (%)
A	13	10	10,200	1,020	10	77
B	10	8	9,000	720	8	80

9 Irradiance is the power of the sunlight striking the PV array per unit area, measured in W/m^2.

10 The solar spectrum refers to the variation of energy at different wavelengths found within sunlight. The spectrum is dependent on the air mass (a value derived from the distance the sunlight travels through the atmosphere). The effect of the solar spectrum on PV system performance is not considered in this work.

2.1.2 Benchmark of performance

Five previous studies have been chosen to illustrate typical annual performance ratio values for domestic PV systems (Table 2-2). The studies represent a broad cross section of different locations and system designs relevant to the UK context. An IEA report (IEA, 2004d) described 170 PV systems in six countries monitored between 1996 and 2002 and the average annual performance ratio for each country ranged from 67% to 72%, with maximum values for individual systems around 85%. The performance ratios recorded by two other recent studies (Pearsall and Hynes, 2003; Oozeki et al., 2003) showed similar values to the IEA report. The Oxford Solar House study (Roaf and Fuentes, 1999) described the performance of one of the first domestic PV systems to be installed in the UK. The performance ratio of 64%, monitored in 1996 to 1998, was slightly lower than the UK systems monitored in later years by Pearsall and Hynes (69%). In the German 1000 roofs programme of 1993 to 1995 (Kiefer et al., 1995), the performance ratios were low (66%) in comparison with later installations in Germany reported in the IEA report (71%). The German 1000 roofs programme study also illustrated how very low annual performance ratio values are possible, with the lowest performance ratio of an individual system at 28%.

Based on these five studies, a rough benchmark was developed for use with the PV systems monitored in this work. For PV systems installed in the late 1990s an average annual performance ratio of around 70% can be expected, with maximum values for individual systems as high as 85%. Annual performance ratios have risen since 1993, as shown in the UK and German PV systems in Table 2-2 and in the paper by Jahn and Nasse (Jahn and Nasse, 2004) described in Section 1.2. Thus the performance ratios of recently installed systems (i.e. later than 2002) may be even higher then the late 1990s benchmark values. Analysis of the distribution of performance ratios for the six countries in the IEA study shows that the majority of systems have annual performance ratios above 55%. This provides a rough benchmark for minimum acceptable annual performance ratios and systems with performance ratios below this figure are almost certainly not performing as well as expected.

Table 2-2: Annual performance ratios from worldwide studies

Study	Location	Years monitored	Number of PV systems	Average annual performance ratio (%)	Range of annual performance ratio (%)
IEA: Country reports on PV system performance (IEA, 2004d)	Austria	1997 - 2001	9	67	50 - 75
	Germany	1996 - 2002	55	71	50 - 85
	Italy	1999 - 2002	20	70	45 - 80
	Japan	1997 - 2000	46	71	55 - 85
	Netherlands	1997 - 1999	8	72	65 - 80
	Switzerland	1996 - 2002	32	70	55 - 85
Monitoring of Domestic PV Installations (Pearsall and Hynes, 2003)	UK	1999 - 2003	6	69	60 - 77
SV Method (Oozeki et al., 2003)	Japan	1995 - 1999	421	67	not provided
Oxford Solar House (Roaf and Fuentes, 1999)	UK	1996 - 1998	1	64	-
German 1000 roofs programme (Kiefer et al., 1995)	Germany	1993 - 1995	100	66	28 - 83

2.1.3 Limitations

The use of annual monitoring is a simple and effective method of evaluating the performance of PV systems. However there are disadvantages to the approach. Annual performance ratios show when systems are performing poorly (by a low performance ratio) but their use cannot explain why this poor performance occurs. They also fail to explain why some PV systems work better than others.

The analysis of annual results is simply not detailed enough to investigate the effect of the many factors which affect PV system performance. Monitoring must be carried out at a much higher resolution, for example daily or hourly, to identify and quantify the many energy losses that occur during PV system operation. Once the energy losses are understood, the reasons for any poor performance can be determined.

2.2. Energy losses and faults

2.2.1 Classification

Many types of energy losses occur in PV systems as part of the sunlight to useful electricity conversion. This work takes a new approach by classifying the energy losses into two separate categories: *operational losses* and *faults*. PV system performance is described as occurring in three states: ideal, normal and actual (Figure 2-2). *Ideal operation* represents the PV system operating at ideal conditions, with system efficiency equal to the PV module rated efficiency and no other losses (as described in the performance ratio calculations in Section 2.1.1). *Normal operation* describes the expected operation of a well-designed and performing PV system. The system efficiency at normal operation is lower than the ideal because of operational losses: inherent, unavoidable losses that occur in all installed PV systems. *Actual operation* represents the monitored performance of the PV system. System efficiency at actual operation may be lower than at normal operation due to faults, additional energy losses in the system which are considered avoidable and not a part of normal operation.

The operational losses are caused by environmental factors, for example the level of solar radiation or temperature, or the physical properties of the system components, for example the resistive energy loss in the DC cables or the energy loss due to the inverter DC to AC conversion process. The faults are due to poor system design (for example shading), component malfunction or problems with the mains electricity grid. The separation of energy losses into the two categories is useful when investigating possible improvements in PV systems operation. With better design and operation, faults can be minimised or even removed entirely. However, with the technology used in contemporary PV systems, operational losses will always be present to some degree.

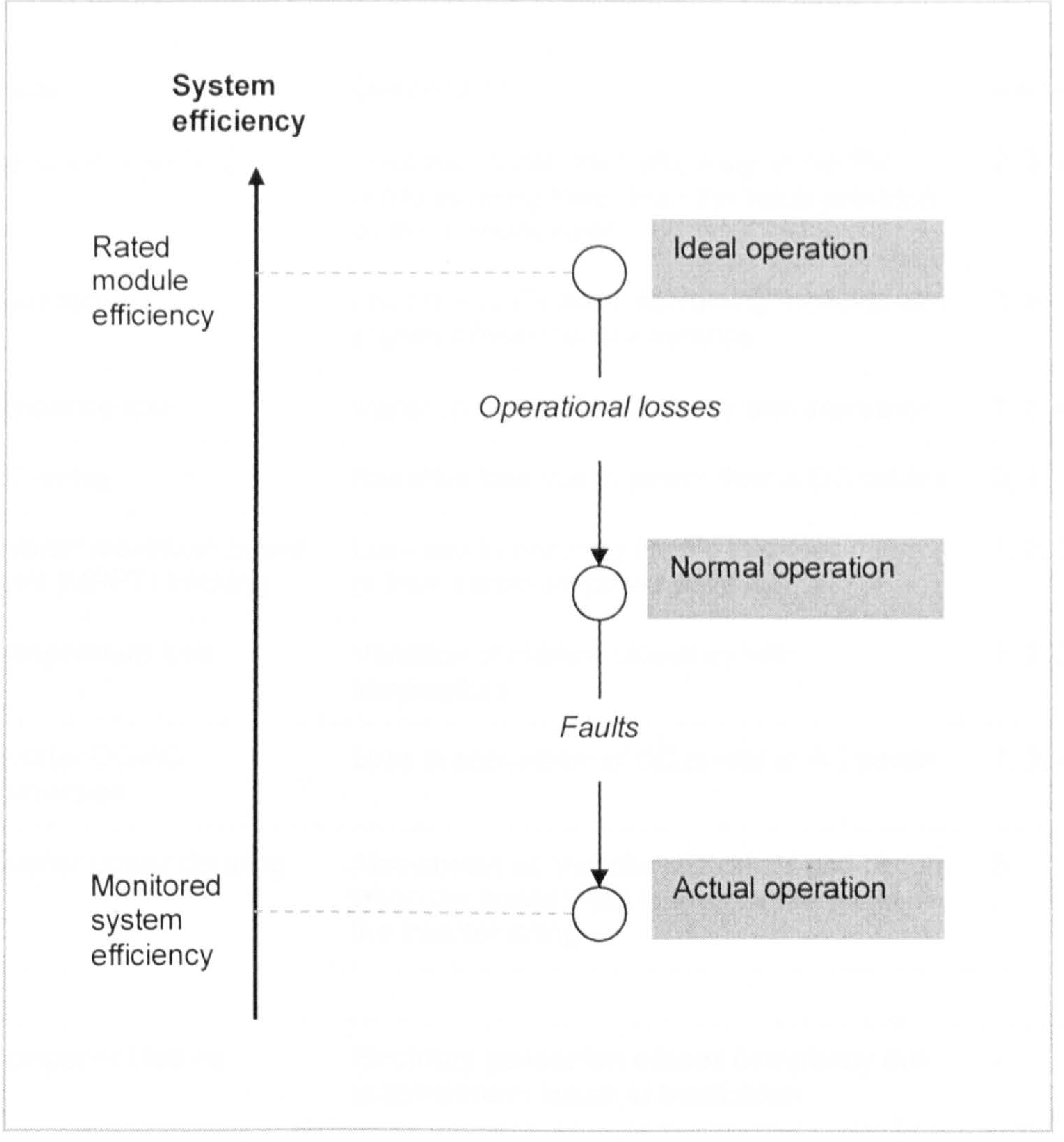

Figure 2-2: Schematic diagram of system efficiency at the three states of operation.

2.2.2 Identification

Six sources, a combination of monitoring studies and technical documentation, have been used to develop a list of operational losses and faults (Table 2-3). Eight types of operational losses and five types of faults are identified. These energy losses are used to investigate the performance of the PV systems monitored in this work. The operational losses and faults identified do not represent a complete list of all possible energy losses but instead those which are appropriate for analysis in this study. The descriptions given in the list are intended as a brief summary of each loss and a full literature review of the losses is provided in Chapters 6 and 7.

Table 2-3: List of operational losses and faults considered in this work

	Name	Description	Source
OPERATIONAL LOSSES	Deviation from STC	Loss due to the rated efficiency of the PV modules being lower than the value provided by the manufacturer	2, 3, 4
	Mismatch	Loss due to PV array containing modules with slightly different characteristics	3, 4
	Irradiance loss	Variation of module efficiency with irradiance	2, 3, 4
	DC wiring	Resistive loss due to power flow in DC cables	3, 4
	Inverter maximum power point (MPPT) tracking	Loss due to ensuring the PV modules operate at their maximum power point	1, 2, 3
	Temperature loss	Variation of module efficiency with temperature	1, 2, 3, 4
	Inverter DC-AC conversion	Loss in conversion of DC power to AC power	1, 3, 4
	Inverter power derating	Also known as 'inverter saturation' and occurs when the power input to the inverter exceeds the inverter rating	5
FAULTS	Component failure	Electricity generation ceases completely due to component failure or breakdown	-
	System isolation	Electricity generation ceases completely due to the system being isolated (i.e. switched off for maintenance work)	
	Inverter shutdown	Electricity generation ceases completely due to a power cut or variation in the grid voltage	6
	Shading	Solar radiation blocked by external shading objects, i.e. buildings, trees	1, 2, 3, 4
	Inverter maximum power point (MPP) tracking failure	When MPP tracking causes a significant reduction in efficiency. Also known as 'inverter dropout'.	-

Sources: 1 - SV Method (Oozeki et al., 2003); 2 - PVSAT-2 (Stettler et al., 2005); 3 - TEAMS (Reinders et al., 1999); 4 - 2250 PV roofs in Germany (Kiefer et. al, 1995); 5 – (Ransom and Funtan, 2005); 6 - inverter technical documentation (SMA, 2005)

In this work shading refers significant energy losses caused large external objects blocking the solar radiation. The losses could be avoided by better design of the positioning of the PV system. Shading is classified as a fault as there is a distinct difference in the performance of a PV system when it is shaded and when it is not.

In PV systems there will always be some shading at very low sun angles (normally around sunrise and sunset) which often cannot be avoided and this could be classified as a normal operation energy loss. However this loss is not investigated as it is considered to be small (due to the low solar radiation levels at sunrise and sunset) and the losses are not easily detectable in the monitored data.

There are further energy losses in PV systems which have been identified by other studies but which are not considered suitable for this study. Orientation loss is the effect on solar radiation energy input due to non-ideal orientation and tilt of a PV array (Reinders et al., 1999). It is calculated by comparing the energy yield to that of a PV system with ideal orientation and tilt. This requires the energy yield of the ideal system to be simulated and does not form a part of performance analysis in line with the aims of this work. Incidence angle reflection loss, described as the loss due to reflection of solar radiation at the surface of the PV modules (Oozeki et al., 2003; Reinders et al., 1999), and spectral effects (Reinders et al., 1999) cannot be studied due to the types of radiation sensors used. Other losses, for example the difference between static and dynamic maximum power point tracking (Reinders et al, 1999), are not considered as the measurements required to analyse these losses were not recorded.

2.3. High resolution monitoring and simulation

2.3.1 Previous studies

Four studies which quantify the energy losses in PV systems have been identified (Table 2-4). The recording intervals[11] range from 10 minutely to hourly and the use of data with a short recording interval, from seconds up to hourly intervals, is termed *high resolution monitoring*. The high resolution data provides a more detailed picture of the system performance and allows individual energy losses to be identified. The studies use either a monitoring only approach or monitoring plus simulation. Monitoring only analysis is based on a small number of measured parameters with a short recording interval. Information on the PV system performance is obtained by investigating the trends and patterns in the monitored data. The simulation approach uses models of PV system operation to simulate the

[11] The recording interval is the time period between each recorded measurement

electricity output. The simulated results are compared with the monitored data and the differences are used to investigate the energy losses.

Table 2-4: Losses quantified by previous studies.

		SV Method (Oozeki et al., 2003)	TEAMS (Reinders et al., 1999)	Data Analysis (Baltus et al., 1998)	German 1000 roofs programme (Kiefer et al., 1995)
Number of systems monitored		421	1	1	1
Monitoring interval		hourly	10 minutes	10 minutes	hourly
Simulations used		no	yes	no	yes
		Loss in annual performance ratio (in performance ratio percent)			
OPERATIONAL LOSSES	Deviation from STC	9	5.7	-	0.3
OPERATIONAL LOSSES	Mismatch	-	[1]	[2]	4.4
OPERATIONAL LOSSES	Irradiance	-	11.8	5.8	3.7
OPERATIONAL LOSSES	Inverter maximum power point (MPP) tracking	9	1.5	[2]	1.2
OPERATIONAL LOSSES	Temperature	4	6.1	2.4	3.3
OPERATIONAL LOSSES	DC wiring	-	[1]	0.9	-
OPERATIONAL LOSSES	Inverter DC-AC conversion	6	12.1	4.8	9.3
FAULTS	Shading	4	-	-	-

[1] In the TEAMS method the mismatch and DC wiring loss are given as a combined total of 3.9

[2] In the Data Analysis method, the mismatch and inverter MPP tracking losses are given as a combined total of 16.3

The Sophisticated Verification method (SV method), presented by Oozeki et al. (Oozeki et al., 2003) and demonstrated by Sugiura et al.(Sugiura et al., 2003), is a high resolution monitoring only approach. In-plane irradiance, PV module temperature, DC power output from the array and AC power output from the inverter were recorded at hourly intervals and used to quantify the energy losses. The monitored data was separated into months and each month was analysed separately. The only fault identified was shading, which was estimated based on the expected performance at different times of day. The Data Analysis method by Baltus et al. (Baltus et al., 1998) was also a monitoring only study in which ten minute data was used to estimate the energy losses.

The TEAMS (Reinders et al., 1999) and the German 1000 roofs programme (Kiefer et al., 1995) studies both used simulation. Losses which could be investigated directly from the monitored data were quantified and the remainder, in particular the mismatch and DC cabling losses, were estimated using simulated results. The simulations required models of the components of the PV systems and detailed measurements of the PV system before operation (such as I-V curve measurements[12]). These measurements could also be used to calculate other losses, such as the actual STC rating of the modules compared to the manufacturers stated rating. Faults were not identified by the simulation studies.

The four studies provide significantly different values of the operational losses. For example irradiance loss is estimated from 3.7% to 11.8% and MPP tracking loss from 1.2% to 9%. Three of the studies are based on single PV systems and this variation could be the result of different design or components.

Fault detection was carried out in only one of the four studies (the SV method estimated shading) and other studies have demonstrated fault detection techniques. Pearsall and Hynes (Pearsall and Hynes, 2003) detected faults in PV systems using five minute interval monitored data. The monitored data was separated into daily sections and visual inspection the data revealed examples of shading and inverter power derating. However the effect of these faults on overall system performance was not quantified. Another fault detection method is the PVSAT project, an initiative to detect faults in PV systems using solar radiation data derived from satellite data (Stettler et al., 2005). The method used the INSEL

[12] The IV curve of a PV system is the relationship of the current (I) and voltage (V) of the array over a variety of loads, from short circuit to open circuit.

simulation tool and satellite data is used to estimate the energy output of the PV system. Faults are detected and identified by comparing the simulated and actual monitored results from a single day, 7 days or 30 days. PVSAT does not attempt to quantify the energy lost due to faults.

2.3.2 Limitations of previous studies

There is no single approach which investigates the effect on performance of both the operational losses and the faults. The SV method provided a technique of estimating the operational losses from monitored data, but because it used hourly data, it did not provide information on the majority of faults. At the hourly level, a fault which occurred for only a few minutes would not show up in the data. A higher resolution recording interval, such as the five minute interval used by Pearsall and Hynes, revealed faults but there was no established method to quantify the losses.

The simulation studies of TEAMS and the German 1000 roof programmes quantified the operational losses but did not identify the faults. Faults were identified through simulation by PVSAT but only at the hourly level and again the effects on performance were not quantified. Models tend to suit the general case rather than specific cases and applying a model to a particular PV system can be difficult. The model may need calibrating to match the characteristics of the PV system and this requires detailed knowledge of the system components, normally acquired through on-site measurements at the start of system operation. These measurements add an extra level of complexity and cost onto the simulation approach.

A further limitation of the approaches is the requirement to separate data into discreet sections. For example the SV method analyses data on a month-by-month basis and the TEAMS approach separates the data into daily sections to analyse shading. This is a time-consuming approach for large datasets and it is possible that long term trends in the data may go unnoticed.

2.3.3 Approach taken in this study

Monitoring only analysis, without simulation, is used as the approach to PV system performance analysis in this work. This decision was made partly through necessity and partly through a rational appraisal of the different performance analysis techniques. The monitoring systems for the PV systems under study were designed and installed without reference to this work (see Section 3.2) and the style of monitoring (a small number of measured parameters at a five minute recording interval) suited the monitoring only approach. There was also little opportunity for additional measurements which are required for simulation techniques.

In addition, as the recording interval of the monitored data decreases, the need for a model of PV system operation becomes less. If the operation of a PV system is measured on a second-by-second or minute-by-minute basis then it is possible that all the information required to understand the system operation is available within the data. The use of models, with their added complexity, is more difficult to justify. The monitoring only approach, especially if used in combination with high resolution data, can potentially provide a near real time assessment of the system performance and be capable of detecting and identifying faults.

The remainder of this thesis presents the work carried out in developing a new performance analysis method based on the monitored five minute interval data. The approach is designed to investigate both operational losses and faults, thus overcoming the limitations of previous methods. The approach also analyses datasets spanning large time periods (a year or greater) and does not require the data to be separated into smaller sections. This allows the identification of patterns and trends in the data but retains the detail of the high resolution measurements.

2.4. Summary

A review of worldwide monitoring studies provides a benchmark for PV system performance. The average annual performance ratios for PV systems installed in the late 1990s was around 70%. Performance ratios had risen over the past decade and higher values could be expected from the monitored PV systems in this study, all of which were installed after 2001. The limitation of annual monitoring was that it could not explain the difference in performance between systems.

Energy losses in PV systems have been classified into the two categories: operational losses; and faults. Thirteen different types of energy losses were considered in this work, based on a survey of six previous studies. A discussion of studies which quantify these losses showed that energy loss due to faults had not been investigated in detail. Models and simulations of PV systems were used in some of the studies, which added a layer of complexity and cost to the analysis process.

The analysis approach taken in this work used monitored data only (which avoided the use of simulation). The value of using a five minutely recording interval to identify and quantify the energy losses is explored. The methods used to collect and process the monitored data is the subject of the next chapter.

3. The Field Trials: Data Measurement, Collection and Processing

The performance analysis techniques developed in this thesis are based on monitored data from UK domestic PV systems and this chapter describes the measurement, collection, transfer and processing of the monitored data. One hundred and nine PV systems were monitored for this study. The PV systems were on five sites, each with between twelve and thirty systems, and the sites were located throughout the UK. The systems were installed and monitored under the UK Government's PV Domestic Field Trial (DFT), a fully funded government programme intended as the first step in the creation of a significant domestic PV market.

The crucial aspect of the DFT programme relevant to this work is the monitoring of the operation and performance of the PV systems. The monitoring systems installed at the five PV sites were designed to meet a specific set of requirements as part of the DFT contract. The types of sensors and data loggers were chosen to meet this specification. Methods of data transfer and processing were developed and software was chosen to analyse the monitored data. Examples of the data analysis methods are given and the results of the data analysis form the content of Chapters 5 to 7.

This chapter describes a combination of work undertaken by the PV installation companies and the author of this thesis. The PV installers were responsible for designing and installing all of the PV systems and all of the monitoring systems except for the Ashley Vale site, where the author took part in the monitoring system installation. The author also developed the data transfer routines (Section 3.2.5) and the data processing routines (Section 3.3).

3.1. The UK Photovoltaic Domestic Field Trial

3.1.1 Background

The DFT was set up by the UK Government in May 2000 (BRE, 2003). Funded by the Department for Trade and Industry (DTI, 2005c), its main aim was to install a large number of domestic grid-connected PV systems throughout the UK. This would provide a significant learning opportunity for government, developers, planners, housing associations, utility companies and the PV industry. It would also stimulate the UK market in order to streamline the design and installation processes and drive down costs. The DFT management contractors were Future Energy Solutions (FES, 2005), the Building Research Establishment (BRE, 2005) and IT Power (IT Power, 2005). The monitoring specialists for the project were the Energy Monitoring Company (EMC, 2005) and the Northumbria Photovoltaic Applications Centre (NPAC, 2005) at the University of Northumbria.

The DFT sought to install PV systems on clusters of houses throughout the UK and to involve as many participants as possible. Thirty one sites were chosen and over 750 domestic buildings were fitted with PV systems. The sites were geographically chosen so each District Network Operator (DNO) of the national electricity grid was involved with at least one project. A wide range of built forms were chosen. Two thirds of the sites were social housing or mixed developments. Seventeen sites were new build (the PV was installed at the same time as the properties were constructed), thirteen were retrofit (the PV was installed into existing housing) and one site was a mix of both. The design, installation and operation of the PV systems were managed by project teams, usually a partnership between the property owners, energy consultants and PV installation firms.

The DFT was fully funded by the DTI. As part of the funding requirements, each site was required to have a comprehensive monitoring system and to collect performance data over a two year period. It was the responsibility of the project teams to carry out the monitoring. The aim of the monitoring was to make a detailed assessment of the operation, reliability and performance of the PV systems and to feed this information back to the developers, owners, tenants and the PV industry.

Information was also gathered on the design of the PV systems and the management of the installation process. For each site a design report, a procurement report, an installation report, a commissioning report and several monitoring reports were produced by the project teams. A social survey was carried out by the project teams, based on a questionnaire specific to the DFT, to provide information on the user satisfaction and opinions of the owners or tenants involved.

3.1.2 Sites monitored in this study

The PV systems studied in this work were installed at five of the DFT sites: Corncroft (Nottingham), Heron Close (Leeds), Panmure Street (Glasgow), Newbiggin Hall (Newcastle) and Ashley Vale (Bristol) (Table 3-1 and Figure 3-1). The sites were a mixture of new build and retrofit developments. Four of the sites are social housing projects and the PV was installed onto properties rented by tenants. Ashley Vale is unique in the DFT as it is a self build development. The individuals own their properties and the PV systems, and they installed the PV systems themselves. All of these sites were project managed by the energy consultants Energy for Sustainable Development Ltd. (ESD, 2005), who co-funded this study.

Table 3-1: Details of the PV sites: location and built forms

Site	Acronym	Location	New-build or Retrofit	Social housing or private	Type of buildings
Corncroft	CC	Nottingham	New-build	Social	Bungalows
Heron Close	HC	Leeds	Retrofit	Social	2 storey blocks and flats
Panmure Street	PS	Glasgow	New-build	Social	One block of 12 flats
Newbiggin Hall	NB	Newcastle	Retrofit	Social	Block of flats
Ashley Vale	AV	Bristol	New-build (self build)	Private	Mixture of detached, semidetached, terrace and flats.

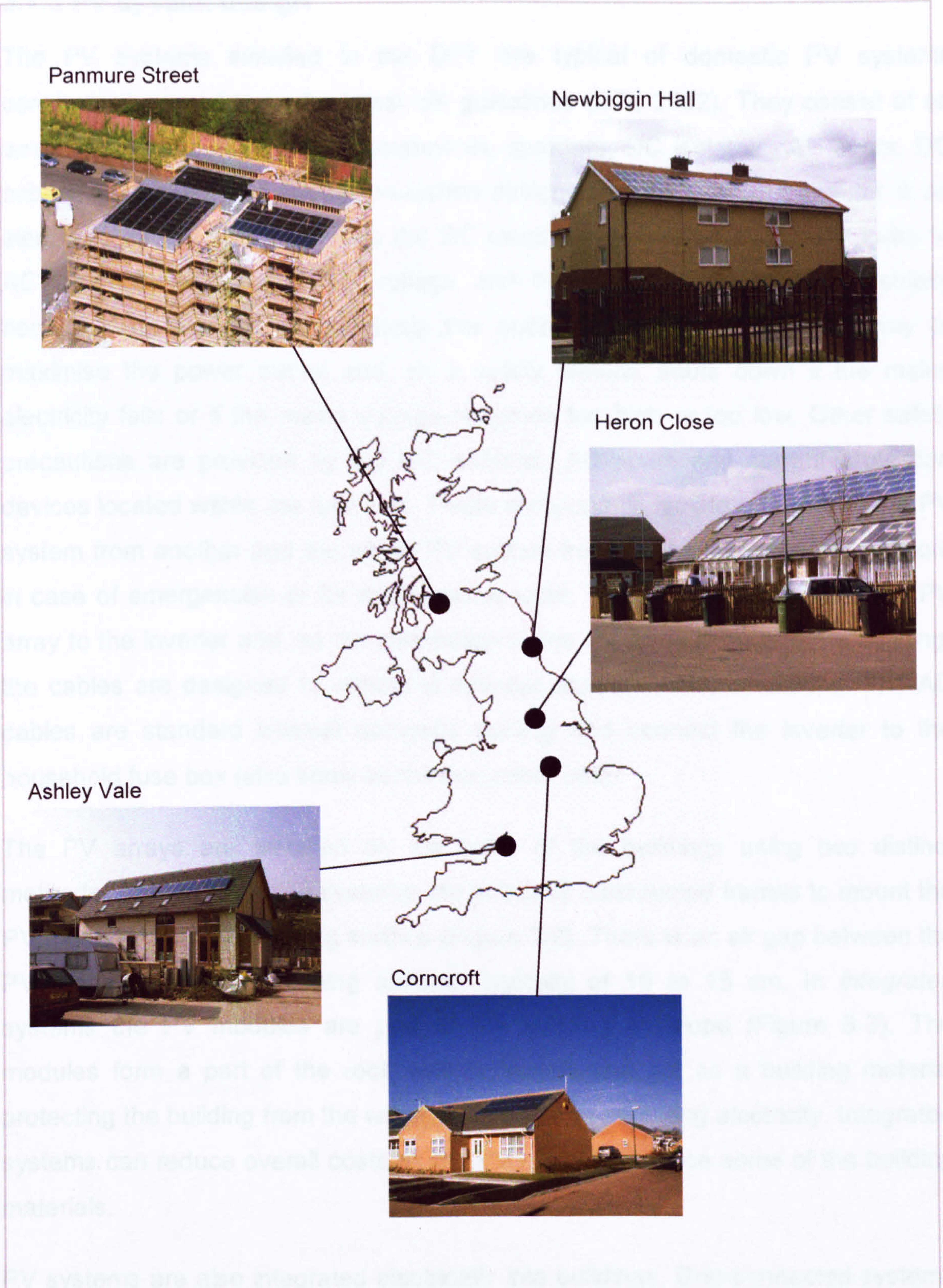

Figure 3-1: The five PV sites in this study

3.1.3 PV system design

The PV systems installed in the DFT are typical of domestic PV systems constructed according to the latest UK guidelines (DTI, 2002). They consist of an array and balance of system components: inverters, DC isolators, AC spurs, DC cables, AC cables and current protection devices (Figure 3-4). The inverter is an electronic device which converts the DC electricity generated by the PV array to AC electricity with the same voltage and frequency as the mains electricity network. The inverter also controls the operating voltage of the PV array to maximise the power output and, as a safety feature, shuts down if the mains electricity fails or if the mains voltage becomes too high or too low. Other safety precautions are provided by the DC isolators, AC spurs and current protection devices located within the fuse box. These components isolate one part of the PV system from another and the whole PV system from the mains electricity network in case of emergencies or for maintenance work. The DC cables connect the PV array to the inverter and, as the connection to the PV array is outside the building, the cables are designed to withstand external environmental conditions. The AC cables are standard internal domestic cabling and connect the inverter to the household fuse box (also know as the consumer unit).

The PV arrays are installed on the roofs of the buildings using two distinct methods. *Bolt-on* mounting systems use specially constructed frames to mount the PV modules over the building surface (Figure 3-2). There is an air gap between the PV modules and the building surface, typically of 10 to 15 cm. In *integrated* systems the PV modules are part of the building envelope (Figure 3-3). The modules form a part of the roof, wall or façade and act as a building material protecting the building from the weather as well as generating electricity. Integrated systems can reduce overall costs as the PV modules replace some of the building materials.

PV systems are also integrated electrically into buildings. Grid-connected systems are normally connected to the building circuitry at the consumer unit or fuse box (Figure 3-4). PV generated electricity is automatically used by the appliances in the building and reduces the import of electricity from the mains electricity network. This contributes to savings on electricity bills. If, at any one moment, the amount of PV electricity being generated is greater than the demand of the building appliances then the excess is exported to the mains electricity network. The exported electricity may be sold to the electricity distribution company.

Figure 3-2: A single PV module on a bolt-on mounting system (Heron Close)

Figure 3-3: A complete PV array integrated into a roof (Corncroft)

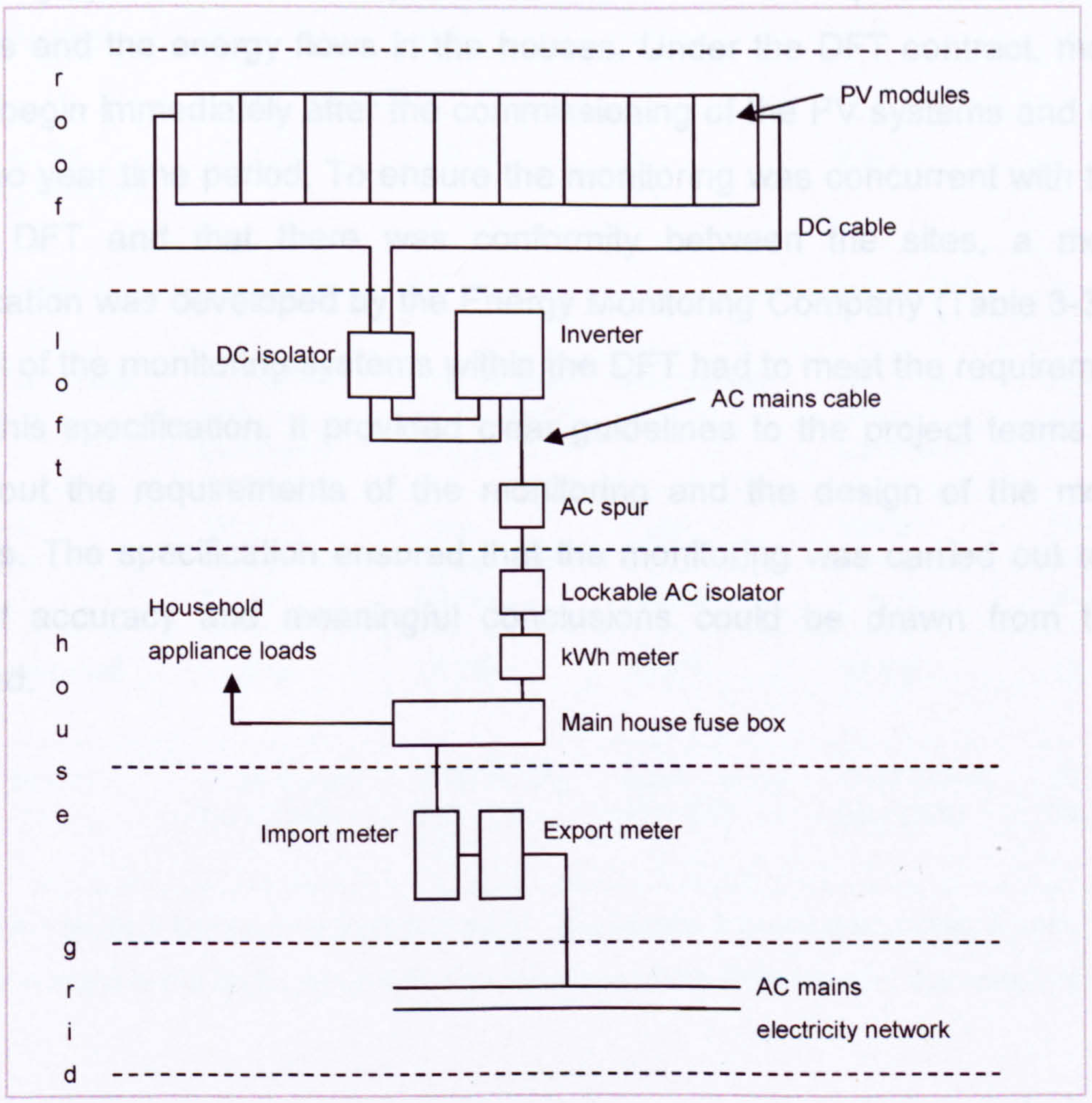

Figure 3-4: Schematic diagram of the main system components

3.1.4 PV systems specifications

There were between 12 to 30 PV systems installed at each site and the total installed PV capacity was from 13 kWp to 40 kWp (Table 3-2). The systems were installed between early 2002 and June 2004 and monitoring began from June 2002 to November 2004. Individual system size varied from 0.77 kWp to 2.55 kWp and the PV array area from 5.7 m^2 to 19.0 m^2. The arrays had a variety of orientations and contained between 9 and 30 PV modules. Two types of PV modules were used: BP Solar 585 laminates and Astropower AP modules. These modules are both crystalline silicon PV modules and have rated efficiencies of 13.8% and 12.3% respectively. Throughout all five sites a range of SMA Sunny Boy inverters are used, with power ratings from 700 W to 2500 W.

3.2. Monitoring system design

3.2.1 The DFT monitoring specification

Monitoring systems were set up at each site to record the performance of the PV systems and the energy flows in the houses. Under the DFT contract, monitoring had to begin immediately after the commissioning of the PV systems and continue for a two year time period. To ensure the monitoring was concurrent with the aims of the DFT and that there was conformity between the sites, a monitoring specification was developed by the Energy Monitoring Company (Table 3-3, Figure 3-5). All of the monitoring systems within the DFT had to meet the requirements set out in this specification. It provided clear guidelines to the project teams at each site about the requirements of the monitoring and the design of the monitoring systems. The specification ensured that the monitoring was carried out to a high level of accuracy and meaningful conclusions could be drawn from the data recorded.

Table 3-2: Details of the PV installations

Site	Corncroft	Heron Close	Panmure Street	Newbiggin Hall	Ashley Vale
Number of PV systems	22	30	12	25	20
Installed PV capacity (kWp)	34	40	13	38	25
Installation date	Early 2002	Aug to Dec 2002	Sept 2003	June 2004	Early 2004
Start of monitoring period	June 2002	Feb 2004	June 2004	Aug 2004	Nov 2004
Size of PV systems (kWp)	1.53 to 1.7	0.88 to 1.92	1.08	0.77 to 2.55	1.08
Mounting system	Roof integrated	Bolt on	Bolt on	Roof integrated	Bolt on
Array orientation (°)[1]	-22	Various: -50 to 40	10	85, -5, 95	Various, -20 to 20
Array inclination (°)[2]	30	37.5	30	40	40
Number of PV modules per array	18 to 20	7 to 16	9	9 to 30	9
Area of array (m^2)	11.1 to 12.3	7.8 to 15.6	11.7	5.7 to 19.0	11.7
PV module model	BP Solar 585 laminates	Astropower AP55, AP75 and AP 120	Astropower AP120	BP Solar 585 laminates	Astropower AP120
PV module technology	Mono-crystalline silicon	Poly-crystalline silicon	Poly-crystalline silicon	Mono-crystalline silicon	Poly-crystalline silicon
PV module rated efficiency	13.8%	12.3%	12.3%	13.8%	12.3%
Inverter model	SMA Sunny Boy 2500	SMA Sunny Boy 700 – 1100	SMA Sunny Boy 850	SMA Sunny Boy 2500	SMA Sunny Boy 850

[1] Orientation angle is the bearing from due south, where east is positive and west is negative

[2] Inclination angle is the angle made between the slope of the PV array and the horizontal

Table 3-3: The DFT monitoring specification (reproduced from the DFT tender documentation; DFT, 2002)

Measured parameter	Locations on site	Specified required resolution	Specified required accuracy	Specified sampling interval
Solar irradiance on the horizontal	Once for the whole site	0.25 W/m^2	± 5%	10 sec
Ambient air temperature	Once for the whole site	0.1 °C	± 0.5 °C	1 min
Solar irradiance in plane of array	Once for each set of arrays with different orientation	0.25 W/m^2	± 5%	10 sec
Array temperature	Once for each set of arrays with different orientation	0.1 °C	± 0.5 °C	1 min
DC electrical power output of PV array	For each PV system	1 W	± 4%	Continuously integrated or 10 sec
AC electrical power output of inverter	For each PV system	1 W	± 2%	Continuously integrated
Electricity imported to building	For each PV system	1 W	± 2%	Continuously integrated
Electricity exported from building	For each PV system	1 W	± 2%	Continuously integrated

The specification defined the measured parameters, location of sensors, resolution, accuracy, sampling interval and recording interval required for the DFT monitoring. All the measured parameters were sampled at ten second or one minute intervals and were recorded at five minute time intervals. Measurements that were regularly sampled (such as irradiance or temperature) were averaged for each five minute period and the average value was stored. Continuously integrated measurements (such as the import and export measurements which were measured by an electric pulse from the sensor for every Wh of electricity flow) were continuously recorded and the values totalled for each five minute period.

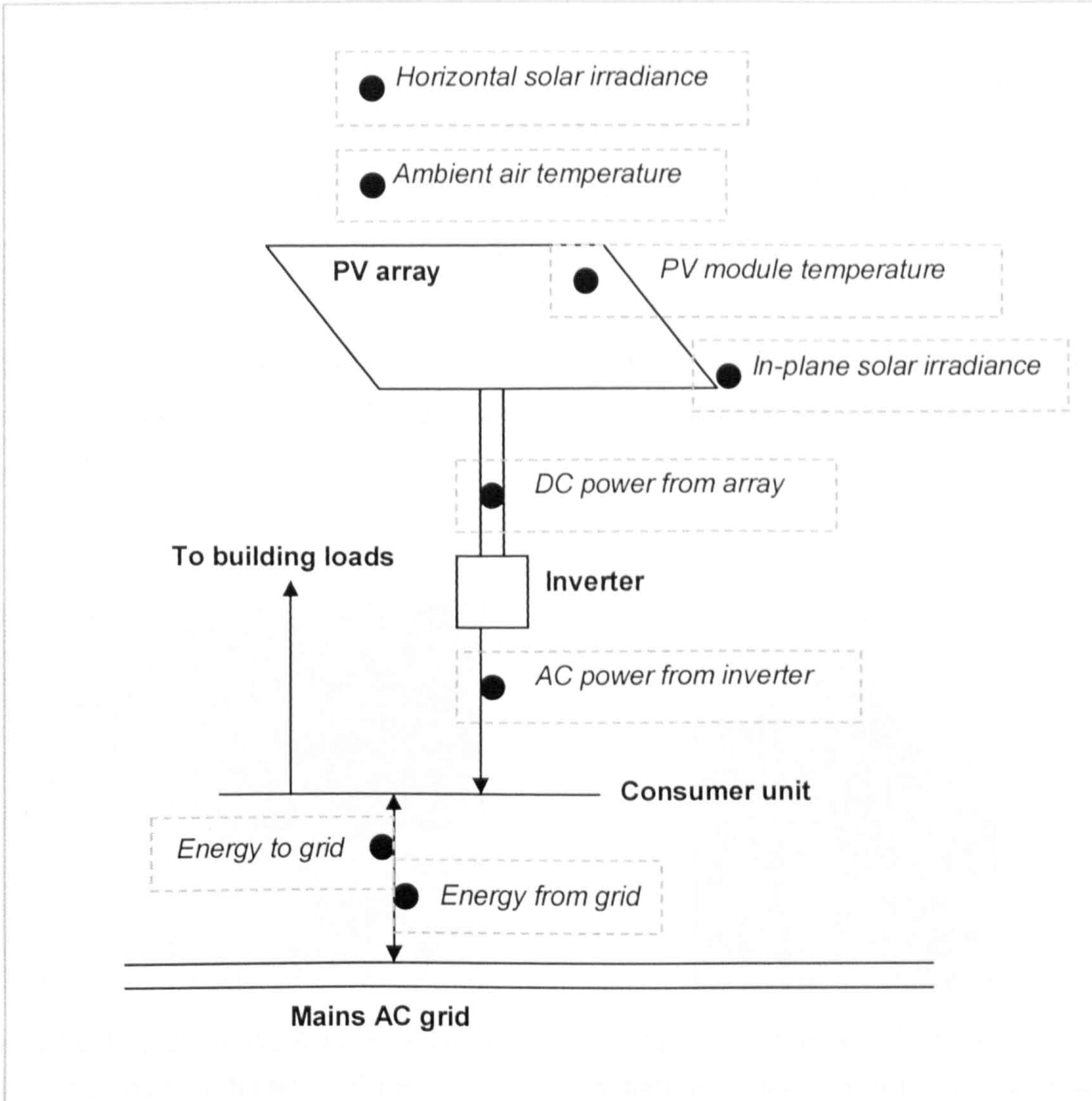

Figure 3-5: Schematic of measured parameters in DFT monitoring specification

The measured parameters of irradiances, temperatures, DC power and AC power were used to develop the performance analysis techniques. The electricity imported and exported by the house did not form a part of the analysis and the data was not used in this study. The data has been useful to the work of others, in particular the development of a domestic energy consumption model (Stokes, 2005).

3.2.2 Solar radiation sensors

As already mentioned, solar radiation was measured both horizontally and in the plane of the PV array. The horizontal radiation was measured at one location for each site and the in-plane solar radiation was measured for each group of PV arrays with similar orientations (only once if all the arrays on site had the same orientation). The radiation sensors should be unshaded throughout the year and if possible were placed above the ridge of the roof (Figure 3-6 and Figure 3-7). There were instances when the radiation sensors were shaded and the effect of this is discussed in Chapter 5.

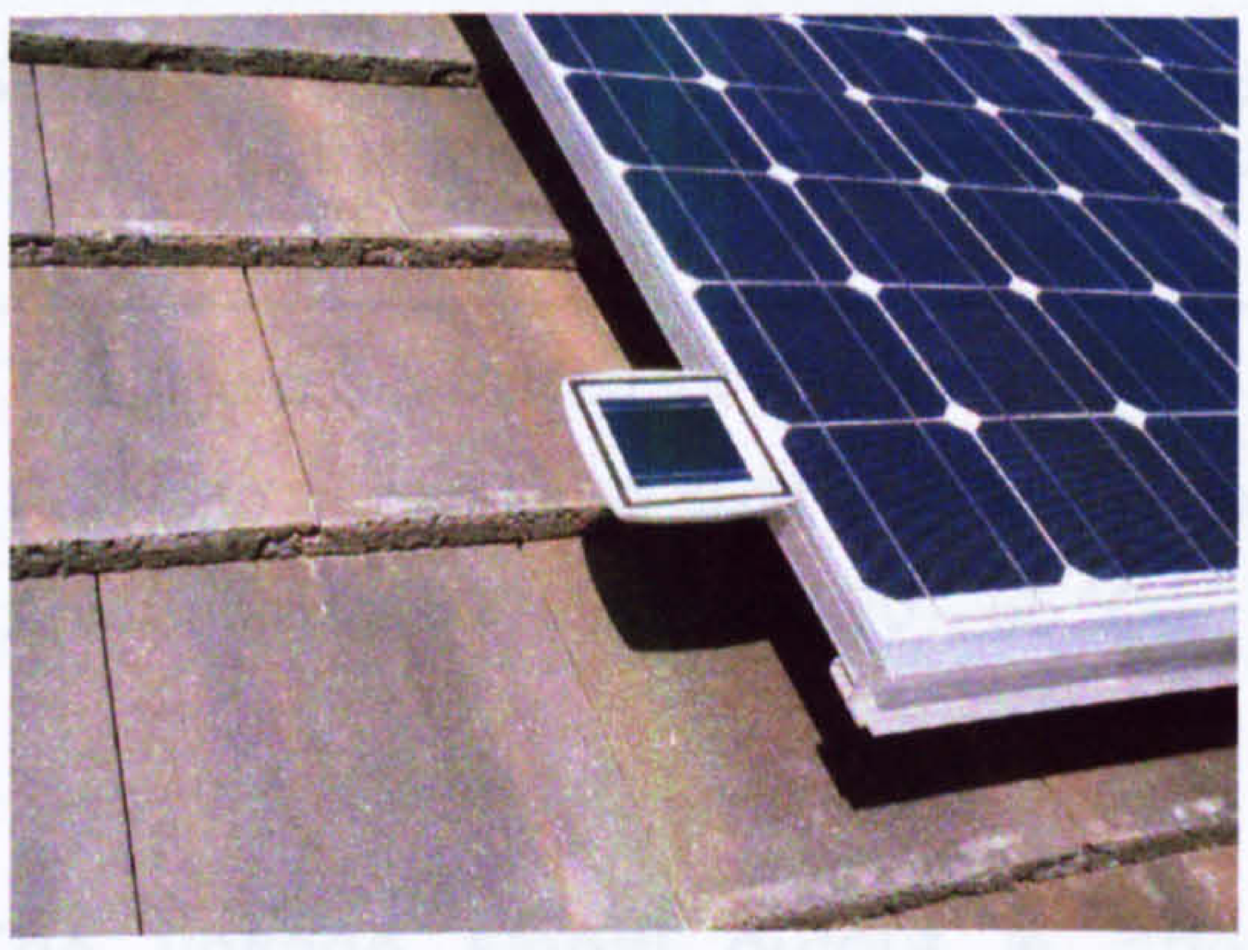

Figure 3-6: In-plane Sensol solar radiation sensor mounted on the edge of a PV array at Heron Close

Figure 3-7: Horizontal and in plane radiation sensors mounted on a bracket above the ridge of the roof at Corncroft. The ambient temperature sensor is also mounted on the bracket.

EETS (EETS, 2005) and Sensol (ISET, 2005) radiation sensors are used, both consisting of a small PV cell of crystalline semiconductor silicon (Table 3-4). The short circuit current[13] of the PV cell is measured and used to calculate the solar irradiance. As the short circuit current in a PV cell varies proportionally with the number of photons absorbed by the cell (as described in Green (Green, 1982)), the sensor is essentially a photon counter. The sensors output a voltage signal which is proportional to the short circuit current of the PV cell. The voltage signal, typically around 0 mV to 60 mV, is measured by the data loggers and used to calculate the

[13] The current under a load of zero resistance

irradiance. The radiation sensors were calibrated against reference sensors under laboratory conditions. The relative measurement uncertainties of the radiation sensors were within the requirement of ±5% set by the DFT monitoring specification.

Table 3-4: Details of the radiation sensors

Solar radiation sensor model	Manufacturer	Voltage signal at STC	Relative measurement uncertainty	Method of temperature measurement	Temperature coefficient of voltage signal
EETS in house	Energy Equipment Testing Services (EETS, 2005)	29.48 mV	± 0.06% [1]	Open circuit voltage of silicon cell	+ (0.007 ± 0.001) mV / °C [3]
Sensol	Institut für Solare Energieversorgungstechnik (ISET, 2005)	≈ 60 mV	± 3% [2]	PV array temperature	+ (0.039 ± 0.009) mV / °C

[1] This figure is provided for STC only

[2] Refers to a confidence level of 95%. It is not clear if this figure applies to all irradiance levels.

[3] Applicable for 800 W/m^2 and 20 – 65 °C

The voltage signal output is affected by temperature. To account for the temperature effect the voltage signal should be temperature corrected[14] to an equivalent signal at 25 °C using the temperature coefficients provided by the manufacturers. The EETS sensor readings were corrected using temperature values calculated from the open circuit voltage of the silicon cell. Although the Sensol sensors have a built-in temperature sensor, this was not measured by the monitoring systems and no temperature correction was made. At high temperatures, this could result in the Sensol measurements being slightly higher than the true irradiance values. For example, an increase in temperature of 40 °C, at irradiance of 1000 W/m^2, would result in a 2.6% increase in the irradiance measurements.

3.2.3 Temperature sensors

Ambient air temperature was measured at one location at each PV site and the PV

[14] Temperature correction is discussed in detail in Section 6.2.3

module temperature for each group of PV arrays with similar orientations. Ideally, the ambient air temperature sensor is placed out of direct sunlight and is usually located under the eaves of a roof on the north side of a house (Figure 3-8). The PV module temperature sensor was fixed to the underside of a PV module, preferably at the centre of the module and at the centre of a cell (Figure 3-9). Although the temperature of a PV array will vary at different locations of the array, only a single temperature measurement was made.

Figure 3-8: Ambient temperature sensor at Ashley Vale. The sensor is placed under the eaves on the north side of the house to avoid any direct solar radiation.

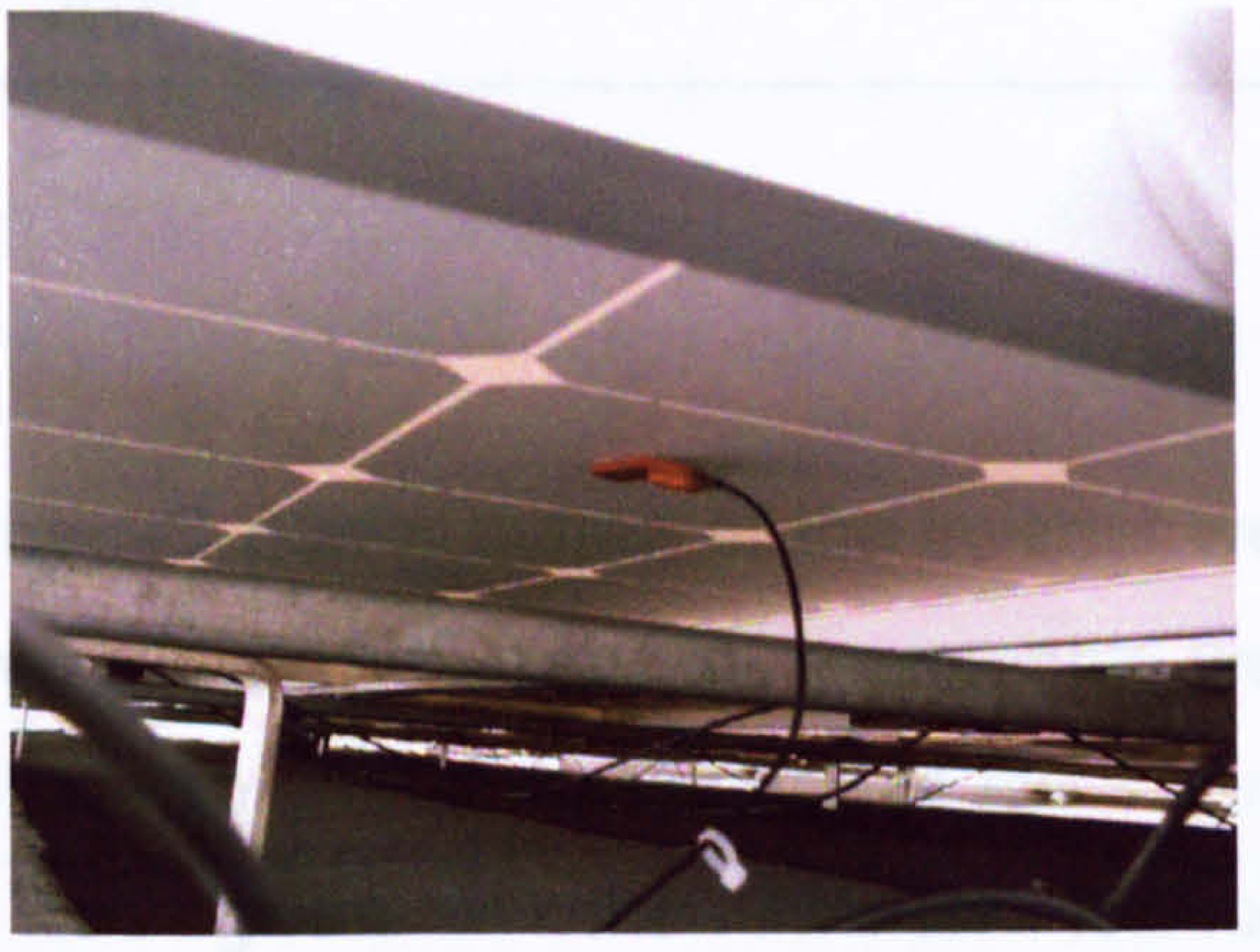

Figure 3-9: PV module temperature sensor fixed to the back of a PV module at Heron Close. Note how the sensor is placed in the middle of one of the PV cells.

The same types of ambient air and PV module temperature sensor are used at all five sites (Table 3-5). The ambient air temperature sensor had a plastic and aluminium alloy screen to minimise the effect of solar radiation, precipitation and wind speed on the measurements. Both sensors used Class B PT100 elements, platinum temperature sensing resistors with a resistance of 100 Ohms at 0 °C. The measurement inaccuracy of ambient and PV module temperature sensors was the same. At a temperature of 80 °C the inaccuracy was low (± 0.34 °C) and within the ± 0.5 °C range required by the DFT specification (Section 3.2.1).

Table 3-5: Details of the temperature sensors

Temperature sensor	Sensor type	Sensor model	Manufacturer	Measurement Inaccuracy	Measurement inaccuracy at 80°C
Ambient air	Shielded PT100	Air Temperature Mini-Screen T351-PX	Vector Instruments Ltd. (Vector Instruments, 2005)	± (0.3°C + 0.005t)[1]	± 0.34°C
PV module	PT100 with an adhesive patch	-	Labfacility Ltd. (Labfacility, 2005)	± (0.3°C + 0.005t)[1]	± 0.34°C

[1] t is temperature in °C

3.2.4 DC and AC power

The DC power output of the array and the AC power output of the inverter were measured for every PV system at the five sites. The power measurements were made by the SMA inverters using in-built sensors. The inaccuracy of the inverter DC and AC power measurements was given in the inverter technical documentation (Table 3-6); this was outside the limit set by the DFT monitoring specification (± 4% for DC power and ± 2% for AC power). The use of SMA inverter measurements was discussed in the Second Annual Report of the DFT (BRE, 2003) and, as SMA inverters were used in the majority of the DFT projects, the inaccuracy limits of the monitoring specification was relaxed.

Table 3-6: SMA inverter measurement accuracy (SMA, 2005)

DC / AC	Inaccuracy of current measurements[1]	Inaccuracy of voltage measurements[1]	Inaccuracy of power measurements[2]
DC	± 4%	± 2%	± 6%
AC	± 2%	± 1%	± 3%

[1] The inaccuracy is referred to as 'maximal failure' in the technical documentation and based only on a temperature of 25 °C

[2] Calculated according to error analysis theory by addition of the current and voltage inaccuracies

It has been anecdotally reported within the PV research community that the DC current measurements made by SMA inverters may be inferred from other measurements rather than measured directly. There is no reference in the literature and it has not been possible to find out from the manufacturer the exact nature of the DC current sensor in SMA inverters. This effect, if present, could in part explain the inaccuracy in the DC power measurements.

3.2.5 Data collection and data transfer

Data collection, the process of reading the measurements made by the sensors and recording the measured values, was carried out by the data loggers, electronic equipment designed specifically for this purpose. Different approaches were taken to data collection on the five sites (Table 3-7). Two types of data loggers were used: Sunny Boy Control Plus (SBC+) units manufactured by SMA, the inverter manufacturer (SMA, 2005); and systems based on a personal computer (PC). A consequence of the difference in the monitoring system design was the variation in the sampling rate at the sites, from around 10 to 60 seconds.

Table 3-7: Design of the monitoring systems

Site	Solar radiation sensor model	Number of in-plane irradiance measurements per site[1]	Number of PV module temperature measurements per site[1]	Data loggers	Number of phone lines	Sampling rate (seconds)
Corncroft	EETS	1	1	One SBC+, one PC	1	≈ 60
Heron Close	Sensol	2	2	Eight SBC+	8	≈ 10
Panmure Street	Sensol	1	1	Three SBC+	1	≈ 10
Newbiggin Hall	EETS	3	3	PC	1	≈ 60 (estimate)[2]
Ashley Vale	Sensol	4	4	Six SBC+	0	≈ 10

[1] In-plane irradiance and PV module temperature is measured for each group of arrays on a site with a different orientation

[2] This figure is an estimate as no direct access to the monitoring PC was provided at this site

The stored data was transferred to a central off-site PC on a regular basis. The data loggers were connected to the public telephone network using modems and the collected data was regularly downloaded. Laplink software (Laplink, 2005) was used for the PC data transfer and SMA Sunny Data Control software for the SBC+ sites. The latter process was automated with routines written by the author in Macro Scheduler (Mjtnet, 2005).

The SMA SBC+ unit is a data logger designed for monitoring PV systems (Figure 3-10). The sensors were connected directly to the SBC+ unit and the SBC+ read and stored the sensor outputs. Each SBC+ unit monitored a maximum of four houses because there was a limit on the number of channels available for the import and export data. Because of the small number of inverters connected to each SBC+, the sampling rate was fast (around 10 seconds). The Heron Close, Panmure Street and Ashley Vale monitoring systems used only SBC+ units. The number of SBC+ units depended on the total number of systems to be monitored. At Heron Close, each SBC+ was connected to a modem and a phone line to transfer the data off site. The SBC+ units at Panmure Street were networked together and connected to a single modem and phone line for data collection. At Ashley Vale the data was collected by personnel on-site.

Corncroft and Newbiggin Hall used PCs to support the data collection. A PC was used to record and store the measured parameters, and was connected to a single modem and phone line for data transfer (Figure 3-11). At Corncroft a single SBC+ unit was used to monitor the AC and DC measured parameters and the data was transferred to the PC daily. At Newbiggin Hall all the measured parameters were recorded directly by the PC. In both cases the sampling rate was slow (at around 60 seconds or greater) for all the measured parameters as the monitoring systems had to cycle through each of the PV systems. This sampling rate was outside the DFT monitoring specification for some of measured parameters and the consequence of the slow sampling rate is discussed in Section 4.2.4.

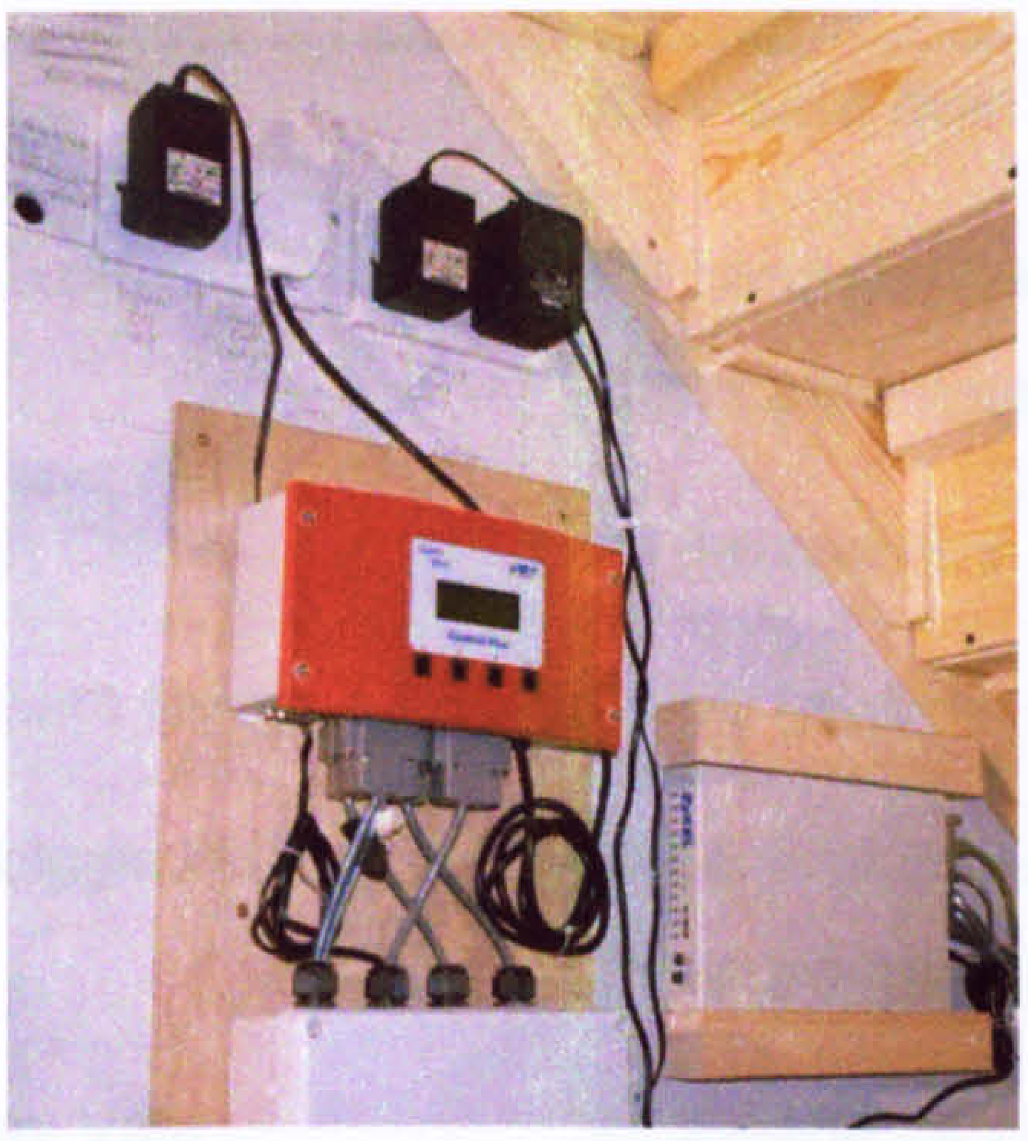

Figure 3-10: A Sunny Boy Control Plus (SBC+) data logger installed at Ashley Vale

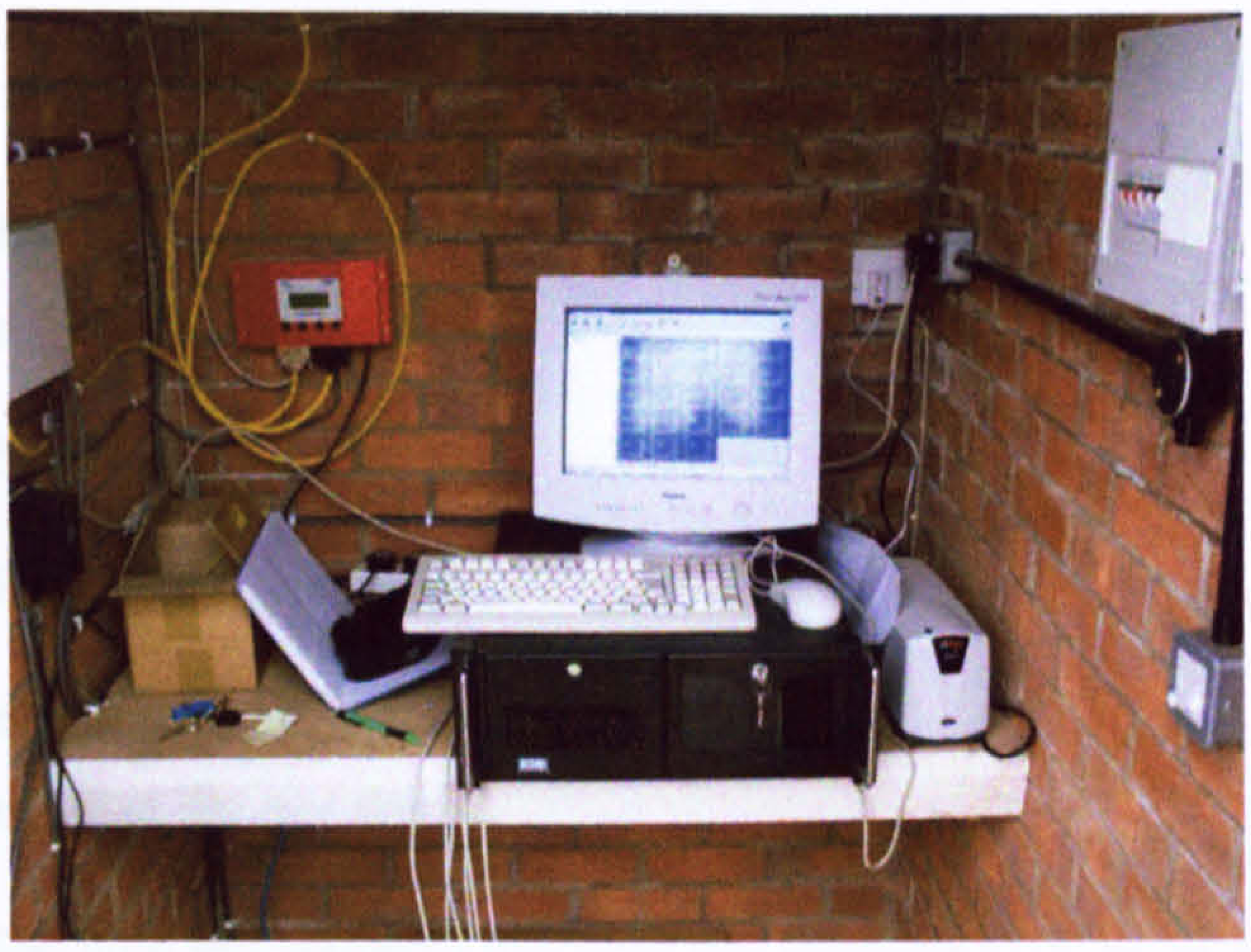

Figure 3-11: PC monitoring system at Corncroft

3.3. Programming for data processing and analysis

3.3.1 Format of raw data

The data recorded at the PV sites was in a variety of formats (Table 3-8 and Figure 3-12). The raw data files varied in length from a single day to a month and different measured parameters were recorded in separate data files. The raw data was processed to convert all the data into a series of standard file formats. The processed data could then be easily accessed and used in data analysis procedures.

An automated method of data processing was necessary because of the large amount of data collected by the monitoring systems (due to the number of measured quantities, the number of houses under study and the duration of the monitoring programme). The size of the datasets in this study can be simply illustrated with the following example. Over a 12 month period a measured parameter recorded every 5 minutes will generate 105,120 data values. At the Corncroft site 22 houses were monitored, each with up to eight different parameters, so approximately 18.5 million data values were recorded to describe the PV systems' behaviour for one year.

Table 3-8: Format of raw data files

Site	Raw data files created
Corncroft	PV temperature: one text file per day Other parameters: one Excel file per month
Heron Close	All parameters: eight Excel files per month
Panmure Street	All parameters: three Excel files per month
Newbiggin Hall	Meteorological parameters: three text files per day Other parameters: one Excel file per day
Ashley Vale	All parameters: six Excel files per month

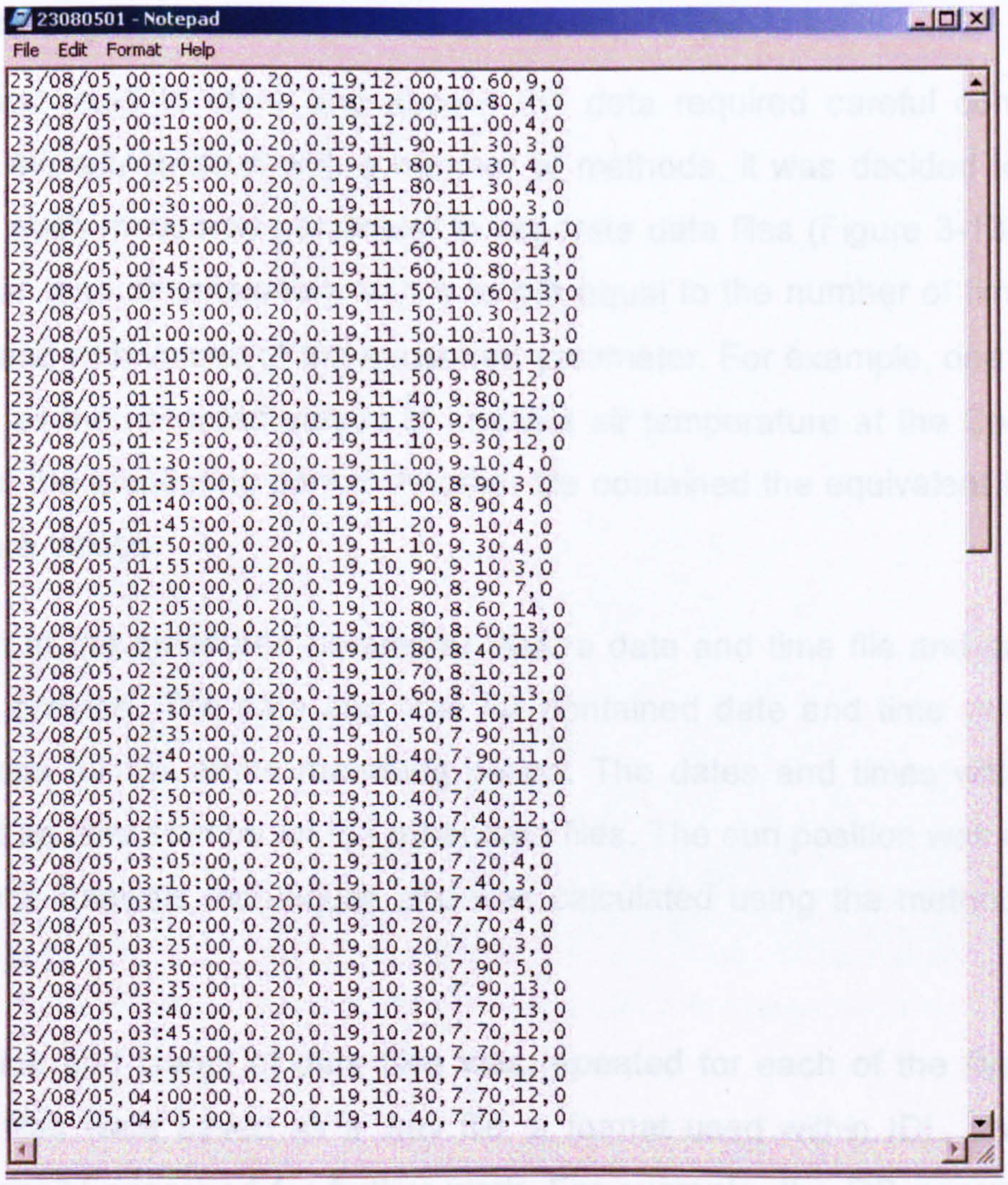


```
23/08/05,00:00:00,0.20,0.19,12.00,10.60,9,0
23/08/05,00:05:00,0.19,0.18,12.00,10.80,4,0
23/08/05,00:10:00,0.20,0.19,12.00,11.00,4,0
23/08/05,00:15:00,0.20,0.19,11.90,11.30,3,0
23/08/05,00:20:00,0.20,0.19,11.80,11.30,4,0
23/08/05,00:25:00,0.20,0.19,11.80,11.30,4,0
23/08/05,00:30:00,0.20,0.19,11.70,11.00,3,0
23/08/05,00:35:00,0.20,0.19,11.70,11.00,11,0
23/08/05,00:40:00,0.20,0.19,11.60,10.80,14,0
23/08/05,00:45:00,0.20,0.19,11.60,10.80,13,0
23/08/05,00:50:00,0.20,0.19,11.50,10.60,13,0
23/08/05,00:55:00,0.20,0.19,11.50,10.30,12,0
23/08/05,01:00:00,0.20,0.19,11.50,10.10,13,0
23/08/05,01:05:00,0.20,0.19,11.50,10.10,12,0
23/08/05,01:10:00,0.20,0.19,11.50,9.80,12,0
23/08/05,01:15:00,0.20,0.19,11.40,9.80,12,0
23/08/05,01:20:00,0.20,0.19,11.30,9.60,12,0
23/08/05,01:25:00,0.20,0.19,11.10,9.30,12,0
23/08/05,01:30:00,0.20,0.19,11.00,9.10,4,0
23/08/05,01:35:00,0.20,0.19,11.00,8.90,3,0
23/08/05,01:40:00,0.20,0.19,11.00,8.90,4,0
23/08/05,01:45:00,0.20,0.19,11.20,9.10,4,0
23/08/05,01:50:00,0.20,0.19,11.10,9.30,4,0
23/08/05,01:55:00,0.20,0.19,10.90,9.10,3,0
23/08/05,02:00:00,0.20,0.19,10.90,8.90,7,0
23/08/05,02:05:00,0.20,0.19,10.80,8.60,14,0
23/08/05,02:10:00,0.20,0.19,10.80,8.60,13,0
23/08/05,02:15:00,0.20,0.19,10.80,8.40,12,0
23/08/05,02:20:00,0.20,0.19,10.70,8.10,12,0
23/08/05,02:25:00,0.20,0.19,10.60,8.10,13,0
23/08/05,02:30:00,0.20,0.19,10.40,8.10,12,0
23/08/05,02:35:00,0.20,0.19,10.50,7.90,11,0
23/08/05,02:40:00,0.20,0.19,10.40,7.90,11,0
23/08/05,02:45:00,0.20,0.19,10.40,7.70,12,0
23/08/05,02:50:00,0.20,0.19,10.40,7.40,12,0
23/08/05,02:55:00,0.20,0.19,10.30,7.40,12,0
23/08/05,03:00:00,0.20,0.19,10.20,7.20,3,0
23/08/05,03:05:00,0.20,0.19,10.10,7.20,4,0
23/08/05,03:10:00,0.20,0.19,10.10,7.40,3,0
23/08/05,03:15:00,0.20,0.19,10.10,7.40,4,0
23/08/05,03:20:00,0.20,0.19,10.20,7.70,4,0
23/08/05,03:25:00,0.20,0.19,10.20,7.90,3,0
23/08/05,03:30:00,0.20,0.19,10.30,7.90,5,0
23/08/05,03:35:00,0.20,0.19,10.30,7.90,13,0
23/08/05,03:40:00,0.20,0.19,10.30,7.70,13,0
23/08/05,03:45:00,0.20,0.19,10.20,7.70,12,0
23/08/05,03:50:00,0.20,0.19,10.10,7.70,12,0
23/08/05,03:55:00,0.20,0.19,10.10,7.70,12,0
23/08/05,04:00:00,0.20,0.19,10.30,7.70,12,0
23/08/05,04:05:00,0.20,0.19,10.40,7.70,12,0
```

Figure 3-12: Sample text file containing radiation and temperature data for one day at Newbiggin Hall. Each row represents a new set of five minute values.

To begin with macros within Excel (Microsoft, 2005) were written to process the raw data, based on the Visual Basic for Applications (VBA) language. The macros placed the raw data for each site and for each month into a spreadsheet. The spreadsheets were used to check the data, produce monthly summary graphs and to provide a method of accessing the data for the performance analysis procedures. An advantage of using Excel was that the programming code could be easily shared as no specialist software was required. However the data processing within Excel was slow and complex and, as the amount of monitored data grew, it was decided to use IDL (RSI, 2005), a sophisticated data analysis software package. IDL, with its ability to manipulate large amounts of data, was more suited to the large data files that were being generated.

3.3.2 Data organisation

The method used to store and access the data required careful consideration. Following experimentation with a number of methods, it was decided to store the data from each measured parameter in separate data files (Figure 3-13). The files were scalar (one dimensional), with a length equal to the number of time intervals recorded and with values of the measured parameter. For example, one of the files contained all the recorded values of ambient air temperature at the Corncroft site throughout the monitoring period. Another file contained the equivalent PV module temperature values.

In addition to the measured parameter files, a date and time file and sun position files were created. The data and time file contained date and time values at five minute steps for the entire recording period. The dates and times within this file were used as time stamps for the other data files. The sun position was used in the performance analysis techniques and was calculated using the methods given in Appendix A.1.

The creation and layout of data files was repeated for each of the five PV sites. The data files were saved as a .sav file, a format used within IDL, and the data could be easily accessed for further work. For example, the DC energy recorded for house 6 at Corncroft for the whole monitoring period was saved as 'PV_Data_Head_Folder/Corncroft/DC_power/06.sav'.

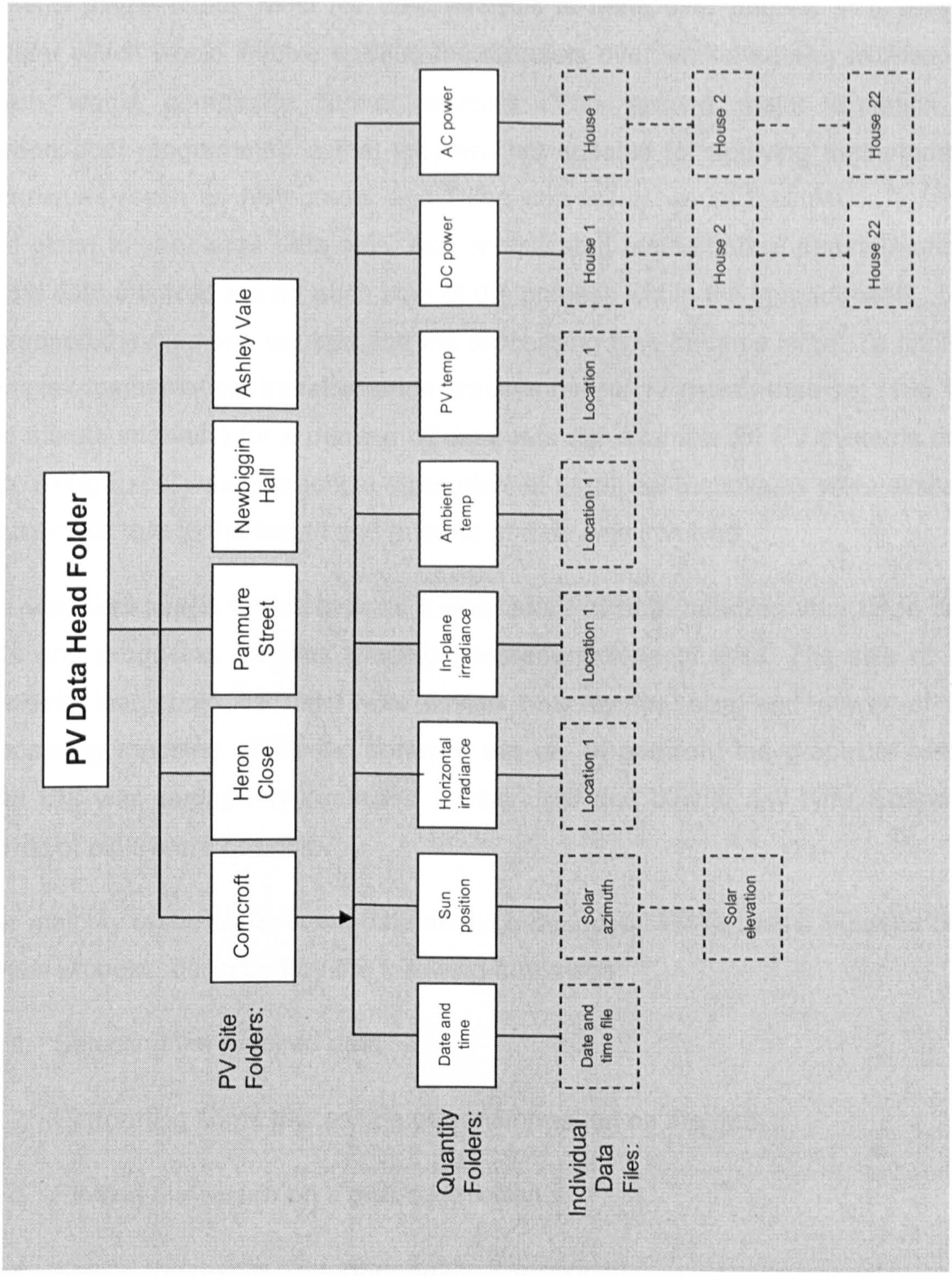

Figure 3-13: Directory layout of measured and calculated parameters for Corncroft

3.3.3 Data analysis procedures

Excel was also used for the initial analysis of the monitored data. However it soon became apparent that the quantity of data was beyond its capability. One immediate limitation was that around 65,000 rows were available in a worksheet and so it was only possible to store about 8 months of five minute interval data within a single sheet. Most PV data analysis is done over periods of a year or greater which would involve splitting the datasets over worksheets or workbooks, which would complicate further analysis. The second major limitation of spreadsheet programmes is that they are not suitable for applying mathematical techniques (such as histograms and fitting curves) or visual techniques (graphs and plots) to very large data sets. Any complicated mathematical transformations of the data involved saving each step of the process within the spreadsheets. This increased the memory required and the processing time became large. To apply a complex mathematical transformation process over a 12 month data set (105,120 five minute intervals) for a number of data sets (for example 30 PV systems on a site) using Excel was impractical. Spreadsheet graphical techniques were similarly problematic due to the length and number of data sets involved.

IDL was well suited to this task as it was adept at both handling very large data sets and producing complex graphical representations of data. The size of the datasets that could be used was limited only by the size and power of the processing machine which the software ran on. In addition, the graphical output from IDL was exclusively controlled by the user and almost any type, shape or format of plots were possible.

The majority of the subsequent data analysis described in this thesis is based on a simple process, described by the following four steps:

1. Selecting the required data
2. Performing some processing or transformation on the data
3. Plotting the results on a graph (optional)
4. Saving the results for further analysis (optional)

A variety of data analysis tasks could be carried out using this process (Table 3-9). The date and time file was used to select certain time periods for analysis if required (for example a particular month or year). Mathematical transformations and other data processing were carried out on the data as required by the aims of the analysis. The results were then output as graphs for visual inspection and inclusion in reports or saved as data files for further analysis.

Table 3-9: Examples of simple IDL data processing routines

	Aim	Data files imported	Data processing	Graphical output	Data file output
Example 1	Plot of AC power for house 2 at Corncroft against date and time for June 2002	Corncroft date and time file Corncroft power 2 AC energy file	Select only data occurring in June 2002	Plot on date and time vs. power axes	-
Example 2	Create annual totals of DC energy generated by each system at Heron Close in 2004	Heron Close date and time file All Heron Close DC power files	Select only data occurring in 2004 Sum the DC values for each house for the annual totals	Plot a bar chart on house number vs. energy axes	Output results to a .sav file for further use
Example 3	Plot of five minute system efficiency for house 5 at Corncroft against in-plane solar irradiance during the first year of operation	Corncroft date and time file Corncroft house 5 in-plane irradiance file Corncroft house 5 AC energy file	Select only data occurring in first year of operation Calculate the system efficiency values from irradiance and AC data	Plot data points on in-plane irradiance (x axis) versus system efficiency (y axis) graph	-

3.4. Summary

One outcome of the DFT programme was the generation of five minute interval monitored performance data from 109 PV systems. The methods of data measurement and collection have been described and the differences in the monitoring systems explained. One consequence of using PCs as data loggers at Corncroft and Newbiggin Hall was slow sampling times of 60 seconds or greater. At the other sites the data was sampled at 10 second intervals or less.

The different forms of the raw data were manipulated so that the data from all the sites was stored in the same format. This prepared the data for analysis using the IDL software. Before analysis of the monitored data could begin, checks were made on the plausibility and quality of the recorded data. These checks are described in the next chapter.

4. Monitored Data: Quantity, Quality and Plausibility

This chapter presents an overview of the amount, the quality and the plausibility of the data recorded using the methods described in Chapter 3. Knowledge of the quality and plausibility is essential in drawing meaningful result and conclusions from the monitored data.

There were problems with the quality of the data recorded. The monitoring systems occasionally failed due to loss of power, failure of the data loggers, a break in the communications network or failure of the sensors. This caused periods of missing data in the datasets. The amount of missing data is quantified and the methodology developed for dealing with any periods of missing data is described. Some monitoring systems used more than one clock to time stamp the data sets. In some cases these clocks were not synchronised and data recorded at slightly different times was given the same date and time stamps. This causes difficulties for further data analysis. At Corncroft the DC power recorded at low irradiance levels was not correct and a step in DC power from zero to a fixed point is noticeable. There was also inherent inaccuracy in the measurements taken due to the accuracy of the sensors and the measurement of sensor output. The extent of the inaccuracy and the effect on further data analysis is considered.

Data plausibility is an investigation of the monitored data to assess whether it is realistic and has expected patterns and trends. The solar radiation and temperature data was compared with measurements from nearby meteorological stations. The PV electrical output was compared with the expected maximum power output of the arrays. The assessment of the plausibility of the data provides confidence in the conclusions drawn from the datasets in Chapters 5 to 8.

4.1. Datasets collected and missing data

4.1.1 Quantity of data collected

The installation of the PV systems and the start of the data monitoring period occurred at different dates for each site (Figure 4-1). Data recorded up to the end of July 2005 was used in the development of the performance analysis techniques in this work. The Corncroft site was monitored for twenty six months and had completed its two year monitoring period. The remaining sites were still being monitored at the end of July 2005. Heron Close had eighteen months of data recorded, Panmure Street had fourteen months, Newbiggin Hall had twelve months and Ashley Vale had eight months.

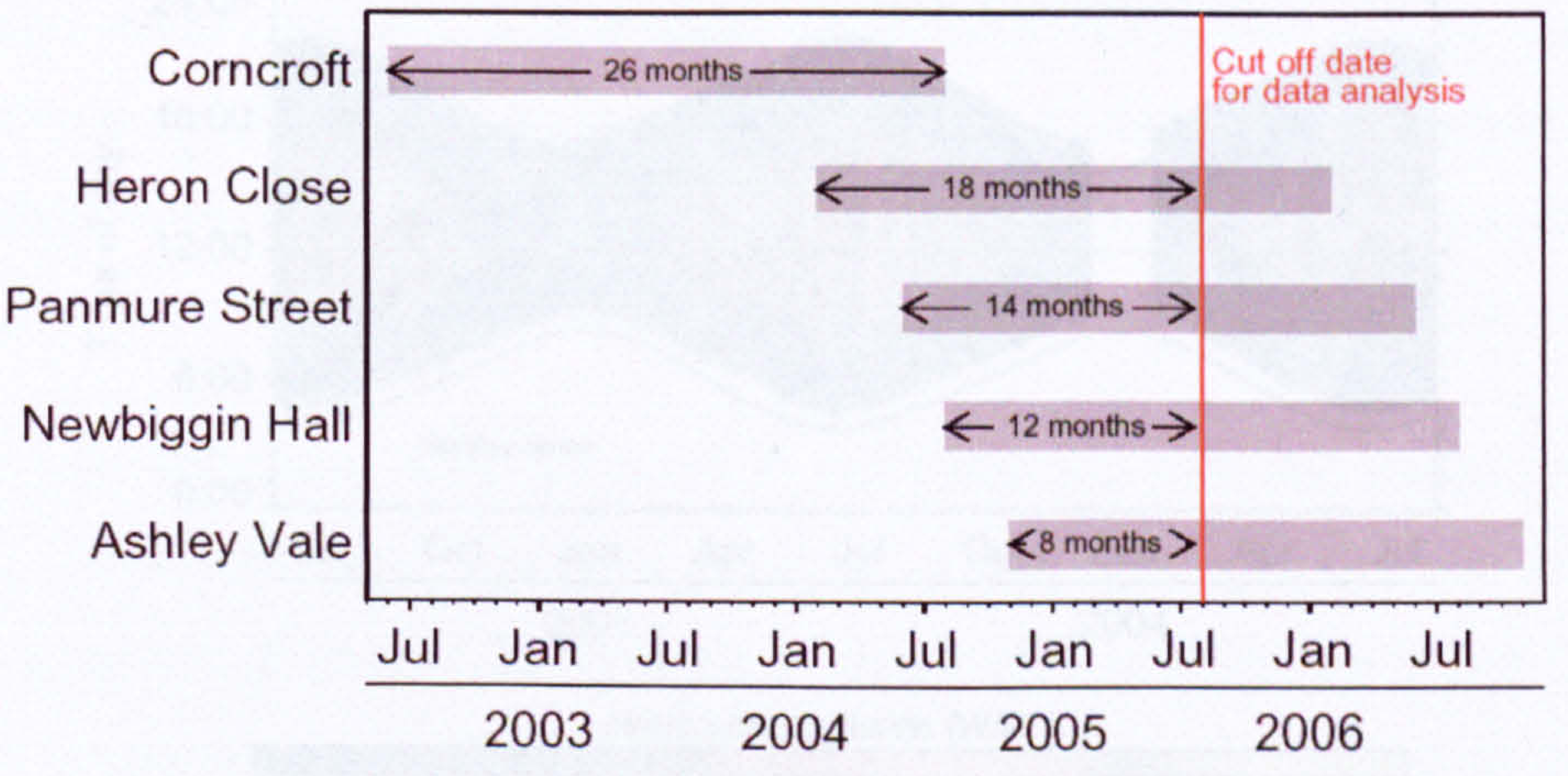

Figure 4-1: Data collection schedule and amount of data available by July 2005

The analysis techniques were designed to investigate the annual performance of the PV systems and to quantify the annual energy losses. A full year of data was required and for this reason the data monitored at Ashley Vale was excluded from any further analysis. Data from the four other sites was considered in data analysis procedures described below and in Chapters 5, 6 and 7.

4.1.2 Date and time stamps

The data from the five sites was recorded either in Greenwich Mean Time (GMT) or, one hour ahead, in British Summer Time (BST). As the sun position routines (Appendix A.1) were based on GMT, and a consistent clock time would allow comparison between sites, all the data is converted to GMT. At some sites it was not possible to directly view the recording clock and determine if BST or GMT was being used, so an alternative method was developed. Taking Corncroft as an example, a plot of the horizontal irradiance measurements against time and date illustrated this method (Figure 4-2). Two lines representing sunrise and sunset times (GMT), and a further line for noon (GMT), are shown. Positive horizontal irradiance values should occur only between the sunrise and sunset times and peak values will generally occur around noon. The horizontal irradiance at Corncroft had these characteristics, but an hour later than expected, indicating that the data was recorded as BST. All the Corncroft data was converted to GMT. At the other sites a mixture of GMT and BST recording was observed and similar date and time stamp checks for the other sites are given in Appendix B.1.

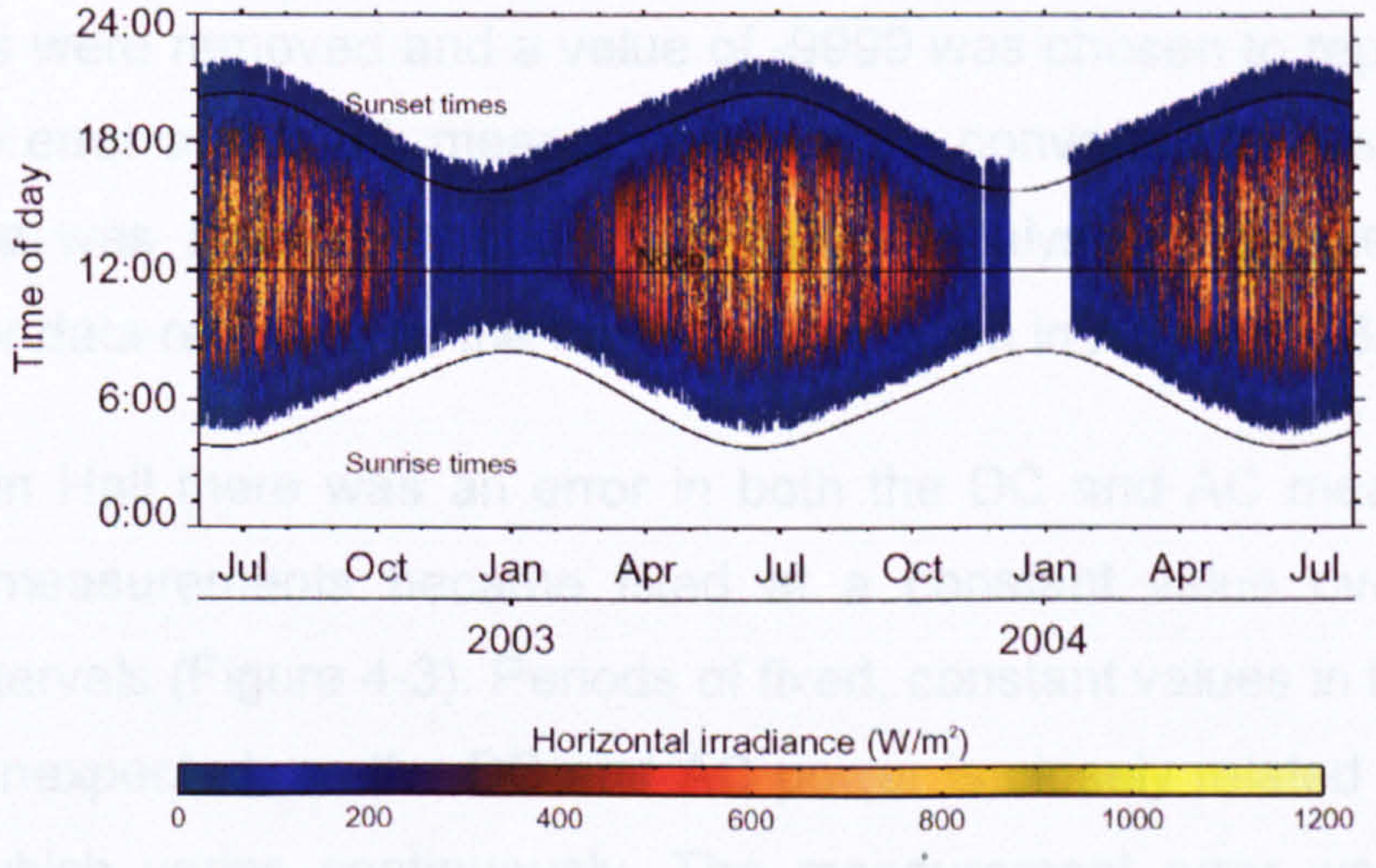

Figure 4-2: Horizontal irradiance at Corncroft plotted on date and time axes. White space represents zero or missing data values.

4.1.3 Correction of night time power output values

The DC and AC power measurements were made whilst the inverter was operating and no measurements were recorded at night time. Throughout all the datasets the night time values of DC and AC power were recorded as missing data. To correct this, any night time readings of missing data in the DC or AC power datasets were converted to a value of zero, as the output from the PV system must be zero at night time. To establish when night time occurred two conditions were used: when the horizontal irradiance measurements were zero and when the elevation of the sun was below the horizon. This ensured that any day time missing data remained identified as such.

4.1.4 Data screening

During the monitoring, errors occurred due to faults in the sensors and the data loggers. Such errors were recorded in the data as large, negative or zero values. During or immediately after maintenance work negative values in the DC and AC power measurements were often observed. Negative values were not possible as the PV arrays cannot draw power and their energy output must always be zero or greater. Occasionally the sensors produced no output signal and this was recorded as zeros. This was misleading as it suggested that the measured parameter was constantly at zero rather than that the sensor was not recording. Other faults in the monitoring caused blank spaces rather than numbers to be recorded.

These errors were removed and a value of -9999 was chosen to represent missing data. All the error and blank measurements were converted to this value and the missing data was ignored in subsequent data analysis. Examples of the data screening for data recorded at the four sites are given in Appendix B.2.

At Newbiggin Hall there was an error in both the DC and AC measurements. At times, the measurements became fixed at a constant value over consecutive recording intervals (Figure 4-3). Periods of fixed, constant values in the DC and AC data were unexpected, as the DC and AC power is closely related to the in-plane irradiance which varies continuously. The measurement error was identified by selecting values which were constant for two or more recording intervals and the errors were converted to missing data.

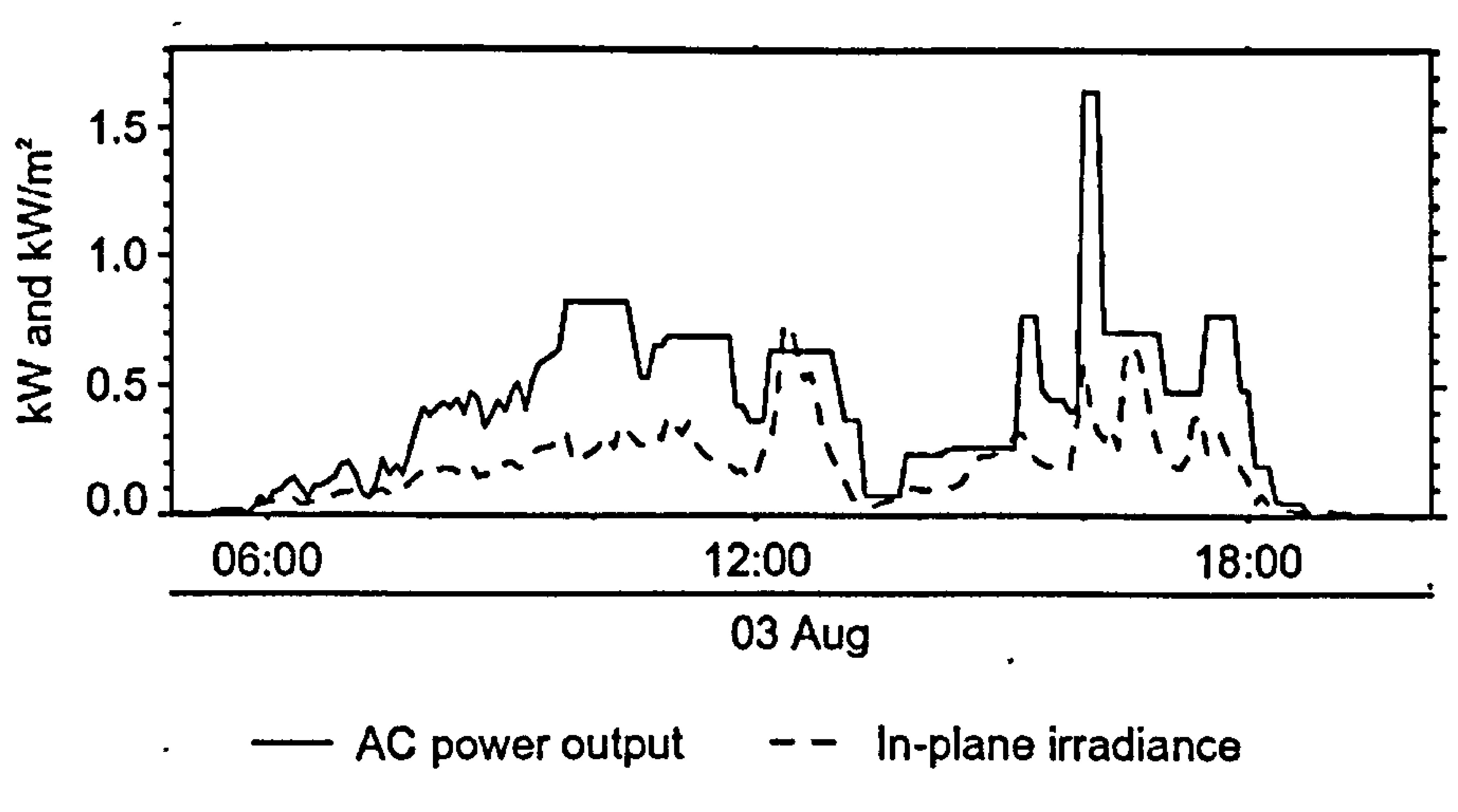

Figure 4-3: In-plane irradiance and AC power on 3rd August 2004 for a Newbiggin Hall PV system. This plot illustrates the constant values in the AC measurements.

4.1.5 Missing data

The data monitoring was a complex process of recording many quantities at high resolution over a long period of time. Inevitably in all the data sets there were periods of missing data. The monitoring systems consisted of many components and these were subject to occasional failures. Loss of mains power, failure of the data loggers, a break in the communications network or sensor failure all contributed to periods when data was not recorded. The data screening process also contributed to the amount of missing data by removing any error values from the datasets.

It is important to assess the amount of missing data present in the datasets because this could influence the results and the conclusions drawn. Taking the Corncroft site as an example, the daily percentages of missing data for all measured parameters for the entire recording period can be shown using a single plot (Figure 4-4). The amount of missing data in each day was calculated as a percentage of the total number of possible values recorded in the day (288 for a five minute recording interval). The percentages are calculated for each measured parameter and each day of the recording period. The percentage values are shown as bars of colour, corresponding to the values given by the legend at the bottom of the figure. As an example, a day with around 10% missing data (28 data values missing out of a possible 288) is shown as a thin blue bar and a day with around 90% missing data is shown as a thin yellow bar. Where missing data occurs over several continuous days this appears as a continuous block of colour.

In the Corncroft datasets there is a period of missing data, in December 2003 and January 2004, where no data was recorded on the site for around 20 days due to a malfunction in the on-site PC. This is shown in the temperature data sets as a 100% daily missing data. For the other parameters this appears as around 35% daily missing data because, after the addition of zero values at night time, only the day time values are recorded as missing. There are occasional other instances of missing data, but these are minor.

The five minute analysis presented in Chapters 6 and 7 utilised the recorded five minute values directly and excluded any occurrences of missing data. However missing data cannot be ignored when calculating the annual totals of the recorded data in Chapter 5. In the case of the Corncroft site, the total missing data was 12.5% for the PV temperature data, 7.1% for the ambient air temperature data and then around 1.9% for all other parameters. The low amount of missing data in the irradiance, DC and AC power measurements was considered suitable for data analysis at the annual and five minute level. The missing data at the end of 2003 may cause some difficulties for monthly or annual totals at that time, but as this occurs when the PV generation is at its minimum, the overall effect on annual totals will be small. The suitability of the data from the other PV sites, where in some cases missing data is much more prevalent, is discussed in Appendix B.3.

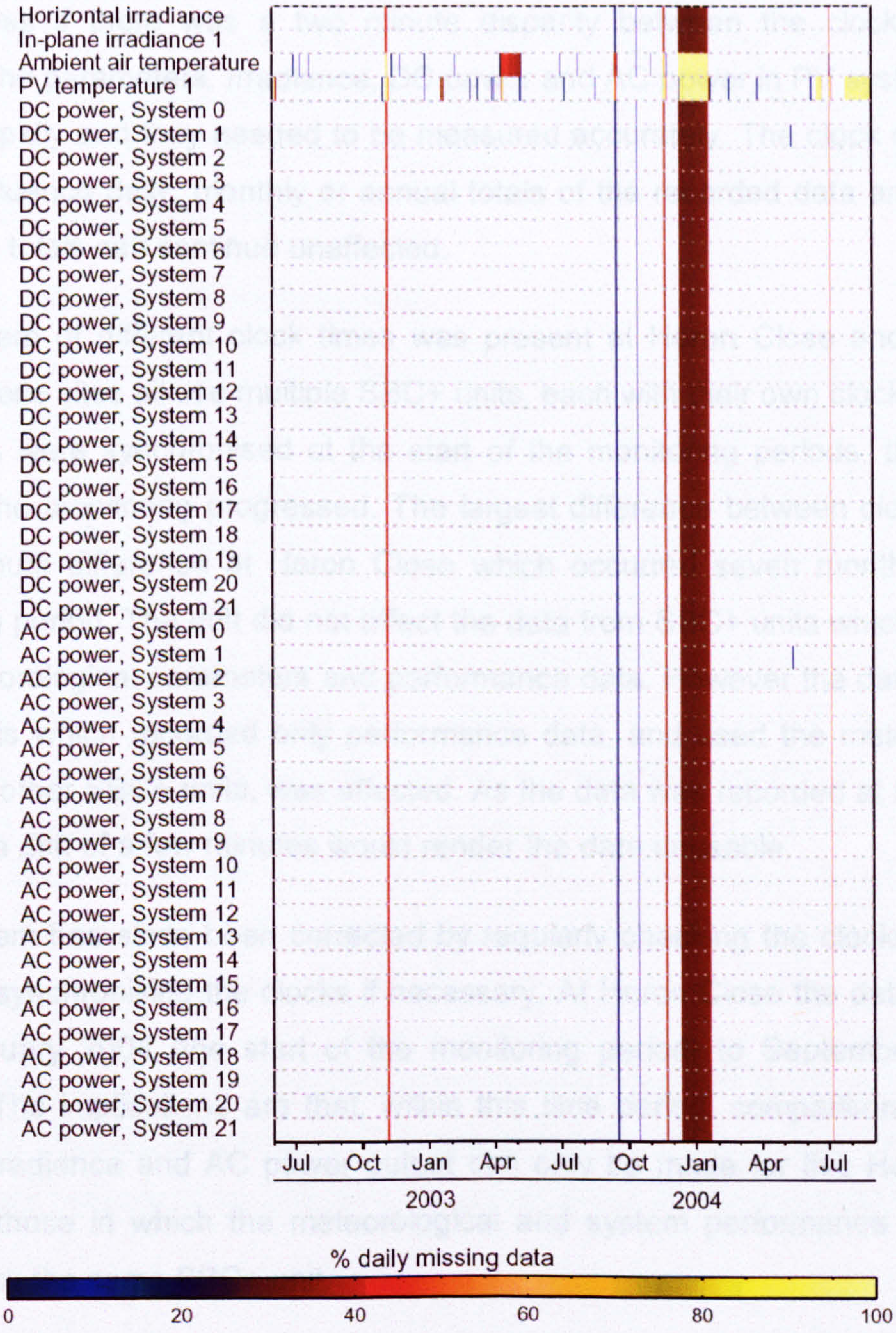

Figure 4-4: Daily percentage of missing data within the Corncroft datasets. The percentage of missing data on each day is indicated by the colour scale in the legend. White space indicates that there was no missing data.

4.2. Data quality

4.2.1 Clock drift

Where several different clocks were used within the same monitoring system there was a possibility that the clocks would not all be synchronised to the same time. This creates problems when comparing measurements recorded using different clocks, especially at the five minutely level. For example, a comparison of five minutely interval values of AC power output to in-plane solar irradiance becomes meaningless if there was a two minute disparity between the clocks used to measure the parameters. Irradiance, DC power and AC power in PV systems could change rapidly and they needed to be measured accurately. The clock differences did not influence daily, monthly or annual totals of the recorded data and analysis with these totals can continue unaffected.

The problem of different clock times was present at Heron Close and Panmure Street. These sites all use multiple SBC+ units, each with their own clock. Although the clocks were synchronised at the start of the monitoring periods, they drifted apart as the monitoring progressed. The largest difference between clocks was a seven minute difference at Heron Close which occurred seven months into the monitoring period. The drift did not affect the data from SBC+ units which recorded both meteorological parameters and performance data. However the data from the SBC+ units which recorded only performance data, and used the meteorological data from other SBC+ units, was affected. As the data was recorded at five minute intervals, a drift of a few minutes would render the data unusable.

The problem has since been corrected by regularly checking the clocks on these sites and synchronising the clocks if necessary. At Heron Close the data recorded from February 2004 (the start of the monitoring period) to September 2004 is affected. The implications are that, within this time period, comparisons between in-plane irradiance and AC power output can only be made for five Heron Close systems, those in which the meteorological and system performance data were recorded by the same SBC+ unit.

4.2.2 Orientation of radiation sensors

A further difficulty in comparing irradiance to power output of the PV systems was the orientation of the in-plane radiation sensors. This issue affected the data monitored at Heron Close because the PV arrays have five different orientations but only two in-plane radiation sensors were used. For example, one radiation sensor was mounted on a block of properties with orientation of 20° and was used to measure the irradiance for the four PV systems on the block. A similar block of properties at orientation of 40° was without a radiation sensor and the irradiance measurements made at 20° were used instead. The difference in orientation had little effect on analysis over large recording intervals (for example hourly or daily). However the effect on five minute analysis was significant and rendered the comparison of irradiance and AC power output impractical. At Newbiggin Hall, the other site with multiple PV array orientations (Table 3-2), an in-plane radiation sensor was used for each orientation.

4.2.3 Low DC power measurement

The DC power measurements at the Corncroft site showed an irregularity at low levels of in-plane irradiance. Whilst the DC power output was zero at zero irradiance, as soon as the irradiance becomes non-zero there was a step change in the measured DC power output (Figure 4-5). There were a number of such steps up to a DC output of 100 W. Below irradiance levels of 50 W/m^2 the DC power converged to one of the discrete values. In contrast the DC power output at Heron Close showed a smooth rise from zero at zero irradiance as expected. Investigation of the low DC power readings at Corncroft revealed that DC power steps were caused by step change of the measured current from the PV arrays. In further analysis of the DC power output at Corncroft, values recorded at low irradiance (less than 100 W/m^2) were excluded to remove the effect of the discrete step changes.

The error at low DC power was not present at Newbiggin Hall which used the same make of PV modules as Corncroft. This suggested that the error was caused either by the power sensors of the inverter or by a fault in the monitoring system.

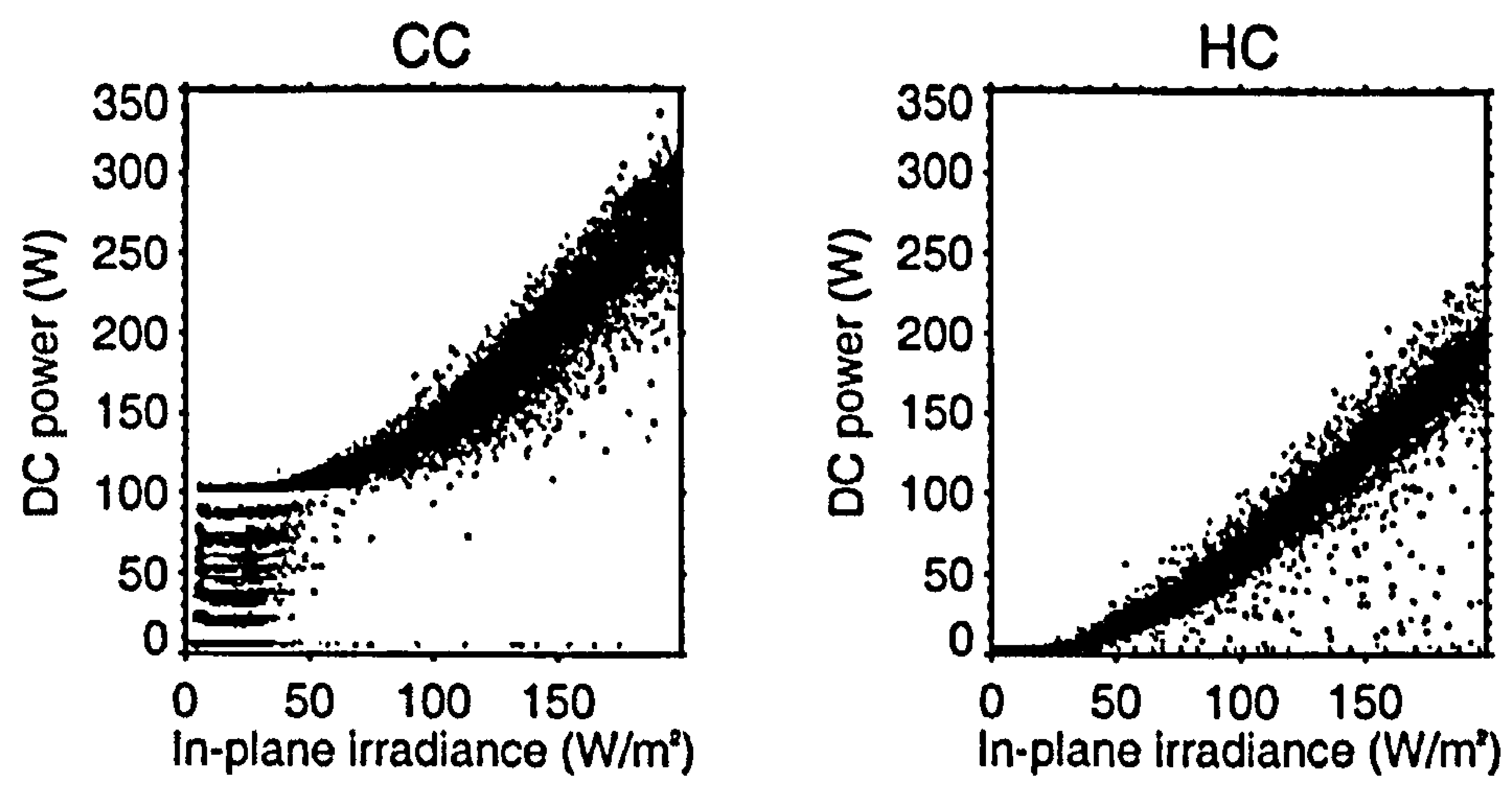

Figure 4-5: DC power measurements at low irradiance levels for a Corncroft and Heron Close PV system.

4.2.4 Measurement inaccuracy

All measurements contain a certain level of inaccuracy. In this study the majority of the inaccuracy within the data was considered to be caused by two reasons. Firstly there was the inaccuracy of the sensors themselves, as discussed in Section 3.2. The second reason was the sampling time used by the monitoring systems. The recorded data was not the instantaneous measurements made by the sensors but five minute averages of sensor readings. As an example, the horizontal solar irradiance was sampled at a sixty second interval at Corncroft and the average of the readings over five minutes was recorded. However if the five readings were made when the irradiance was relatively low and during the intervening time the irradiance was high (this scenario is possible due the variable nature of solar radiation) then the average value recorded would be too low. The same measurement made by the Heron Close monitoring system, with a ten second sampling rate, would record an average irradiance value closer to the true value. Slow sampling rates were present at Corncroft and Newbiggin Hall and may cause a relatively higher level of measurement inaccuracy at these sites. However the effect of the slow sampling at Corncroft and Newbiggin Hall is difficult to quantify.

Measurements taken at a system at Newbiggin Hall on the 1st and 2nd August 2004 provide an example of the possible measurement inaccuracy (Figure 4-6). The system efficiency is not expected to rise above the module rated efficiency, but on 2nd August this happened repeatedly. Closer inspection of the in-plane irradiance and AC power measurements on this day revealed that they did not always appear to rise and fall at the same time as expected since AC power output is approximately proportional to the in-plane irradiance. This resulted in the improbably high system efficiencies (as well as occurrences of low values) and may be an effect of the slow sampling interval at Newbiggin Hall. The effect was not continuous and is not seen in the 1st August measurements. The implications of this measurement error for the analysis of the Newbiggin Hall data are discussed in Section 5.2.2.

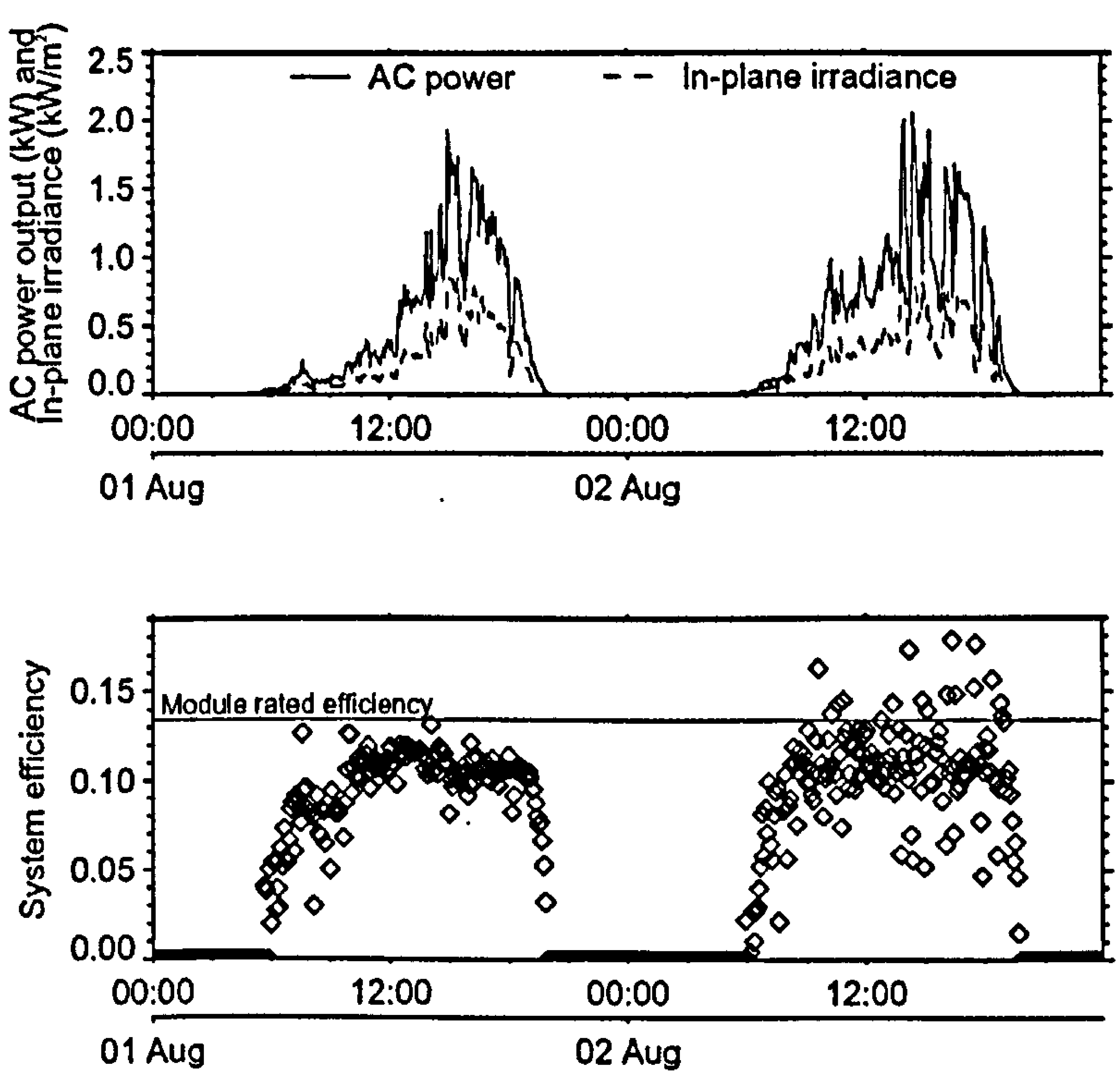

Figure 4-6: Data for a Newbiggin Hall system on 1st and 2nd August 2004. The upper plot shows in-plane irradiance and AC power plotted against time and date. The lower plot shows system efficiency vs. time of day.

4.3. Data plausibility

4.3.1 Definition

In this thesis data plausibility testing means the comparison of the actual monitored data to the expected value. In many situations the monitored data should follow trends or rules according to the type of measurement being recorded. For example, it is expected that solar radiation measurements are generally at a maximum around noon, with greater peaks in summer than in winter and zero at night time. If the recorded data follows the expected trend then it can be considered plausible, or realistic. This is an important part of establishing confidence in the datasets before using them to develop results and conclusions.

The plausibility of a dataset can be assessed in one of three ways: comparison with expected results from references and models; comparison with another dataset recorded on site; and comparison to an external independent source of data. This section investigates the plausibility of the datasets recorded at the five sites and provides examples of potentially unrealistic values. The plausibility of the DC and AC power measurements are not considered in this chapter as these measurements were studied in detail in Chapters 5 and 6. This later analysis highlighted some implausible values within the DC and AC datasets.

4.3.2 Horizontal irradiance

Solar radiation had both seasonal (time of year) and diurnal (time of day) trends but the five minute interval values were highly variable. The best method of checking the plausibility of the irradiance measurements was to make a comparison with an external, independent source of measurements. Such a source was not always available so this method could not be applied in every case. An external source of horizontal irradiation measurements was found for comparison with the Corncroft site data from the Geography Department at Loughborough University (LUMetS, 2005), a distance of about 8 miles from the Corncroft site. The Loughborough University data was recorded at hourly intervals using a pyranometer[15] and the Corncroft data was averaged over hourly intervals to allow comparison between the two datasets.

Daily totals of horizontal irradiation for the Corncroft and Loughborough University sites from June 2002 to April 2003 show similarity throughout the time period (Figure 4-7). Direct comparison of the hourly data showed a strong similarity on clear days but some differences on days with passing cloud (Figure 4-8). Although

[15] A pyranometer is a solar radiation measurement instrument which uses a thermopile to measure the difference in heating of a black surface (which absorbs most of the solar radiation) and a white surface (which reflects most of the solar radiation).

the two locations are only 8 miles apart and the climates are similar, there will be variation in the amount of cloud cover between the two sites and this will cause differences in the measured irradiance values.

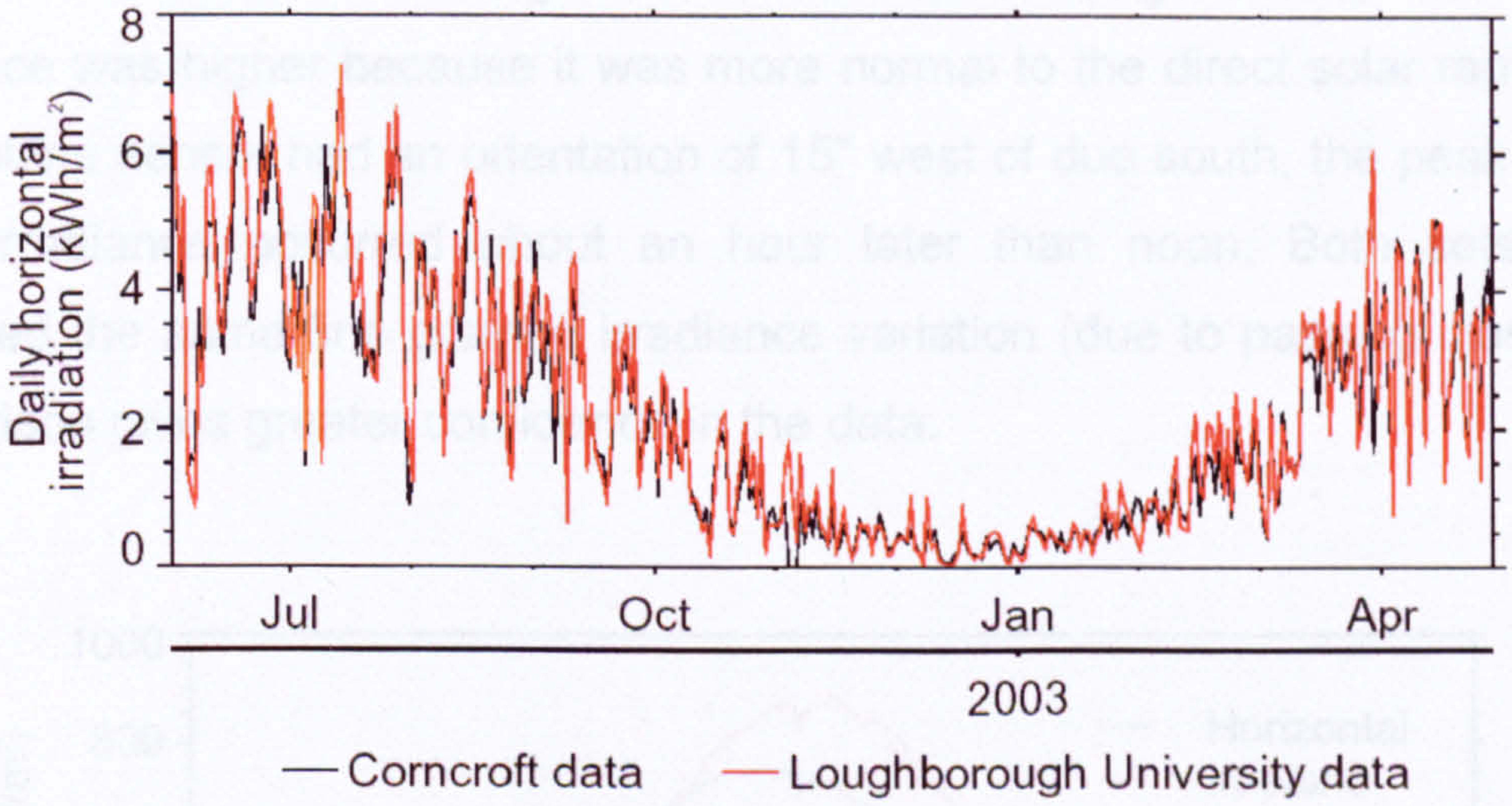

Figure 4-7: Daily totals of horizontal solar irradiation measurements recorded by Corncroft and Loughborough University

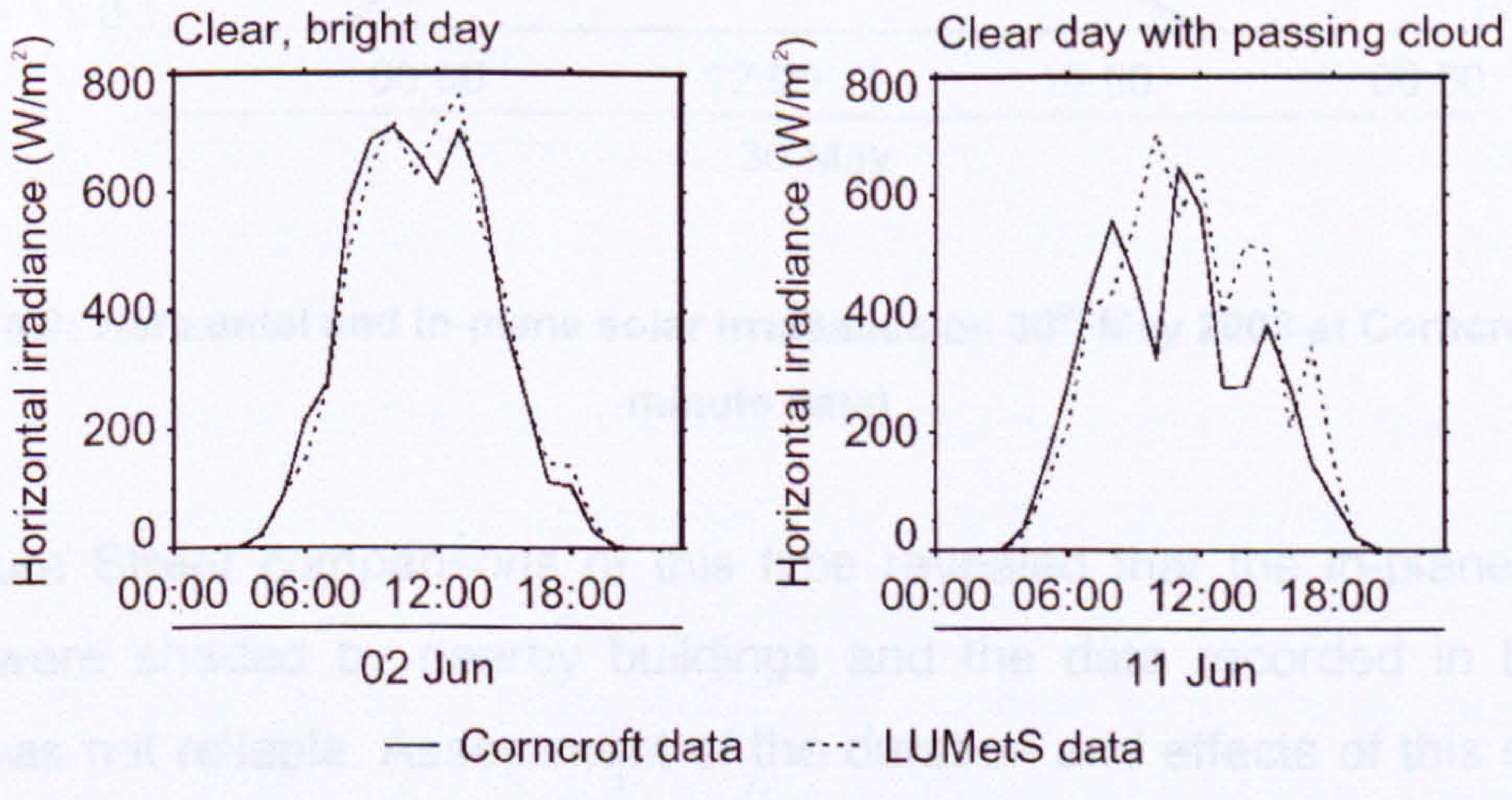

Figure 4-8: Horizontal irradiance measurements recorded by Corncroft and Loughborough University for two days in June 2002 (hourly data)

4.3.3 In-plane irradiance

External independent measurements to compare with the in-plane solar radiation are more difficult to source (external data needs to be measured with the same azimuth and inclination to be useful for comparison and such external measurements are unlikely to be found). A more practical method of assessing the plausibility of the in-plane solar irradiation measurements was to compare them to other data recorded at the site. As a simple example, comparison of the horizontal and in-plane irradiance data on a clear day at Corncroft shows that the in-plane measurements reached a higher maximum value (Figure 4-9). The in-plane irradiance was higher because it was more normal to the direct solar radiation. As the in-plane sensor had an orientation of 15° west of due south, the peak in the in-plane irradiance occurred about an hour later than noon. Both sets of data contained the same fine grained irradiance variation (due to passing clouds). The comparison gives greater confidence in the data.

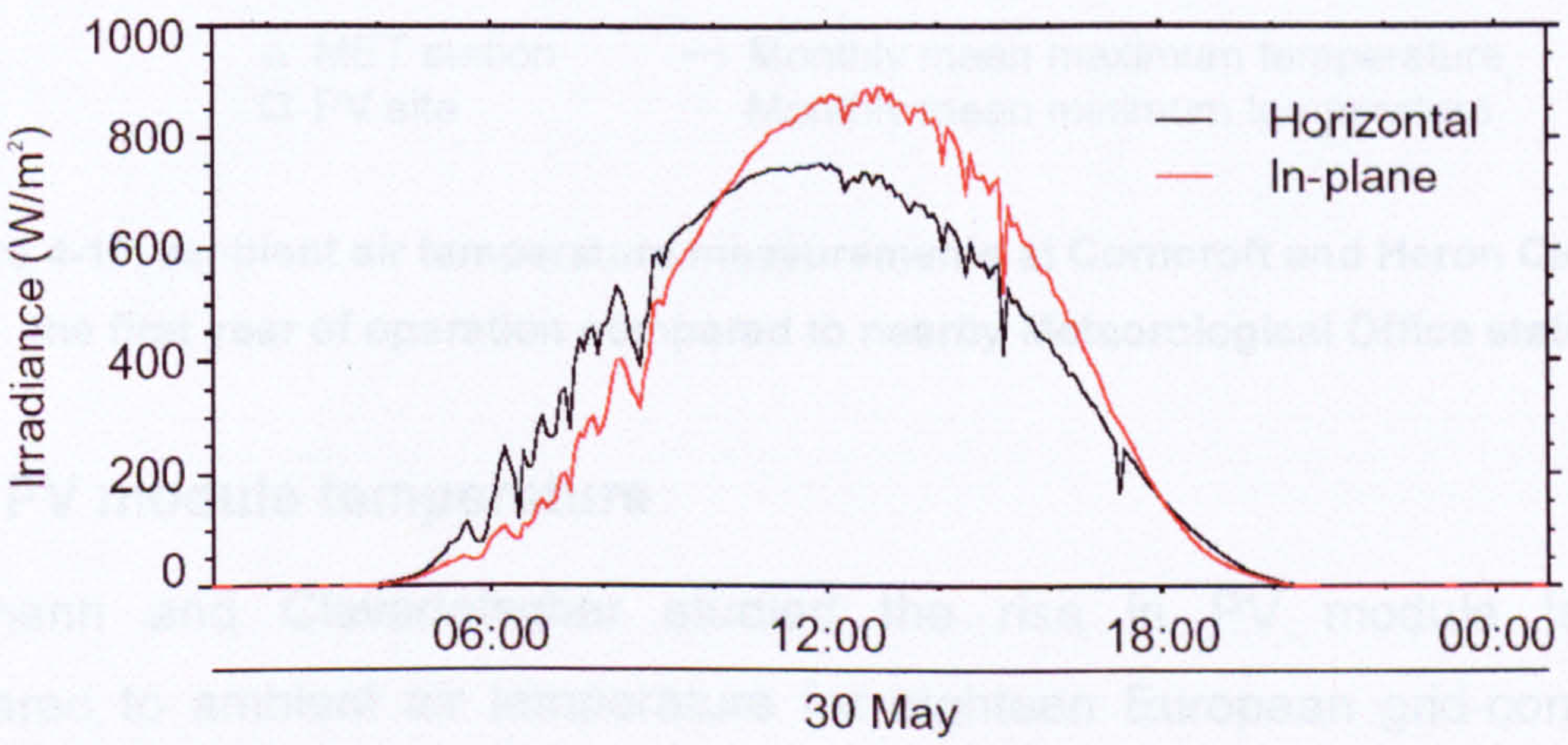

Figure 4-9: Horizontal and in-plane solar irradiance on 30th May 2003 at Corncroft (five minute data)

At Panmure Street comparisons of this type revealed that the in-plane radiation sensors were shaded by nearby buildings and the data recorded in the winter months was not reliable. Assessment of the duration and effects of this shading is given in Appendix B.4.1.

4.3.4 Ambient air temperature

As with solar radiation, ambient air temperature had seasonal and diurnal trends but its exact value was determined by local weather conditions. An external source of measurements was found for Corncroft and Heron Close from meteorological stations (MET stations) run by the Meteorological Office (Met Office, 2005). The MET stations are located throughout the UK and monthly data are available. The monthly mean maximum and minimum temperatures[16] show similarity between the PV site data and the external MET data (Figure 4-10).

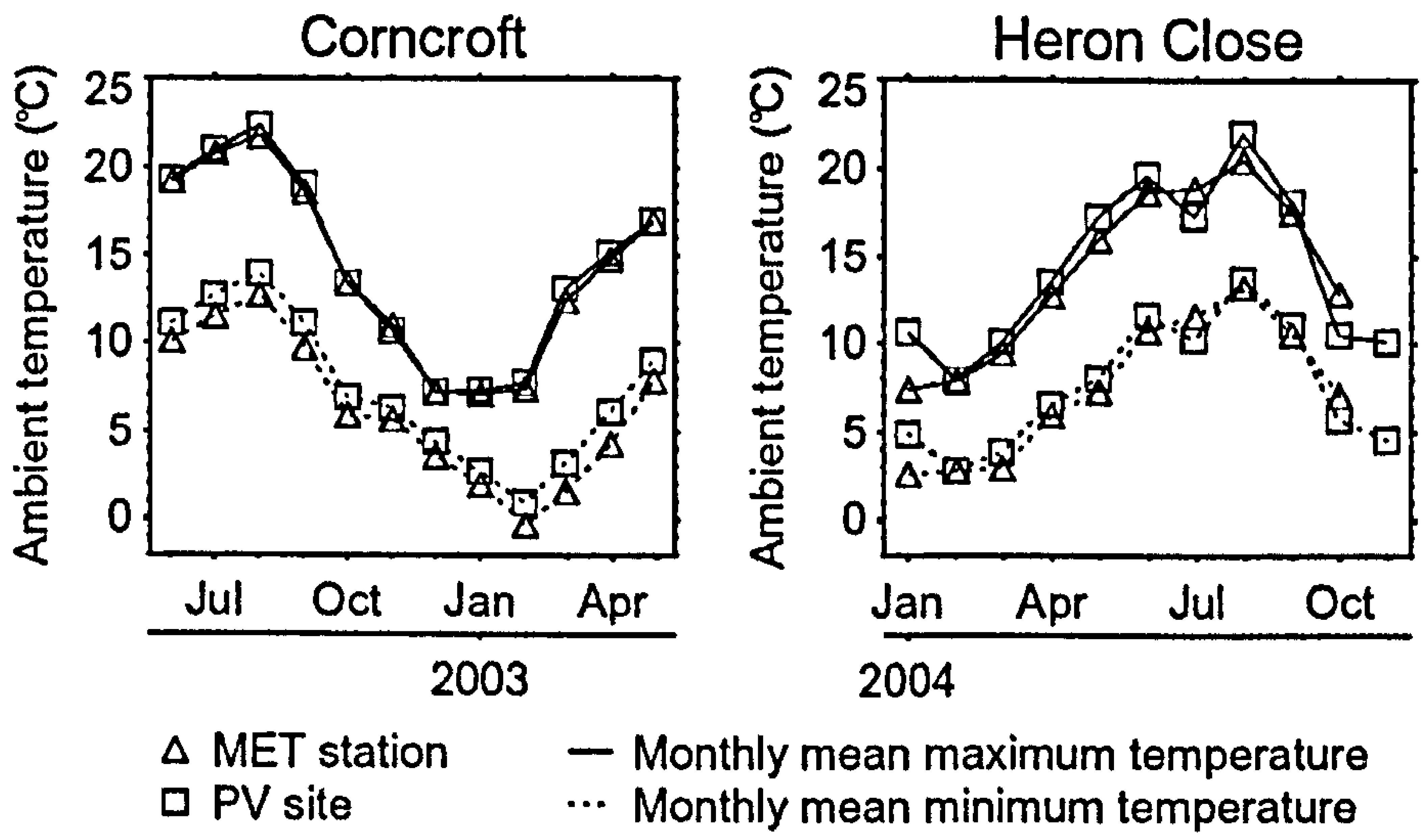

Figure 4-10: Ambient air temperature measurements at Corncroft and Heron Close during the first year of operation compared to nearby Meteorological Office stations

4.3.5 PV module temperature

Nordmann and Clavadetscher studied the rise in PV module temperature compared to ambient air temperature for eighteen European grid-connected PV systems which had a variety of mounting methods (Nordmann and Clavadetscher, 2003). They showed that PV module temperatures can rise from 20 °C to 50 °C above ambient air temperatures at in-plane irradiances of 1000 W/m^2. Plots of the PV module temperature rise above ambient against the in-plane irradiance for Corncroft and Heron Close show how the monitored data compared to Nordmann and Clavadetscher study (Figure 4-11). PV module temperature elevations at Corncroft and for the second set of Heron Close temperature measurements matched the results of the study and were considered realistic. However for the first set of Heron Close measurements, the rise above ambient temperature at 1000 W/m^2 was low. It was felt that the data could not be used with confidence,

[16] The monthly mean maximum temperature is the average of the maximum temperature recorded on each day in the month. A similar calculation using the minimum daily temperature provides the monthly mean minimum temperature.

perhaps because the sensor had become detached from the back of the PV module and was measuring the air temperature in the gap between the PV modules and the roof rather than the module temperature itself. This set of temperature measurements was not used in further analysis in this work and the second set of Heron Close PV module temperatures were substituted in their place[17]. Similar examples for the Panmure Street and Newbiggin Hall PV module temperature data is given in Appendix B.4.2.

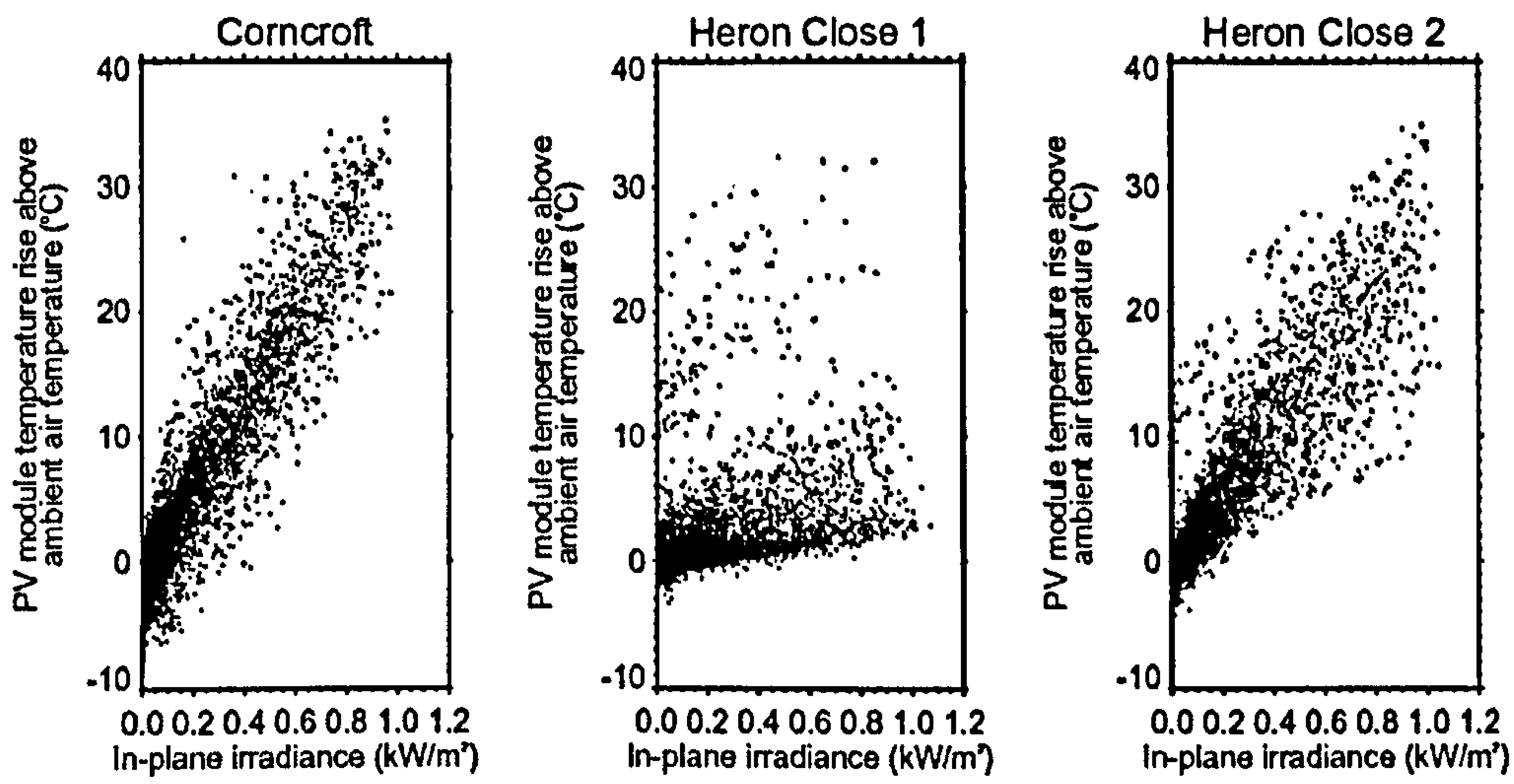

Figure 4-11: PV module temperature rise above ambient vs. in-plane irradiance for first year of operation at Corncroft and Heron Close (hourly data)

4.4. Summary

This chapter reviewed the quantity, quality and plausibility of the monitored data. The data from each site was assessed for its suitability in further data analysis (Table 4-1). The main issues with the monitored data were:

- The Ashley Vale site was not used in the performance analysis as less than a year of monitored data had been collected at the time of writing this thesis (Section 4.1.1)

- Many of the Heron Close PV systems had to be excluded from the analysis due

[17] This substitution was considered acceptable because the PV module temperature has a significantly lower impact than irradiance on PV system performance. Throughout this work a single PV module temperature reading was taken to represent the temperature of all PV arrays of similar orientation throughout each site.

to clock differences (Section 4.2.1), orientations which differed from that of the radiation sensors (Section 4.2.2) and missing data (Appendix B.3.)

- The DC and AC measurement error at Newbiggin Hall may result in unreliable results from the data (Section 4.1.4).

- The slow sampling rate (60 seconds or greater) at Corncroft and Newbiggin Hall may cause difficulties in analysing the data at the five minute level (Section 4.2.4)

- Shading of the radiation sensors in winter at Panmure Street meant the affected data was excluded from the five minute data analysis (Appendix B.4.1)

- The first set of PV module temperature data at Heron Close was not recorded correctly and was not used in later analysis (Section 4.3.5)

The analysis of the quality and plausibility of the data highlights the importance of monitoring system design on the recorded data. In addition to the measurement inaccuracies of the sensors, the quality of the data is influenced by missing data, clock drift, measurement error and slow sampling intervals. In particular the sampling interval has a strong impact in PV monitoring, due to the highly variable nature of the solar irradiance.

This chapter demonstrated the importance of undertaking quality and plausibility tests before using the data in analysis. The next chapter discusses the annual performance of the PV systems and the initial steps of the analysis of the five minutely performance data.

Table 4-1: Quality assessment of data sets

	Missing data	Data accuracy	Data plausibility	Consequences for further data analysis
Corncroft	No data recorded Dec 2003 to Jan 2004 Minimal missing data elsewhere	Sampling rate of 60 seconds	-	Five minute analysis may be affected by the measurement inaccuracy
Heron Close	Substantial missing data. Houses 20, 21, 22, 23, 27, 28 and 29 excluded from further analysis.	Different clock times from Feb to Sept 2004. Only houses 4, 5, 6, 7 and 12 were not affected. Different orientations from the radiation sensors. Houses 0 to 7, 11 and 12 not affected	PV temperature 1 measurements appear low.	Houses 0, 1, 3, 4, 5, 6, 7, 8, 9, 10, 12, 13, 14, 15, 16, 17, 19, 24, 25 and 26 considered in annual analysis Houses 4, 5, 6, 7 and 12 considered in five minute analysis PV temperature 1 data not used
Panmure Street	Minimal	-	Shading of radiation sensors from Sept 2004 to mid April 2005	Shaded irradiance data excluded in the five minute analysis
Newbiggin Hall	Low levels of missing data (2 to 4%) in the DC and AC data due to measurement errors	Measurement inaccuracy in the DC and AC measurements Sampling rate greater than 60 seconds	PV temperature 3 data was unreliable	Five minute analysis may not be possible due to measurement inaccuracy Annual and five minute analysis results may be unreliable due to the DC and AC measurement error
Ashley Vale	Excluded due to not having a complete year of monitored data			

5. PV System Operation: Annual and Five Minutely Analysis

This chapter introduces annual and five minutely analysis of the monitored PV system performance data described in Chapters 3 and 4. This initial analysis provides the foundation for developing the new PV system monitoring techniques, the main aim of this study. For the four PV sites, annual results are investigated by considering the first twelve months of operation at three sites and the first twenty four months of operation at one site. These annual results are compared to reported values in previous studies and are used to determine which PV systems are performing poorly.

The five minutely recorded data provides a more detailed, near real time picture of the performance of the monitored PV systems. The basic analysis technique is to compare the five minutely values of in-plane solar irradiance to the five minutely values of system efficiency. This shows, for each five minute period of operation, how well the PV system converts the sunlight it receives into useful electrical energy. The analysis demonstrates the additional detail provided by five minutely recorded data in comparison with analysis based on half hourly or hourly data. It also illustrates how such a high level of detail could be exploited to yield an improved understanding of PV system performance.

In Chapter 2 PV system operation was separated into two states: normal operation and faults. Normal operation represents times when the PV system is working well with high efficiencies within an expected range. Faults are times of unexpected low efficiencies. A technique to identify the normal operation and faults of PV systems using five minutely recorded data is developed. New PV system monitoring techniques are developed for the two states of PV system operation separately in Chapters 6 and 7.

5.1. Analysis of annual results

5.1.1 Site results

Annual results were calculated for the four PV sites: Corncroft, Heron Close, Panmure Street and Newbiggin Hall (Table 5-1). The results from the first year of operation at each site are given and also the second year at Corncroft (as the site was monitored for more than two years). The dates of the monitoring period, the number of the system monitored and the annual totals of horizontal and in-plane irradiation are shown. The PV system performance is described using annual totals of DC and AC energy yield and four calculated annual performance indicators: final yield[18]; performance ratio; system efficiency; and inverter efficiency[19]. Performance ratio and system efficiency were defined in Section 2.1.1. For each site, the mean, standard deviation and range (from minimum to maximum) values are given for the six annual energy yields and performance indicators. Individual system results are shown in Appendix C.1.

A rough benchmark for annual performance ratios of recently installed PV systems was developed in Section 2.1.2. This stated that for a group of PV systems, installed in the late 1990s, an average annual performance ratio of around 70% was expected (for well operating systems), with the highest values of individual annual performance ratio around 85%. The average annual performance ratio values for Corncroft (76% and 73%) and Newbiggin Hall (77%) compared well to this benchmark and the systems may be said to be performing well. The average annual performance ratios at Heron Close (60%) and Panmure Street (67%) were lower than the benchmark value which suggests the systems were not operating as well as expected.

[18] Final yield is defined as the AC energy output from the inverter normalised by the system rating (in kWh/kWp). Final yield is useful for comparing the AC energy output from systems of different ratings.

[19] Inverter efficiency is the ratio of AC energy output from the inverter to DC energy input to the inverter

Table 5-1: Results of annual monitoring

Site (Monitoring dates)	Number of systems	Solar irradiation (kWh/m²) Horizontal / In-plane	DC energy output from array (kWh)	AC energy output from inverter (kWh)	Final yield (kWh/kWp)	Performance ratio (%)	System efficiency	Inverter efficiency (%)
			Average of annual values; *(standard deviation)*; range - minimum to maximum					
Corncroft Year 1 (Jun 2002 to May 2003)	22	858 1024 [1]	1440 *(131)* 965 to 1605	1198 *(118)* 766 to 1356	775 *(72)* 501 to 836	76 *(7.0)* 49 to 82	0.101 *(0.009)* 0.066 to 0.109	83 *(1.1)* 79 to 85
Corncroft Year 2 (Jun 2003 to May 2004)	22	854 1027 [1]	1367 *(204)* 597 to 1571	1152 *(179)* 482 to 1343	745 *(111)* 315 to 834	73 *(10.8)* 31 to 81	0.097 *(0.015)* 0.041 to 0.109	84 *(1.0)* 81 to 86
Heron Close (Feb 2004 to Jan 2005)	20 *(10 systems excluded)*	858 895 [2] and 940 [3]	846 *(216)* 417 to 1196	763 *(197)* 268 to 1071	544 *(90)* 256 to 672	60 *(9.9)* 29 to 75	0.073 *(0.012)* 0.035 to 0.093	90 *(0.9)* 88 to 92
Panmure Street (Jun 2004 to May 2005)	12	790 919 [4]	637 *(107)* 343 to 718	571 *(97)* 304 to 645	528 *(90)* 281 to 597	67 *(11.4)* 36 to 76	0.082 *(0.014)* 0.044 to 0.093	90 *(0.4)* 89 to 90
Newbiggin Hall (Aug 2004 to July 2005)	25	720 683 [5], 714 [6] and 904 [7]	1108 *(283)* 453 to 1769	982 *(258)* 392 to 1591	648 *(53)* 512 to 722	77 *(7.0)* 63 to 88	0.103 *(0.009)* 0.084 to 0.118	89 *(0.7)* 86 to 90

Orientation angle of in-plane irradiance sensors: [1] -22°; [2] -50°; [3] 20°; [4] 10°; [5] 85° ; [6] -95°; [7] -5° (defined in Table 3-2)

Tilt angle of in-plane irradiance sensors: [1,4] 30°; [2,3] 37.5°; [5,6,7] 40°

The inverter efficiency values at Corncroft (83% and 84%) are lower than for the other sites (from 89% to 90%). The inverters were oversized at Corncroft and the low annual inverter efficiencies may be caused by the inverter operating in the lower part of its efficiency curve for prolonged periods. The other sites had slightly undersized inverters which would therefore tend to operate at greater efficiencies throughout the year. Inverter efficiency curves are discussed further in Section 6.2.3.

5.1.2 Performance ratio distributions

The variation of performance ratios at each site was investigated by considering the frequency distributions obtained by placing the performance ratio values into bins of 2.5% (Figure 5-1). This clearly highlighted the differences in performance between the sites. At Corncroft the majority of systems had annual performance ratios from 67.5% to 82.5%. One system was below this range in the first year of monitoring and three systems in the second year.

At Newbiggin Hall most of systems had similar performance to those at Corncroft with annual performance ratios from 62.5% to 80%. There were six systems with very high performance ratios at Newbiggin Hall (85% to 90%) which exceed the maximum benchmark value of 85%. These systems faced west whilst the other Newbiggin Hall systems all faced east or south. The efficiency of the west facing systems was higher at low irradiance than the other systems and a possible explanation for the high performance ratios is that the inverters were recording the power measurements above their true value. The west facing systems had inverters with high ratings (1700 W and 2500 W) compared to the inverters of the other systems (850 W and 1100 W).

Panmure Street had most of its annual performance ratios from 62.5% to 77.5%, a similar range to Newbiggin Hall, and two systems with low performance ratios. Heron Close had generally poorer performance than the other sites, with the majority of systems within a large range of annual performance ratios from 50% to 77.5%. There was one system at Heron Close with a low annual performance ratio of 29%.

The annual results show which systems and which sites perform better than others. Many of the systems had low performance ratios lower than 60% and the reasons for this cannot be determined by annual analysis. In order to improve the performance of the systems, and the design of future PV installations, it is essential to understand why these differences in performance occur. The annual analysis does not provide sufficient information on which to make recommendations for future system designs. Analysis of monitored data at a higher resolution (such as five minutely, half hourly or hourly) can provide this level of understanding and an initial study of the five minutely data from the monitored PV systems is described in the next section.

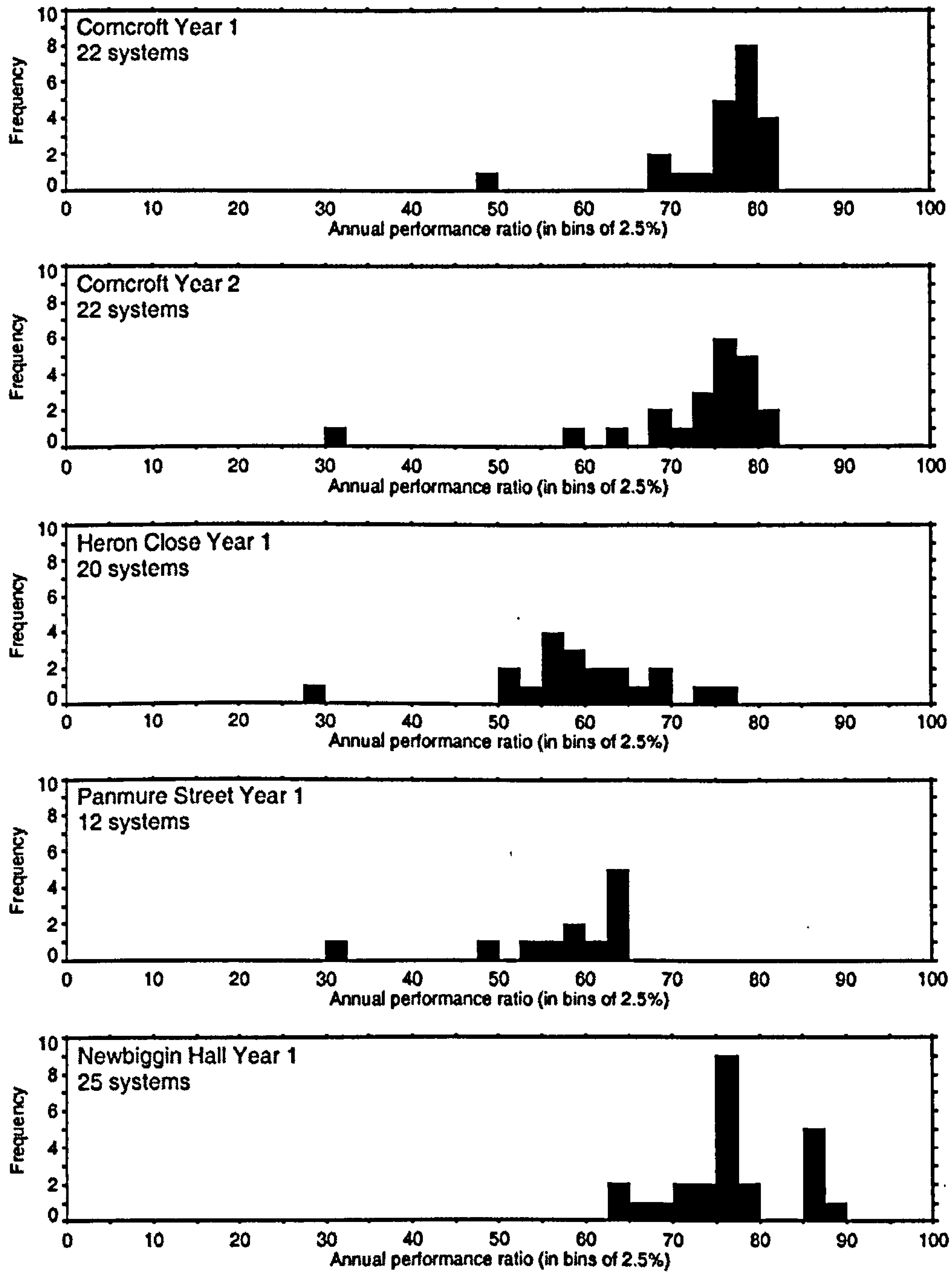

Figure 5-1: Distribution of annual performance ratios at each site. The system annual performance ratios are placed into bins of 2.5%.

5.2. Performance at the five minutely level

5.2.1 PV module efficiency curves

The initial analysis of the monitored data at the five minutely level is based on the relationship of in-plane irradiance to system efficiency. System efficiency is primarily influenced by the PV module efficiency, defined as the ratio of the DC energy output from the PV array to the solar irradiation received by the array. Four studies which describe PV module efficiency for a range of PV modules are reported by Gxasheka et al. (Gxasheka, 2005), Stamenic et al. (Stamenic et al., 2004), Eikelboom and Jansen (Eikelboom and Jansen, 2000) and Bucher and Kunzelmann (Bucher and Kunzelmann, 1998). For crystalline silicon PV modules, the PV module efficiency rises from zero at zero irradiance to a near constant value at irradiances above around 500 W/m^2. The curve described by the relationship of PV module efficiency to in-plane solar irradiance is known as the *PV module efficiency curve*. At STC[20], typical rated PV module efficiencies range from 12% to 15% for monocrystalline PV modules (IEA, 2005c).

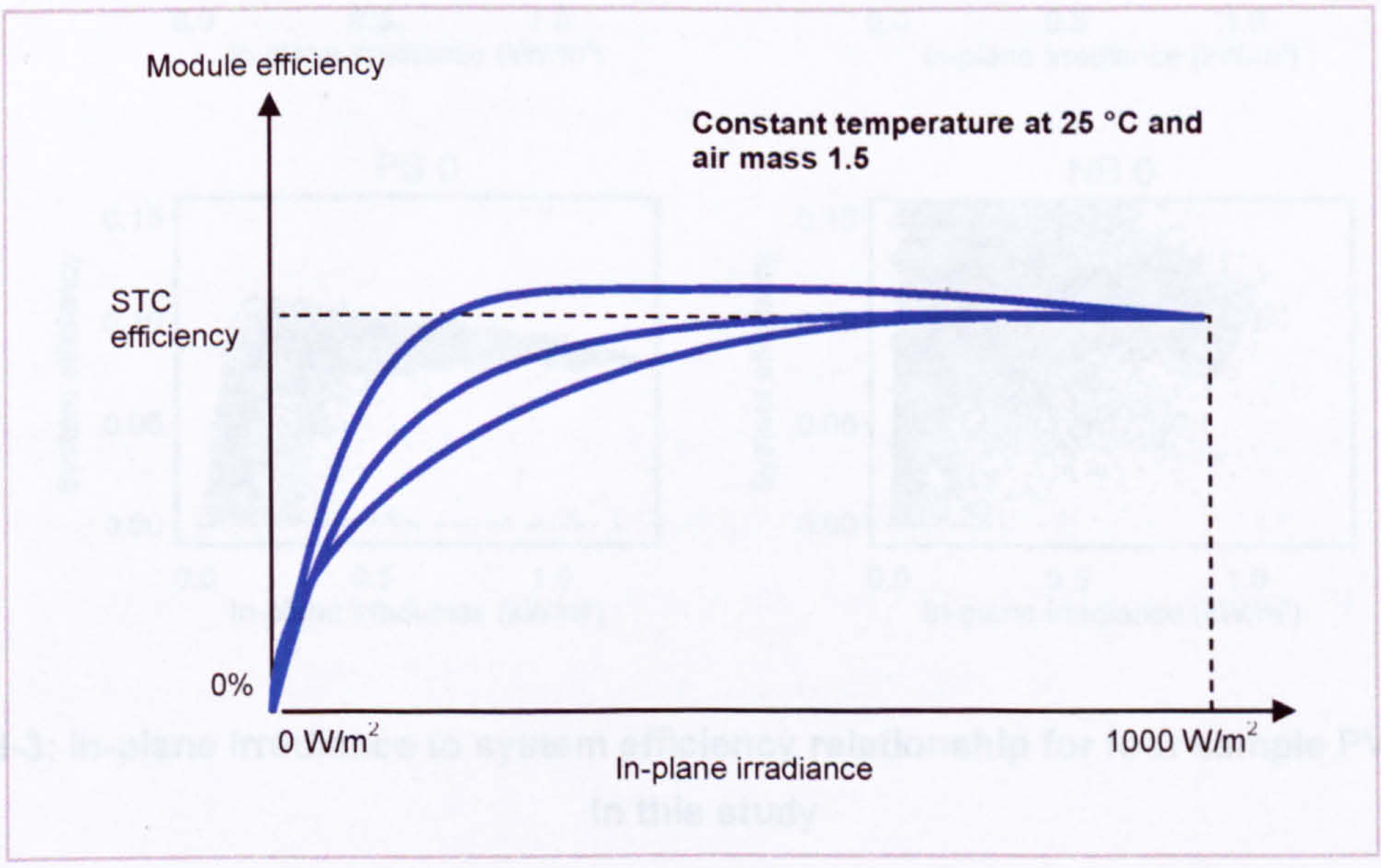

Figure 5-2: Examples of crystalline silicon PV module efficiency curves for three PV modules (reproduced from Bucher and Kunzelmann, 1998).

---

[20] STC is defined in Section 2.1.1

5.2.2 Efficiency to irradiance relationship at the five minute level

Plots of the measured five minutely in-plane solar irradiance against the system efficiency values produced a boomerang-shaped cloud of points (Figure 5-3). One system from each site is shown and the titles of the plots are the two letter acronym of the site (CC for Corncroft; HC for Heron Close; PS for Panmure Street and NB for Newbiggin Hall) and the system number (which starts at zero). For Corncroft, which recorded over two years data, the suffix 'Y1' denotes that the data is from the first year of operation. The PV systems chosen are well operating systems with a high annual performance ratio. Plots for all the monitored PV systems at each site are given in Appendix C.2.

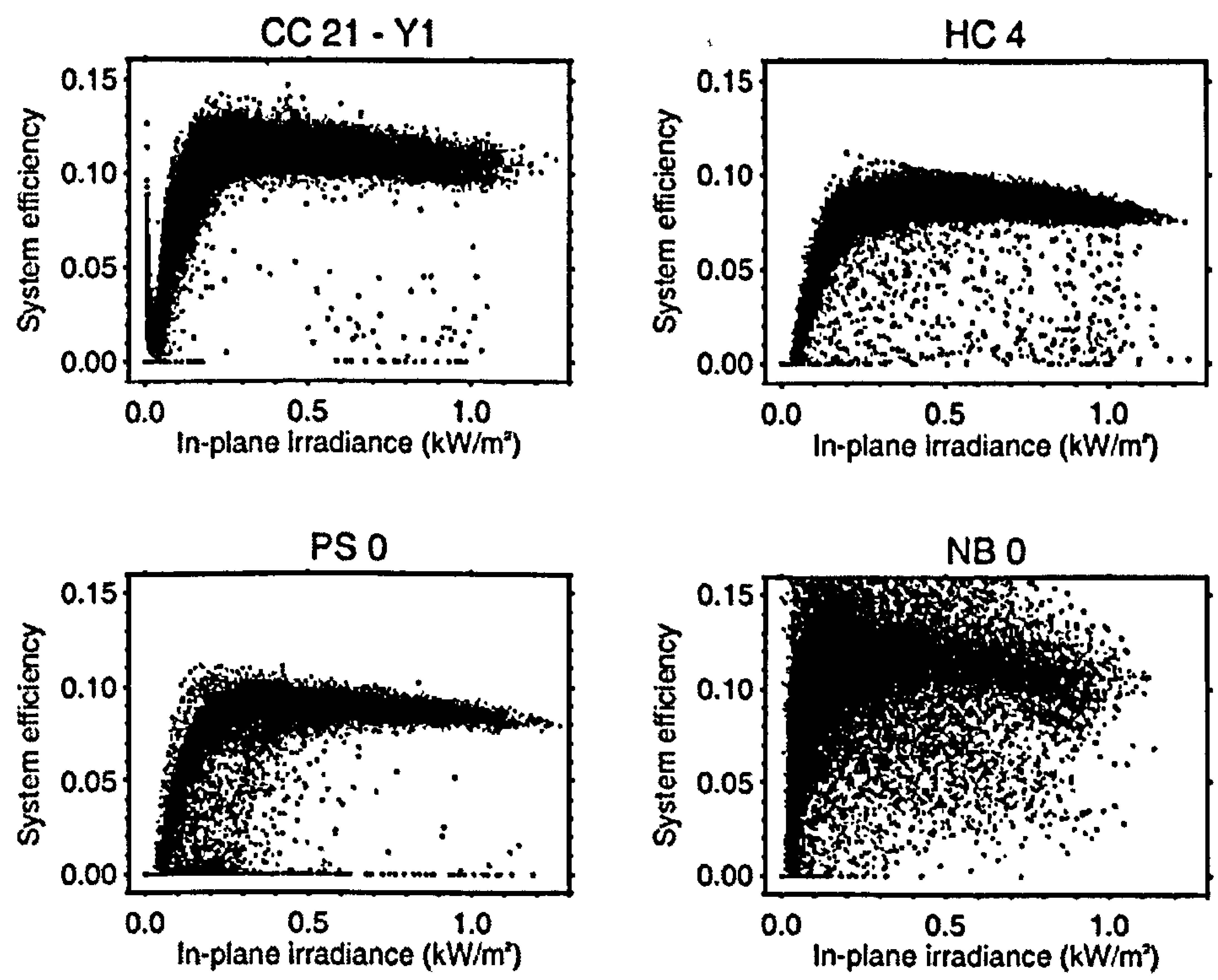

Figure 5-3: In-plane irradiance to system efficiency relationship for four sample PV systems in this study

The irradiance to efficiency relationship at the Corncroft, Heron Close and Panmure Street produces a boomerang-shaped cloud of points. The shape of this cloud was similar to the general shape of the PV module efficiency curves in Figure 5-2. The efficiency was zero at zero irradiance and rose steeply to a relatively constant value at irradiance above 300 to 500 W/m^2. At Corncroft there was an unexpected rise in efficiency at irradiance close to zero, assumed to be caused by measurement error at the low irradiance and power levels (Section 4.2.3). The system efficiency values formed a cloud of points due to the losses that occur in normal operation: the operational losses described in Section 2.2.1. At a particular level of irradiance, the system efficiency may be high or low depending on the operation losses. For example, high temperatures or high MPP tracking loss will reduce the system efficiency to the lower boundary of the cloud of points (the effect of the operational losses are discussed in detail in Chapter 6). A similar plot can be seen for a single PV system in the study by Kiefer et al. (Kiefer et al., 1995) which is based on one minute data. Oozeki et al. (Oozeki et al., 2003) also show this effect but instead use hourly data and AC power output rather than system efficiency.

At Newbiggin Hall the system irradiance to efficiency relationship was less clearly defined and the cloud of points much more dispersed. Due to intrinsic losses during operation, the monitored system efficiency values should be lower than the rated PV module efficiency (13.4% at Newbiggin Hall) but there were many efficiency values above this figure. This suggests the data at Newbiggin Hall was unreliable, possibly caused by the slow sampling time (discussed in Section 3.2.5). The removal of values suffering from the DC and AC measurement error (Section 4.1.4) may have been incomplete and also contribute the errors in the data. One method of using the Newbiggin Hall data is to analyse half hourly averaged values rather then five minute values (Figure 5-4). Whilst error values still remained in the half hourly data, a cloud of points similar to that seen at the other sites was more clearly visible. There are however still many points above the maximum feasible efficiency of 13.4%. The analysis in this work only considers five minute data and so, from hereon, the Newbiggin Hall data has been ignored.

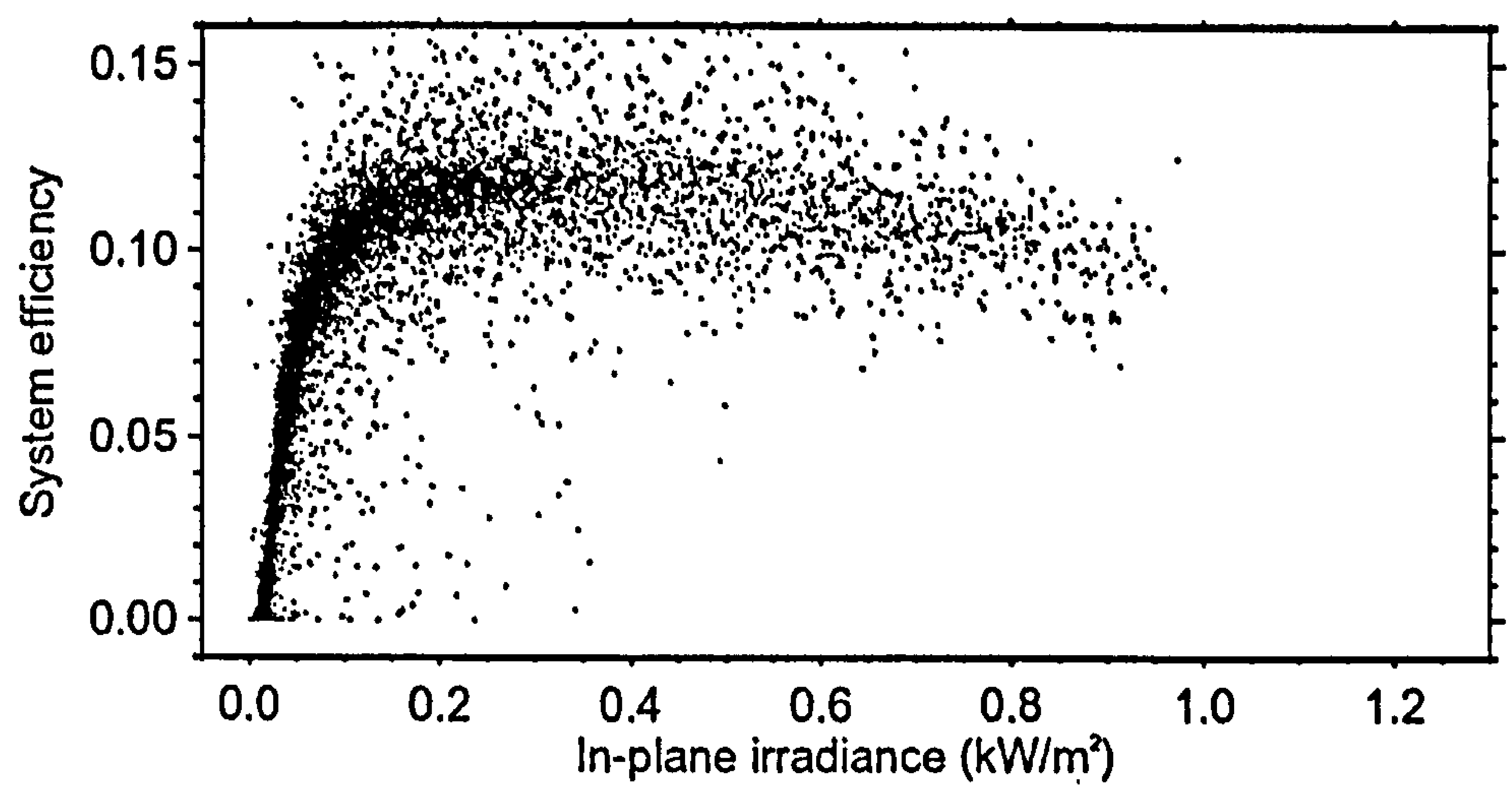

Figure 5-4: Half hourly in-plane irradiance to system efficiency relationship for System 0 at Newbiggin Hall

5.2.3 Explaining the variation in normal operation

The assertion in this work is that the dense cloud of points seen in the system irradiance to efficiency relationship represents the normal operation of the PV systems. The system efficiencies which lie within the boomerang shaped cloud were thus assumed to be indicative of a well operating PV system and not caused by faults. The reason for a cloud of points rather than a single line is due to the energy losses in normal operation: deviation from STC; mismatch; DC wiring; maximum power point tracking; temperature; and inverter DC to AC conversion (Section 2.2.2). Specifically the cloud of points is caused by variations in the energy losses for similar irradiance levels and this is thought be primarily determined by the mismatch, inverter MPP tracking and temperature losses. The other normal operation losses of deviation from STC, DC wiring and inverter DC to AC conversion are considered to be approximately constant for specific irradiance levels.

At Heron Close System 4 (HC 4) the reduction in efficiency from the top to the bottom of the cloud of points ranges from approximately 0.04 at irradiance of 250 W/m^2 to 0.015 at irradiance of 1000 W/m^2 (Figure 5-3). This variation can be compared to the results of previous studies. The combined totals of the mismatch, inverter MPP tracking and temperature losses for the four previous studies discussed in Section 2.2.2 range from a 8.9% to 18.7% performance ratio percent reduction in annual performance ratios (Table 5-2). For Heron Close System 4 (HC

4) with a rated efficiency of 0.123 this represents a 0.011 to 0.023 reduction in annual system efficiency. This reduction in annual efficiency can be thought of as the average efficiency reduction throughout the monitoring period. Assuming the average efficiency reduction in the measured five minutely values is approximately half that of the maximum reduction, the average efficiency reductions in the cloud of points at HC4 ranges from approximately 0.020 at irradiance of 250 W/m^2 to 0.0075 at irradiance of 1000 W/m^2. These figures are roughly comparable with the annual efficiency reductions from previous studies.

Table 5-2: Mismatch, inverter MPP tracking and temperature combined losses from previous studies

	SV Method (Oozeki et al., 2003)	TEAMS (Reinders et al., 1999)	Data Analysis (Baltus et al., 1998)	German 1000 roofs programme (Kiefer et al., 1995)
Combined mismatch, inverter MPP tracking and temperature loss (in annual performance ratio %)	13	11.5	18.7	8.9
Reduction in annual efficiency assuming a rated efficiency of 0.123	0.016	0.014	0.023	0.011

System efficiency values below the cloud were assumed to be caused by faults. The faults lowered the system efficiency values below the expected values for normal operation.

5.3. Describing normal operation

5.3.1 Variable irradiance bins

The five minute system efficiency values included the combined effects of both the normal operation and the faults. This made it difficult to individually investigate the effects of either the operational losses or the faults. For example, studying the effects of temperature on array efficiency was not possible if the array efficiencies were very low due to shading. A method to identify normal operation was developed which used mathematical descriptions to describe the normal operation efficiency values for each PV system. The initial step in this process was the use of variable irradiance bins.

The analysis techniques relied on the principal of separating the irradiance values into bins and investigating the values in each bin. This removed the influence of irradiance from the analysis. For example, a study on the efficiency values within the irradiance bin from 999 W/m^2 to 1001 W/m^2 could investigate the effects of factors other than irradiance on efficiency values at high irradiance. A difficulty when choosing irradiance bins was that the majority of irradiance values occurred at low levels of irradiance. Using bins of constant size (for example 50 W/m^2) meant that the low irradiance bins (i.e. 100 W/m^2 to 150 W/m^2) contained many more values than the high irradiance bins (i.e. 900 W/m^2 to 950 W/m^2). Small bin sizes were required at low irradiance to account for the rapid change in system efficiency (as shown in the examples of Figure 5-3). However small bin sizes at the higher irradiances meant that some bins would not contain any efficiency values at all, as there were much less high irradiance values.

The problem was overcome by using irradiance bins of variable size so than they contained a constant number of values. At Corncroft, the lower boundary of the bins was chosen as 100 W/m^2 to avoid the measurement error in the Corncroft data seen in the system efficiency (Section 5.2.2) and in the DC power measurements (Section 4.2.3). At Heron Close and Panmure Street, the lower boundary was set at 50 W/m^2. Taking, as an example, Heron Close system 4, if the constant number of values per bin was set at 300 then the first 300 irradiance values above 50 W/m^2 were placed in the first bin, the next 300 irradiance values were placed in the second bin, and the process was repeated for the whole range of irradiance values (Figure 5-5).

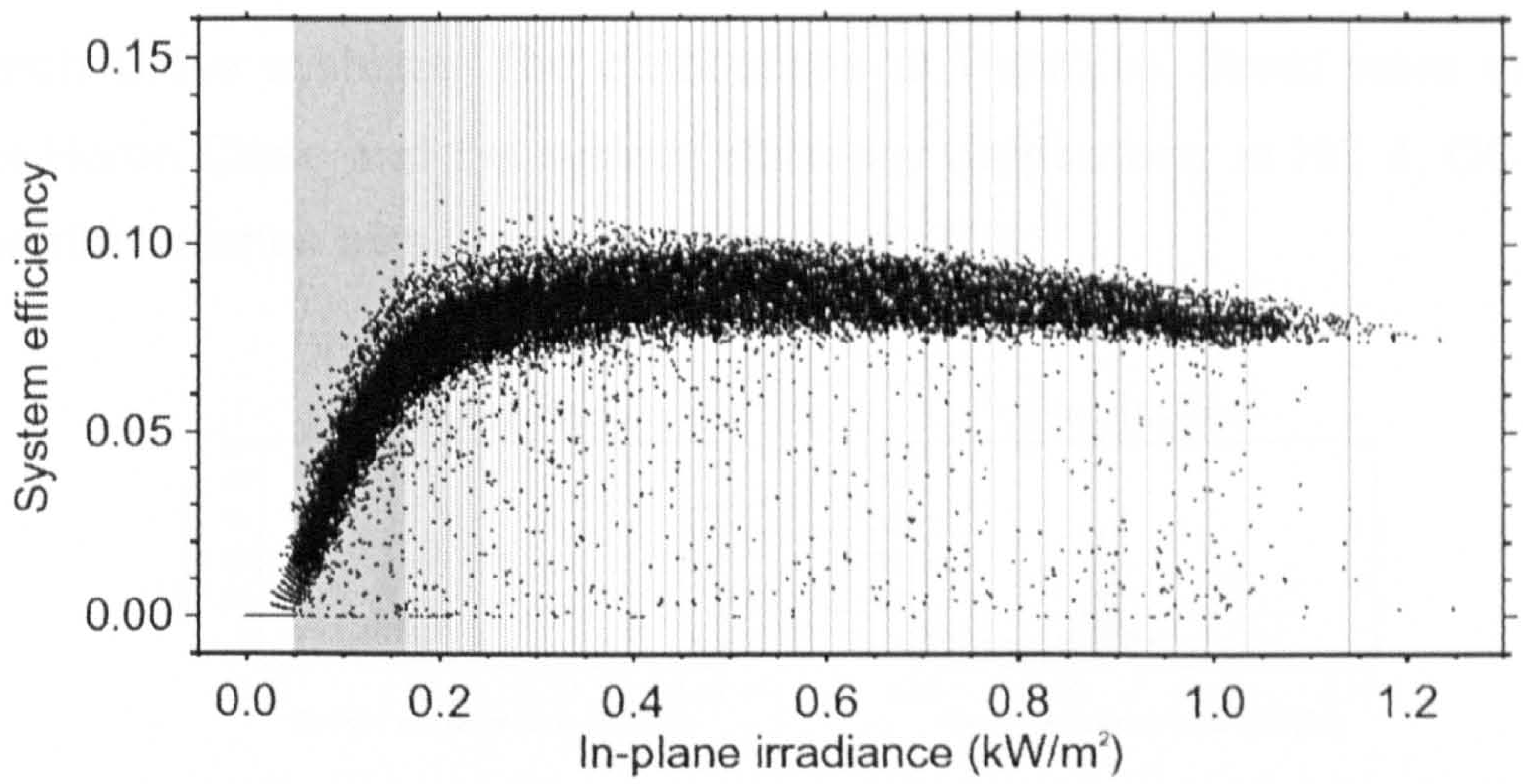

Figure 5-5: Irradiance to system efficiency relationship at HC 4 with the variable irradiance bins. The upper and lower boundaries of the irradiance bins are shown by the grey lines.

5.3.2 Distribution of efficiency values within irradiance bins

The normal operation of the PV systems was investigated by considering the distribution of the 300 system efficiency values in each irradiance bin. The distribution of efficiency in each irradiance bin was calculated by placing the efficiency values into constant bins of 0.001 width. For HC 4, the distributions of system efficiency values within bins of different irradiance levels were similar (Figure 5-6).

The distributions showed that the monitored system efficiencies within a small range of irradiances approximated a Gaussian distribution. In each bin, the majority of the efficiency values were clustered around a central value with a modal frequency at or near this central value. The frequency of occurrence of efficiencies decreased above or below the central value. The efficiencies around the central value were within the boomerang cloud of points seen in Section 5.2.2 and were a part of the normal operation of the PV system. Efficiencies which were significantly lower than the central value (to the left in Figure 5-6) were caused by faults. Similar results are seen for the frequency distribution of system efficiencies within irradiance bins at Corncroft system 21 (Figure 5-7). However the distributions at in low irradiance bins at CC 21, below around 200 W/m^2, had lower frequencies and were more widely spread than their equivalents at HC 4. This was a possible consequence of the slower sampling at Corncroft resulting in more variability in the measured efficiency values. This difference was observed in all the of Corncroft and Heron Close systems. The distributions at Panmure Street were similar to those at Heron Close and the system efficiency distributions at HC 4, CC 21 and PS 0 for all irradiance bins are given in Appendix C.3.

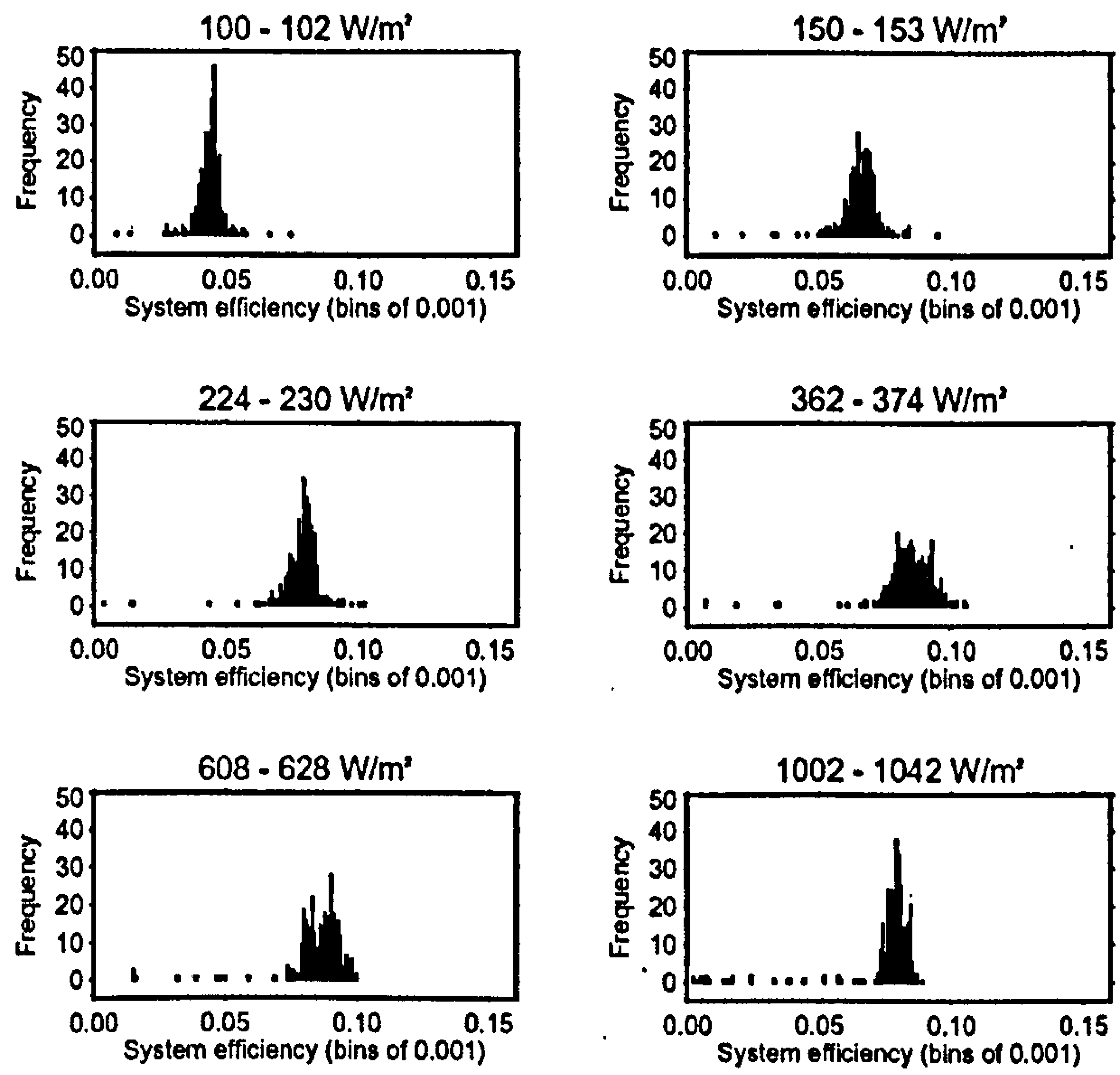

Figure 5-6: Frequency distributions of the system efficiency within six sample irradiance bins for Heron Close system 4 (HC 4)

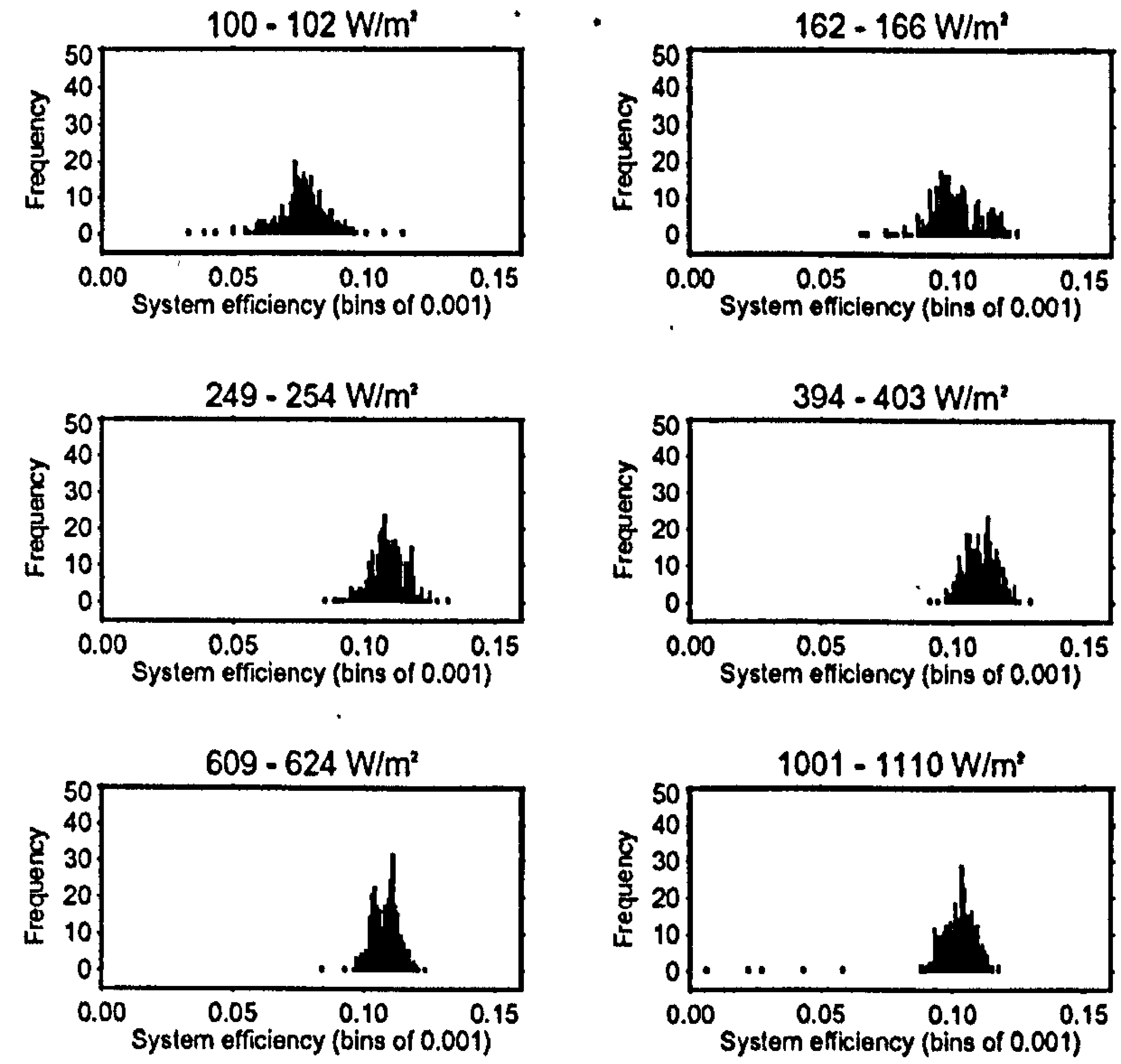

Figure 5-7: Frequency distributions of the system efficiency within six sample irradiance bins for Corncroft system 21 (CC 21)

5.3.3 Modelling normal operation with Gaussian distribution curves

The Gaussian distribution is used in many applications to describe the errors in experimental measurements (Mathworld, 2005). It is defined in IDL (RSI, 2005) by the equation:

$$f(x) = A_0 e^{-(x-\mu)^2 / (2\sigma^2)}$$

where f(x) represents the value of the function at a value x, A_0 is the height of the distribution, μ is the mean and σ is the standard deviation. The distribution was fitted to the efficiency frequency distribution in each irradiance bin using a least squares fitting procedure. The sum of the squares of the difference between a Gaussian distribution and the actual distribution was calculated. The Gaussian distribution which had the lowest least squares value was chosen as the best fit to the measured efficiency distribution. The least squares fit was carried out using in-built routines of IDL.

Continuing with the example of HC 4, a Gaussian distribution was fitted to the efficiency frequency distributions within one of the irradiance bins (Figure 5-8). The height, mean (called alpha on the figure) and standard deviation (called sigma) of the Gaussian distribution are shown. The shape of the Gaussian distribution curve approximated the efficiency distribution and the mean represented the central point about which the majority of the efficiency values occurred. An advantage of using Gaussian distributions and the least squares fitting method is that a few low efficiency values do not unduly affect the fit of the Gaussian distribution curve.

In a Gaussian distribution with mean α and standard deviation σ there is a 5% probability than a value will lie above or below α ±1.64 σ. There is a 2.5% probability at α ±1.95 σ and 1% probability at α ±2.33 σ. The boundaries of these probabilities (shown by the dotted lines in Figure 5-8) enclose the majority of the system efficiency values at HC 4. This provides the basis of the technique to separate the system efficiencies of normal operation and faults, which is described in the next section. Further examples of fitted Gaussian distributions for CC 21, HC 4 and PS 0, are given in Appendix C.4.

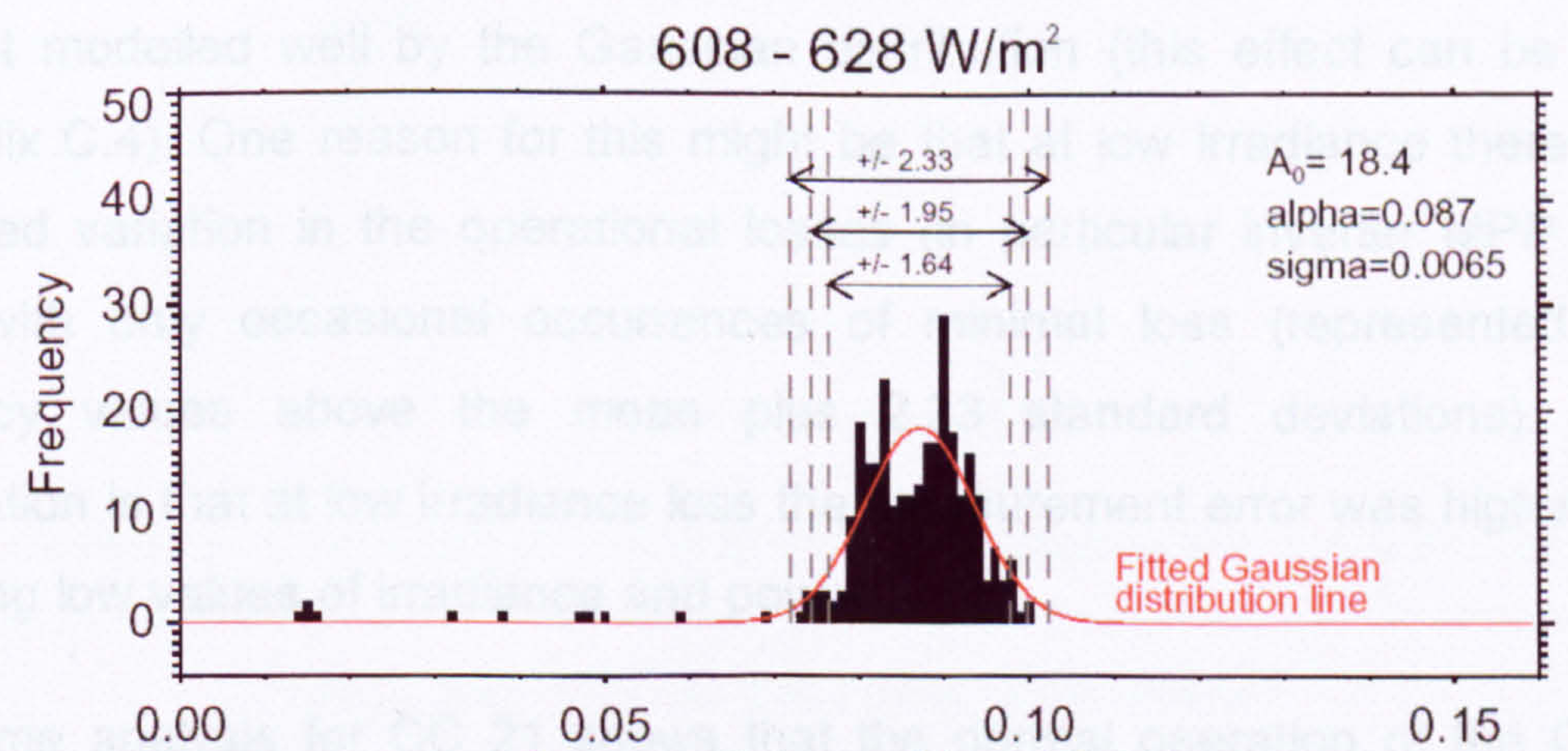

Figure 5-8: Gaussian distribution fit to the efficiency distribution of HC 4 in the 608 W/m^2 to 628 W/m^2 irradiance bin

5.4. Developing efficiency curves and identifying normal operation

5.4.1 Gaussian distribution curves

The normal operation of a PV system was described by using the fitted Gaussian distributions. For the example of HC 4, the means of the Gaussian distributions are shown on the system efficiency to in-plane irradiance relationship (Figure 5-9). The red line shows the curve formed by the mean values of the Gaussian distributions for all the irradiance bins. The blue lines show the curves formed by the mean values plus or minus 2.33 standard deviations. The dense boomerang-shaped cloud of points represented the normal operation of the system (Section 5.2.2). The normal operation was described by the area enclosed by the means of the Gaussian distribution plus or minus 2.33 standard deviations. Assuming the normal operation can be approximated to Gaussian distributions, there is a 99% probability that the efficiencies of normal operation will lie within this area. At irradiances below 250 W/m^2 there were many efficiency values that were slightly above or below this area which suggested that the frequency distribution of normal operation was not modelled well by the Gaussian distribution (this effect can be seen in Appendix C.4). One reason for this might be that at low irradiance there was an increased variation in the operational losses (in particular inverter MPP tracking loss), with only occasional occurrences of minimal loss (represented by the efficiency values above the mean plus 2.33 standard deviations). Another explanation is that at low irradiance loss the measurement error was higher, due to recording low values of irradiance and power.

The same analysis for CC 21 shows that the normal operation of the Corncroft systems can also be modelled by the area enclosed by the means of the Gaussian distributions plus or minus 2.33 standard deviations (Figure 5-10). A similar effect to HC 4 is seen at low irradiances where many efficiency values fall slightly outside the 99% probability range.

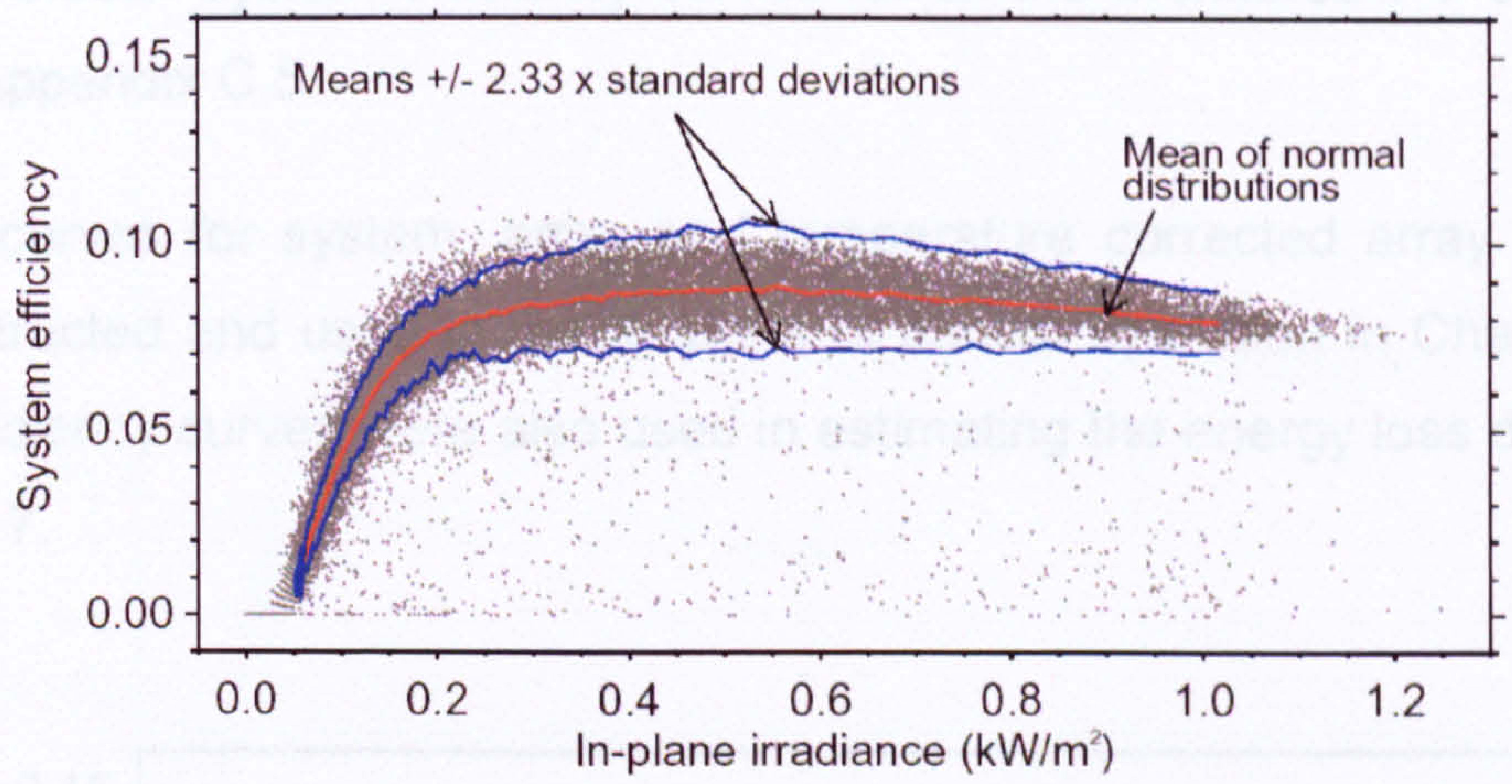

Figure 5-9: Mean and standards deviation of normal distribution fits for HC 4. The red line shows the curve formed by the mean values. The blue lines show the curves formed by the means plus or minus 2.33 standard deviations.

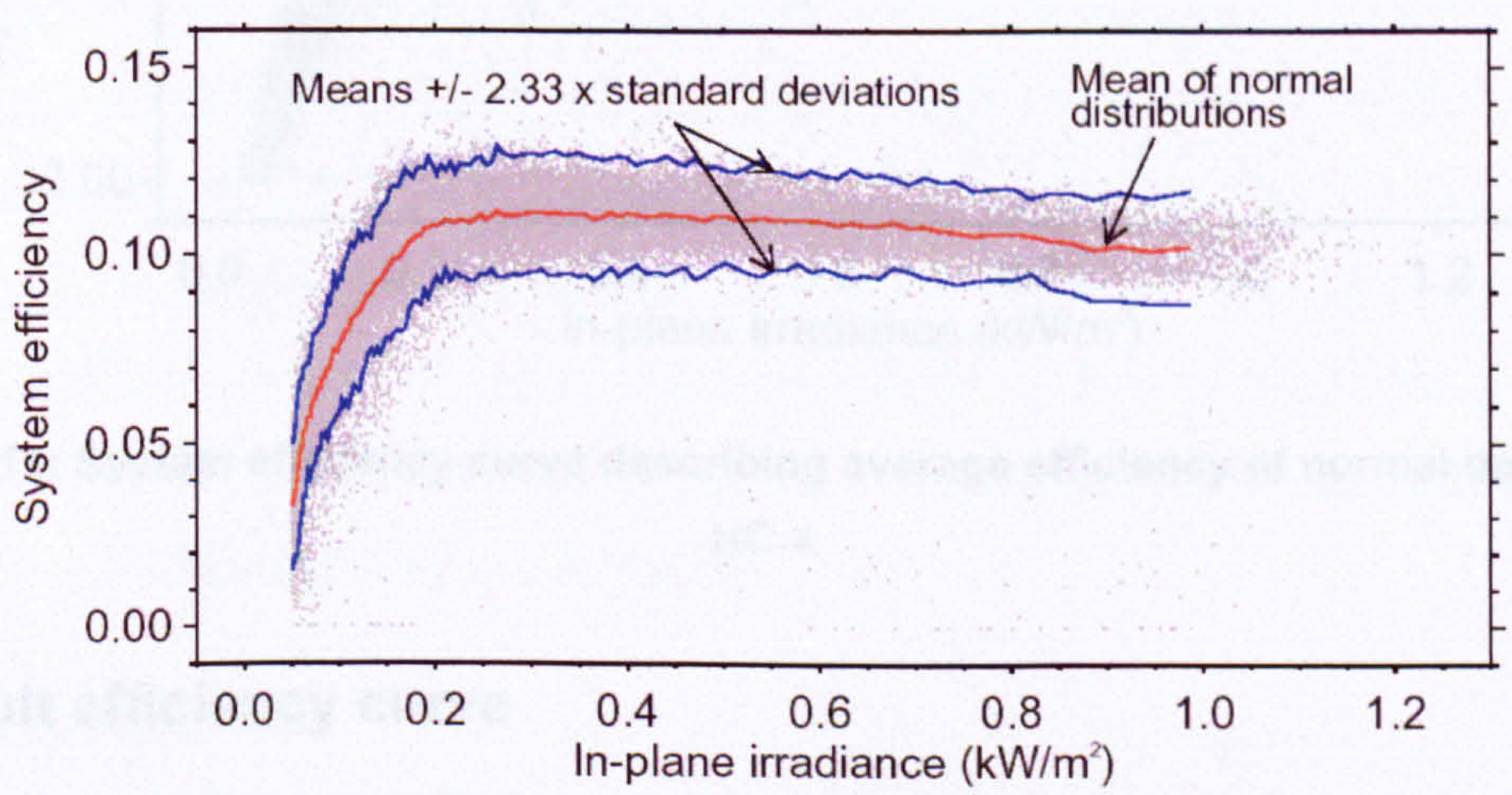

Figure 5-10: Mean and standards deviation of normal distribution fits for CC 21. The red line shows the curve formed by the mean values. The blue lines show the curves formed by the means plus or minus 2.33 standard deviations.

5.4.2 Efficiency curves

The fitted Gaussian distributions were used to develop efficiency curves, the relationship of irradiance to efficiency for the normal operation of the PV systems. The efficiency curve is constructed from the means of the Gaussian distributions. As an example, the system efficiency curve at HC 4 was calculated using the system efficiency values (Figure 5-11). The curve represents the average system efficiency during normal operation over the range of irradiance. For example, at irradiance of 600 W/m^2, the average system efficiency during normal operation at

HC 4 was 0.082. System efficiency curves for all the monitored PV systems are shown in Appendix C.5.

Efficiency curves for system, array and temperature corrected array efficiencies were constructed and used in the analysis of normal operation in Chapter 6. The system efficiency curves were also used in estimating the energy loss due to faults in Chapter 7.

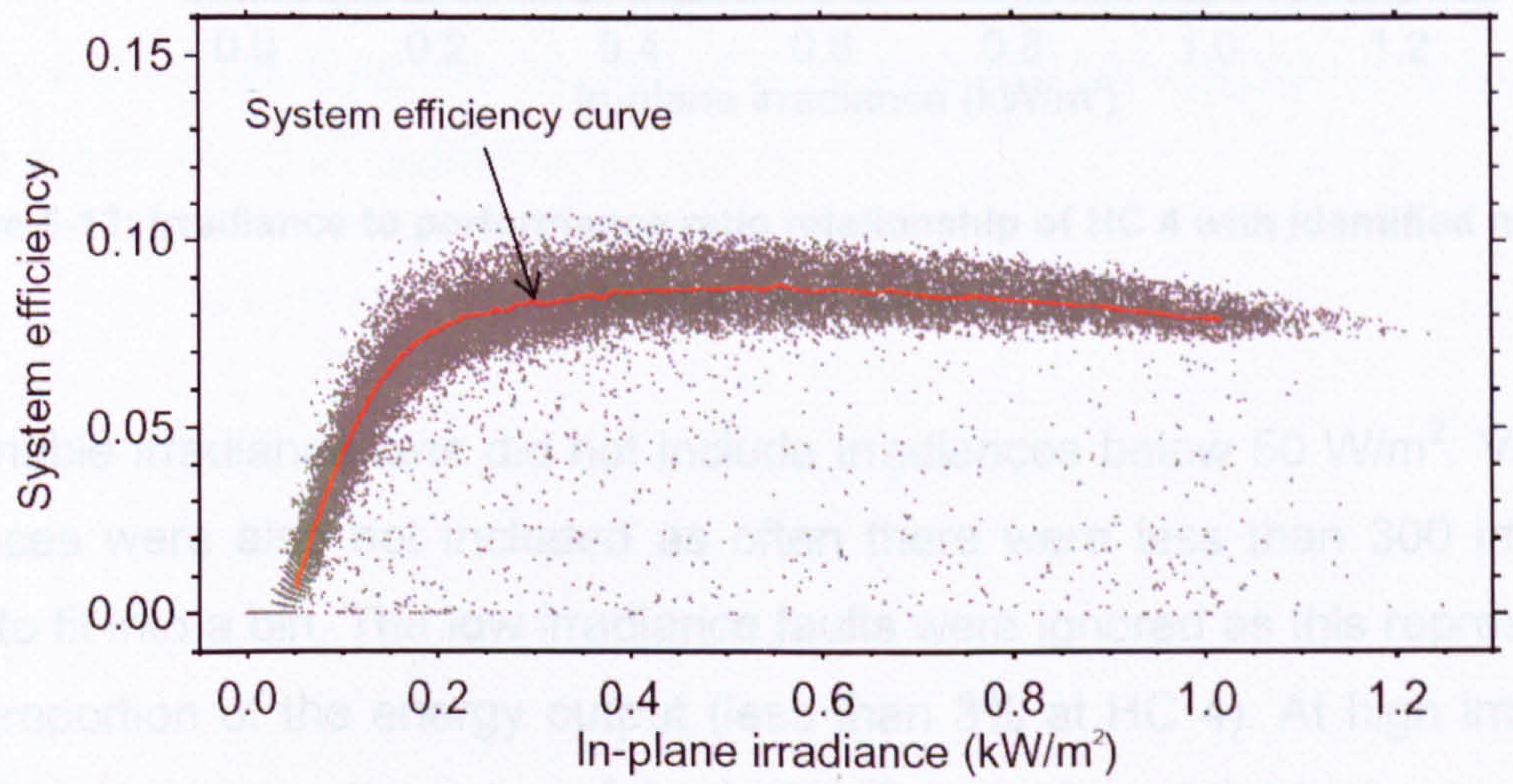

Figure 5-11: System efficiency curve describing average efficiency of normal operation at HC 4

5.4.3 Fault efficiency curve

The normal operation and faults were identified by constructing a *fault efficiency curve*. Efficiencies above the fault efficiency curve were identified as normal operation and below as faults. The fault efficiency curve was defined as the means of the Gaussian distribution minus 2.33 standard deviations. The faults were therefore the efficiency values with less than a 1% chance of occurring during normal operation and which were lower than the normal operation efficiencies. Using the example of HC 4, the fault efficiency curve enabled the separation of normal operation and poor performance (Figure 5-12). Similar plots are shown for all the monitored PV systems in Appendix C.6.

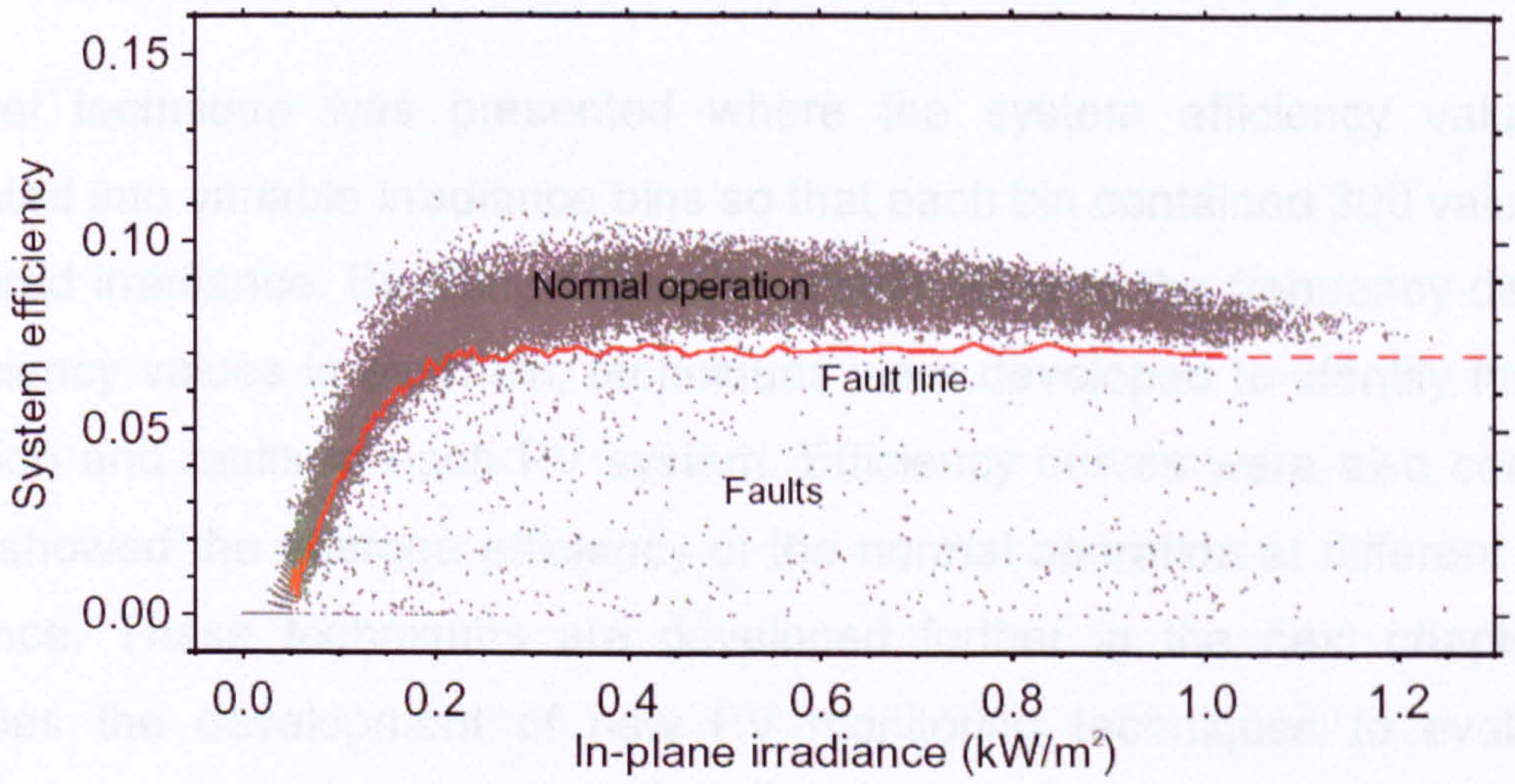

Figure 5-12: Irradiance to performance ratio relationship of HC 4 with identified normal operation and faults

The variable irradiance bins did not include irradiances below 50 W/m^2. Very high irradiances were also not included as often there were less than 300 irradiance values to fit into a bin. The low irradiance faults were ignored as this represented a small proportion of the energy output (less than 3% at HC 4). At high irradiance, any efficiencies below the value of the fault efficiency line at the highest irradiance (0.07 efficiency at 1020 W/m^2 at HC 4) were identified as faults (this process is shown by the dotted red line in the figure).

5.5. Summary

Annual results of the monitored PV systems show that the Corncroft and Newbiggin Hall sites were performing well. Heron Close and Panmure Street did not perform as well as expected and had some systems with low annual performance ratios. The annual results cannot be used to investigate why some systems performed better than others.

The relationship of in-plane irradiance to system efficiency at the five minute level showed that for Corncroft, Heron Close and Panmure Street a cloud of points occurred which follow a similar pattern to the PV module efficiency curve. The skewed boomerang-shaped cloud was assumed to represent the normal operation of the system and efficiencies below this cloud taken to be faults. The five minute data at Newbiggin Hall contained much more noise and did not show this relationship. It was suggested that this was caused by the slow sampling rate and the Newbiggin Hall data was excluded from the five minute analysis.

A novel technique was presented where the system efficiency values were separated into variable irradiance bins so that each bin contained 300 values of the measured irradiance. By fitting Gaussian distributions to the frequency distribution of efficiency values in each bin, techniques were developed to identify the normal operation and faults in each PV system. Efficiency curves were also constructed which showed the average efficiency of the normal operation at different levels of irradiance. These techniques are developed further in the next chapter which describes the development of new PV monitoring techniques to evaluate the normal operation of PV systems.

6. Normal Operation Monitoring Analysis Techniques

This chapter describes the development of new monitoring analysis techniques to analyse the normal operation of PV systems. The techniques are based on the five minutely monitored data from the PV sites and methods to identify normal operation in the monitored data were described in Chapter 5. The use of five minutely data provides the opportunity to gain additional understanding into the normal operation of PV systems and the monitoring techniques are developed to maximise the benefits of this high resolution data.

Normal operation represents times when the PV system is working well and all faults are excluded. PV system performance at normal operation is influenced by the design of the PV systems, the system components and the local climate. These factors cause energy losses in the sunlight to electricity conversion process and this group of energy losses is defined as the operational losses. A literature review of each loss is presented and the effects on efficiency are discussed.

Monitoring techniques are developed to identify each of the operational losses. The techniques are mostly graphical and are based on the five minutely monitored data from the PV sites. The normal operation data is used to construct a series of 'efficiency curves' for each system which describe the typical performance of the system. Original monitoring techniques are described and applied including: a study of the effect of inverter power derating at different levels of irradiance; and a study of the inverter maximum power point (MPP) tracking loss at different irradiance levels. The techniques are demonstrated throughout this chapter by reference to three example PV systems from Corncroft, Heron Close and Panmure Street.

The monitoring techniques are applied to the monitored data recorded at the PV sites and the losses in annual performance ratio are calculated for each operational loss. The annual results are compared to previous studies to assess the plausibility of the results and to evaluate the monitoring techniques.

6.1. Review of operational losses

6.1.1 Types of operational losses

The operational losses were defined in Section 2.2.1 as the energy losses which reduce the efficiency from ideal operation to normal operation. Eight operational losses were identified: 1) inverter power derating; 2) inverter DC to AC conversion; 3) DC wiring loss; 4) temperature loss; 5) inverter maximum power point (MPP) tracking; 6) irradiance loss; 7) mismatch; and 8) deviation from STC. Prior to developing techniques to identify these losses, a literature review of each operational loss was undertaken and the results are presented in this section.

6.1.2 Inverter power derating

Inverters are given different ratings according to their maximum AC power output. For example an 850 W inverter will output a maximum AC power of 850 W no matter how high the DC power input from the PV array. Inverter rating is chosen in relation to the size of the PV array and inverters are often deliberately undersized. The PV array rarely generates very high DC powers (only during times of high irradiance) and costs are reduced by using smaller inverters. For example, for Heron Close system 4 (HC4) a 1100 W inverter was used with a 1.44 kWp array. Inverters with ratings of 700 W, 850 W, 1100 W and 2500 W were used at Corncroft, Heron Close and Panmure Street (Table 6-1). The ratio of the inverter rating to the PV array rating ranged from 0.59 (undersized) at Heron Close to 1.63 (oversized) at Corncroft.

Table 6-1: Array and inverter ratings

Site	System number(s)	Array rating (kWp)	Inverter rating (W)	Ratio of inverter to array rating
CC	All	1.53 or 1.7	2500	1.63 or 1.47
HC	4, 5 and 6	1.44	1100	0.76
HC	7	1.68	1100	0.65
HC	12	1.44	850	0.59
PS	All	1.08	850	0.79

The energy loss caused by the reduction in AC energy output is defined as *inverter power derating loss.* A study by Ransome and Funtan (Ransome and Funtan, 2005) demonstrated the effect of inverter power derating. During the operation of a PV system with a significantly undersized inverter, the AC output power did not rise above a certain 'saturation' power limit, equal to the inverter rating. If the inverter had been oversized then the AC power output would not have been limited.

6.1.3 Inverter DC to AC conversion

The energy loss in the conversion from DC power to AC power by the inverter is defined as the *inverter conversion loss.* The loss is described by the inverter efficiency, defined as the ratio of the AC energy output from the inverter to the DC energy input to the inverter. Inverter efficiency varies with the amount of electrical power that is being converted and the *inverter efficiency curve* is defined as the relationship between AC power output and inverter efficiency. The curve for a 1100 W rated SMA Sunny Boy inverter was provided in the inverter technical documentation (SMA, 2005), with the AC power output normalised by the inverter rating (Figure 6-1). At AC powers above 10% of the rated power (110 W), the inverter efficiency is greater than 80%, with a maximum efficiency of 93% at around 40% of rated power (440 W). Below 10% rated power, the inverter efficiency falls to zero. SMA inverters were used in all the monitored PV systems and had similar efficiency curves.

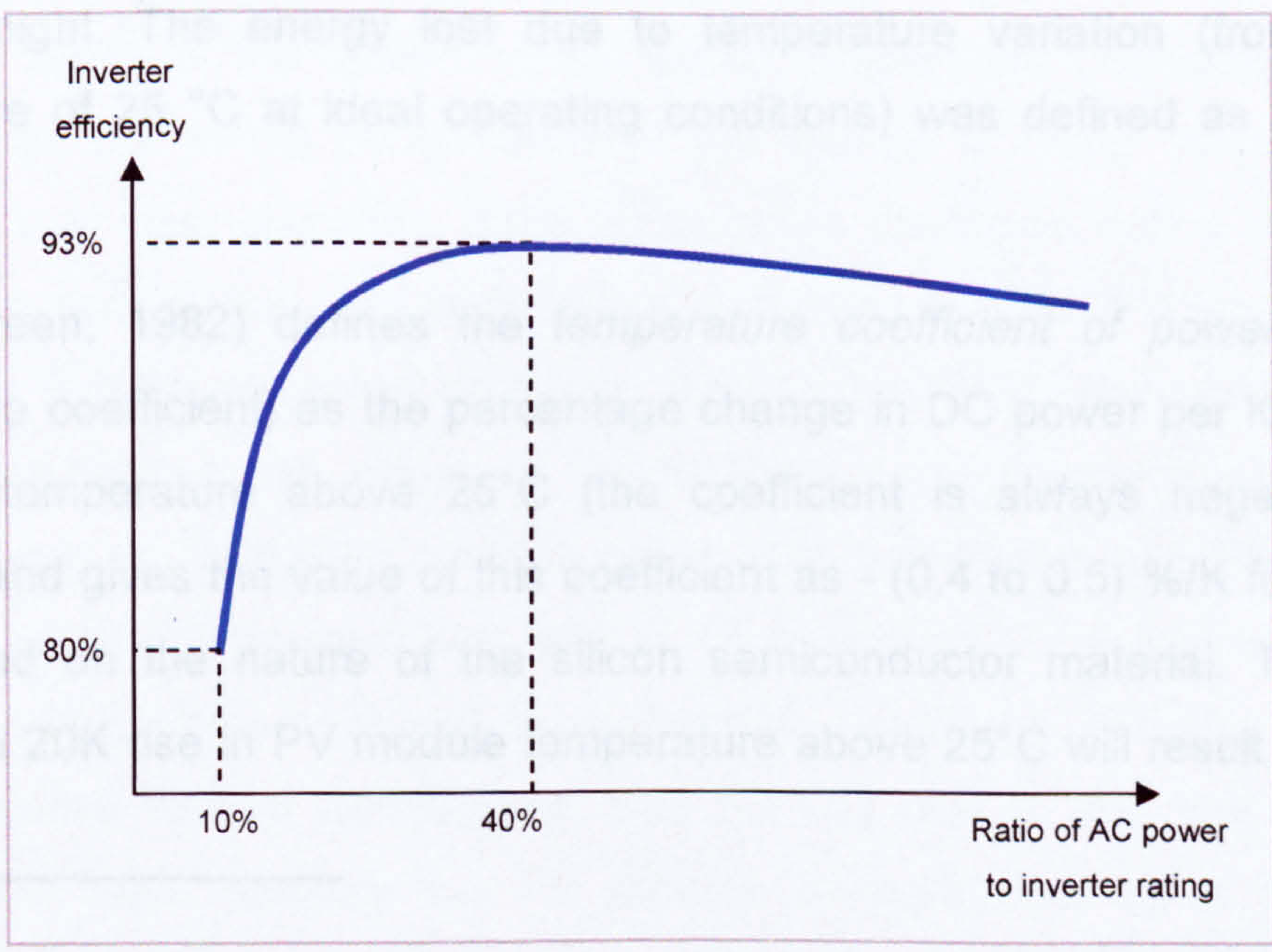

Figure 6-1: Inverter efficiency curve for a SMA 1100 W inverter (reproduced from SMA, 2005)

6.1.4 DC wiring

DC wiring loss is defined as the energy lost due to the resistive losses in the DC cables that connect the PV array to the inverter. In the DC cables the electrical energy is converted to heat at the rate:

$$P_{DC,LOSS} = I_{PV}^{\ 2} R$$

where $P_{DC,LOSS}$ is the power loss due to the resistance (Watts), I_{PV} is the DC current of the PV array (Amps) and R is the resistance of the DC cables connecting the PV array to the inverter (Ohms).

DC wiring loss increases with both the DC current output (at its highest during times of high solar irradiance) and the length of the DC cables. In a study of a 3.3 kWp PV system in the Netherlands, Baltus et al. (Baltus et al., 1997) estimated the reduction in annual performance ratio due to DC wiring loss at 1.2%.

6.1.5 Temperature

The temperature of PV modules affects the efficiency of the sunlight to electricity conversion process due to the properties of the crystalline silicon semiconductor material[21]. As the module temperature increases, a decrease occurs in the module efficiency. The effect of temperature on efficiency constantly changes as the modules are heated by the solar radiation in the day time and then cool down again at night. The energy lost due to temperature variation (from the STC temperature of 25 °C at ideal operating conditions) was defined as *temperature loss*.

Green (Green, 1982) defines the *temperature coefficient of power* (or simply temperature coefficient) as the percentage change in DC power per K increase in operating temperature above 25°C (the coefficient is always negative for PV modules) and gives the value of this coefficient as - (0.4 to 0.5) %/K for silicon PV cells, based on the nature of the silicon semiconductor material. Thus, as an example, a 20K rise in PV module temperature above 25°C will result in an 8% to

---

[21] All of the PV systems in this work had crystalline silicon PV modules

10% decrease in DC power output. The manufacturers of the PV modules used in this study provided the temperature coefficients at STC (Table 6-2).

Table 6-2: Temperature coefficients for the PV modules used in this study

Manufacturer	Model	Temperature coefficient of power at STC
BP Solar (BP Solar, 2005)	Saturn 585	- (0.5 ± 0.05) %/K
Astropower (Astropower, 2004)	AP 55, AP 75 and AP 120	-0.473 %/K

Gxasheka et al. (Gxasheka et al., 2005) described the temperature dependence of the power output of a number of silicon PV modules using indoor testing. The power output of the modules, based on STC measurements but with increasing temperature, was shown to decrease linearly as temperature increased. Temperature coefficients for the modules were calculated as -0.40 to -0.56 %/K. In an outdoor study of PV modules, Nishioka et al. (Nishioka et al., 2003) determined a temperature coefficient of -0.4 %/K for a crystalline silicon module, based on the mean efficiency values for different temperature ranges.

Temperature loss is defined as the difference between the estimated energy output of a PV system operating at constant PV module temperature of 25°C and the measured output of the system under actual temperature conditions. This loss applies when the actual performance of the system is being compared to the performance at ideal operation. If the temperature conditions during operation are low the temperature loss can be negative, indicating that the PV array generated more power than its equivalent operating at a constant 25°C. None of the reviewed studies investigated the effect of irradiance on the temperature coefficient. Previous work by Nordmann and Clavadetscher (Nordmann and Clavadetscher, 2003) calculated the temperature loss in 17 monitored PV systems as 1.7% to 11.3% of annual performance at ideal operating conditions. A further PV system had a negative annual temperature loss (-2.1%) due to the low ambient air temperatures (and therefore low PV module temperatures) at its high altitude location.

6.1.6 Inverter maximum power point tracking

A study by Haeberlin et al. (Haeberlin et al., 2005) described the relationship of operating voltage to module efficiency for a typical crystalline silicon PV module (Figure 6-2). PV module efficiency varies with the operating voltage and has a maximum at a certain operating voltage, defined as the *maximum power point* (MPP). To maximise the module efficiency the operating voltage must be kept at the MPP voltage. If the array operating voltage moves away from the MPP voltage then the module efficiency decreases below its maximum value.

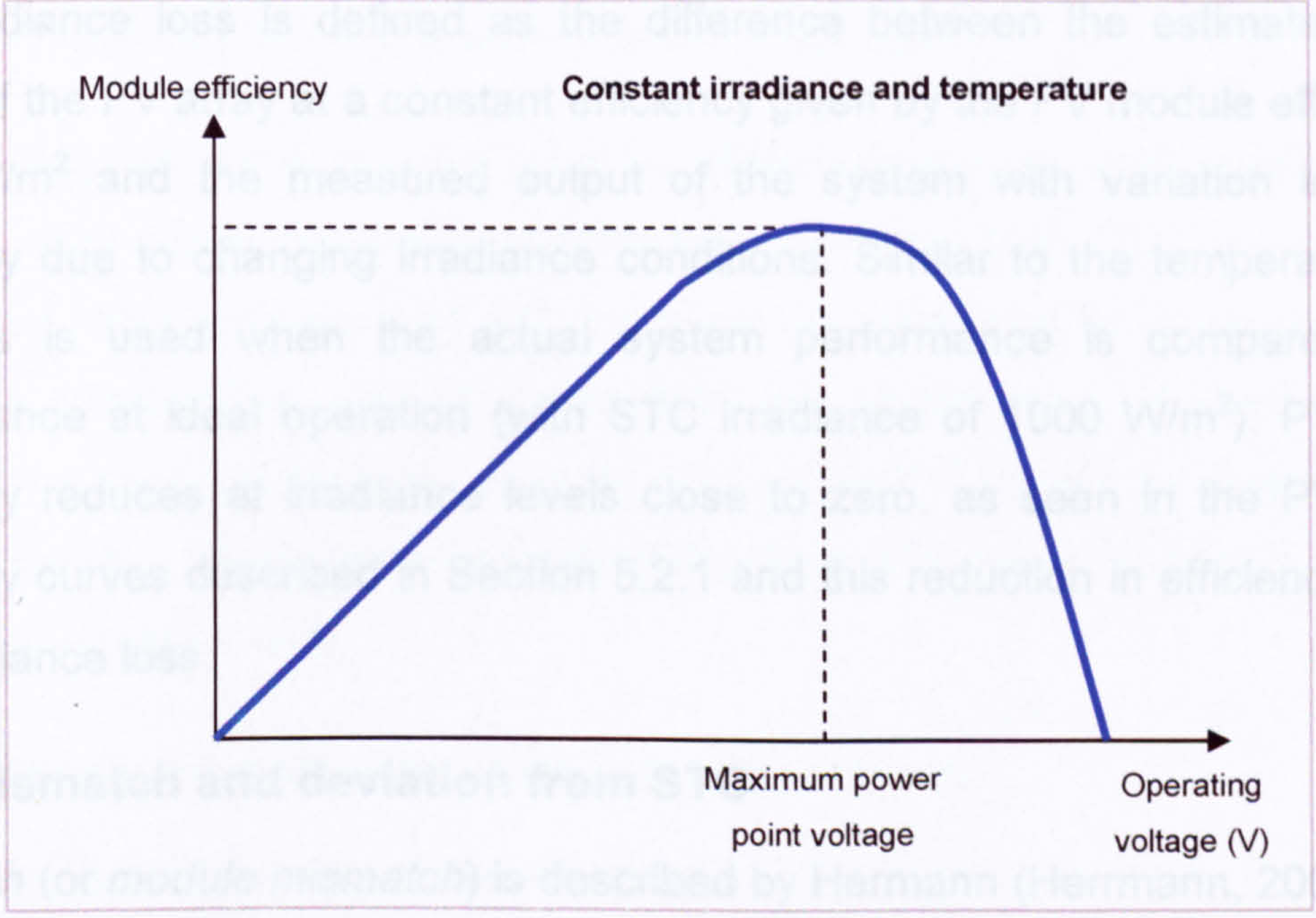

Figure 6-2: Relationship of operating voltage and module efficiency for a typical crystalline silicon PV module (reproduced from Haeberlin et al., 2005)

The MPP voltage is influenced by irradiance and temperature conditions and in installed PV systems is constantly changing. The operating voltage is constantly adjusted (by the inverter) to match the MPP voltage and thus maximise efficiency. This process is known as *inverter MPP tracking*. The study by Haeberlin et al. (Haeberlin et al., 2005), and another by Jantsch et al. (Jantsch et al., 1997), describe this process. The inverter MPP tracking worked well during times of steady, incremental changes in the solar irradiance such as bright, clear days. However, at times of large and rapid irradiance changes, such as bright summer days with passing cloud, the MPP tracking struggled to keep up with changes in the MPP voltage and significant losses could result. However in neither study was the energy lost due to MPP tracking quantified.

A separate study on MPP tracking for amorphous silicon PV modules by Infield et al. (Infield et al., 2001) describes the laboratory testing of inverters using an electronic solar simulator in place of an actual PV array. A tracking efficiency term was defined as the ratio of the measured DC energy over a test period to the calculated DC energy assuming ideal MPP tracking operation. In tests in which an amorphous silicon PV array was simulated, it was shown that the tracking efficiencies for three different inverters ranged from 70% to 98%.

6.1.7 Irradiance

The irradiance loss is defined as the difference between the estimated energy output of the PV array at a constant efficiency given by the PV module efficiency at 1000 W/m^2 and the measured output of the system with variation in module efficiency due to changing irradiance conditions. Similar to the temperature loss, this loss is used when the actual system performance is compared to the performance at ideal operation (with STC irradiance of 1000 W/m^2). PV module efficiency reduces at irradiance levels close to zero, as seen in the PV module efficiency curves described in Section 5.2.1 and this reduction in efficiency reflects the irradiance loss.

6.1.8 Mismatch and deviation from STC

Mismatch (or *module mismatch*) is described by Hermann (Herrmann, 2005) as the loss due to the variation in electrical characteristics of PV modules within a PV array. In PV modules the current and voltage characteristics vary slightly due to tolerances in the manufacturing process. This causes the MPP voltage between modules to vary slightly. When PV modules are connected in series in an array, the array MPP voltage will be a combination of the individual module MPP voltages and the modules cannot all operate at their MPP voltage simultaneously. The power output of the array is therefore lower than the sum of the power outputs of the individual modules and the reduction in efficiency is defined as the *mismatch loss*. Hermann showed that in one experiment the maximum power of modules of the same make and model varied from 145.8 to 155.6 W and a power loss of 0.4% to 0.5% could be attributed to module mismatch in an array of these modules. Mismatch is the reason why modules of different power ratings are not used in the same PV array.

A further source of mismatch can occur during operation if the PV modules in an array are subjected to different irradiance or temperature conditions. Variation in irradiance levels over the array is typically caused by shading (see Section 7.1.5). Variation in module temperatures over the array is caused by the difference in ventilation of the modules. For example, air drawn under an array will cool the modules down most at its point of entry (at the bottom of the array). As the air rises underneath the PV array the air temperature increases and the cooling effect on the PV modules decreases. This means that temperature gradients can form across the PV array and across PV modules in the array. Mismatch caused by these temperature gradients is termed *thermal mismatch*.

The result by Hermann, that PV modules of the same make and model can have different rated power, illustrates another loss: *deviation from STC*. In some cases the actual rated efficiency of PV modules (for example as measured before operation commences) can be lower than the single value of rated efficiency provided by the manufacturer. A study of a single PV system by Reinders et al. (Reinders et al., 1999) showed that deviation from STC accounted for 5.7% loss in annual performance ratio.

6.2. Development of monitoring techniques

6.2.1 A model of the operational losses

The operational losses can operate simultaneously which makes it difficult to identify them separately in the monitored data. To simplify the development of new PV monitoring techniques a model of the energy flows in a PV system has been developed to approximate the actual physical system (Figure 6-3). This model places the operational losses in a specific order and it is assumed that the losses occurred in this sequence. The order is determined by the needs of the analysis and does not necessarily represent the actual order of the system losses which is difficult to assess.

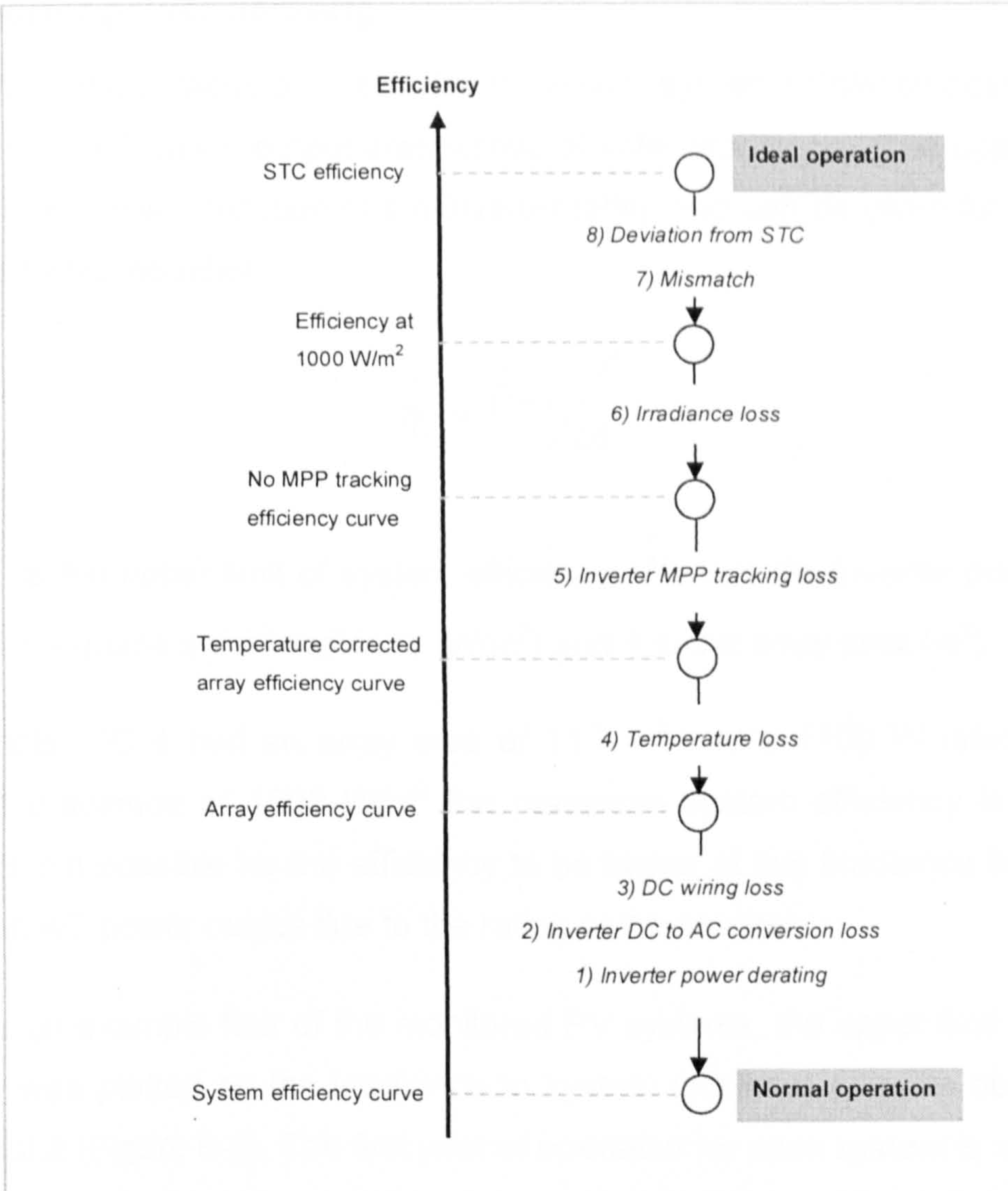

Figure 6-3: Schematic diagram of reduction in efficiency due to operational losses

The reduction in efficiency from ideal operation to normal operation is split into stages corresponding to a series of six efficiency curves: system; array; array temperature corrected; no inverter MPP tracking; irradiance at 1000 W/m^2; and STC efficiency (Figure 6-3). These curves describe the typical efficiency of the PV system at the different stages of normal operation and are constructed using new techniques based on the five minutely monitored data. The system efficiency curve is based on the AC power measurements and the STC efficiency curve on the rated efficiency of the modules. The remaining four efficiency curves are based on the DC power measurements. This section describes new methods to analyse the operational losses and the development of the efficiency curves.

6.2.2 Inverter power derating

The inverter rating places a limit on the maximum system efficiency possible (due to the limit on AC power output irrespective of solar irradiance). The upper limit of system efficiency is a function of the inverter rating and can be given for a specific irradiance by the equation:

$$\hat{\eta}_i = \hat{P}_{INV} / iA$$

where $\hat{\eta}_i$ is the upper limit of system efficiency; $\hat{P}_{INV}$ is the inverter power rating (W), i is the in-plane solar irradiance (W/m^2) and A is the array area (m^2).

For example, HC 4 had an array area of 11.7 m^2 and a 1100 W rated inverter. Under an irradiance of 1000 W/m^2 the maximum system efficiency is therefore 0.094. It is not possible for the efficiency to be higher at this irradiance because of the limit on AC power output due to the rating of the inverter.

Taking as an example four of the monitored PV systems, the upper limit of system efficiency was plotted on the irradiance to system efficiency plots as described in Section 5.2.2 (Figure 6-4). The first year of operation for each system is shown and only the normal operation efficiencies are plotted, as determined from the Gaussian distribution techniques in Section 5.4.3. The faults were ignored in all the analysis techniques in this chapter. At Corncroft, irradiance values below 100 W/m^2 were not included in the plots, due to the occurrence of measurement inaccuracy at low irradiance (Section 4.2.3). At Heron Close and Panmure Street the minimum irradiance used was 50 W/m^2 as this was the minimum value used in the variable irradiance bin technique (Section 5.3.1). Similar plots for the other Heron Close and Panmure Street systems are given in Appendix D.1.

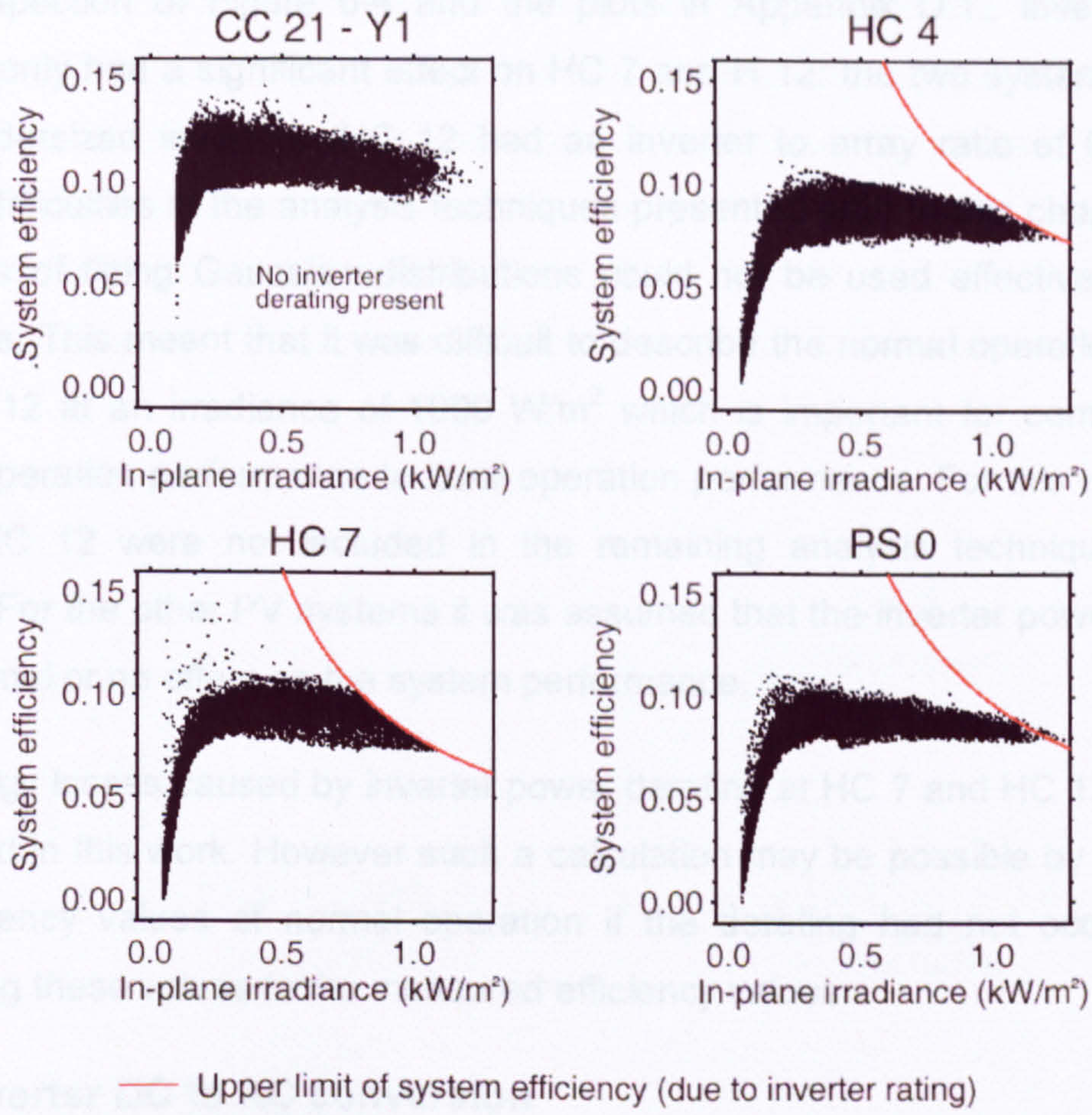

Figure 6-4: Irradiance to system efficiency relationships for selected systems. The upper limit of system efficiency, caused by inverter power derating, is shown by the red line.

At CC 21 there was no inverter power derating because the inverter was significantly oversized compared to the PV array (Section 6.1.2). This was true for all Corncroft systems. At HC 4 the inverter derating effect was minimal as the recorded efficiencies only approached their upper limit at irradiances of around 1200 W/m^2 or greater. This high level of irradiance occurred rarely during operation. The inverter was significantly undersized at HC 7 with an inverter to array ratio of 0.65 (Table 6-1) and the effect on efficiency can be clearly seen. There was a sharp decline in efficiency values recorded at irradiances of around 800 W/m^2 or greater due to the limiting effect of the inverter. Surprisingly, at PS 0 some efficiency values above the theoretical maximum did occur. This is because the inverters at Panmure Street allowed an output power up to around 900 W which was slightly higher than their rated power of 850 W. The effect of inverter power derating at PS 0 was similar to HC 4 and only efficiencies at very high irradiances were affected.

From inspection of Figure 6-4 and the plots in Appendix D.1., inverter power derating only had a significant effect on HC 7 and H 12: the two systems with the most undersized inverters (HC 12 had an inverter to array ratio of 0.59). This caused difficulties in the analysis techniques presented later in this chapter as the technique of fitting Gaussian distributions could not be used effectively for high irradiance. This meant that it was difficult to describe the normal operation of HC 7 and HC 12 at an irradiance of 1000 W/m^2 which is important for comparing the normal operation performance to ideal operation performance. For this reason, HC 7 and HC 12 were not included in the remaining analysis techniques in this chapter. For the other PV systems it was assumed that the inverter power derating had minimal or no effect on the system performance.

The energy losses caused by inverter power derating at HC 7 and HC 12 were not calculated in this work. However such a calculation may be possible by estimating the efficiency values of normal operation if the derating had not occurred and comparing these values to the measured efficiency values.

6.2.3 Inverter DC to AC conversion

The effects of the inverter conversion loss were simple to investigate as both the DC and AC power measurements were recorded. The inverter efficiency curves at the three example PV systems were, as expected, similar to the manufacturer's efficiency curves as described in Section 6.1.3 (Figure 6-5). HC 7 was excluded from the analysis due to the significant amount of inverter power derating as discussed in Section 6.2.2. Inverter efficiency curves for all the PV systems are shown in Appendix D.2.

The inverter curves for HC 4 and PS 0 showed more variation in efficiency than CC 21. This may be an effect of the different sampling rates used at the sites[22]. The maximum AC power output from CC 21 reached only around 60% of the inverter rating, as the inverter was oversized (a 2500 W inverter for a 1.53 kWp system). At HC 4 and PS 0 the inverters were slightly undersized and the maximum AC power output was similar to the inverter rating.

[22] Comcroft had a sampling rate of around 60 seconds. Heron Close and Panmure Street both had sampling rates around 10 seconds (Section 3.2.5)

At CC 21, the system would operate at the low efficiency section of the curve (to the left of the curve in Figure 6-5) for a longer period of time than the other two systems. As all the inverters at Corncroft were oversized, this would explain the low annual inverter efficiencies in the annual results (Section 5.1.1). At HC 4 and PS 0 there were some efficiency values greater than 1 and this suggested that there must be some measurement error in the Heron Close and Panmure Street values.

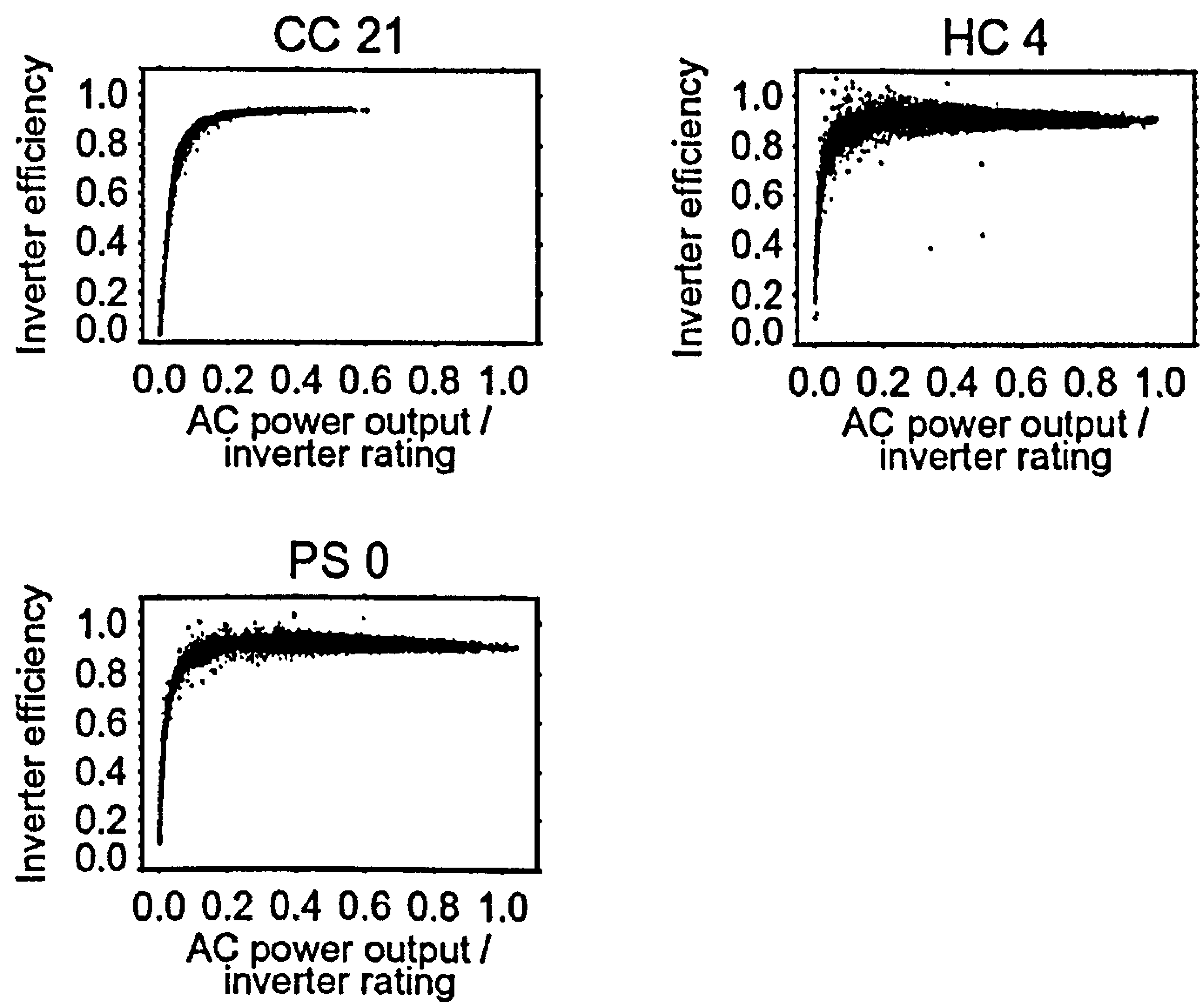

Figure 6-5: Inverter efficiency curves for selected systems

6.2.4 DC wiring

The equation of power loss in the DC cables was defined in Section 6.1.4. All the monitored systems had similar DC cables with a cross sectional area of 2.5 mm^2. Based on this cross sectional area, the resistance of the cable was estimated at 8.2 Ω per km (Powerstream, 2005). It was assumed that at each PV system the DC cable run was 10 m in length (a pair of 5 m cables connecting the array to the inverter). Thus the resistance R of the DC cables at each system was estimated as 0.082 Ω.

The DC current I_{PV} in the DC cables was calculated from the DC power input to the inverter and the DC voltage at the inverter input. The DC power input to the inverter was provided by the recorded DC power measurements. The DC voltage was not measured and it was assumed that the DC voltage remained constant at the value of MPP voltage at STC provided by the module manufacturers (18 V for the Corncroft modules and 16.9 V for the Heron Close and Panmure Street modules). Thus the power loss in the DC cables is given by:

$$P_{DC,LOSS} = I_{PV}^{2} R = \left(\frac{P_{DC,INV}}{nV_{MPP}} \right)^{2} \times R$$

where n is the number of PV modules in the PV array and V_{MPP} is the MPP voltage at STC provided by the module manufacturers (V).

For example, on a bright sunny day the PV array at HC 4 could have a DC power output of 1000 W. There were 12 PV modules in the PV array and the MPP voltage at STC is provided by the manufacturer as 16.9 V. The DC current output of the array is estimated as 4.93 A and the power loss in the DC cables as 2 W. This suggests that the power loss in the DC cables has a minimal effect on the power output of the system.

6.2.5 System efficiency and array efficiency curves

Array efficiency is calculated using the DC power output from the PV array (Section 5.2.1). These DC power values were not measured directly but were calculated as the sum of the DC power measurements (recorded at the input to the inverter) and the DC wiring losses (calculated using the method described in Section 6.2.4). This is described by the equation:

$$P_{DC,ARRAY} = P_{DC,LOSS} + P_{DC,INV}$$

where $P_{DC,ARRAY}$ is the DC power output from the PV array (W); $P_{DC,LOSS}$ is the power loss in the DC cables (W); and $P_{DC,INV}$ is the DC power input to the inverter (W).

For the three example PV systems the difference between array efficiency and system efficiency is clearly observed (Figure 6-6). Similar plots are provided for all the monitored PV system in Appendix D.3. The reduction from array efficiency to system efficiency (calculated from the AC power output from the inverter) was due to the energy losses in the DC wiring and in the inverter DC to AC conversion process (Figure 6-3). System efficiency curves and array efficiency curves were constructed from the efficiency values using the techniques described in Section 5.4.2.

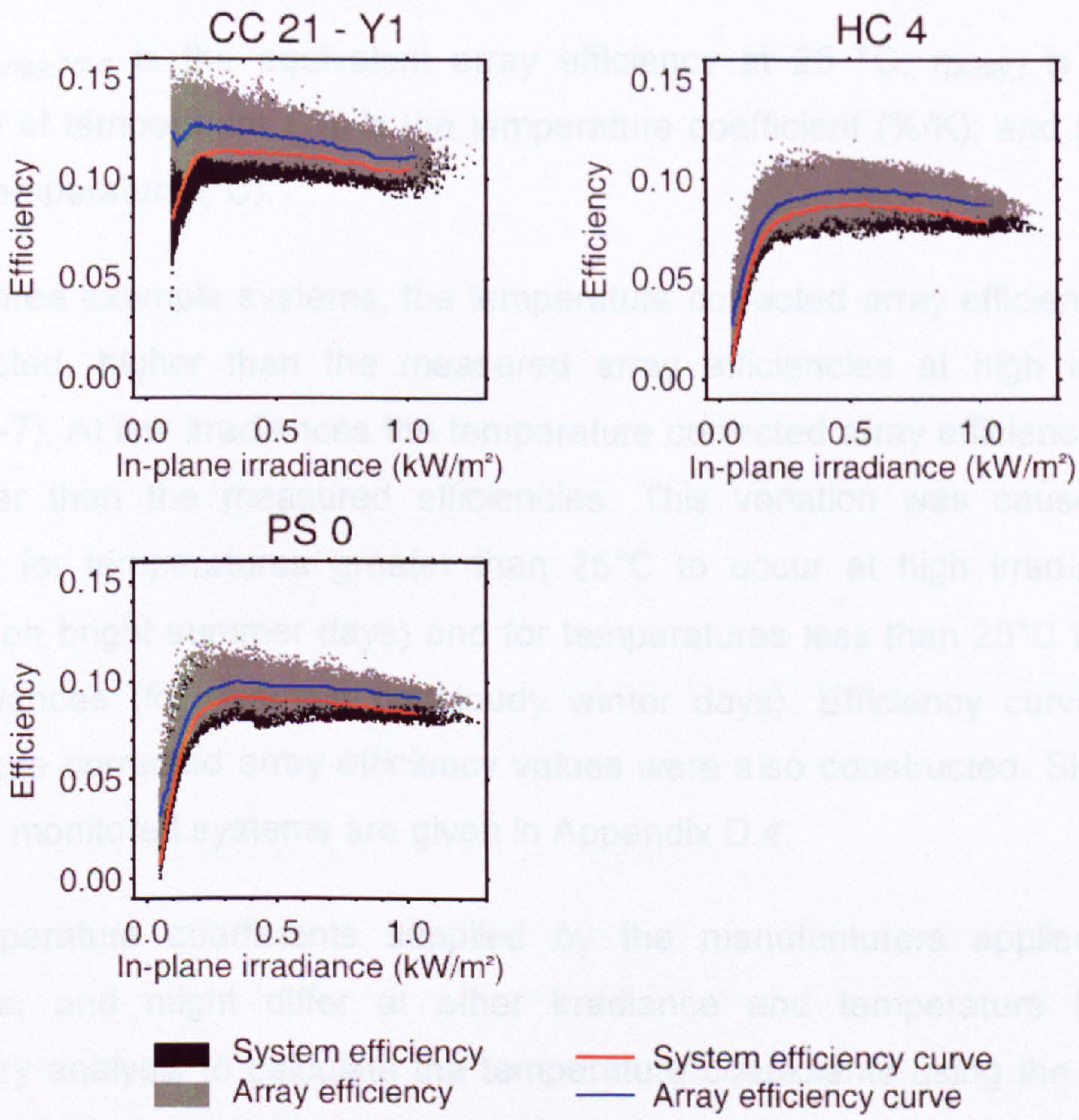

Figure 6-6: System efficiency and array efficiency to irradiance relationships for selected systems.

6.2.6 Temperature correction

The array efficiency values were temperature corrected to exclude the effect of temperature from the data and to allow the investigation of the other operational losses. The same approach was taken as used in other studies (for example Oozeki et al., 2003; Kiefer et al., 1995) in which the array efficiencies were corrected to an equivalent value at 25°C. The temperature coefficients supplied by the manufacturers (Table 6-2) were used in the temperature correction calculations. Although the PV module temperature measurements were only made for one array at Corncroft and Panmure Street and for two arrays at Heron Close (Table 3-7), these measurements were used for the temperature correction of all the systems on each site. The temperature correction of the array efficiency values was carried out using the following formula:

$$\eta_{array,25^\circ C} = \eta_{array,t} \times \alpha_t (t - 25)$$

where $\eta_{array,25^\circ C}$ is the equivalent array efficiency at 25 °C, $\eta_{array,t}$ is the array efficiency at temperature t, α_t is the temperature coefficient (%/K); and t is the PV module temperature (°C).

For the three example systems, the temperature corrected array efficiencies were, as expected, higher than the measured array efficiencies at high irradiances (Figure 6-7). At low irradiances the temperature corrected array efficiencies were a little lower than the measured efficiencies. This variation was caused by the tendency for temperatures greater than 25°C to occur at high irradiances (for example on bright summer days) and for temperatures less than 25°C to occur at low irradiances (for example on cloudy winter days). Efficiency curves for the temperature corrected array efficiency values were also constructed. Similar plots for all the monitored systems are given in Appendix D.4.

The temperature coefficients supplied by the manufacturers applied at STC conditions, and might differ at other irradiance and temperature levels. An exploratory analysis to calculate the temperature coefficients using the monitored data was attempted and this is discussed in Appendix D.5.

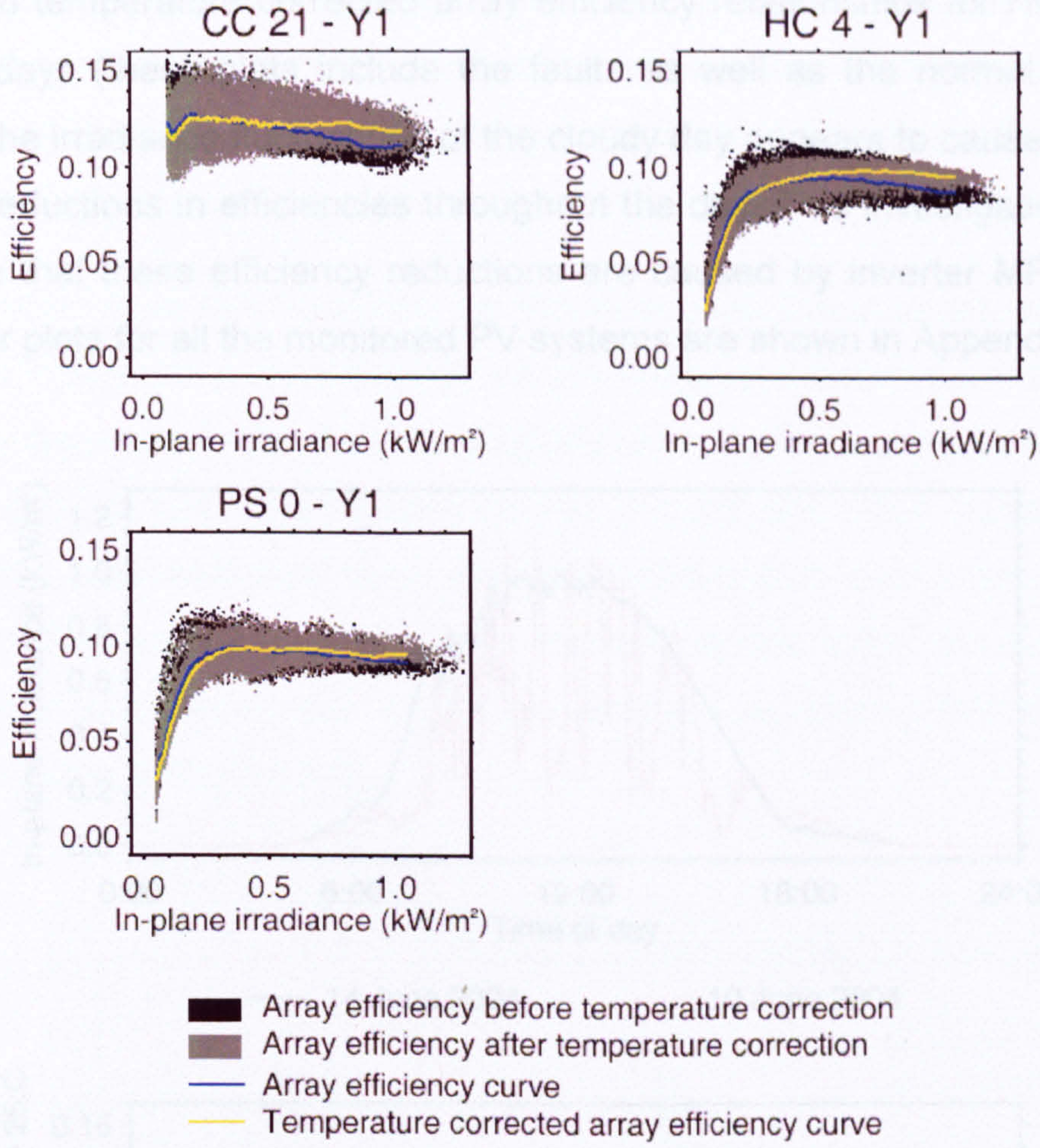

Figure 6-7: Irradiance to array efficiency relationships for selected systems before and after temperature correction

6.2.7 Inverter maximum power point tracking

The temperature corrected array efficiencies showed a cloud of points when plotted against in-plane irradiance (Figure 6-7). The main reason for the variation in efficiency at similar irradiance levels was assumed to be the losses caused by inverter MPP tracking. This assumption was checked by investigating the efficiencies on a clear day (with no passing cloud) and a cloudy day (with passing cloud and large fluctuations in irradiance). It was expected that inverter MPP tracking loss would be minimal on the clear day and significant on the cloudy day, due to the changes in the inverter MPP voltage that occur during times of irradiance fluctuations (as described Section 6.1.6). For the Heron Close site, 14^{th} June 2004 was identified as a clear day and 10^{th} June 2004 as a cloudy day. A plot of time of day against in-plane irradiance for the two days clearly shows the passing clouds cause large irradiance fluctuations (Figure 6-8). A plot of the irradiance to temperature corrected array efficiency relationships for HC 4 on the same two days (these plots include the faults as well as the normal operation) show how the irradiance fluctuations of the cloudy day appears to cause both large and small reductions in efficiencies throughout the day. This investigation is taken to conclude that these efficiency reductions are caused by inverter MPP tracking loss. Similar plots for all the monitored PV systems are shown in Appendix D.6.

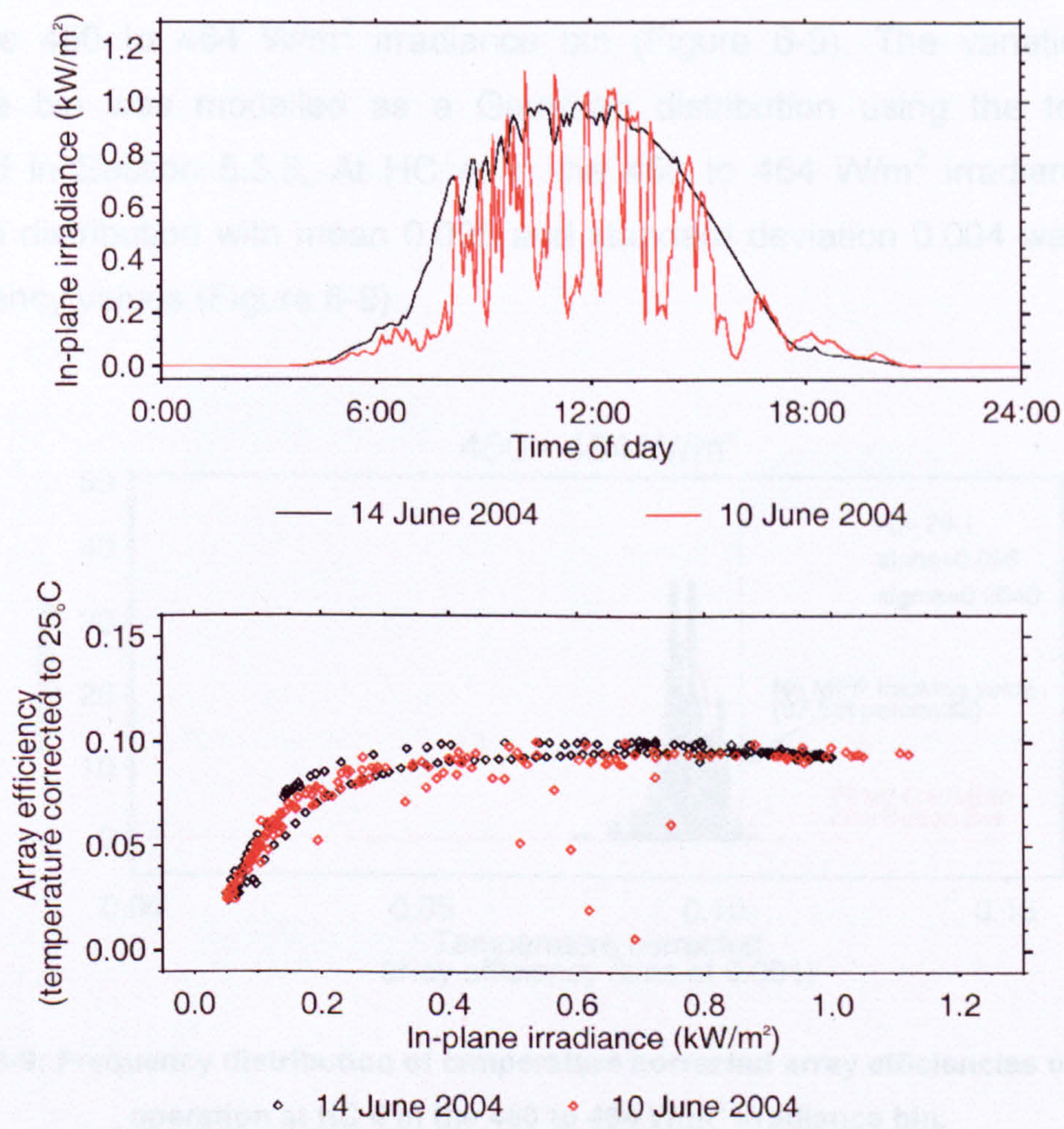

Figure 6-8: Time of day against in-plane irradiance for Heron Close on a clear and cloudy day and irradiance to efficiency for HC 4 on the same days.

On the clear day there is a noticeable effect of two distinct curves of efficiency values. The higher curve occurs before midday and the lower curve after midday. The reasons for this variation in efficiency are not clear but are thought to be either caused by thermal mismatch (Section 6.1.8), inaccuracies in the temperature correction procedure (Section 6.2.6) or inaccuracies in the temperature measurements. As only one PV module temperature measurement is made for each orientation of PV arrays on each site, it is difficult to determine the cause of the variation seen on clear days. For this reason it is assumed that the variation seen in the temperature corrected efficiency values are caused solely by inverter MPP tracking in the remainder of the analysis in this work.

The effect of inverter MPP tracking on efficiency was investigated by analysing temperature corrected array efficiency values separated into the irradiance bins. Taking HC 4 as an example, there was significant variation in the efficiency values within the 450 to 464 W/m^2 irradiance bin (Figure 6-9). The variation in the irradiance bin was modelled as a Gaussian distribution using the techniques described in Section 5.3.3. At HC 4, in the 450 to 464 W/m^2 irradiance bin, a Gaussian distribution with mean 0.095 and standard deviation 0.004 was fitted to the efficiency values (Figure 6-9).

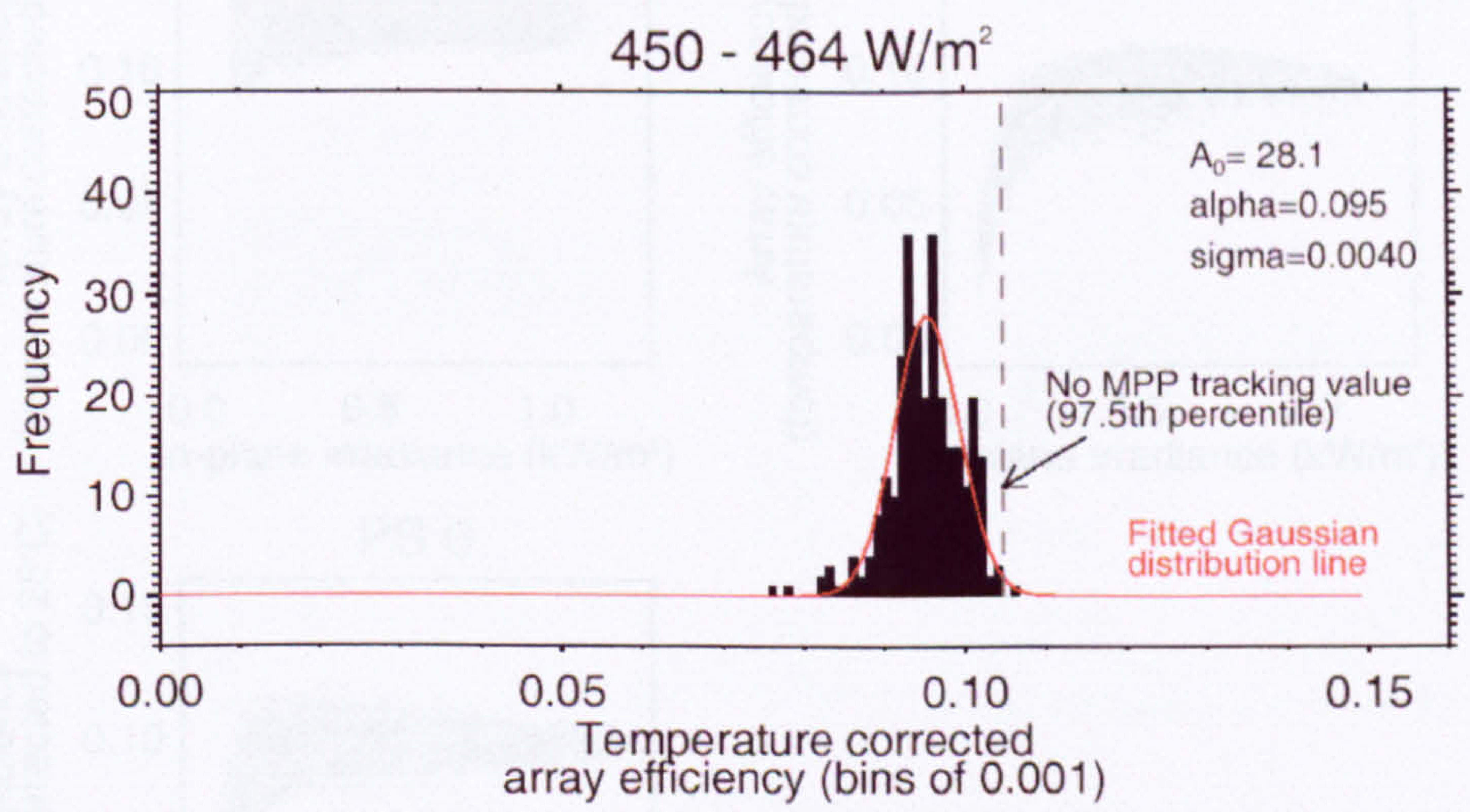

Figure 6-9: Frequency distribution of temperature corrected array efficiencies of normal operation at HC 4 in the 450 to 464 W/m^2 irradiance bin.

The value of efficiency at which no inverter MPP tracking losses occurred was defined as the *no MPP tracking value*. If the variation in efficiency within the irradiance bin was caused by inverter MPP tracking, then the no MPP tracking efficiency would lie at the right hand side of the efficiency distribution (Figure 6-9). Theoretically the maximum efficiency value in each bin should represent the no MPP tracking value. However in the monitored data there were occasional examples of efficiencies which were significantly higher than the rest of the values. It was assumed that these unusual high values could be caused by measurement error and thus not used to estimate the no MPP tracking value. To overcome this problem, the no MPP tracking value was calculated as the 97.5th percentile of the fitted Gaussian distributions for each irradiance bin.

The no MPP tracking values were used to construct curves for each PV systems which represented the temperature corrected array efficiency values with zero inverter MPP tracking losses. These curves are defined as *no MPP tracking efficiency curves*. For the three example PV systems, the efficiency to irradiance plots show that the no MPP tracking efficiency curves follow the upper boundary of the cloud of temperature corrected array efficiency values. Similar plots for all the monitored PV systems are given in Appendix D.7.

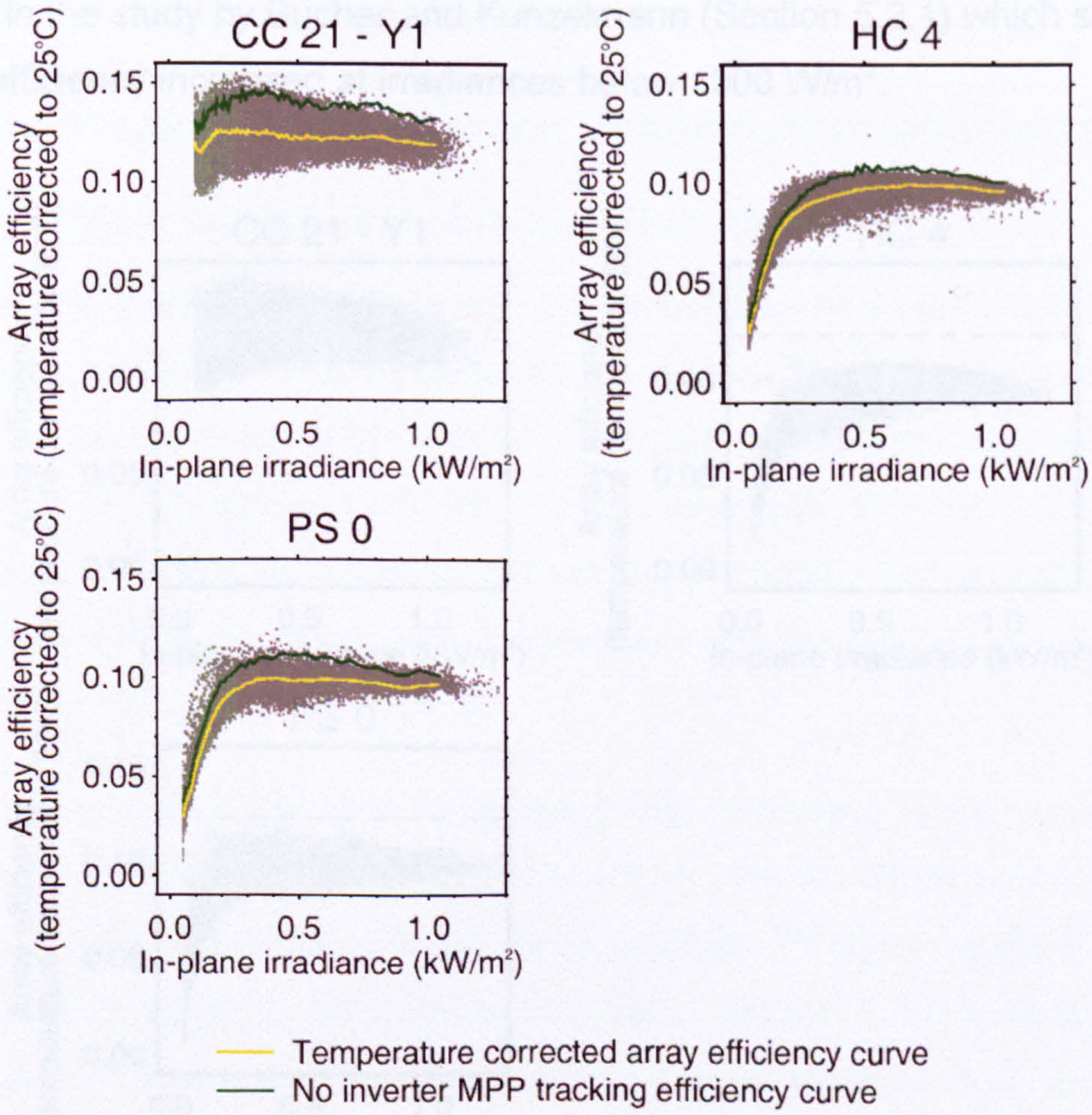

Figure 6-10: Irradiance to temperature corrected array efficiency relationships for selected systems showing the no MPP tracking curves.

6.2.8 Irradiance, mismatch and deviation from STC

Irradiance loss was investigated by considering the difference between the variation of efficiency with irradiance and the value of efficiency at an irradiance of 1000 W/m^2 (the irradiance level of STC). In this analysis the temperature corrected array efficiencies with no inverter MPP tracking loss were used, as described by the no inverter MPP tracking efficiency curves (Figure 6-10). The values of these efficiencies at 1000 W/m^2 was determined for each monitored PV system.

For the three example PV systems, the efficiency values at irradiance of 1000 W/m^2 were plotted on the irradiance to efficiency plots (Figure 6-11). The 1000 W/m^2 efficiency value is shown as a straight line, as its value is assumed constant over all irradiance levels. In all three systems the no MPP tracking efficiencies became slightly higher than the 1000 W/m^2 value at irradiance below 1000 W/m^2 before decreasing sharply at low irradiance. Such a result has previously been reported in the study by Bucher and Kunzelmann (Section 5.2.1) which showed PV module efficiency increased at irradiances below 1000 W/m^2.

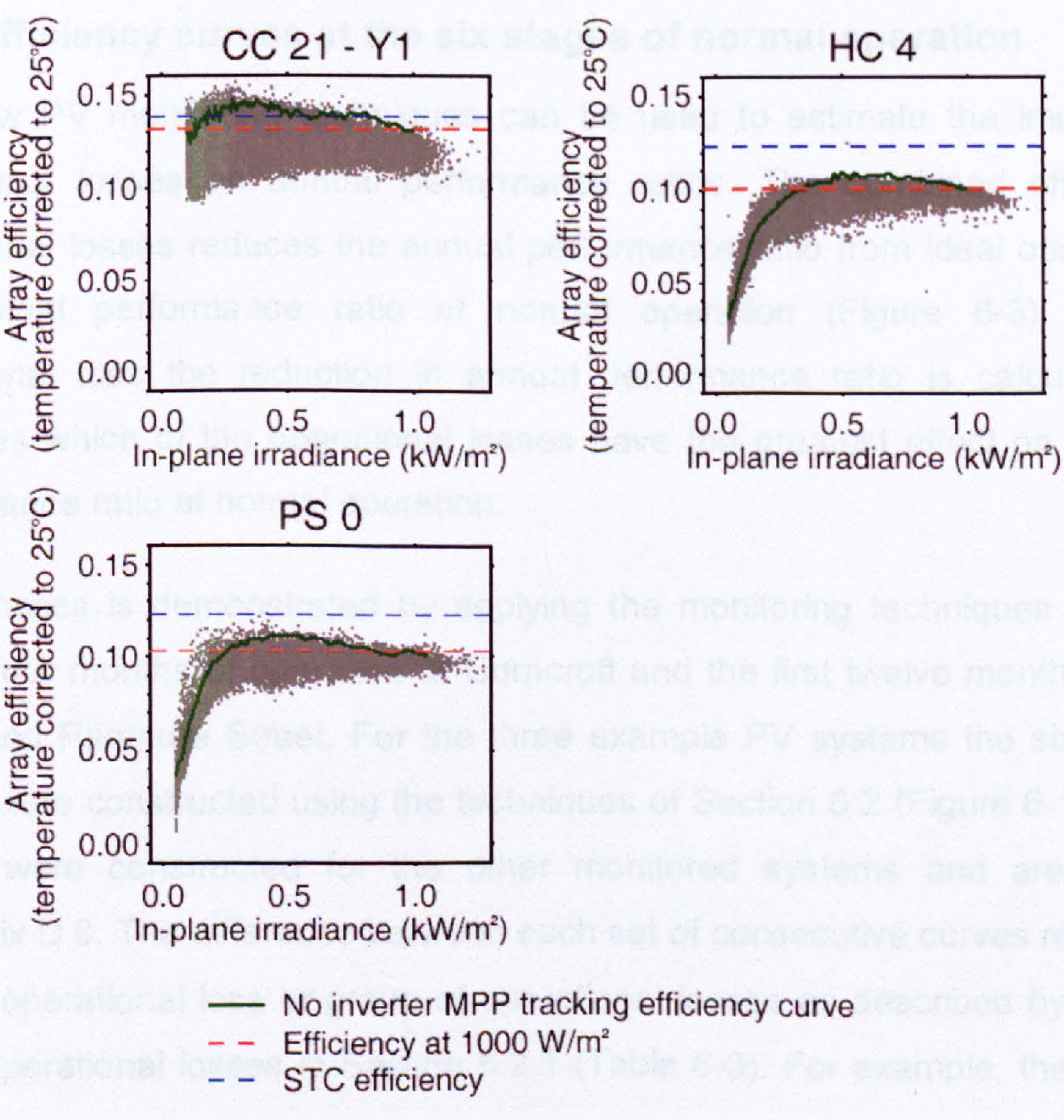

Figure 6-11: Irradiance to temperature corrected array efficiency relationships for selected systems

The STC efficiency, the rated efficiency of the PV modules, is also shown on the irradiance to efficiency plots as a constant value over all levels of irradiance (Figure 6-11). The difference between the STC efficiency and the efficiency at 1000 W/m^2 represents the mismatch loss and deviation from STC loss (Figure 6-3). More detailed measurements would be required to separate these losses and in this analysis the combined effects of mismatch and deviation from STC were considered.

At CC 21 there were temperature corrected array efficiency values higher than the STC efficiency for irradiances from 100 W/m^2 to around 700 W/m^2. This suggested a possible error in the efficiency values as it was unlikely that that the recorded efficiencies would rise above the rated efficiency of the PV modules. This observation is discussed further in Section 6.3.4.

6.3. Application and evaluation of monitoring techniques

6.3.1 Efficiency curves at the six stages of normal operation

The new PV monitoring techniques can be used to estimate the impact of the operational losses on annual performance ratios. The combined effect of the operational losses reduces the annual performance ratio from ideal operation[23] to the annual performance ratio at normal operation (Figure 6-3). For each operational loss the reduction in annual performance ratio is calculated. This illustrates which of the operational losses have the greatest effect on the annual performance ratio at normal operation.

This process is demonstrated by applying the monitoring techniques to the first twenty four months of operation at Corncroft and the first twelve months at Heron Close and Panmure Street. For the three example PV systems the six efficiency curves were constructed using the techniques of Section 6.2 (Figure 6-12). Similar curves were constructed for the other monitored systems and are shown in Appendix D.8. The difference between each set of consecutive curves represents a distinct operational loss or group of operational losses as described by the model of the operational losses in Section 6.2.1 (Table 6-3). For example, the difference

[23] By definition the annual performance ratio at ideal operation is unity for all PV systems

between efficiency at no MPP tracking efficiency curve and efficiency at temperature corrected array efficiency curve is taken to be the reduction in efficiency due to inverter MPP tracking.

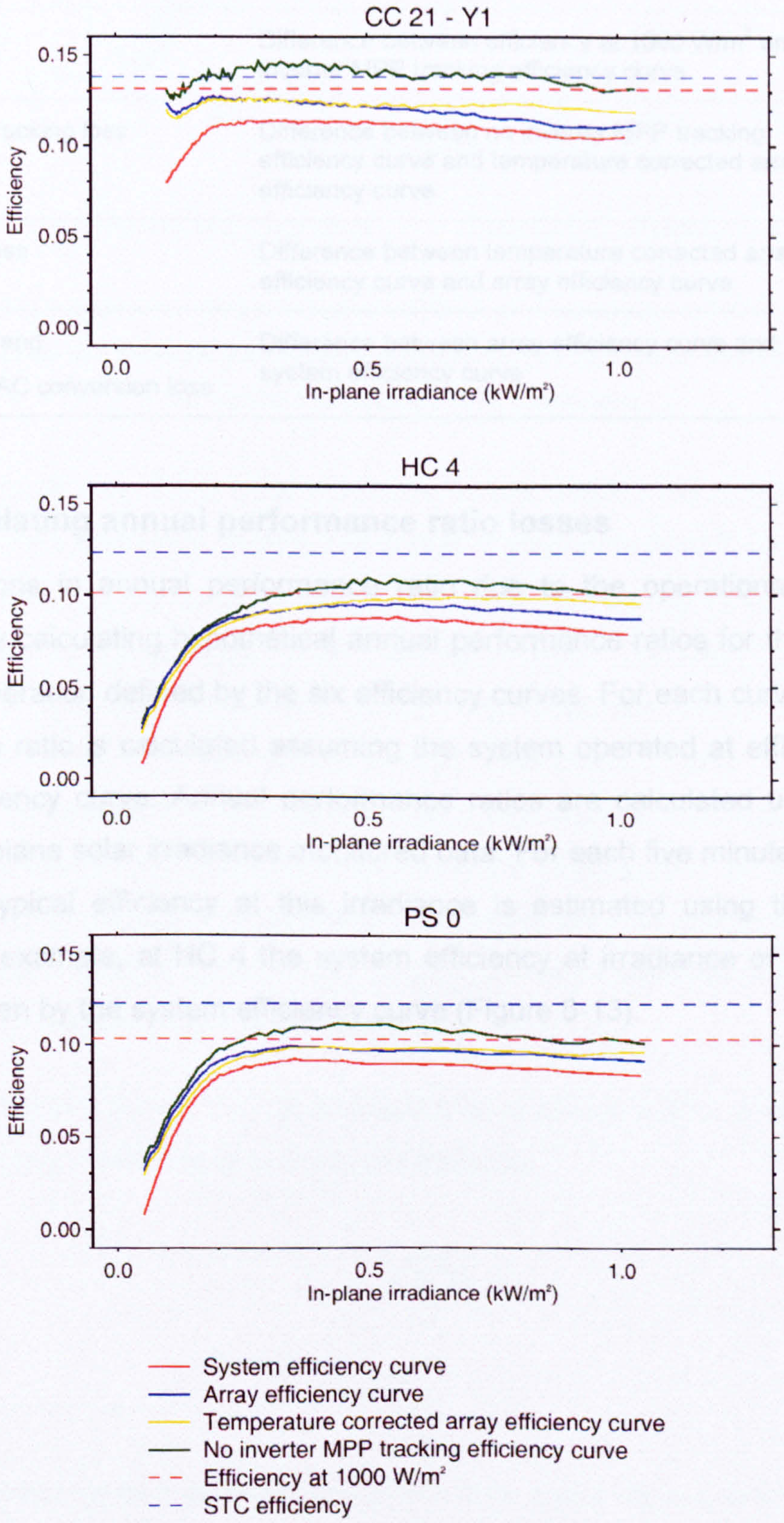

Figure 6-12: Efficiency curves describing normal operation for selected systems

Table 6-3: Graphical definition of operational losses

Operational loss	Described by:
Mismatch and deviation from STC	Difference between STC efficiency and efficiency at 1000 W/m^2
Irradiance loss	Difference between efficiency at 1000 W/m^2 and no inverter MPP tracking efficiency curve
Inverter MPP tracking loss	Difference between no inverter MPP tracking efficiency curve and temperature corrected array efficiency curve
Temperature loss	Difference between temperature corrected array efficiency curve and array efficiency curve
DC wiring loss and inverter DC to AC conversion loss	Difference between array efficiency curve and system efficiency curve

6.3.2 Calculating annual performance ratio losses

The reductions in annual performance ratio due to the operational losses are estimated by calculating hypothetical annual performance ratios for the six stages of normal operation defined by the six efficiency curves. For each curve the annual performance ratio is calculated assuming the system operated at efficiency given by the efficiency curve. Annual performance ratios are calculated using the five minutely in-plane solar irradiance monitored data. For each five minutely irradiance value, the typical efficiency at this irradiance is estimated using the efficiency curves. For example, at HC 4 the system efficiency at irradiance of 600 W/m^2 is 0.087 as given by the system efficiency curve (Figure 6-13).

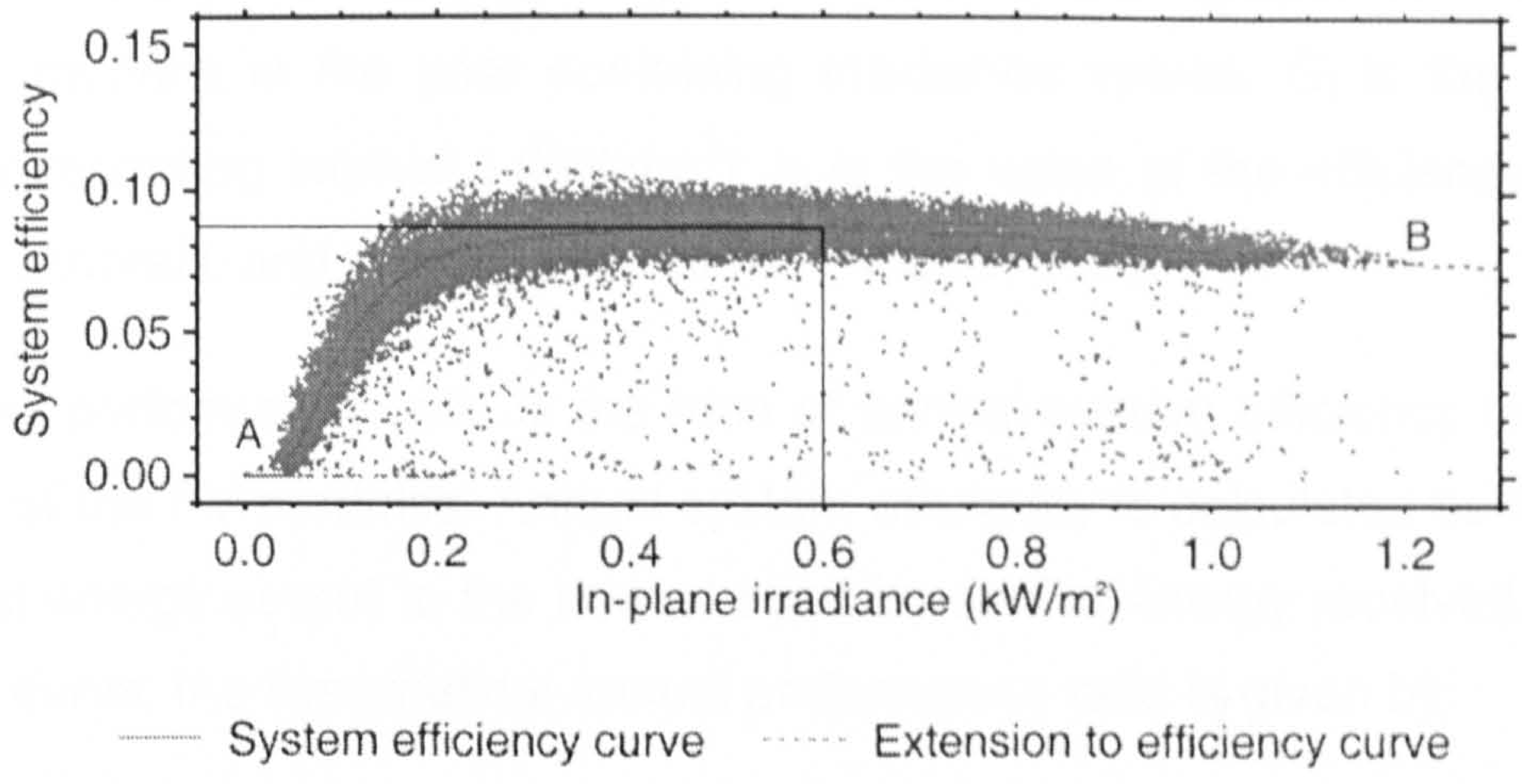

Figure 6-13: In-plane irradiance to system efficiency relationship at HC 4. The system efficiency curve, the value of the system efficiency curve at 600 W/m^2 and the extension to the system efficiency curve are shown.

In the monitored data there were irradiance values outside the range of irradiance described by the efficiency curves. The range of irradiance described by the curves is from 50 W/m^2 (at Heron Close and Panmure Street) or 100 W/m^2 (at Corncroft) up to a maximum irradiance value (usually around 1000 W/m^2). To estimate efficiency for recorded irradiances outside this range the efficiency curves are extended to cover very low and very high irradiances (Figure 6-13). For low irradiances, a straight line is fitted from zero efficiency at zero irradiance to the efficiency curve at its minimum irradiance (line A on the figure)[24]. At high irradiance the efficiency curves are extended using a straight line with gradient equal to that of a straight line fitted to the efficiency values between irradiance of 600 W/m^2 and the maximum irradiance (line B in the figure).

For each efficiency curve, the hypothetical annual energy output is estimated from the five minutely irradiance data using the equation:

$$E_G = A\sum_{i=1}^{n} G_i \eta_i$$

[24] There is an abrupt change in gradient in the extension of the system efficiency curve at low irradiance. However this is considered to have a minimal impact on the calculated annual energy yields as energy generation at such low irradiance is minimal.

where E_G is the annual energy output (kWh); n is the number of five minutely recording intervals in the year containing irradiance values; G_i is the irradiation energy for recording interval i (kWh/m^2); η_i is the value of the efficiency curve for recording interval i; and A is the area of the PV array (m^2).

The annual performance ratio is the ratio of annual system efficiency to the rated efficiency of the PV modules. Annual system efficiency is calculated as the ratio of the annual energy output to the annual solar irradiation energy received. For each efficiency curve, the hypothetical annual performance ratio is given by:

$$PR = \frac{E_G / G_I}{\eta_{STC}}$$

where PR is the annual performance ratio; G_I is the annual solar in-plane irradiation (kWh/m^2); and η_{STC} is the rated efficiency of the PV modules.

As an example, the hypothetical annual performance ratios were calculated for the first year of operation at HC 4 (Table 6-4). The area of the PV array was 11.7 m^2, the annual in-plane solar irradiation was 895 kWh/m^2 and the rated efficiency of the PV modules was 0.123. The reduction in annual performance ratio due to the operational losses is given by the difference between hypothetical annual performance ratios of consecutive efficiency curves (as defined in Table 6-3). The annual operational losses were calculated as (expressed in annual performance ratio percent): mismatch and deviation from STC losses 18.1%; irradiance loss 5.8%, inverter MPP tracking loss 5.6%, temperature loss 2.0%; and the combined DC wiring and inverter conversion loss 6.8%. The annual performance ratio loss due to DC wiring was calculated separately as 0.1% (based on the calculation of power loss in the DC cables described in Section 6.2.4) and this gives the inverter DC to AC conversion loss as 6.7%.

Table 6-4: Annual energy outputs and performance ratios for the different stages of normal operation at HC 4

Efficiency curve used	Annual energy output (kWh)	Annual performance ratio (%)
STC efficiency	895	100.0
Efficiency at 1000 W/m^2	733	81.9
No inverter MPP tracking efficiency curve	681	76.1
Temperature corrected array efficiency curve	631	70.5
Array efficiency curve	613	68.5
System efficiency curve	552	61.7

This process was repeated for the first and second year of operation at Corncroft and the first year of operation at Heron Close and Panmure Street (Table 6-5). For each category of operational loss the mean value, standard deviation and range (minimum value to maximum value) of performance ratio loss is shown and all values are in performance ratio percent. For example, an annual loss calculated as 5 performance ratio percent could represent a reduction in annual performance ratio from 80% to 75%. The sum of the operational losses is equal to the difference between annual performance ratio at ideal operation (100%) and annual performance ratio at normal operation. Full results for each system are given in Appendix D.9.

Table 6-5: Estimated reductions in annual performance ratio during normal operation

Site	Mismatch and deviation from STC loss	Irradiance loss	Inverter MPP tracking loss	Temperature loss	DC wiring loss	Inverter DC to AC conversion loss	Annual performance ratio of normal operation
	Loss in annual performance ratio (in performance ratio percent)						(%)
	Average; *(standard deviation)*; range – minimum to maximum						
Corncroft	3.7	-4.1	12.6	2.0	0.1	8.2	77.6
Year 1	*(1.3)*	*(1.6)*	*(0.8)*	*(0.2)*	*(0.0)*	*(0.3)*	*(2.4)*
(22 systems)	1.3 to 7.2	-6.4 to -0.3	10.7 to 14.6	1.6 to 2.5	0.1 to 0.1	7.5 to 8.6	71.8 to 81.5
Corncroft	5.4	-4.4	12.1	2.0	0.1	7.9	76.9
Year 2	*(1.2)*	*(2.2)*	*(1.0)*	*(0.6)*	*(0.0)*	*(0.3)*	*(2.1)*
(22 systems)	2.7 to 7.2	-8.1 to 1.7	9.6 to 14.6	-0.5 to 2.7	0.1 to 0.1	7.2 to 8.4	72.9 to 80.8
Heron Close	12.4	8.3	6.0	2.0	0.1	7.0	64.2
Year 1	*(5.0)*	*(2.1)*	*(0.4)*	*(0.2)*	*(0.0)*	*(0.3)*	*(2.5)*
(3 systems)	8.5 to 18.1	5.9 to 9.9	5.6 to 6.3	1.8 to 2.3	0.1 to 0.1	6.8 to 7.3	61.6 to 66.5
Panmure Street	14.3	6.7	8.0	-0.3	0.1	7.2	64.1
Year 1	*(2.0)*	*(1.9)*	*(1.3)*	*(0.6)*	*(0.0)*	*(0.2)*	*(2.4)*
(12 systems)	11.0 to 16.8	3.9 to 11.2	5.9 to 10.0	-1.9 to 0.4	0.1 to 0.2	6.6 to 7.4	59.2 to 67.1

6.3.3 Evaluation of the monitoring techniques

An evaluation of the PV monitoring techniques is made by checking the plausibility of the annual results. The annual performance ratio losses for the monitored PV systems at Corncroft, Heron Close and Panmure Street were compared with the annual performance ratio losses calculated in four previous energy loss studies discussed in Section 2.3.1 (Table 6-6).

Table 6-6: Annual average performance ratio losses compared to results from previous studies

Operational loss	Previous studies (Table 2-4)				Average results from this study [2] (Table 6-5)			
	SV Method[1] (Oozeki et al., 2003)	TEAMS (Reinders et al., 1999)	Data Analysis (Baltus et al., 1998)	German 1000 Roofs programme (Kiefer et al., 1995)	Corncroft Year 1	Corncroft Year 2	Heron Close	Panmure Street
	Loss in performance ratio (in performance ratio percent)							
Deviation from STC	9	5.7	-	0.3	3.7	5.4	12.4	14.3
Mismatch	-	[3]	[4]	4.4				
Irradiance	-	11.8	5.8	3.7	-4.1	-4.4	8.3	6.7
Inverter maximum power point (MPP) tracking	9	1.5	[4]	1.2	12.6	12.1	6.0	8.0
Temperature	4	6.1	2.4	3.3	2.0	2.0	2.0	-0.3
DC wiring	-	[3]	0.9	-	0.1	0.1	0.1	0.1
Inverter DC-AC conversion	6	12.1	4.8	9.3	8.2	7.9	7.0	7.2

[1] Values shown for the SV Method are the average values for 421 systems

[2] Values shown for Corncroft, Heron Close and Panmure Street are average values for each site

[3] In the TEAMS method the mismatch and DC wiring loss are given as a combined total of 3.9%

[4] In the Data Analysis method, the mismatch and inverter MPP tracking losses are given as a combined total of 16.3%

There was a large difference between the average annual deviation from STC and mismatch losses at Corncroft (3.7% and 5.4%) compared to Heron Close (12.4%) and Panmure Street (14.3%). The Corncroft losses were comparable to the TEAMS study (5.7%) and the German 1000 Roofs study (4.7%). The losses at Heron Close and Panmure Street were higher than maximum reported by the previous studies (9% by the SV Method study).

Average annual irradiance losses at Heron Close and Panmure Street (8.3% and 6.7%) were comparable with the previous studies (from 3.7% to 11.8%). The average annual irradiance losses at Corncroft were calculated as negative values (-4.1% and -4.4%). This suggested a problem with the monitoring techniques as all the other reported values were positive.

At Corncroft the average annual inverter MPP tracking losses (12.6% and 12.1%) were higher than Heron Close (6.0%) and Panmure Street (8.0%). These values compared well with the values of the SV Method study (9%) and the Data Analysis study (16.3%, which included mismatch losses). The TEAMS study and the German 1000 Roofs study estimated annual inverter MPP tracking loss at values significantly lower (1.2% and 1.5%). These two studies used simulation models of inverter MPP tracking, rather than data analysis techniques, which may account for the difference. The study by Infield et al. reported MPP tracking efficiencies from 70% to 98% (Section 6.1.6). The tracking efficiencies at the PV sites can be calculated from the annual average performance ratio losses and range from 87.5% to 92.4% which compares well with the study.

The average annual temperature losses at Corncroft and Heron Close (all at 2.0%) were slightly lower than in the previous studies (from 2.4% to 6.1%). This effect could be caused by the colder climate of the UK. Panmure Street had a negative annual average temperature loss (-0.3%) and may be caused by the low temperatures at the Panmure Street site. In a study of an Austrian PV system Nordmann and Clavadetscher (Nordmann and Clavadetscher, 2003) showed that negative temperature loss of -2.1% occurred due to conditions of low ambient air temperatures.

The average annual DC wiring losses at the PV sites (all at 0.1%) were lower than the value suggested by the Data Analysis study (0.9%). Average annual inverter DC to AC conversion losses at Corncroft (8.2% and 7.9%) were slightly higher than Heron Close (7.0%) and Panmure Street (7.2%). This may be caused by the oversized inverters at Corncroft. The calculated values were within the range of inverter conversion loss in previous studies (4.8% to 12.1%).

This comparison suggests that the new PV monitoring techniques are providing reasonable and realistic values of annual performance ratio losses for the majority of the operational losses. The techniques are more comprehensive than previous studies and, with the exception of the deviation from STC and mismatch losses, they provide more detail on the effects of individual losses. The irradiance losses at Corncroft appeared to be in error which suggests a problem in the monitoring techniques. This is discussed further in the next section.

6.3.4 Limitations of the monitoring techniques

At Corncroft the calculated annual irradiance losses were negative and significantly lower than the results of previous studies and the calculated values at Heron Close and Panmure Street. The source of this problem was first seen during the development of the monitoring techniques when it was noted that at Corncroft there were recorded efficiencies higher than the rated efficiencies of the PV modules (Section 6.2.8). The high efficiencies occur at irradiances below around 700 W/m^2. It is these high efficiency values which cause the negative annual irradiance losses as the hypothetical annual energy generated at the no inverter MPP tracking efficiency curve (constructed using the high efficiencies) is greater that the hypothetical annual energy generated at constant efficiency at 1000 W/m^2.

This illustrates a weakness of the monitoring techniques: the techniques rely on high measurement accuracy in the monitored data. It is believed that the high efficiency values recorded at Corncroft are caused by measurement inaccuracy in the DC power measurements. The PV installation company for Corncroft have studied the DC power measurements at a site similar to Corncroft and found that measurements made with separate energy meters produce different results to measurements made by the inverter (Kreutzer, 2006). The measurements made by the separate meter produce a narrower cloud of points on the irradiance to efficiency plots with a smaller spread in efficiency within specific irradiance bins. This suggests the DC power measurements at Corncroft may be recorded as higher or lower than their true value at certain times. The measurement error at Corncroft may be due to the oversized inverters at the site which operate at a low percentage of their rated power for long time periods and the in-built DC power sensors at very lower powers may be inaccurate. The slow sampling time used by the monitoring system at Corncroft may also influence the measurement accuracy of the DC power.

A further possibility which could explain the inaccuracy in the DC power measurements at Corncroft is that, due to the step change in power levels at low irradiance observed in Section 4.2.3, the Corncroft DC power measurements are recorded at 100 W above their true value. An exploratory analysis to investigate this possibility is discussed in Appendix D.10 and concludes that an on-site check and calibration of both the DC and AC power measurements at Corncroft is highly recommended.

Another limitation of the monitoring techniques is that they rely on the efficiency measurements at irradiance of 1000 W/m^2 to estimate the operational losses. However if inverter derating reduced the efficiency values at this irradiance then the present techniques could not be applied. Significant inverter power derating caused difficulties with the analysis and two Heron Close systems were excluded from the analysis due to inverter derating (Section 6.2.2).

6.4. Summary

New PV monitoring techniques have been developed to analyse the normal operation of PV systems. The techniques construct a series of six efficiency curves based on five minutely monitored performance data. These curves have been used to calculate the annual performance ratio losses caused by the operational losses.

The monitoring techniques were applied to the monitored data from the Corncroft, Heron Close and Panmure Street sites and annual losses in performance ratio were calculated. The results were compared to previous studies and the monitoring techniques were shown to produce estimates comparable to the previously reported values. One exception was the annual irradiation losses at Corncroft which were calculated as negative values. This problem was investigated and it was concluded that measurement inaccuracy of the DC power at Corncroft was the cause of this unrealistic result. The limitations of the new monitoring techniques are discussed.

The annual results showed that all the monitored systems had the potential to perform well, within a range of around 60% to 80% in annual performance ratio at normal operation. In reality, many of the systems suffered from faults which reduced their performance. New techniques to identify the faults, based on the five minutely monitored data, are discussed in the next chapter.

7. Faults in PV Systems

This chapter introduces new techniques to identify faults in PV systems based on the five minutely performance data described in Chapter 4. Faults were defined as low operational efficiencies which could not be explained by normal operation and were detected using the Gaussian distribution techniques demonstrated in Chapter 5. The different types of faults considered were listed in Chapter 2 and a literature review of each fault is presented in this chapter. By studying the characteristics of the faults, and their impact on the five minutely efficiency values, new techniques for diagnosing faults have been developed. These techniques are illustrated throughout this chapter by reference to four example PV systems.

The high resolution monitored data meant that faults with short time periods (with a minimum duration of about five minutes) could be observed. If the recording interval had been half hourly or hourly, the short time period faults may not have been visible. Faults were detected by studying the efficiency to irradiance plots and identifying the data which was outside the bounds of normal operation. Three diagnostic techniques have been developed to identify the faults. The first technique identified faults with zero efficiency, when power output stopped completely during operation. The second technique identified shading based on the positions of the sun throughout the year. The shading analysis relied solely on the five minutely interval data and did not require any knowledge of the site layout or the shading objects. Thirdly, any remaining faults which were not identified as zero efficiency or shading faults were attributed to inverter MPP tracking failure.

The amount of energy lost due to each type of fault has been calculated and the results used to assess the effects of the faults on the annual performance of the PV systems. Conclusions have been drawn on the presence and impact of faults in the monitored PV systems and recommendations are made to minimise faults in future projects.

7.1. Review of faults

7.1.1 Types of faults

The five types of fault considered in this study (listed in Section 2.2.2) were: component failure; inverter shutdown; system isolation; shading; and inverter MPP tracking failure. Three diagnostic methods were used to identify these faults: i) zero efficiency faults, ii) shaded faults and iii) non-zero efficiency non-shaded faults (Table 7-1). The zero efficiency faults were investigated further by studying the duration of the faults. A zero efficiency fault that was sustained over a long time period (i.e. a day or more) was identified as component failure or system isolation. Brief zero efficiency faults were identified as inverter shutdown, system isolation or extreme cases of shading or inverter MPP tracking.

Table 7-1: Fault diagnostic methods

Name of diagnostic method	Faults identified		Diagnostic method
Zero efficiency faults	Sustained faults	Component failure System isolation	Identify faults with zero efficiency (no power output) and long time periods
	Brief faults	Inverter shutdown System isolation Extreme shading or MPP tracking	Identify faults with zero efficiency (no power output) and short time periods
Shading faults	Shading		Identify faults based on the sun positions when the faults occur
Non-zero efficiency non-shaded faults	Inverter MPP tracking failure Other faults		The faults remaining after the zero efficiency and shading faults have been isolated.

Normal operation was defined in Section 2.2.1 as the operation of a well designed PV system with no faults occurring. The system efficiency curves developed in Section 5.4.2 predict the average efficiency at normal operation for different irradiance levels. The effect of the faults can be described as the reduction in efficiency from normal operation to the actual measured efficiency (Figure 7-1). To simplify the fault analysis, it was assumed that only a single type of fault could occur in each five minute recording period. For example, a fault detected in a five minute recording interval could be identified as either shading or a non-zero efficiency non-shaded fault, but not as a combination of the two. Descriptions and a review of the literature for each type of fault are presented below.

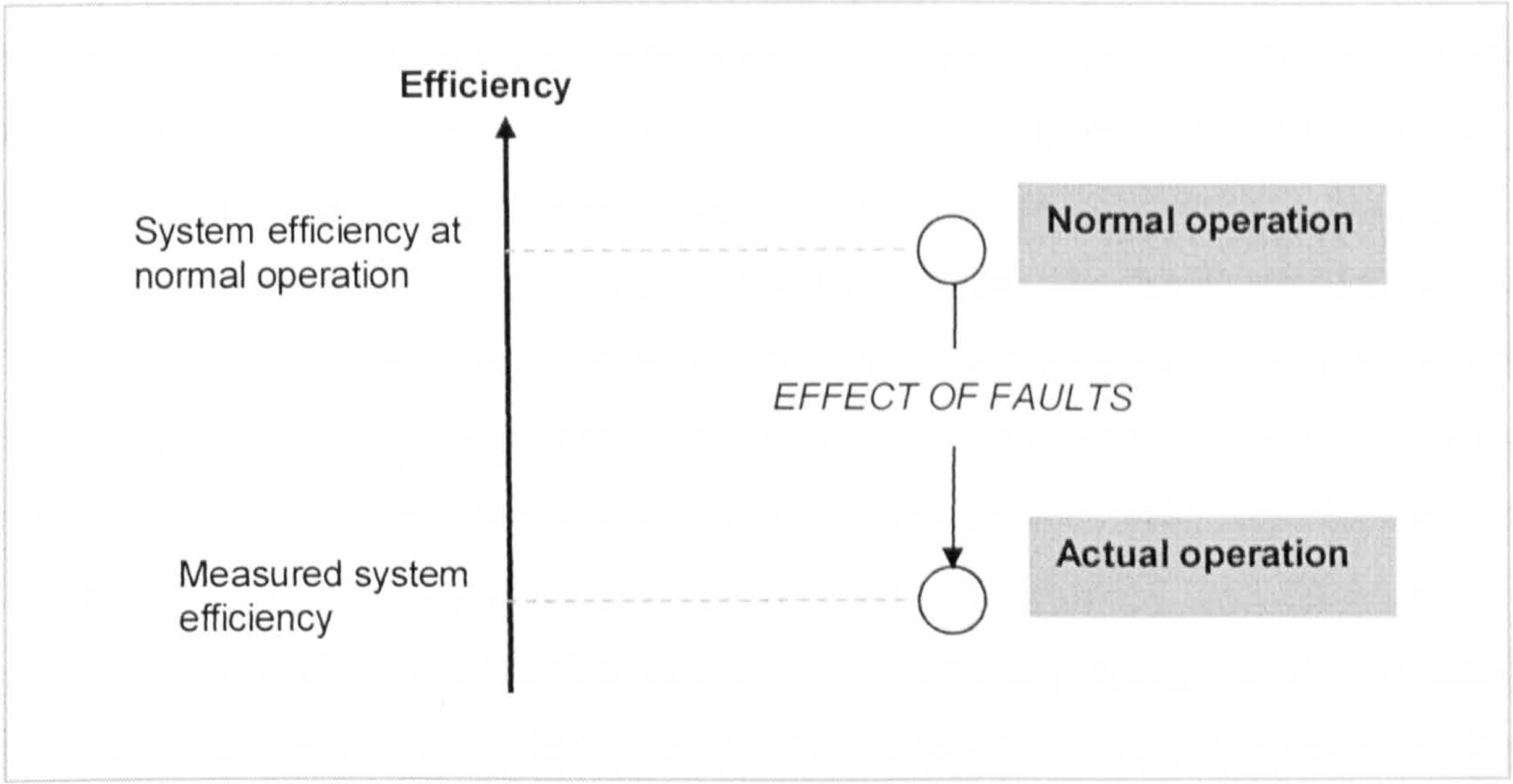

Figure 7-1: Schematic diagram of reduction in efficiency due to faults

7.1.2 Component failure

Failure of a component in a PV system which results in a complete stop in electricity generation is defined as *component failure*. The components of the monitored PV systems are subject to occasional failure and in such cases maintenance work or replacement of the component is usually required. Reasons for component failure are: a failure in the PV modules; a malfunction of the inverter; a break in the continuity of the DC or AC cabling; and failure in the other balance of system components. Component failure is likely to cause long periods of zero power output due to the time taken between the failure occurring and the maintenance work being carried out.

7.1.3 System isolation

System isolation is defined as times when a PV system is isolated from the mains electricity grid by the household consumer unit, the AC lockable isolator, AC spur or DC isolator (see Figure 3-4). Once isolated, the system would have zero power output. This fault occurs if the system is isolated for regular electrical maintenance work on the house. The system could also be automatically isolated by the household consumer unit. Whether the fault occurs for a short or long period of time depends on how soon the system is reconnected to the mains grid.

7.1.4 Inverter shutdown

The inverters have in-built safety procedures which shut down the inverter if necessary and stop all electricity generation. This type of fault is defined as *inverter shutdown* and had two main causes. If the inverter detects the loss of the AC mains electricity grid then shutdown occurs. This can be caused by a failure in the mains grid (a power cut) and prevents the PV system operating independently of the grid, a process known as *islanding*. The mains grid provides a stabilising effect on the voltage and frequency of the AC power output from the inverter and without this stabilising effect the output voltage or frequency can vary significantly. High voltages can lead to dangerous conditions within the building and damage to the electrical appliances. To avoid this situation inverters are designed only to operate if connected to the mains electricity grid. This safety feature is common to all grid connected inverters.

The inverters have a further safety feature which shuts down the inverter if the voltage of the mains electricity is too high or too low. The UK Engineering Recommendation G83/1 states that inverters must switch off if the mains voltage rises above 264 V (Energy Networks Association, 2006). At weak points in the mains electricity network, for example at the end of a low-voltage distribution line, the grid voltage can rise or fall significantly. Inverter shutdown is a precautionary measure as the PV systems themselves could be contributing to the change in voltage.

Like component failure and system isolation, inverter shutdown is indicated by zero power output being recorded during daylight hours. As inverter shutdown is caused by transient effects of the mains grid the faults are likely to be brief and, unless the auto-restart failed, not continue for many hours or days.

7.1.5 Shading

Shading reduces the amount of solar irradiation received by a PV array and thus lowers the system efficiency. The effect of shading is most pronounced during bright, clear conditions when external objects block the direct beam solar radiation[25]. In cloudy conditions with a high proportion of diffuse solar radiation[26] the effect of shading is reduced. Some PV arrays can be self-shading if the modules are in different planes (for example an array of tilted modules mounted in rows one behind the other). For most building integrated PV systems (including the systems in this study) the modules are in a single plane and shading is caused by surroundings object such as chimneys, stacks, aerials, other buildings, street furniture (for example signs or lamp posts) and trees.

A study by Kawamura et al. (Kawamura et al., 2003) showed the current and voltage behaviour of PV modules under shadow. Different transmittance values of shadow (from 25% to 100%) and a number of different irradiance levels were used. The current output of a PV module decreased significantly, by over 50% in some cases, when a small proportion of the module area (a single cell) was under a shadow of 35% transmittance. A literature review of the effects of shading by Woyte et al. (Woyte et al., 2003) stated that this effect was similar for PV arrays and the shading of part or all of one module could significantly decrease the array power output (quoted from Kovach, 1995).

The effects of shading on the performance of PV systems have been estimated using several techniques. A simple analysis, presented by Decker and Jahn, compared the electricity generation of two identical, nearby PV systems, one of which was strongly shaded (Decker and Jahn, 1997). The difference in the performance of the two systems was used to identify the shading effect. A study by Ransome et al. (Ransome et al., 2004) also used comparisons between shaded and non-shaded systems, and measurements of array current and voltage, to identify shading. A modelling approach taken by Kovach and Schmid (Kovach and Schmid, 1996) used a three dimensional building model, a ray tracing technique and a PV cell model to simulate the shading losses. Photographic techniques, by Heilscher et al. (Heilscher et al., 1998) and Oozeki et al. (Oozeki et al., 2005), used fish-eye photography to estimate the sun positions when shading would occur and

[25] The direct beam component of solar radiation is the radiation that passes straight through the atmosphere without scattering before it reaches the Earth's surface

[26] The diffuse solar radiation is the component of the radiation which has been scattered by particles in the atmosphere before reaching the Earth's surface

to quantify the energy loss due to shading.

A technique to calculate a 'shading factor' was presented by Uchida et al. (Uchida et al., 2001). This approach used hourly monitored data from PV systems and was unique because the shading effect could be identified solely from monitored data. No site visits or comparisons with other nearby non-shaded systems were required. The hourly data was split into separate months and for each month the maximum values of energy generation for each hour (i.e. 00:00, 01:00 ... 23:00) were extracted. It was assumed that the maximum values represented the PV system operating on a bright clear day with high direct beam solar radiation. Any difference between the maximum energy generation values and the expected energy generation (calculated using irradiance data) was identified as an effect of shading. The shading effects were investigated for each month in turn and a monthly shading factor (the percentage energy loss due to shading) was calculated.

7.1.6 Inverter MPP tracking failure

In normal operation there is a continual and fluctuating loss in power output due to inverter MPP tracking (as observed in Section 6.2.7). *Inverter MPP tracking failure* occurs if the operating voltage of the PV array moves far away from the MPP voltage and thus causes a significant decrease in power output. This can occur if there are large rapid changes in the MPP voltage (for example during times of shading or of large irradiance fluctuations) such that the MPP tracking routines in the inverter cannot react fast enough to match the change in the MPP voltage. In such a situation, it can take some time for the MPP tracking routines to return the operating voltage to the MPP voltage, resulting in low efficiency for this period of time. No reference to this effect has been found in the literature but the effect is known within the PV community, sometimes under the name 'inverter dropout'.

7.2. Fault detection and identification

7.2.1 Detection of faults

The faults were detected in the monitored data using the Gaussian distribution techniques to separate normal operation and faults as demonstrated in Section 5.4.3. Fault detection was carried out at Corncroft for the first and second year of operation and at Heron Close for the first year of operation. At Panmure Street, because the majority of the winter data was not reliable (due to the shading of the radiation sensor described in Section 4.3.2), the faults were not analysed. Unlike the analysis of normal operation, which could assess the performance of the Panmure Street systems based on a proportion of the annual data set, the fault analysis requires accurate irradiance data throughout the year. Taking two Corncroft systems (in their first year of operation) and two Heron Close systems as an example, the fault detection identified the efficiency values caused by faults (Figure 7-2). Similar plots for all the systems at the sites are given in Appendix E.1.

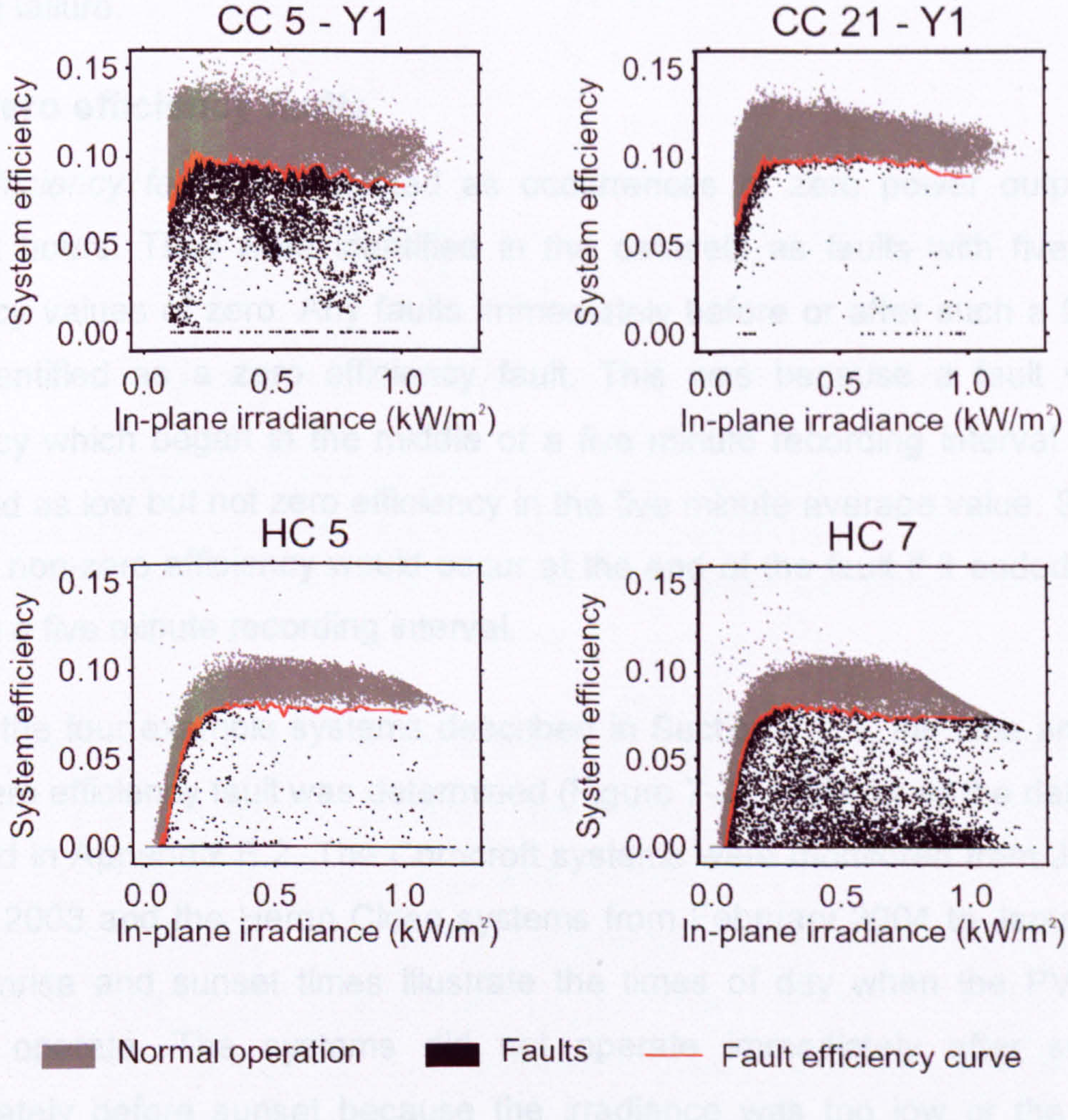

Figure 7-2: Irradiance to system efficiency relationships for selected Corncroft and Heron Close systems. The faults (shown in black) lie below the fault efficiency curve defined in Section 5.4.3 (shown in red).

At CC 5 there were occurrences of zero efficiency and low efficiency values for all levels of irradiance. There were also a significant number of low efficiencies at high irradiance, around 0.8 kW/m^2, which suggested that shading could be the cause of the faults (as the effect of shading is greatest on bright sunny days). CC 21 had fewer faults, mainly concentrated at low irradiance (below 0.3 kW/m^2) and just beneath the fault efficiency curve. Low irradiance faults, with efficiencies slightly lower than normal operation, were observed in all the Corncroft systems (see Appendix E.1.1 and E.1.2). HC 5 also had a small number of faults, but many at zero efficiency. HC 7 had faults throughout the range of irradiances and the efficiencies appeared to concentrate at levels close to, or at, zero. There was no indication of shading at HC 7 and this suggested that the faults may have been caused by component failure, system isolation, inverter shutdown or inverter MPP tracking failure.

7.2.2 Zero efficiency faults

Zero efficiency faults are defined as occurrences of zero power output during daylight hours. They were identified in the datasets as faults with five minutely efficiency values of zero. Any faults immediately before or after such a fault were also identified as a zero efficiency fault. This was because a fault with zero efficiency which began in the middle of a five minute recording interval would be recorded as low but not zero efficiency in the five minute average value. Similarly a low but non-zero efficiency would occur at the end of the fault if it ended part way through a five minute recording interval.

Taking the four example systems described in Section 7.2.1, the time and date of each zero efficiency fault was determined (Figure 7-3). Plots for all the datasets are provided in Appendix E.2. The Corncroft systems were monitored from June 2002 to May 2003 and the Heron Close systems from February 2004 to January 2005. The sunrise and sunset times illustrate the times of day when the PV systems should operate. The systems did not operate immediately after sunrise or immediately before sunset because the irradiance was too low or the sun was behind the plane of the PV array. CC 5 and CC 21 had few zero efficiency faults. HC 5 had a large number of zero efficiency faults which includes a period of sustained faults between June 2004 and January 2005. HC 7 also had a large number of zero efficiency faults, but the faults were brief and rarely lasted for more than an hour.

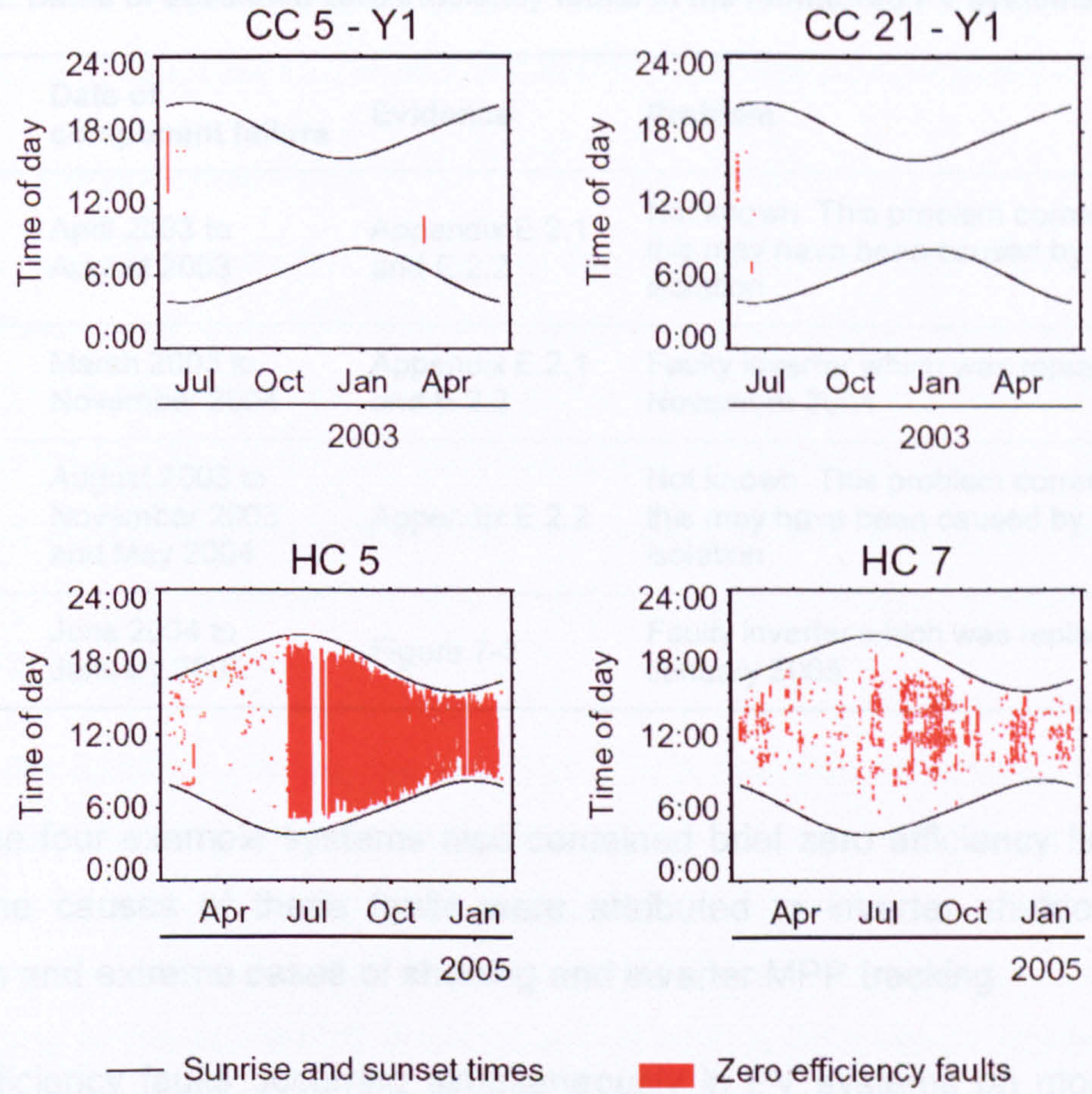

Figure 7-3: Zero efficiency faults on date and time axes for selected Corncroft and Heron Close systems. Each five minute period of a fault with zero efficiency (or adjacent to a zero efficiency fault) is shown as a red point. The times of sunrise and sunset are shown as black lines.

Zero efficiency faults which were sustained for a day or longer were attributed to component failure or system isolation (see Table 7-1). The long period of zero efficiency faults at HC 5 (Figure 7-3) was caused by a faulty inverter which was replaced in mid January 2005. Similar periods of sustained zero efficiency faults were also identified at CC 0, CC 2 and CC 17 through inspection of the datasets (Table 7-2). At CC 0 and CC 17 the problem causing the zero efficiency faults corrected itself and this suggested that the systems had been isolated and not reconnected to the mains for some time. At CC 2 and HC 5 the fault was caused by component failure. The inverters had malfunctioned and needed to be replaced.

Table 7-2: Dates of sustained zero efficiency faults in the monitored PV systems

Site and system	Date of component failure	Evidence	Problem
CC 0	April 2003 to August 2003	Appendix E.2.1 and E.2.2	Not known. This problem corrected itself so this may have been caused by system isolation
CC 2	March 2003 to November 2004	Appendix E.2.1 and E.2.2	Faulty inverter which was replaced in November 2004
CC 17	August 2003 to November 2003 and May 2004	Appendix E.2.2	Not known. This problem corrected itself so this may have been caused by system isolation
HC 5	June 2004 to January 2005	Figure 7-3	Faulty inverter which was replaced in mid January 2005

All of the four example systems also contained brief zero efficiency faults (Figure 7-3). The causes of these faults were attributed to inverter shutdown, system isolation and extreme cases of shading and inverter MPP tracking.

Zero efficiency faults occurring simultaneously in PV systems on more than one building on a site were deemed to be external events, in particular unusual events in the mains voltage or a power cut. This could cause inverter shutdown and, as the systems at each site were connected to the same grid, it was likely that any inverter shutdown would not be an isolated event but observed simultaneously in several systems. In the case of power cuts the effects would be seen at all the systems at the site. Under high or low voltage some inverters may shutdown but others may not, depending on the sensitivity of the inverter voltage sensors. As an example, zero efficiency faults occurred in eleven systems at Corncroft on 1st June 2002 (see Figure 7-3 and Appendix E.2.1). As the faults occurred simultaneously in more than one system, this indicated inverter shutdown due the behaviour of the mains grid. Details of this example are discussed further in Appendix E.2.4.

HC 5 had a large number of brief zero efficiency faults before the component failure occurred (from February to June 2004) and HC 7 had a large number of brief faults throughout the year (Figure 7-3). This suggests a significant problem of inverter shutdown or extreme cases of shading and inverter MPP tracking failure. The other Heron Close systems had fewer zero efficiency faults. There are examples of the zero efficiency faults occurring simultaneously in the Heron Close systems (see Appendix E.2.3) and this is discussed further in Appendix E.2.4.

7.2.3 Shading faults

Shading occurred when the position of the sun was such that an external object was between the sun and the PV array. As the arrays were stationary, and assuming the shading object did not move with time, the position of the sun was the determining factor of the shading effect. In previous studies (for example Uchida et al., 2001) the shading effect was taken to be a function of the time of day and time of year. However the use of sun position removes the need to consider these additional variables.

To identify shading effects, the position of the sun was calculated for each five minute interval using the time and date and the latitude of the PV site. The details of the sun position calculations are provided in Appendix A. Sun position was defined by the solar azimuth α and elevation β. Solar azimuth is the angle between the bearing of the sun and due south, where east is taken to be positive and west negative. Solar elevation is the angle made between the sun and the horizon. As an example, the sun positions for each five minute recording interval at Corncroft for the first day of each month in the first year of operation are shown in Figure 7-4. This illustrates the variation in solar azimuth and elevation throughout the year. Three separate plots are used to cover the time period from June 2002 to May 2003.

The size of shading objects that occur in the built environment meant that, if a fault was caused by shading, it was likely that there would be further faults at nearby sun positions. Thus shading was identified when a high number of faults occurred within a small region of specific sun positions. The shading analysis ignored the zero efficiency faults already identified in Section 7.2.2. It was also found that high concentrations of faults appeared to occur at the beginning and end of each day corresponding to high solar incidence angles[27]. These faults were ignored in the shading analysis so that only shading from significant shading objects (rather than

[27] Solar incidence angle is the angle made between a line drawn between the PV array and the position of the sun and a line normal to the PV array.

from objects close to the horizon) was investigated. Any faults which occurred at solar incidence angles of greater than 80° were ignored in the shading analysis. This process is discussed in detail in Appendix E.3.1.

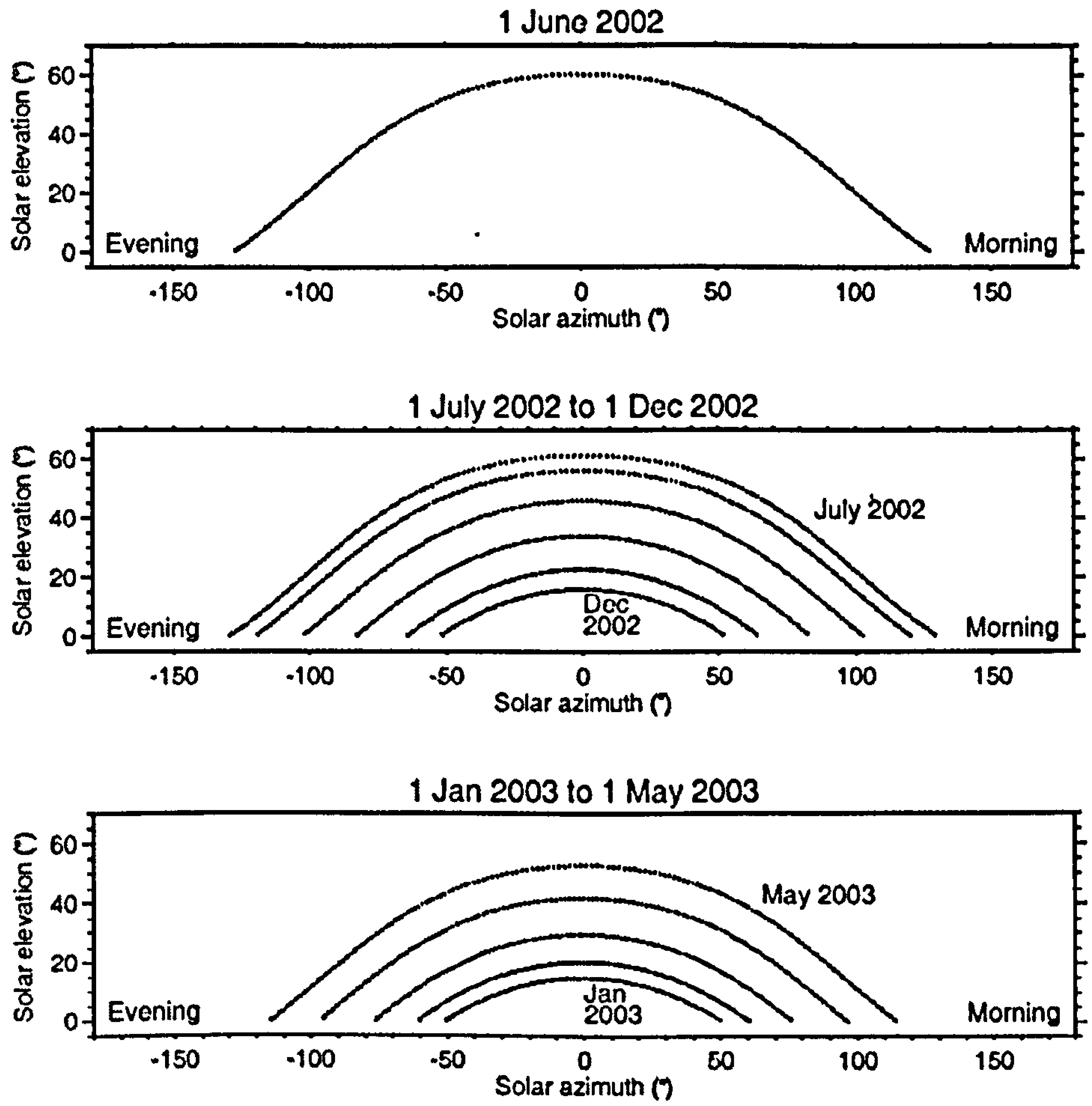

Figure 7-4: Calculated sun positions at five minute intervals for the fist day of every month in the first year of operation at Corncroft, June 2002 to May 2003

The remaining faults were plotted on solar azimuth versus solar elevation axes. For the four example systems, these plots showed the sun position regions where the faults were most concentrated (Figure 7-5). This type of plot has been termed a *sun position fault plot* and similar plots for all the monitored PV systems are shown in Appendix E.3.2 to E.3.4.

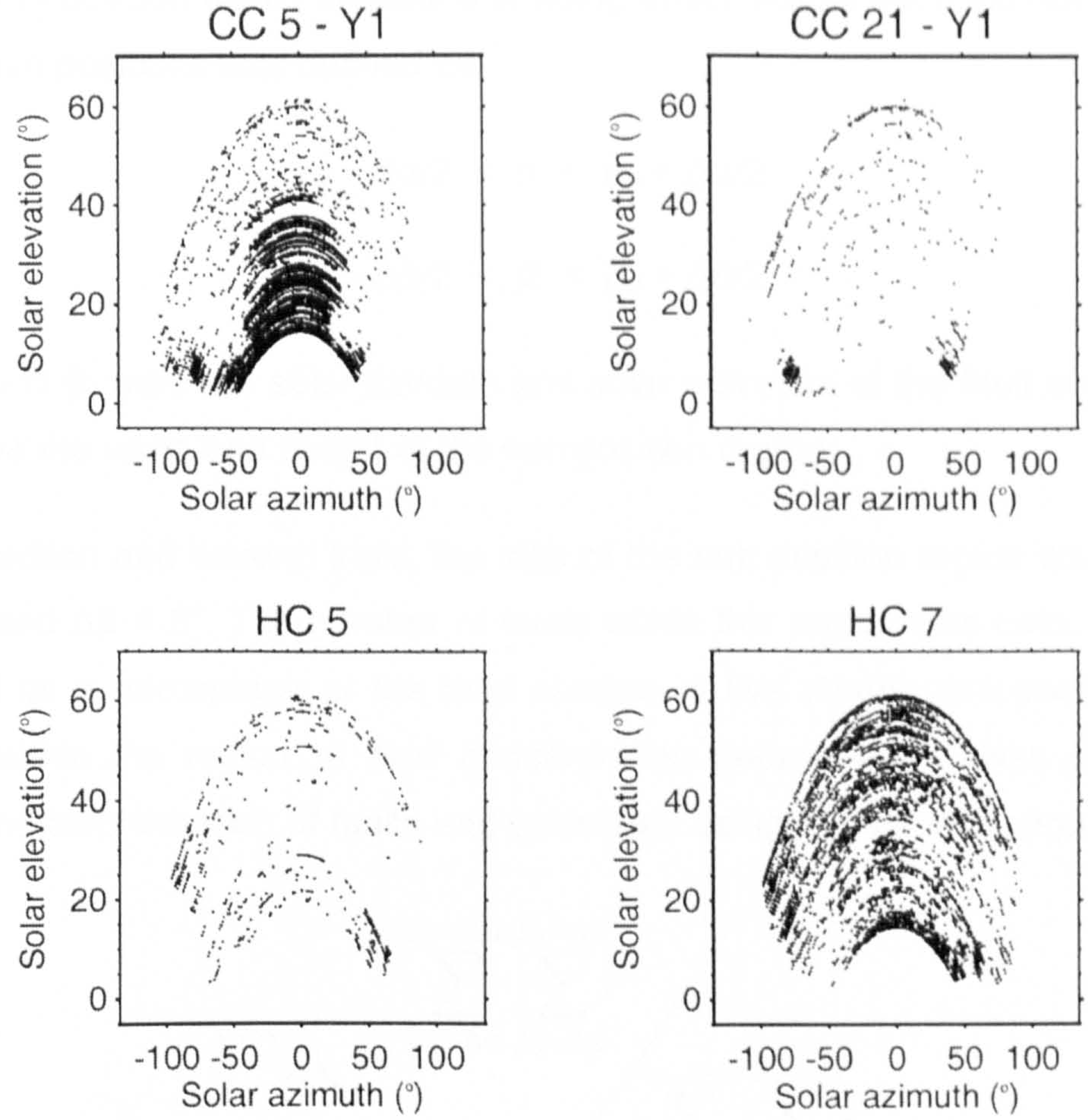

Figure 7-5: Sun position of faults for four systems at Corncroft and Heron Close

CC 5 had a high concentration of faults in the middle of the day ($-40° < \alpha < 40°$) and in autumn, winter and spring ($\beta < 40°$) and a low concentration in summer (at high solar elevations). A large tree was located to the south of the PV array and the high concentration of faults around zero solar azimuth illustrates the shading effect of the tree. CC 21 had no external objects which could block the solar radiation and the sun position fault plot shows minimal concentration of faults around sun positions with low solar elevation. The HC 5 sun position fault plot showed no fault concentration with sun position. HC 7 had many faults which were spread throughout the possible sun positions but with no obvious concentration of points within a particular sun position region.

A rules-based system was developed to identify which of the faults in the sun path plots were caused by shading. It was assumed that shading would occur at similar sun positions and so a concentration of poor performance points in a particular region of sun position would indicate a shading effect. About each individual fault a region of sun positions was defined as:

$$\alpha_0 - \Delta\alpha/2 < \alpha < \alpha_0 + \Delta\alpha/2$$

$$\beta_0 - \Delta\beta/2 < \beta < \beta_0 + \Delta\beta/2$$

where α_0 and β_0 were the solar azimuth and solar elevation of the fault and $\Delta\alpha$ and $\Delta\beta$ describe the width and height of the sun position region.

From inspection and several trials, the size of the sun position region was fixed at $\Delta\alpha = 10°$ and $\Delta\beta = 5°$. The number of faults within this region was calculated and expressed as a percentage of the total number of five minute sun positions that occurred within the region. A *fault concentration* parameter FC was defined to describe the concentration of faults and calculated using the following equation:

$$FC_{\alpha_0\beta_0} = \left. \sum_{\alpha_0-\Delta\alpha}^{\alpha_0+\Delta\alpha} \sum_{\beta_0-\Delta\beta}^{\beta_0+\Delta\beta} F \middle/ \sum_{\alpha_0-\Delta\alpha}^{\alpha_0+\Delta\alpha} \sum_{\beta_0-\Delta\beta}^{\beta_0+\Delta\beta} S \right.$$

where $FC_{\alpha_0\beta_0}$ is the fault concentration about sun position α_0 β_0, F is the number of faults within the sun position region and S is the number of five minute sun positions within the sun position region.

As an example, at CC 5 a fault occurred at sun position $\alpha = 11.5°$ and $\beta = 40.5°$ (Figure 7-6). The sun position region is $6.5° < \alpha < 16.5°$ and $38.0° < \beta < 43.0°$. Sixteen faults occurred in this sun position region during the first year of operation and the total number of five minutely values when the sun was within the region was 160. The fault concentration for this single fault was therefore 0.1 (or 10%).

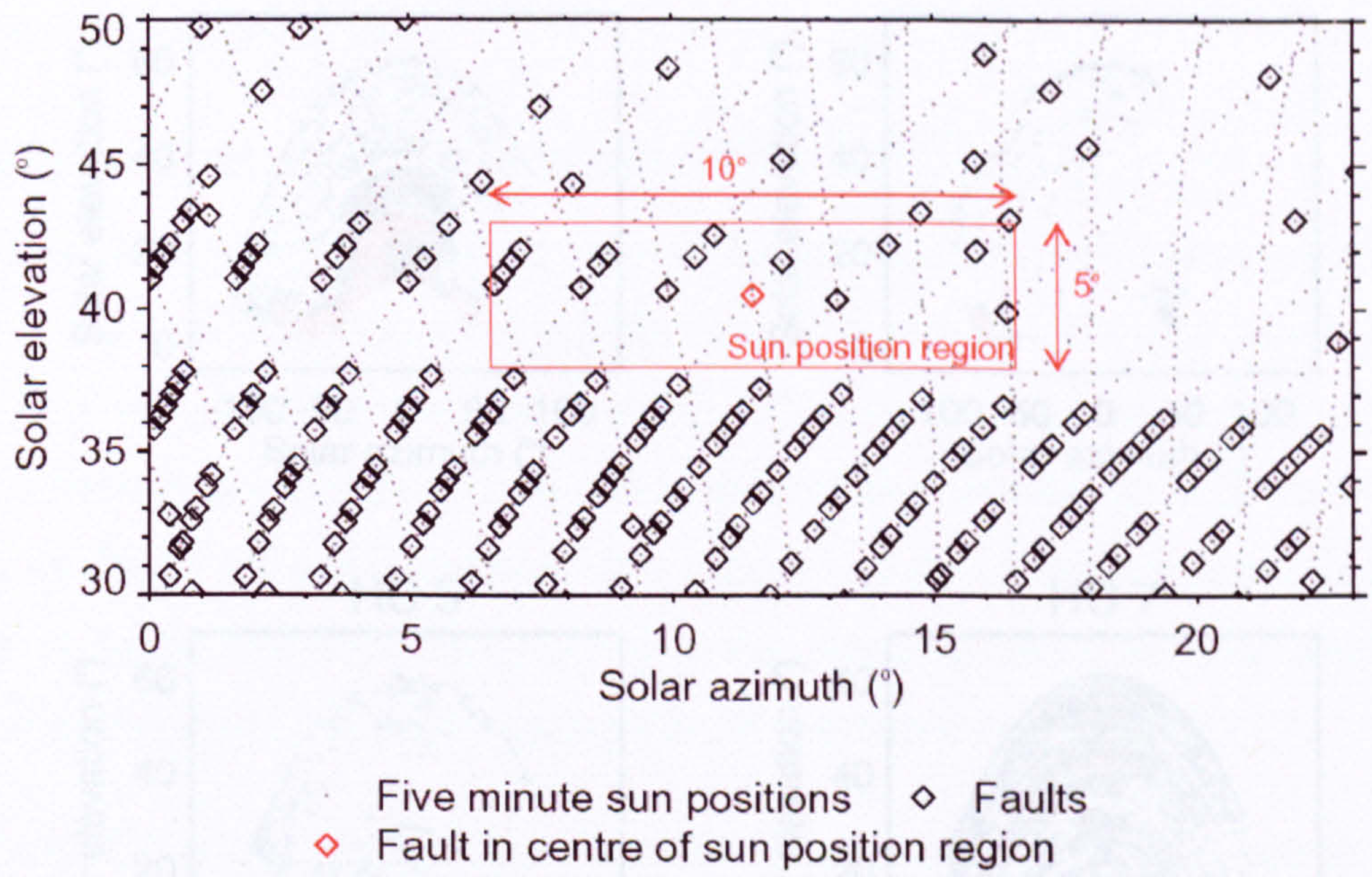

Figure 7-6: Example of the sun position region used in fault concentration calculations for a fault with sun position α = 11.5° and β = 40.5° at Corncroft system 5 in the first year of operation

For the four example PV systems at Corncroft and Heron Close, the fault concentration values were calculated (Figure 7-7). Plots for all the monitored PV systems are shown in Appendix E.4. At CC 5 the fault concentration was greater than 20% for sun positions -40° < α < 40° and β < 40° which suggested shading occurred in this region. There were few high fault concentration values at CC 21 and HC 5 which indicates no shading. At HC 7 a large number of high fault concentrations (greater than 20%) were observed. These were scattered over a wide area of sun positions with many at high solar elevations. This was unlikely to be caused by shading, which would tend to concentrate around smaller ranges of sun position and would not normally occur at high solar elevations (i.e. in the summer) unless very tall or close external shading objects were present. A site visit to Heron Close showed that HC 7 had no external shading objects. The high fault concentrations were instead caused by the high number of non-shading (and non zero efficiency) faults that occurred repeatedly in this system.

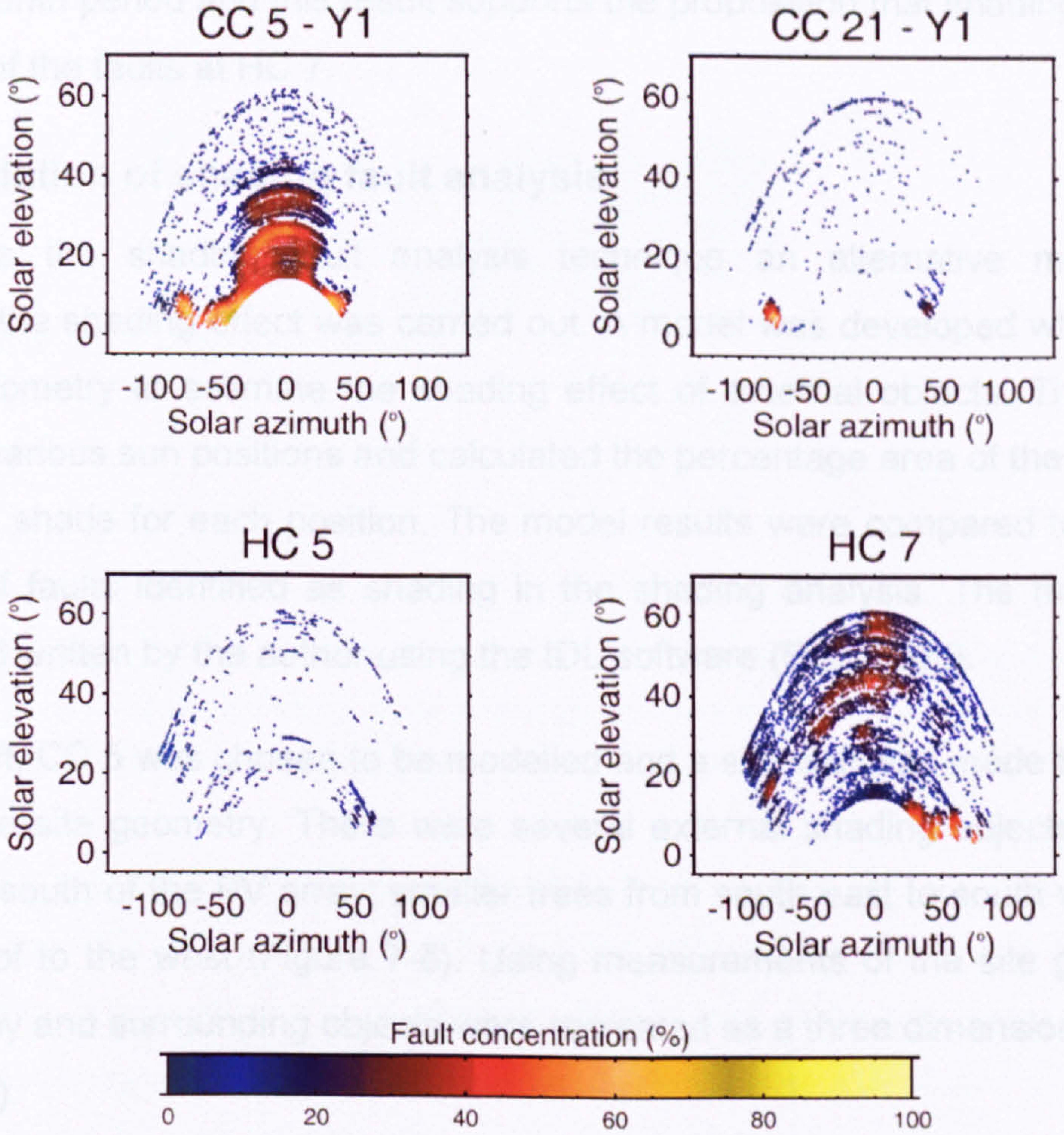

Figure 7-7: Sun position and fault concentration of faults for four systems at Corncroft and Heron Close. The fault concentration of each fault is shown in colour.

One disadvantage of analysing annual datasets was that faults recorded at different times of the year could have similar sun positions and be considered together when calculating the fault concentrations. This was because the position of the sun moved in the same region in a repeating six month cycle from the winter solstice to the summer solstice and vice versa (as shown in Figure 7-4). A shading fault analysis is therefore possible for each distinct six month period and such an approach avoids the overlaying of points on the sun position fault plots. This type of analysis is explored in Appendix E.4.4 and shows that the area of high fault concentrations seen at CC 5 (Figure 7-7) repeated in every 6 month period over the first two years of operation. The size of the high fault concentration area was less in the spring months than the autumn months, an effect that could be explained by the growth of the leaves of the shading tree (the leaves would be larger in autumn). At HC 7 the area of high fault concentration did not repeat in each six month period and this result supports the proposition that shading was not the cause of the faults at HC 7.

7.2.4 Validation of shading fault analysis

To validate the shading fault analysis technique an alternative method of estimating the shading effect was carried out. A model was developed which used the site geometry to estimate the shading effect of external objects. This model simulated various sun positions and calculated the percentage area of the PV array that was in shade for each position. The model results were compared to the sun positions of faults identified as shading in the shading analysis. The model was original and written by the author using the IDL software (RSI, 2005).

At Corncroft, CC 5 was chosen to be modelled and a site visit was made to the site to study the site geometry. There were several external shading objects: a large tree to the south of the PV array; smaller trees from south east to south west; and a porch roof to the west (Figure 7-8). Using measurements of the site geometry, the PV array and surrounding objects were recreated as a three dimensional model (Figure 7-9).

Figure 7-8: Systems 4 and 5 at Corncroft (system 5 is the PV array on the left). The large tree to the south is the middle tree in the photograph. The west porch roof is to the left of the PV array in the photograph and the other surrounding trees can be seen.

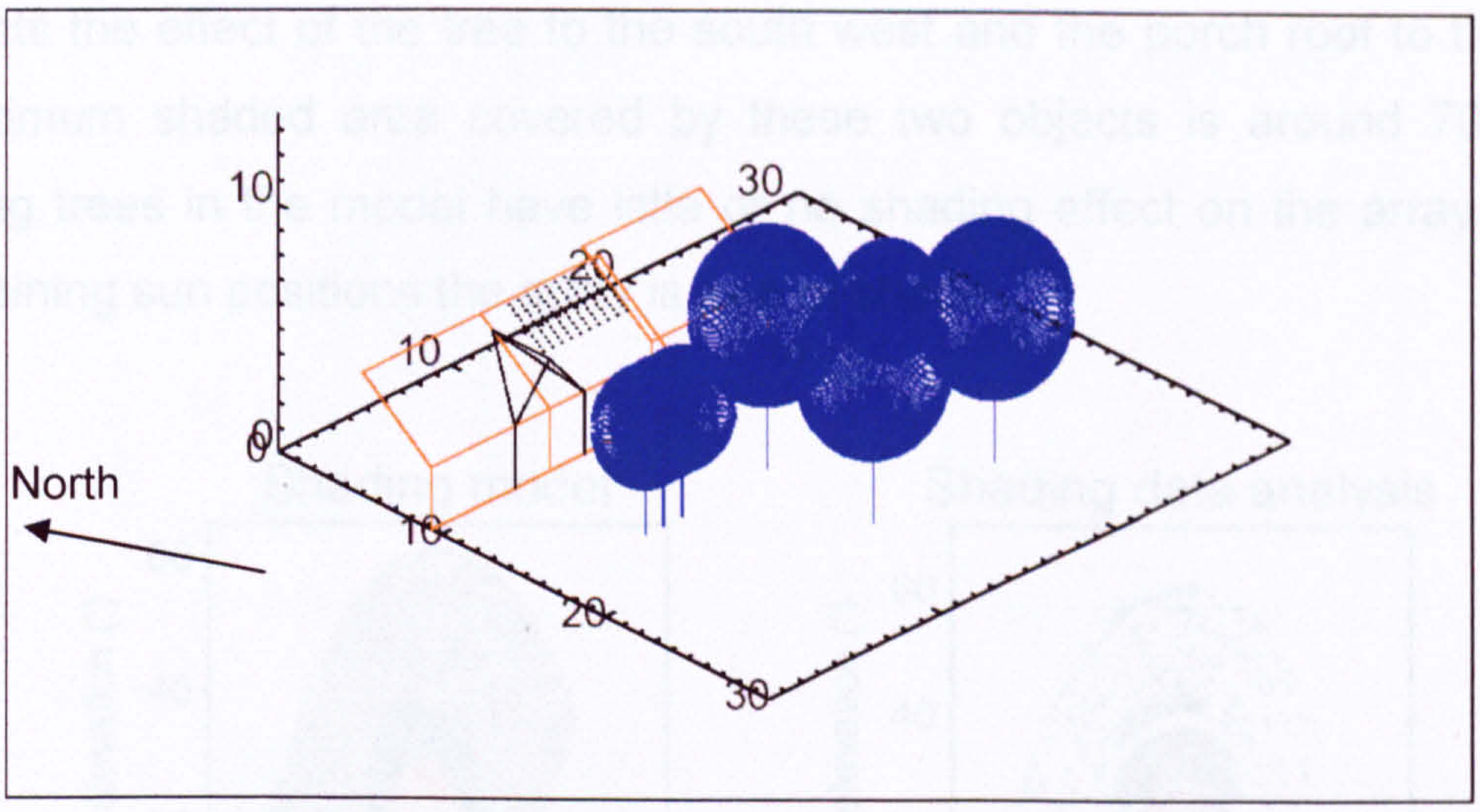

Figure 7-9: 3-D model of site geometry for system 5 at Corncroft. The house walls and roofs are outlined in red and the PV array is the rectangle of black dots. The porch roof to the west of the array is outlined in black and trees are shown in blue.

The PV array was represented as a flat mesh of 100 points. For each sun position throughout the monitoring period, the area of the array under shade was estimated. Only sun positions with solar inclination angle less than 80° were used as described in Section 7.2.3. The solar azimuth and solar elevation for each five minutely interval was calculated using the techniques described in Appendix A. For each sun position, a line was drawn, beginning at each of the mesh points of the PV array in the direction of the solar azimuth and solar elevation. This was equivalent to drawing a line between the mesh point and the sun. If the line passed through any of the external objects (the roofs, wall or trees) then the mesh point was considered to be shaded. If the line did not pass through any external objects then the point was not shaded. For each sun position, the proportion of mesh points under shade was used to calculate the percentage area of the array which was shaded.

The simulation results show when the PV array of CC 5 is under shade during its first year of operation (Figure 7-10). The sun positions are represented by coloured points, where the colour shows the percentage area of the array which is shaded. No shading is represented by grey points. The array is in shade at $-40° < \alpha < 30°$ and $\beta < 40°$, due to the large tree to the south. The percentage area of the array in shade at this sun position varies from 0% at the edge of the shading area to nearly 100% in the middle. The array is also in shade at $\alpha < -40°$ and $\beta < 15°$, which represents the effect of the tree to the south west and the porch roof to the west; the maximum shaded area covered by these two objects is around 70%. The remaining trees in the model have little or no shading effect on the array and for the remaining sun positions the array is free of shade.

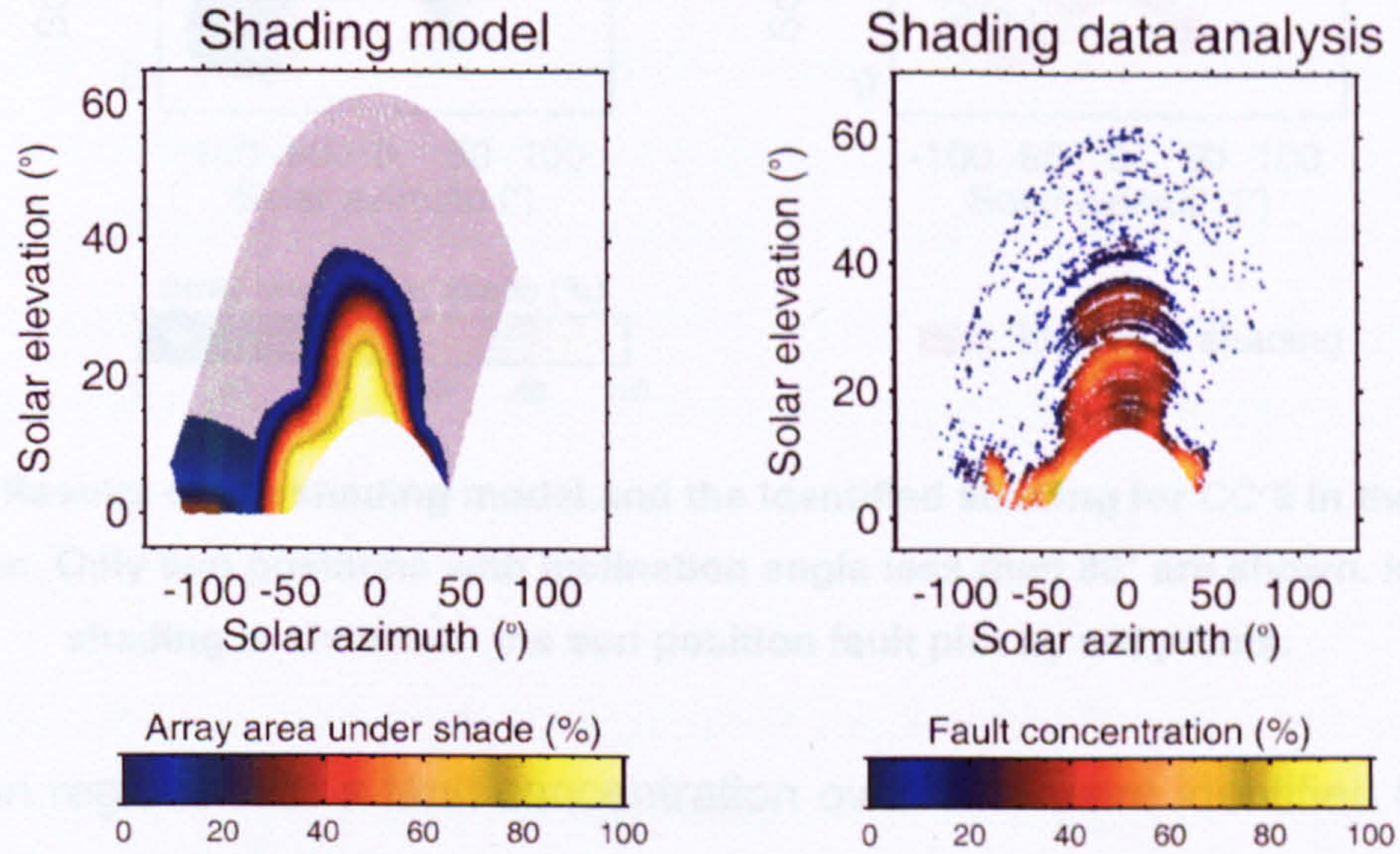

Figure 7-10: Results of the shading model (left) and the fault concentrations (right – from the shading fault analysis in Section 7.2.3) for CC 5 in the first year of operation. Only sun positions with inclination angle less then 80° are used. In the shading model plot, the percentage area of the array in shade is shown by the colours in the legend and no shading is shown by the grey points.

The sun positions for which the model predicted the array at CC 5 to be shaded were similar to the sun positions in the sun path plots of shading faults (Figure 7-10). The effect of the large tree to the south of the array can be seen in both results, although the sun position fault plot derived from the shading fault analysis showed the area of shading to be slightly larger than the model prediction. One reason for this could be that the size of the tree has been underestimated in the model geometry. The comparison of the model and sun path plot results for CC 5 validated the shading fault analysis. The comparison was also used to assess the fault concentration level at which shading occurred and fault concentrations with values of 12% or greater were identified as shading (Figure 7-11).

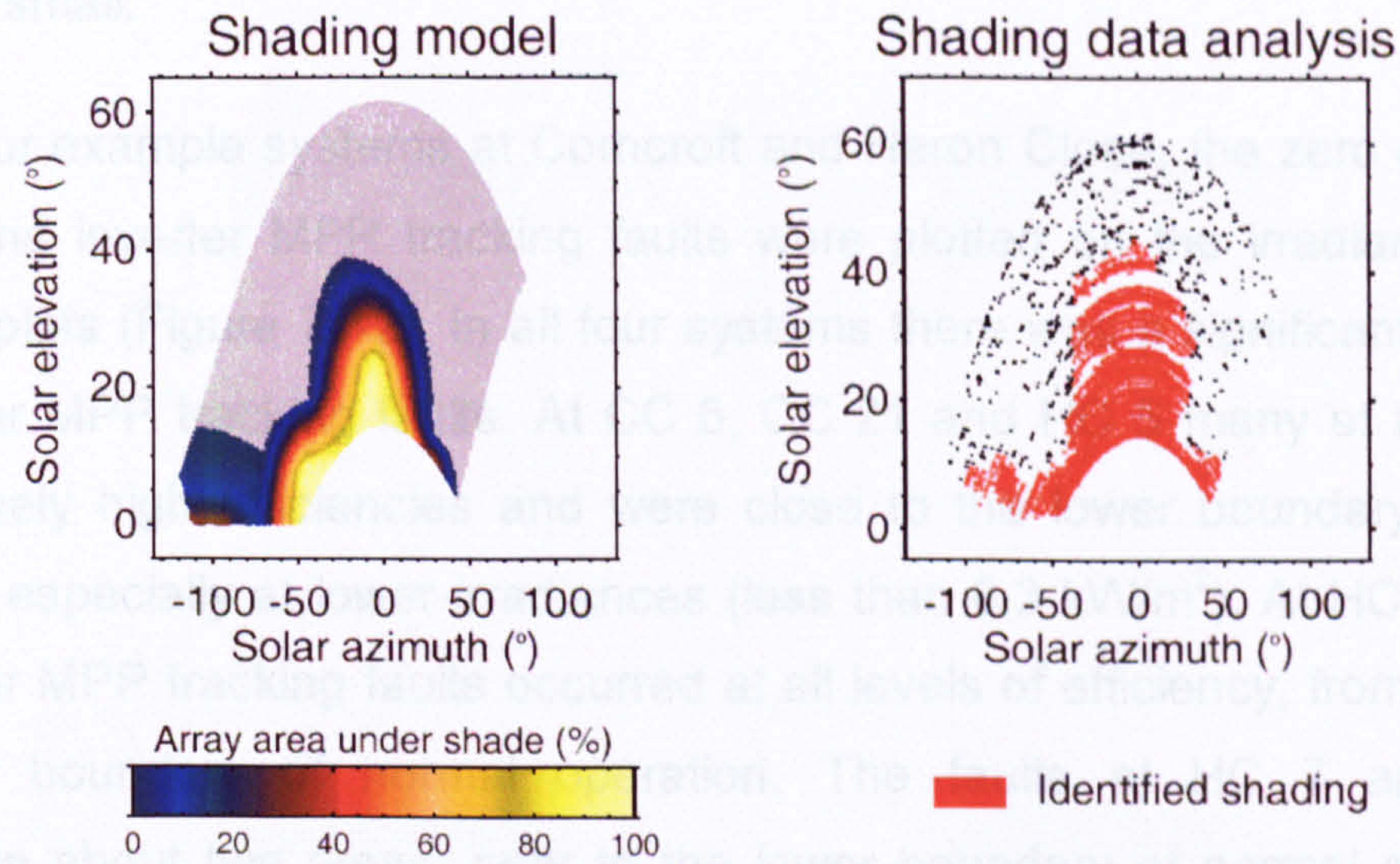

Figure 7-11: Results of the shading model and the identified shading for CC 5 in the first year of operation. Only sun positions with inclination angle less then 80° are shown. Identified shading is shown on the sun position fault plot by red points.

Sun position regions with a fault concentration over 12% were identified for all the monitored PV systems and the results are shown in Appendix E.5. At Heron Close, values of high concentration which did not repeat in subsequent 6 month periods (see Appendix E.4.4.) were not identified as shading.

Further visual verifications of the analysis method were made by comparing other results from Corncroft with the observed site geography. For example, the shading effect of the large tree to the south of CC 5 was also identified in CC 4 (located adjacent to CC 5 to the east) and CC 6 (located adjacent to CC 5 to the west) as shown in the sun position fault plots of Appendix E.5.1 and E.5.2.

7.2.5 Inverter MPP tracking faults

The *inverter MPP tracking faults* are defined as the faults which were not identified as zero efficiency or shading faults. Although this technique of assigning the remaining faults to inverter MPP tracking failure does not actively identify the faults as such, the analysis in this section shows that inverter MPP tracking failure was the likely cause of the majority of the remaining faults. However this definition meant that faults other than inverter MPP tracking faults could be included in the inverter MPP tracking fault category. Such additional faults might include shading faults which were not identified in the shading fault analysis or faults due to unidentified additional causes. It was assumed the occurrence of such additional faults was small.

For the four example systems at Corncroft and Heron Close, the zero efficiency[28], shading and inverter MPP tracking faults were plotted on the irradiance against efficiency plots (Figure 7-12). In all four systems there was a significant number of the inverter MPP tracking faults. At CC 5, CC 21 and HC 5 many of these faults had relatively high efficiencies and were close to the lower boundary of normal operation, especially at lower irradiances (less than 0.3 kW/m^2). At HC 7 however the inverter MPP tracking faults occurred at all levels of efficiency, from zero up to the lower boundary of normal operation. The faults at HC 7 appeared to concentrate about two areas: near to the lower boundary of normal operation at irradiance less than 0.3 kW/m^2; and close to zero efficiency at irradiance greater than 0.3 kW/m^2.

In the cases when two or more inverter MPP tracking faults occurred sequentially in the five minutely data, such occurrences were classified as single faults with durations of greater than five minutes in length. Although there were many inverter MPP tracking faults in the four example systems (Figure 7-12), the majority were brief faults with small durations. Frequency histograms of the fault durations at the four systems show that the most frequent fault duration was five minutes (Figure 7-13). The faults could have been of shorter duration but five minutes is the limit of resolution with the monitored data. At higher values of fault duration, the frequency of faults decreased significantly.

[28] The zero efficiency faults also include faults immediately before or after a zero efficiency fault as described in Section 7.2.2

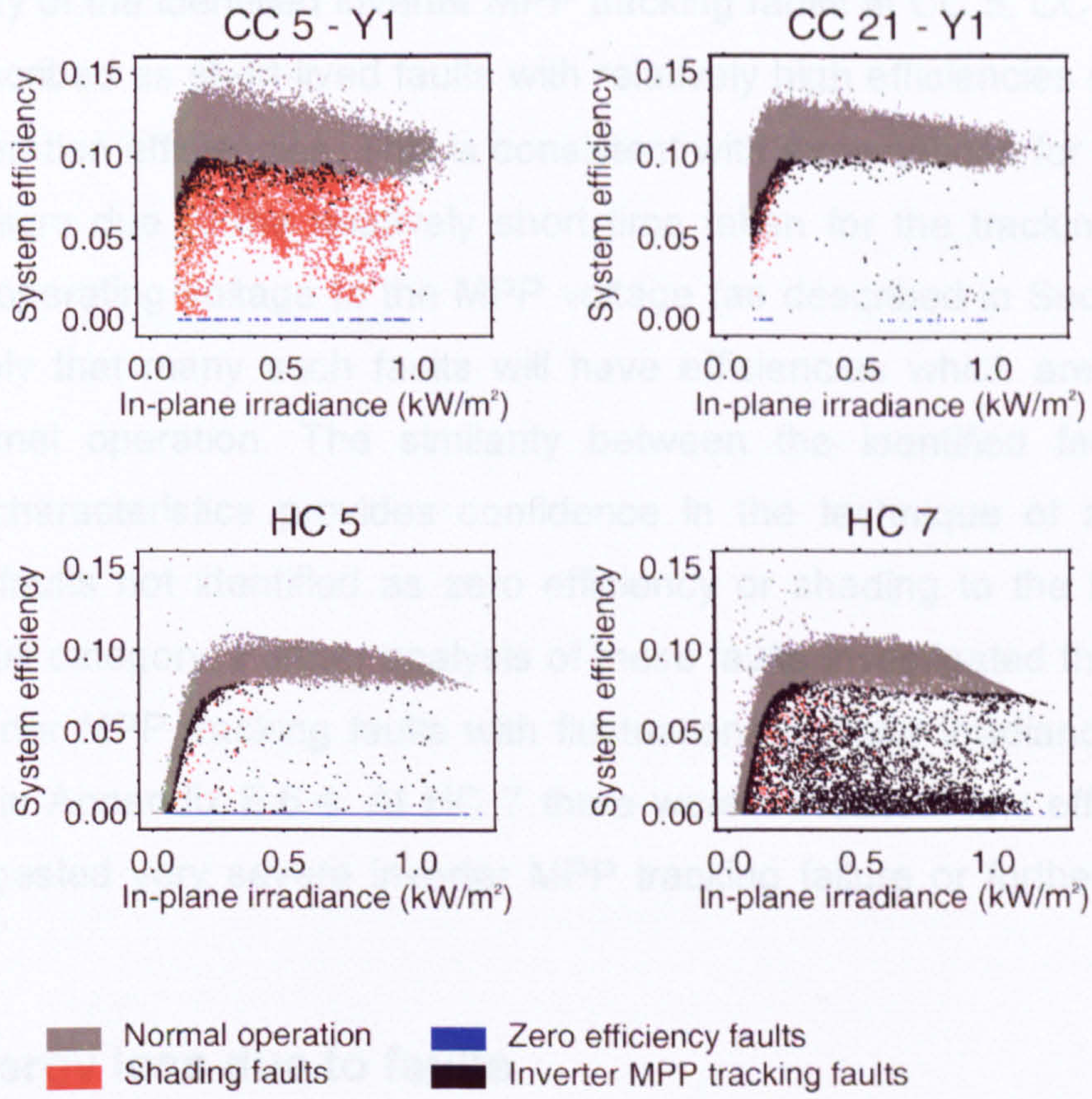

Figure 7-12: Irradiance to system efficiency relationships for selected Corncroft and Heron Close systems. Normal operation is shown in grey, zero efficiency faults in blue, shading faults in red and inverter MPP tracking faults in black.

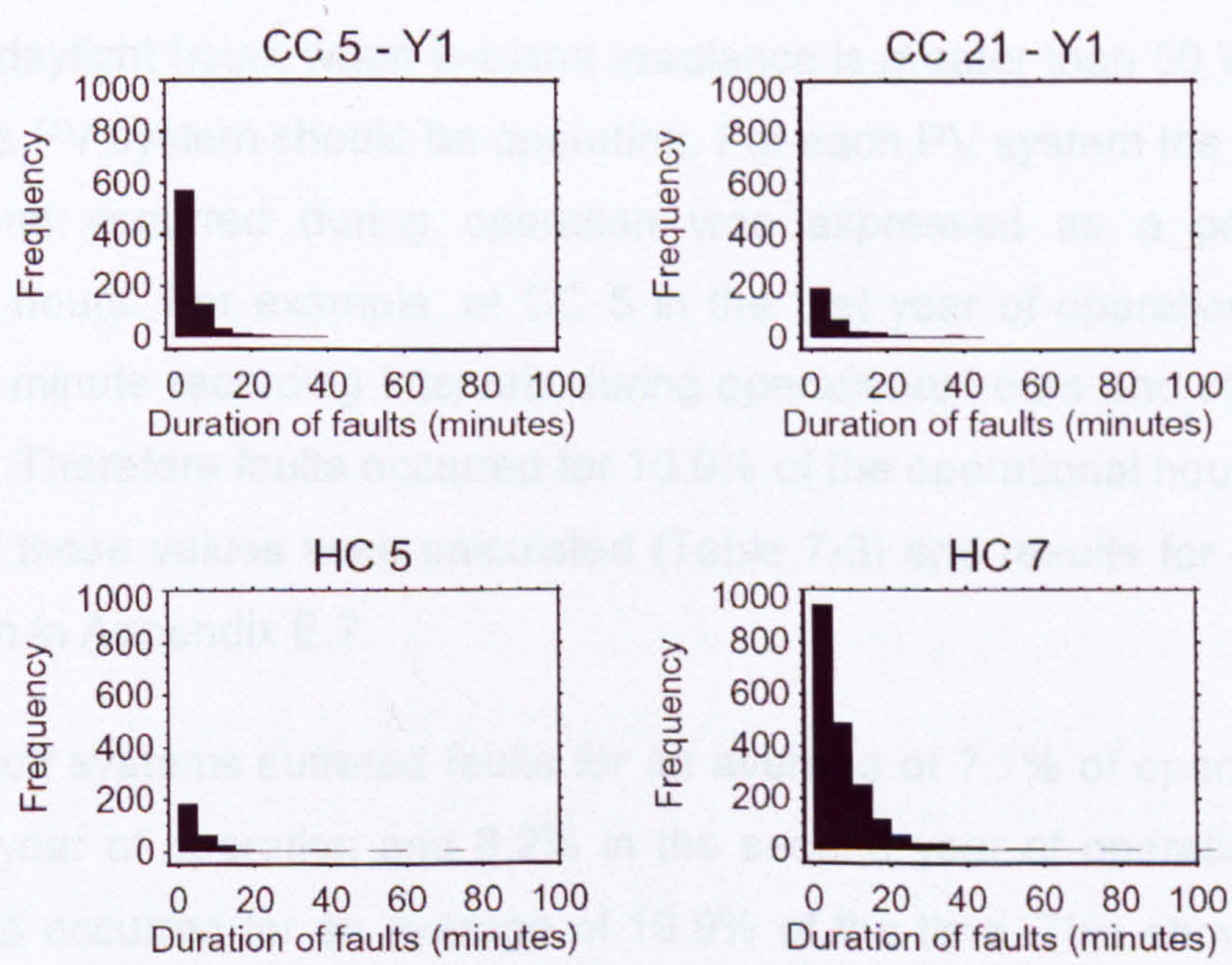

Figure 7-13: Duration of inverter MPP tracking faults for selected Corncroft and Heron Close systems.

The majority of the identified inverter MPP tracking faults at CC 5, CC 21 and HC 5 can be described as short-lived faults with relatively high efficiencies slightly below normal operation efficiencies. This is consistent with expectations for inverter MPP tracking failure due to the relatively short time taken for the tracking routines to return the operating voltage to the MPP voltage (as described in Section 6.1.6). It is also likely that many such faults will have efficiencies which are only slightly below normal operation. The similarity between the identified faults and the expected characteristics provides confidence in the technique of assigning the remaining faults not identified as zero efficiency or shading to the inverter MPP tracking fault category. Further analysis of these faults investigated the occurrence of the inverter MPP tracking faults with fluctuations in solar irradiance and this is discussed in Appendix E.6.4. At HC 7 there were consistent low efficiency faults which suggested very severe inverter MPP tracking failure or further unidentified faults.

7.3. Energy loss due to faults

7.3.1 Number of faults

The techniques in the previous section identified a significant number of faults in the monitored PV systems. To investigate the extent of the faults, the number of faults that occurred during operational hours was calculated. Operational hours are defined as daylight hours when in-plane irradiance is greater than 50 W/m^2, i.e. the time when a PV system should be operating. For each PV system the total number of faults that occurred during operation was expressed as a percentage of operational hours. For example, at CC 5 in the first year of operation there were 36,488 five minute recording intervals during operational hours and of these 3,974 were faults. Therefore faults occurred for 10.9% of the operational hours. Summary statistics of these values were calculated (Table 7-3) and results for each system can be seen in Appendix E.7.

The Corncroft systems suffered faults for an average of 7.1% of operational hours in the first year of operation and 8.2% in the second year of operation. At Heron Close, faults occurred for an average of 19.9% of the time. This shows that faults occurred in significant quantities at both sites. Such a result has not been observed in previous studies and demonstrates the effectiveness of high resolution monitoring in detecting short lived faults.

Table 7-3: Mean and range of percentage of operational hours during which faults occurred

Site	Sustained zero efficiency faults	Brief zero efficiency faults	Shading faults	Inverter MPP tracking faults	Total faults
	Average value (% of operational hours) *Range: min to max (% of operational hours)*				
Corncroft Year 1 (22 systems)	1.1	0.1	3.0	2.9	7.1
	0 to 18.0	*0 to 1.1*	*0 to 8.1*	*1.7 to 4.5*	*1.8 to 27.9*
Corncroft Year 2 (22 systems)	3.4	0.3	3.1	1.3	8.2
	0 to 41.6	*0 to 2.2*	*0 to 9.6*	*0.5 to1.8*	*0.5 to 47.5*
Heron Close (5 systems)	11.7	1.3	0.6	6.2	19.9
	0 to 58.6	*0.1 to 4.9*	*0.1 to 1.5*	*1.6 to 12.9*	*6.0 to 60.7*

7.3.2 Calculation of energy losses

The energy losses due to faults were calculated to assess the effects on the performance of the PV systems. The energy losses were converted into performance ratio losses to investigate the impact on annual performance ratios. It was assumed that, if the faults had not occurred, the PV systems would have operated at normal operation, with an efficiency given by the normal operation system efficiency curves as defined in Section 5.4.2. For each fault, the energy loss was calculated based on the difference between the efficiency whilst operating in a fault manner and the efficiency at the same irradiance under normal operation. Taking as an example a single five minute recording interval at HC 4, a fault occurred at an irradiance of 600 W/m^2 and produced an efficiency of 0.040 (Figure 7-14). If the fault had not occurred, and the system had been at normal operation, then the efficiency can be estimated to be 0.087 (given by the system efficiency curve). The fault therefore caused a 0.047 reduction in efficiency.

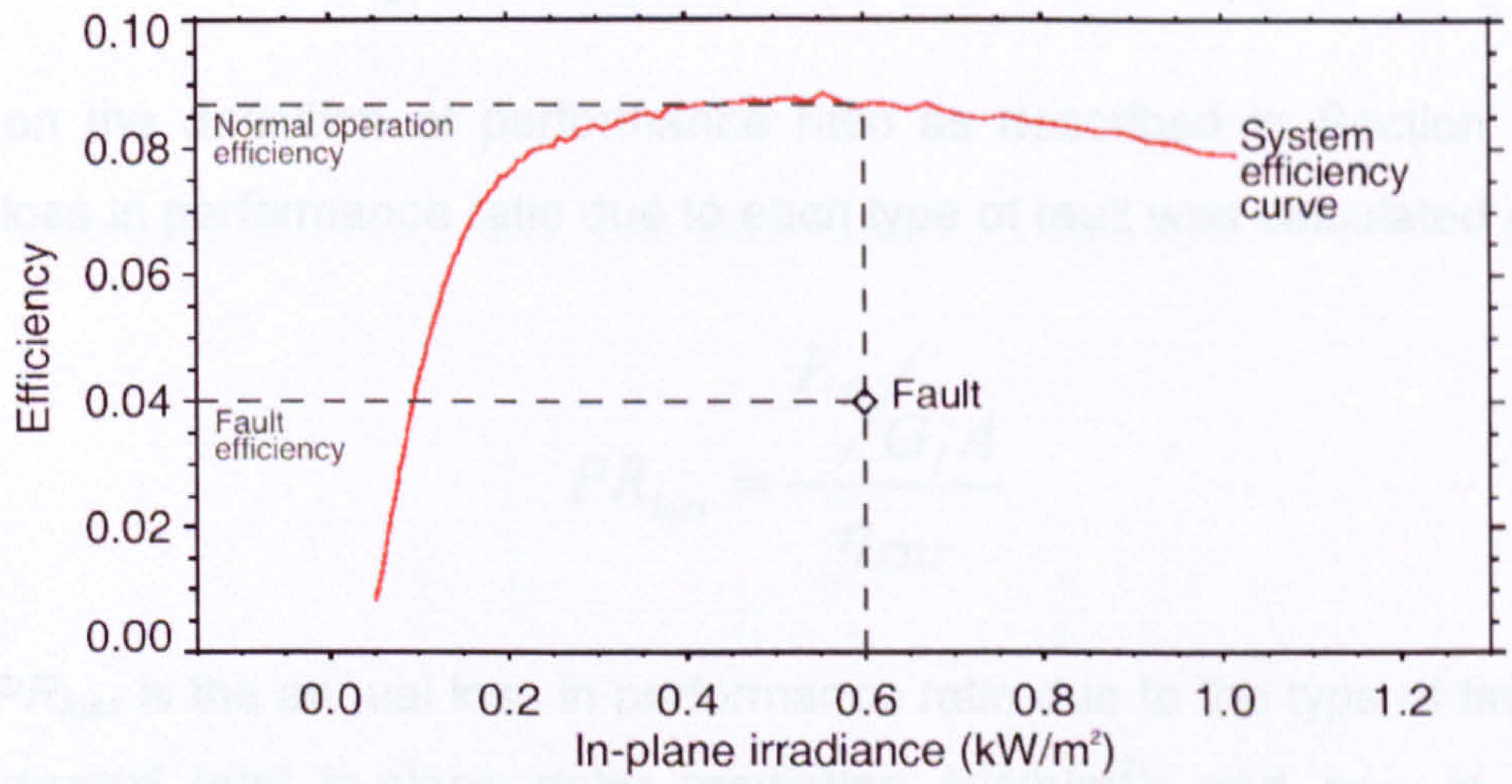

Figure 7-14: Example of fault energy loss calculations using the Heron Close system 4 system efficiency curve (defined in Section 5.4.2)

For each fault the loss in energy was calculated using the following equation:

$$e_F = \left(\eta_{NO,i} - \eta_F\right) \times G_i A$$

where e_F is the energy loss due to an individual fault (kWh); $\eta_{NO,i}$ is the system efficiency of normal operation at irradiance *i*; η_F is the system efficiency of the fault; G_i is the in-plane solar irradiation energy (kWh/m^2); and *A* is the area of the PV array (m^2).

Continuing the example of HC 4 above for a single fault occurring at 600 W/m^2 (Figure 7-14), the fault efficiency was 0.040 and the normal operation efficiency was 0.087. For a five minutely irradiance of 600 W/m^2, the irradiation received over the five minute period was 50 Wh/m^2 and the array of the array was 11.7 m^2. The energy loss due to the fault is calculated as 27.5 Wh.

In Section 7.1.1 four types of faults were identified: sustained zero efficiency; brief zero efficiency; shading; and inverter MPP tracking failure. The annual energy loss was calculated for each type of fault by:

$$E_F = \sum_{1}^{n} e_F$$

where E_F is the annual energy lost due to a type of fault (kWh); and n is the total number of faults of this type in the annual data.

Based on the definition of performance ratio as described in Section 2.1.1, the annual loss in performance ratio due to each type of fault was calculated as:

$$PR_{loss} = \frac{E_F / G_I A}{\eta_{STC}}$$

where PR_{loss} is the annual loss in performance ratio due to the type of fault; and G_I is the annual total in-plane solar irradiation (kWh/m^2); and η_{STC} is the rated efficiency of the PV modules.

7.3.3 Annual energy losses

The reductions in annual performance ratio for each type of fault were calculated for Corncroft in the first and second year of operation and for Heron Close in first year of operation (Table 7-4). The annual performance ratios of normal operation (the estimated performance if no faults had occurred) were calculated from the system efficiency curves as described in Section 6.3.2 and the actual annual performance ratios from the recorded data. The mean, standard deviation and range of values for each set of annual results are shown. Annual results for the individual systems are given in Appendix E.8. The loss due to faults was defined as the difference between the normal operation and actual operation (Section 7.1.1). However in the annual totals the difference between normal operation and actual operation is not precisely equal to the sum of the losses due to faults, because the estimation of the normal operation annual performance ratio is based on the system efficiency curves.

The faults reduced the average annual performance ratios at Corncroft from 77.6% to 75.7% in the first year of operation and from 76.9% to 72.5% in the second. The significant faults at Corncroft are sustained zero efficiency loss (1.0% and 3.2% averages) and shading (1.1% and 1.2% averages). Sustained zero efficiency faults only occurred in three of the systems but it had a dramatic effect on performance ratio, with a maximum loss of 38.5% for one system. The average shading losses at Corncroft were similar in both years and the maximum shading loss was 5.2%. The remaining faults at Corncroft, brief zero efficiency loss (0.1% and 0.3%

averages) and inverter MPP tracking failure loss (0.5% and 0.3% averages), had a smaller effect on performance.

Table 7-4: Annual performance ratio and losses in normal operation

Site	Annual performance ratio of normal operation	Sustained zero efficiency loss	Brief zero efficiency loss	Shading loss	Inverter MPP tracking failure loss	Actual annual performance ratio
	(%)	Loss in annual performance ratio (in performance ratio %)				(%)
	Average; range – minimum to maximum					
Comcroft Year 1 (22 systems)	77.6 71.8 to 81.5	1.0 0 to 16.2	0.1 0 to 1.1	1.1 0 to 3.8	0.5 0.3 to 0.7	75.7 48.9 to 81.7
Comcroft Year 2 (22 systems)	76.9 72.9 to 80.8	3.2 0 to 38.5	0.3 0 to 1.8	1.2 0 to 5.2	0.3 0.1 to 0.4	72.5 30.7 to 81.1
Heron Close Year 1 (5 systems)	64.2 61.6 to 66.5	7.3 0 to 36.7	1.4 0.1 to 5.5	0.2 0 to 0.5	3.1 0.5 to 9.3	51.8 25.9 to 62.9

At Heron Close the faults caused a reduction in average annual performance ratio from 64.2% to 51.8%. This was largely due to high sustained zero efficiency faults, brief zero efficiency faults and inverter MPP tracking failure. The high sustained zero efficiency loss was due to a single system with an individual component failure loss of 36.7%. Brief zero efficiency loss (1.4% average) was low in three of the systems (from 0.1% to 0.3%) but high in two systems (1.1% and 5.5%). The losses due to inverter MPP tracking failure (3.1% average) were also low in the same three systems (from 0.5% to 1.7%) and high in the other two systems (2.8% and 9.3%). Shading loss at Heron Close (0.2% average) was low for all the systems.

Both sites had significant sustained zero efficiency losses caused by component failure which reduced the annual performance ratios of a small number of systems. Component failure could have been minimised by quick detection and correction of the failure (through maintenance work and the replacement of components). Shading loss was higher at Corncroft than Heron Close due to the presence of nearby trees and other shading objects. The slight increase in the shading loss during the two years of operation at Corncroft (from an average of 1.1% to 1.2%) may be the results of the growth of the trees. The maximum shading loss at Corncroft was 5.2%. Although the shading did reduce the performance of the systems, the magnitudes of the shading losses illustrate that it is possible to site PV systems in positions of partial shade and still achieve good annual performance ratios. However such an approach should take into account the possibility of additional stress being placed on the system components due to shading.

The brief zero efficiency loss and inverter MPP tracking failure loss were high at Heron Close. Both losses had their highest values at HC 6 and HC 7 which suggested that these losses may be caused by the same or similar effects. It is not clear why only these two systems at Heron Close had such high losses. Brief zero efficiency loss caused by the mains electricity network (power cuts or voltage variation) should to some degree affect all of the PV systems on the site as they share the same grid. Inverter MPP tracking failure, caused by fast changes in irradiance, should also affect all the systems similarly as they were all subject to the same solar irradiance conditions. One possibility is that the inverters at HC 6 and HC 7 were behaving differently to the others at Heron Close, and the high losses were caused by inverters particularly prone to inverter shutdown, inverter MPP tracking failure or other unidentified faults.

7.3.4 Comparison with previous studies

Previous studies which examined faults in PV systems were discussed in Chapter 2 (Oozeki et al., 2003; Stettler et al., 2005, Baltus et al., 1998; Kiefer et al., 1995) and in the literature review of faults in Section 7.1. In those studies component failure loss was quoted as a reason for low annual performance ratios but the degree of the affect on annual performance ratios was not stated. Inverter shutdown and inverter MPP tracking faults have not been discussed in previous studies because these brief faults can only be detected with the high resolution, short recording interval data as used in this work. Many of these faults were under 15 minutes in length and would not be detected in studies based on data with recording intervals of half hourly or greater (for example Oozeki et al., 2003; Stettler et al., 2005).

Shading loss was difficult to compare to other studies as the magnitude of the loss varied with individual site geometry and external shading objects. Oozeki et al. gives shading losses as 4% on average for 421 systems, Kiefer et al. gives 5% to 10% for six systems and Baltus et al. gives 11% for a single system. The magnitude of estimated shading losses in this work was about 2% to 5% for the shaded systems at Corncroft.

7.3.5 Critical appraisal of this approach

The fault analysis techniques required a high accuracy in the monitored performance data. The data for Panmure Street and many of the Heron Close systems could not be analysed due to measurement errors in the monitored data (as described in Chapter 4). The techniques also required monitored data with a short recording interval to capture the inverter shutdown and inverter MPP tracking faults with short durations. The analysis could be carried out on data with a larger recording interval (for example hourly data) but these faults would not be detected.

The approach did not allow combinations of faults to be identified and each fault was assigned to a single cause. To identify multiple faults would require monitoring of individual system components. Minor faults which caused only a slight drop in efficiency were not detected if the efficiency values still lay within the boundaries of normal operation. This could potentially lead to underestimation of the energy losses for repeated minor faults such as very slight shading.

The techniques identified faults with short time periods of around 5 minutes in the data sets. However the reasons for such faults were not always accurately defined. In particular inverter MPP tracking faults were inferred from the data and not explicitly identified. More detailed monitoring would be required to ascertain the exact nature of these faults.

7.4. Summary

This chapter has demonstrated new monitoring techniques to identify faults in PV systems. Four types of faults were considered: sustained zero efficiency; brief zero efficiency; shading and inverter MPP tracking failure. A literature review of each fault has been presented and the faults were identified through investigation of the patterns and trends in five minutely monitored data. The high resolution monitored data enabled brief faults (of around five minutes in length) to be detected. Such short lived faults have not been reported in previous studies. Zero efficiency faults were analysed in comparison to neighbouring systems and a novel technique identified shading faults by considering the position of the sun where faults occurred.

The monitoring techniques were used to estimate the losses in annual performance ratio caused by the faults for the monitored PV systems at Corncroft and Heron Close. The results were compared to previous studies and a critical appraisal of the techniques has been presented. The monitoring techniques demonstrate a new approach to estimating the effects of faults on PV system performance. These techniques could be used in a wide variety of PV system monitoring applications to minimise the effects of faults. For example, planning decisions could be made based the estimated impact of shading on annual performance ratios. Such an approach could be employed to raise the efficiency of installed PV systems and improve future PV system design.

8. Conclusions and Suggestions for Further Work

This thesis has described the development of new PV monitoring techniques to improve the understanding of PV system performance. The techniques are based on high resolution monitored data from one hundred and nine domestic PV systems installed at five sites throughout the UK. Three of these sites, Corncroft (CC), Heron Close (HC) and Panmure Street (PS), were studied in detail. Solar irradiance, temperature and energy output were recorded at five minutely intervals for periods of up to two years. The suitability and plausibility of the monitored data was checked and the monitoring techniques were developed from data at fifty four of the PV systems. The techniques identify the effects of individual losses on system performance and enable recommendations to be made to raise the efficiency of future PV system designs.

8.1. Main conclusions

A new strategy for monitoring PV systems is proposed. Original analysis techniques are used on high resolution monitored data from a low number of sensors to produce a detailed understanding of system performance. This approach identifies and quantifies more losses than previous studies which use lower resolution data (i.e. hourly) or rely on pre-installation measurements and simulations to generate some of their results. Four monitoring parameters are required: solar in-plane irradiance, PV module temperature, DC power output from the PV array and AC power output from the inverter. The high resolution data is recorded at short intervals (five minutes or less) and is analysed directly without aggregating it into hourly or daily totals. The data plotted on efficiency versus irradiance plots shows a boomerang-shaped cloud of points. Statistical tests applied to this cloud of points enable the data to be separated into normal operation (times when the PV system works well) and faults (times of unexpected low efficiencies). The normal operation data and fault data is analysed separately using original techniques to identify the individual losses within each mode of operation. A series of 'efficiency curves' are constructed which describe the different stages of normal operation. Fault identification techniques include a shading method based on the position of the sun at each five minute interval.

The new monitoring techniques are applied to annual data from the monitored PV systems and used to estimate the reductions in annual performance ratios caused by individual losses. The results show which losses have the greatest effect on system performance and opportunities to minimise the losses are identified. The analysis is used to make recommendations to raise the efficiency of the monitored PV systems and future UK domestic PV systems.

8.2. The new PV monitoring techniques

The first aim of this study was 'to demonstration that high resolution monitoring and analysis can improve our understanding of PV system performance'. This work has proved that clear benefits arise from this approach. In the analysis of normal operation, the following types of energy losses were identified: inverter power derating loss (caused by undersizing the inverters); inverter DC to AC conversion loss; DC wiring resistive loss; temperature loss due to operating at temperatures other than STC temperature (25°C); inverter maximum power point (MPP) tracking loss; irradiance loss due to operating at irradiances other than STC irradiance (1000 W/m^2); and mismatch and deviation from STC losses. The occurrence and magnitude of these losses was determined directly from the high resolution monitored data by analysing the trends and patterns in the relationship between the five minutely irradiance and efficiency values.

Statistical methods were used to construct a series of efficiency curves describing the efficiency to irradiance relationship at different stages of normal operation. This was used to identify inverter MPP tracking losses and the average reduction in annual performance ratio due to this loss was between 6.0% and 12.6% (in performance ratio percent). Mismatch and deviation from STC losses were shown to be high at Heron Close and Panmure Street with average annual performance ratio losses of 12.4% and 14.3% respectively. This explained in part the low annual performance ratios at these sites. At Corncroft the average annual irradiance losses were calculated as negative values, which is unrealistic. Further investigation showed that the likely cause of these negative values was inaccuracy in the DC power output measurements. This highlighted the susceptibility of the monitoring techniques to measurement error in the monitored data.

Four types of faults were identified: sustained zero efficiency faults which represented long periods of no power output; brief zero efficiency faults where there was no power output for short periods; shading caused by external objects; and inverter MPP tracking faults caused by failure to track the array MPP voltage. Brief zero efficiency faults and inverter MPP tracking faults are largely unseen in previous studies which rely on hourly data. Many of these faults lasted for around five minutes and analysing the five minutely data directly allowed the short lived faults to be observed. Sustained zero efficiency faults caused a loss in annual performance ratio of 38.5% for CC 2 (system 2 at Corncroft) where the inverter failed and was not replaced for several months. This illustrates the need for regular monitoring and quick maintenance. For HC 7, brief zero efficiency faults and inverter MPP tracking faults caused high losses in annual performance ratio (5.5% and 9.3% respectively) possibly due to the effects of a faulty inverter.

Shading faults were identified using a novel technique based on plotting each occurrence of faulty performance on a plot of solar orientation and elevation. High concentrations of faults around particular sun position regions were used to identify shading effects. This is an improvement on previous studies which required a site visit to study the site geometry or the separation of the data into months and individual analysis on each month. The largest loss in annual performance ratio due to shading was 5.2% for CC 5 where the PV system was shaded by a large tree to the south. HC 7 also had high fault concentrations but six monthly shading analysis showed that the faults occurred at different sun position regions in each six month period. This demonstrated that shading was not the cause of the high fault concentration seen at this system; a site visit confirmed that the system was indeed unshaded.

This work has shown that the high resolution monitoring techniques have a clear benefit in improving understanding in PV system performance. The techniques enable the effects of individual losses and faults to be quantified and can be used to explain the differences in annual performance ratios of PV systems.

8.3. Recommendations for raising PV system efficiencies

The second aim of the work was 'to demonstrate how such monitoring can be used to raise the efficiency of current and future PV installations'. The application of the new PV monitoring techniques enables such recommendations to be made.

The analysis of inverter power derating and inverter DC to AC conversion loss showed that, for the systems studied, the optimal array to inverter rating ratio was from 0.76 to 0.79 (Section 6.1.2). The systems in this range (HC 4, 5, and 6 and all at Panmure Street) had minimal inverter power derating and the lowest inverter AC to DC conversion losses. Systems with low array to inverter ratios (HC 7 and HC 12, with array to inverter rating ratios of 0.59 and 0.65) had significant inverter derating. Systems with oversized inverters and high array to inverter ratios had high inverter DC to AC conversions losses. At Corncroft, where the systems have array to inverter rating ratios of 1.47 to 1.63, the inverter DC to AC conversion losses resulted in annual average losses in performance ratio of 8.2% in the first year and 7.9% in the second year. This was around 1% higher than the inverter conversion losses at Heron Close and Panmure Street. The oversized inverters at Corncroft also appeared to cause high inverter MPP tracking losses, although this may have been a result of the inaccuracy in the DC power measurements.

Deviation from STC and mismatch caused significant losses at Heron Close and Panmure Street resulting in a reduction in annual performance ratio of 12.4% and 14.3% respectively (Table 6-5). These findings require further validation (for example more detailed measurements of the PV modules) before reliable conclusions can be made about the performance of the modules. However the data suggests that the PV modules at Heron Close and Panmure Street were operating significantly below their rated efficiency. One recommendation is to measure the efficiency of PV modules at the installation stage to ensure that they are performing according to the claims of the manufacturer.

As noted above, component failure can have a large impact on performance (with a 38.5% loss in annual performance ratio at CC 2). It is essential to have monitoring procedures in place which can quickly identify failures so that these can be repaired immediately thereby avoiding significant energy losses.

The maximum calculated shading loss was a 5.2% reduction in annual performance ratio for a system heavily shaded in autumn and winter by a large tree to the south of the PV array. Although this is a significant reduction, it does demonstrate that PV systems can still perform reasonably under shaded conditions. Shading loss can be eliminated or minimised by removing the external shading objects. The analysis techniques can identify the effects of shading in installed PV systems on a case by case basis and this could be used in decision making on the placement and removal of external shading objects. For example, this approach could determine when the cost of removing a shading object is less than the additional revenue generated (through electricity generation) by removing the object.

8.4. Further work

The new PV monitoring techniques could be developed further to improve their scope and increase their ability to provide insight into PV system performance. The techniques could be developed to analyse monitored data from other PV systems with different recording intervals. A study could investigate the benefits of using these techniques on lower resolution data, such as half hourly or hourly recording intervals. The benefits of using higher resolution data, for example with a one minutely recording interval, could also be investigated. If the techniques can provide additional insights using hourly datasets then they could be applied to the data from a large number of PV systems across the world.

The techniques could be validated by conducting further studies with more detailed measurements of PV system performance. Such work would also determine the optimum number of parameters to measure. Additional measurements might include: measurements of voltage and current to assess inverter MPP tracking routines; measurements of the array temperature at multiple locations to better assess the effects of temperature; measuring the solar radiation with pyranometers to improve the accuracy of the data; and measurements of DC and AC power with independent power meters (instead of the in-built inverter sensors) to improve accuracy.

A separate area of further work would be to extend the monitoring techniques to assess the impact of inverter derating on annual performance ratios. Significant inverter derating was observed using the monitoring techniques but its impact was not calculated. One method of assessing the inverter derating could be to develop techniques to estimate efficiency values if the derating had not occurred, and compare these to the loss in efficiency caused by derating. In addition the remaining operational losses were not calculated for systems with severe inverter derating (because the derating affected efficiencies at irradiance of 1000 W/m^2). An improvement to the monitoring techniques would be to remove this limitation. A further study to investigate the brief zero efficiency faults and inverter MPP tracking faults is also required to determine the reason for the high levels of these faults in the Heron Close systems. Such work might include an investigation of the relationship between the occurrence of these faults and fluctuations in solar irradiance levels.

Finally, the import and export of electricity to and from the households was also monitored in this work. Similar high resolution monitoring techniques could be developed to analyse this import and export data. This study would determine which households are most suited to PV systems and the impact of the PV system on electricity bills. This work would investigate the economic benefits of PV systems for users, which is critical in encouraging the uptake of PV systems.

Bibliography

Alsema, 2005. *The real environmental impacts of crystalline silicon PV modules: an analysis based on up-to-date manufacturers data,* 20th European PV Solar Energy Conference, Barcelona, June 2005

Astropower, 2004. Astropower Ltd. website. www.astropower.com. Accessed June 2004

Baltus et al., 1997. *Analytical monitoring of losses in PV systems*, 14th European PV Solar Energy Conference, Barcelona, June 1997

Baltus, 1998. *The suitability of several methods to quantify energy losses in PV systems,* ECN report: ECN-C-98-098. www.ecn.nl. Accessed 29/11/2005

Betcke et al., 2002. *Evaluation of the performance of PV system designs in the Netherlands in 1997 - 2000,* Novem report: NWS-E-2002-45. www.chem.uu.nl/nws. Accessed 29/11/2005

BP Solar, 2005. BP Solar Ltd. website. www.bpsolar.com. Accessed 16/8/2005

BRE, 2003. *PV Domestic Field Trial: second annual technical report,* DTI contractors report: ETSU S/P2/00335/REP/M2, Department of Trade and Industry, UK. www.dti.gov.uk. Accessed on 1/6/2004

BRE, 2005. Building Research Establishment website. www.bre.co.uk. Accessed on 1/4/2005

BSI, 1998. *Photovoltaic system performance monitoring – guidelines for measurement, data exchange and analysis,* British Standards Institution, BS EN 61724:1998

Bucher and Kunzelmann, 1998. *The Fraunhofer ISE PV charts: Assessment of PV Device Performance,* 2nd World Conference and Exhibition on Photovoltaic Solar Energy Conversion, Vienna, Austria, July 1998

Decker and Jahn, 1997. *Performance of 170 grid connected PV plants in Northern Germany – analysis of yields and optimization potentials,* Solar Energy 59, 127 - 133

DFT, 2002. *DFT tender documentation Annex 6.* www.dti.gov.uk. Accessed October 2002

DTI, 2000. *Photovoltaics in Buildings: BIPV Projects. Studio E Architect,.* DTI contractors report: ETSU S/P2/00328/REP. www.dti.gov.uk. Accessed on 1/11/2005

DTI, 2001. *Photovoltaic (PV) Government – Industry Group Final Report: 26/1/2001,* Department of Trade and Industry report. www.dti.gov.uk. Accessed Jan 2003

DTI, 2002. *Our energy future – creating a low carbon economy,* UK Government white paper. www.dti.gov.uk. Accessed 19/4/2005

DTI, 2005a. UK energy sector indicators 2005, Department of Trade and Industry report, June 2005. www.dti.gov.uk. Accessed 24/8/2005

DTI, 2005b. *Second annual report on the implementation of the energy white paper,* Department of Trade and Industry report, July 2005. www.dti.gov.uk. Accessed 24/8/2005

DTI, 2005c. Department of Trade and Industry website. www.dti.gov.uk. Accessed on 1/4/2005

EETS, 2005. Energy Equipment Testing Services Ltd. website. www.eets.co.uk. Accessed on 6/5/2005

Eikelboom and Jansen, 2000. *Characterisation of PV modules of new generations: results of tests and simulations,* Report no: ECN-C-00-067. www.ecn.nl/library/reports/2000e/zon.html. Accessed on 16/8/2005

Energy Networks Association, 2006. *Engineering Recommendation G.83/1, (2003) Recommendations for the connection of small-scale embedded generators (up to 16A per phase) in parallel with public low-voltage distribution networks.* www.energynetworks.org. Accessed on 12/8/2006

EMC, 2005. The Energy Monitoring Company website. users.powernet.co.uk/emc. Accessed on 1/9/2005

Erge et al., 2001. *The German experience with grid-connected PV systems,* Solar Energy 70, no. 6, pp. 479 – 487

ESD, 2005. Energy for Sustainable Development Ltd. website. www.esd.co.uk. Accessed on 2/4/2005

FES, 2005. Future Energy Solutions website. www.etsu.com. Accessed on 2/4/2005

Gottschalg, 2005. *The solar resource.* Distance learning study notes available from CREST, Loughborough University. www.lboro.ac.uk/departments/el/research/crest. Accessed on 24/8/2005

Green, 1982. *Solar cells: operating principles, technology and system applications,* Prentice-Hall Inc., ISBN 0-13-822270-3

Gxasheka et al., 2005. *Evaluation of performance parameters of PV modules deployed outdoors,* Renewable Energy 30, 611 – 620

Haeberlin et al., 2005. *Total efficiency – a new quantity for better characterisation of grid-connected PV inverters,* 20th European PV Solar Energy Conference, Barcelona, June 2005

Heilscher et al., 1998. *Shading analysis with 100 PV-Systems,* 2nd World Conference and Exhibition on Photovoltaic Solar Energy Conversion, Vienna, Austria, 6 – 10 July 1998

Herrmann, 2005. *Analyses of array losses caused by electrical mismatch of PV modules,* 20th European PV Solar Energy Conference, Barcelona, June 2005

IEA, 2000. *Analysis of photovoltaic systems,* IEA PVPS report: T2-01:2000. www.iea-pvps.org. Accessed on 16/8/2005

IEA, 2003. *Trends in photovoltaic applications: Survey report of selected IEA countries between 1992 and 2002,* IEA PVPS report: T1-12:2004. www.iea-pvps.org. Accessed on 8/8/2005

IEA, 2004a. *Trends in photovoltaic applications: Survey report of selected IEA countries between 1992 and 2003,* IEA PVPS report: T1-13:2004. www.iea-pvps.org. Accessed on 8/8/2005

IEA, 2004b. *National Survey Report of PV Power Applications in Japan, 2003.* www.iea-pvps.org. Accessed on 8/8/2005

IEA, 2004c. *National Survey Report of PV Power Applications in the United Kingdom, 2003.* www.iea-pvps.org. Accessed on 8/8/2005

IEA, 2004d. *Country reports on PV system performance,* IEA-PVPS report: T2-05:2004. www.iea-pvps.org accessed on 9/8/2005

IEA, 2005a. *World Energy Outlook 2004.* www.iea-pvps.org. Accessed on 16/8/2005

IEA, 2005b. *Trends in photovoltaic applications: Survey report of selected IEA countries between 1992 and 2004,* report in press. www.iea-pvps.org. Accessed on 8/8/2005

IEA, 2005c. IEA PVPS website. www.iea-pvps.org. Accessed on 16/8/2005

Infield et al., 2001. *Maximum Power Point Tracking Design and Assessment with Emphasis on Thin Film Cells*, Final review report of EPSRC project GR/M16665/01

IPCC, 2001. *Climate Change 2001: Third Assessment Report.* www.ipcc.ch. Accessed on 17/4/2005

ISET, 2005. Institut für Solare Energieversorgungstechnik website. www.iset.uni-kassel.de. Accessed on 6/5/2005

IT Power, 2005. IT power website. www.itpower.co.uk. Accessed 29/11/2005

Jahn and Nasse, 2004. *Operational performance of grid-connected PV systems on buildings in Germany,* Progress in Photovoltaics, 12:441-448 (2004)

Jantsch et al., 1997. *Measurement of PV maximum power point tracking performance,* 14th European PV Solar Energy Conference, Barcelona, June 1997

Kawamura et el., 2003. *Simulation of I-V characteristics of a PV module with shaded cells,* Solar Energy Materials and Solar Cells 75 (2003) 613 – 621

Kiefer et al., 1995. *2250 PV-roofs in Germany – operating results from intensified monitoring and analysis through numerical modelling,* 13th European Solar Energy Conference, Nice, France, October 1995

Kovach and Schmid, 1996. *Determination of energy output losses due to shading of building integrated photovoltaic arrays using a raytracing technique,* Solar Energy 57, No. 2, pp. 117-124, 1996

Kovach, 1995. *Effect of partial shading on the energy performance of photovoltaic arrays integrated onto buildings,* VDI-Verlag, Dusseldorf (cited by Woyte et al., 2003)

Kreutzer, 2006. Personal communication.

Labfacility, 2005. Labfacility website. www.labfacililty.co.uk. Accessed on 5/5/2005

Laplink, 2005. Laplink website. www.laplink.com. Accessed on 5/5/2005

LUMetS, 2005. www.lboro.ac.uk/departments/gy/climate/index.html. The data was recorded by K. Boucher at the Geography Department of Loughborough University.

Mathworld, 2005. Mathworld website. mathworld.wolfram.com. Accessed 29/11/2005

Met Office, 2005. Meteorological office website. www.met-office.gov.uk. Accessed on 1/9/2005

Microsoft, 2005. Microsoft website. www.microsoft.com. Accessed on 5/9/2005

Mjtnet, 2005. Mjtnet website for Macro Scheduler Software. www.mjtnet.com. Accessed on 6/5/2005

Nishioka et al., 2003. *Field test analysis of PV system output characteristics focusing on module temperature,* Solar Energy Materials and Solar Cells 75 (2003) 665-671

Nordmann and Clavadetscher, 2003. *Understanding temperature effects on PV system performance,* IEA-PVPS Task 2 paper. www.iea-pvps.org. Accessed on 23/5/2005.

NPAC, 2005.. Northumbria Photovoltaic Applications Centre website. http://soe.unn.ac.uk/npac/npac.htm. Accessed on 4/9/2005.

Oozeki et al., 2003. *An evaluation method of PV systems,* Solar Energy Materials and Solar Cells 75 (2003) 687 – 695

Oozeki et al., 2005. *An accuracy of the SV method for evaluated shading losses – compared with results using the fish-eye-photogram method,* 20th European PV Solar Energy Conference, Barcelona, June 2005

Pearsall and Hynes, 2003. *Monitoring of domestic PV installations,* DTI contractors report: ETSU S/P2/00319/REP. www.dti.gov.uk. Accessed 20/8/2005

Powerstream, 2005. Powerstream website. www.powerstream.com. Accessed 29/11/2005

Ransome and Funtan, 2005. *Why hourly averaged measurement data is insufficient to model PV system performance accurately,* 20th European PV Solar Energy Conference, Barcelona, June 2005.

Ransome et al., 2004. *Can grid tied PV systems be characterised with only monthly average values of PR?,* 19th European PV Solar Energy Conference, Paris, June 2004

RCEP, 2000. *Energy – the changing climate,* Royal Commission on Environmental Pollution report. www.rcep.org.uk. Accessed on 20/4/2005

Reinders et al., 1999. *Technical and economic analysis of grid-connected PV systems by means of simulation,* Progress in Photovoltaics, 7:71-82 (1999)

Roaf and Fuentes, 1999. *Demonstration project for a 4 kW domestic photovoltaic roof in Oxford,* DTI contractor report: ETSU S/P2/00236/REP/1. www.dti.gov.uk. Accessed 20/8/2005

RSI, 2005. Research Systems Inc. website. www.rsinc.com. Accessed on 5/9/2005

SMA, 2005. SMA Technologie AG website. www.sma.de. Accessed on 5/5/2005

Stamenic et al., 2004. *Low light conditions modelling for building integrated photovoltaic (BIPV) systems,* Solar Energy 77 (2004) 37 – 45

Stettler et al., 2005. *Failure detection routine for grid connected PV systems as part of the PVSAT-2 project,* 20th European PV Solar Energy Conference, Barcelona, June 2005.

Stokes, 2005. *Removing barriers to embedded generation: a fine-grained load model to support low voltage network performance analysis,* PhD thesis, De Montfort University.

Sugiura et al, 2003. *Measurements, analyses and evaluation of residential PV systems by Japanese monitoring program,* Solar Energy Materials and Solar Cells 75 (2003) 767 – 779

Uchida et al., 2001. *Evaluation of effective shading factor by fitting a clear-day pattern obtained from hourly maximum irradiance data,* Solar Energy Materials and Solar Cells 67 (2001) 519-528

UNFCCC, 2005. United Nations Framework Convention on Climate Change website. unfccc.int. Accessed 19/4/2005

Vector Instruments, 2005. Vector Instruments website. www.windspeed.co.uk. Accessed on 9/5/2005

Woyte et al., 2003. *Partial shadowing of photovoltaic arrays with different system configurations: literature review and field test results,* Solar Energy 74 (2003) 217-233

Appendix A. Calculating the Sun Positions

A.1. Sun position calculations

Sun position is described using the parameters of orientation and elevation. Solar orientation α (also known as the azimuth) is the bearing in degrees from due south where east is positive and west is negative. Solar elevation β is the angle made between the sun position and the horizontal.

For each date and time stamp of the five minute recording intervals, the position of the sun was calculated. The positions were saved into a separate data file and could be recalled for use in the later data analysis. In particular the sun position calculations were used in the data plausibility checks of Chapter 4 and the shading analysis technique in Chapter 7.

The method of calculating the sun positions was based on a review of previous studies by Gottschalg (Gottschalg, 2005). This explored different sun position models and presented a simple method to undertake the calculations. It is assumed that the position of the Earth is fixed and the sun orbits the Earth on an ecliptic plane (Figure A-1). The equatorial plane is defined as the plane which passes through the equator of the Earth. The Sun crosses the equatorial plane at the summer and autumn equinoxes. The summer and winter solstice occur then the Sun is furthest from the equatorial plane. The angle made between a line drawn from the centre of the Sun to the centre of the Earth and the equatorial plane is defined as the solar declination δ.

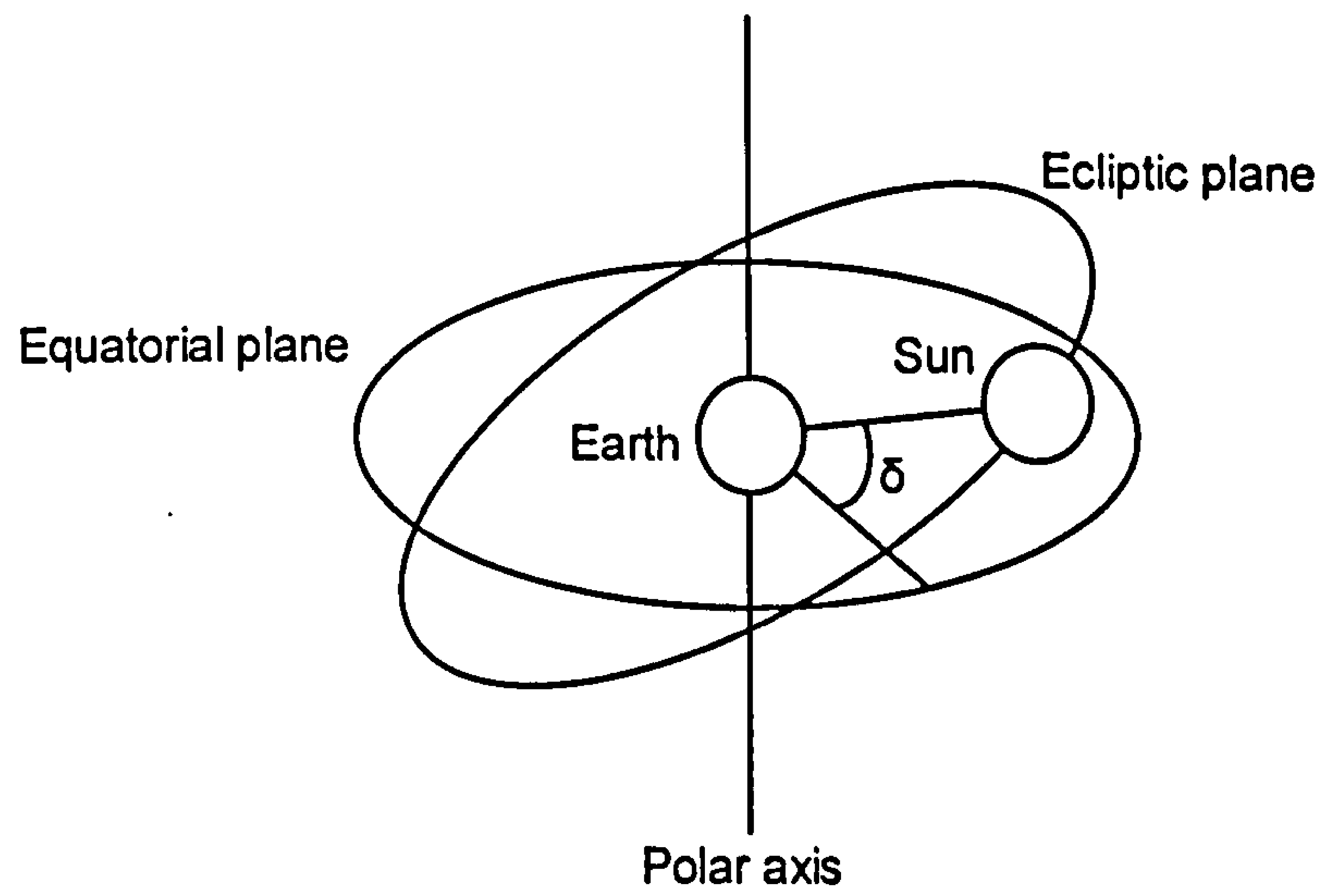

Figure A-1: The Sun – Earth system assuming the position of the Earth is fixed.

The position of the sun is calculated using the following equations:

1. Calculation of solar time using the equation:

The value of time used to calculate the sun differs from the local clock time due to the position of the point of interest on Earth and variations in the Earth's orbit of the sun. Time specific to the sun is defined as solar time and is calculated as:

$$\text{Solar time} = \text{Standard time} + E + 4(L_{st} - L_{loc})$$

where L_{st} is the standard meridian for the local time zone (°), L_{loc} is the longitude of the location (°) and E is the equation of time. The equation of time E varies throughout the year with a maximum value of ± 7 minutes. Its value is calculated as:

$$E = 9.87\sin(2B) - 7.53\cos B - 1.5\sin B$$

where E is the equation of time (minutes) and B is calculated as:

$$B = \frac{360(DoY - 81)}{364}$$

where DoY is the day of year. DoY value varies between 1 and 365 (366 on a leap year).

2. Calculation of the solar declination δ:

Solar declination is defined as the angle between a line drawn between the centres of the Earth and Sun and the equatorial plane. It can be calculated using the day of year as:

$$\delta = 23.45\sin\left(\frac{360}{365}(DoY + 284)\right)$$

where δ is the solar declination (°).

3. Calculation of the hour angle ω:

The hour angle is calculated using the solar time value. It represents the angle between the orientation of the sun at noon and its apparent orientation at the time in question. Each hour of solar time accounts for 15° of hour angle and in 24 hours 360° is described. The hour angle is calculated as:

$$\omega = (12 - solar\_time) * 15°$$

where ω is the hour angle (°).

4. Calculation of solar elevation β:

From the calculated values of solar declination and hour angle, and the latitude of the location, the solar elevation is calculated as:

$$\sin\beta = \sin\delta\sin\phi + \cos\delta\cos\phi\cos\omega$$

where β is the solar elevation (°) and Φ is the latitude of the location (°).

5. Calculation of solar orientation α:

The solar orientation is calculated using the solar elevation, solar declination and the latitude of the location by the following equation:

$$\cos\alpha = \frac{\sin\beta\sin\phi - \sin\delta}{\cos\beta\cos\phi}$$

where α is the solar orientation (°).

Appendix B. Data Quality and Plausibility

B.1. Date and time stamp checks

B.1.1 Corncroft

The Corncroft date and time stamp check was discussed in Section 4.1.2.

B.1.2 Heron Close

The Heron Close data was recorded using six SBC+ units each with a clock. It was possible to view the clocks and all were recording on BST. At house 12 the data was recorded for a period where the clock altered to GMT, shown by plotting the horizontal irradiance data (Figure B-1). The GMT recording occurred between 10th Oct 2004 at 00:00 and 2nd Feb 2005 at 11:00. All the data at Heron Close was converted to GMT except for the data recorded by the SBC+ in house 12 during this time period.

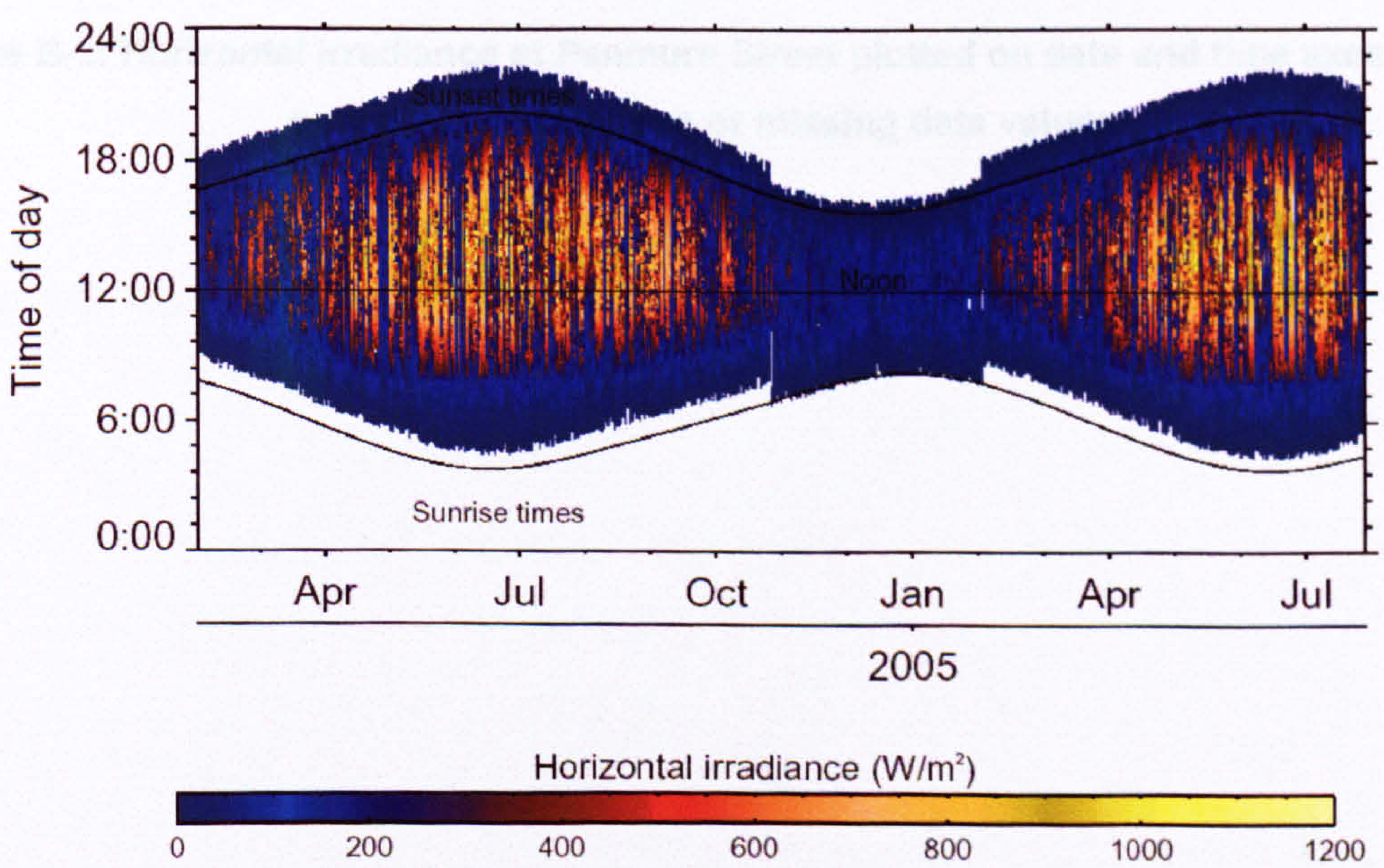

Figure B-1: Horizontal irradiance at Heron Close plotted on date and time axes. White space represents zero or missing data values.

B.1.3 Panmure Street

The Panmure street data was recorded by three SBC+ units with their clocks set to BST (Figure B-2). All the data was converted to GMT.

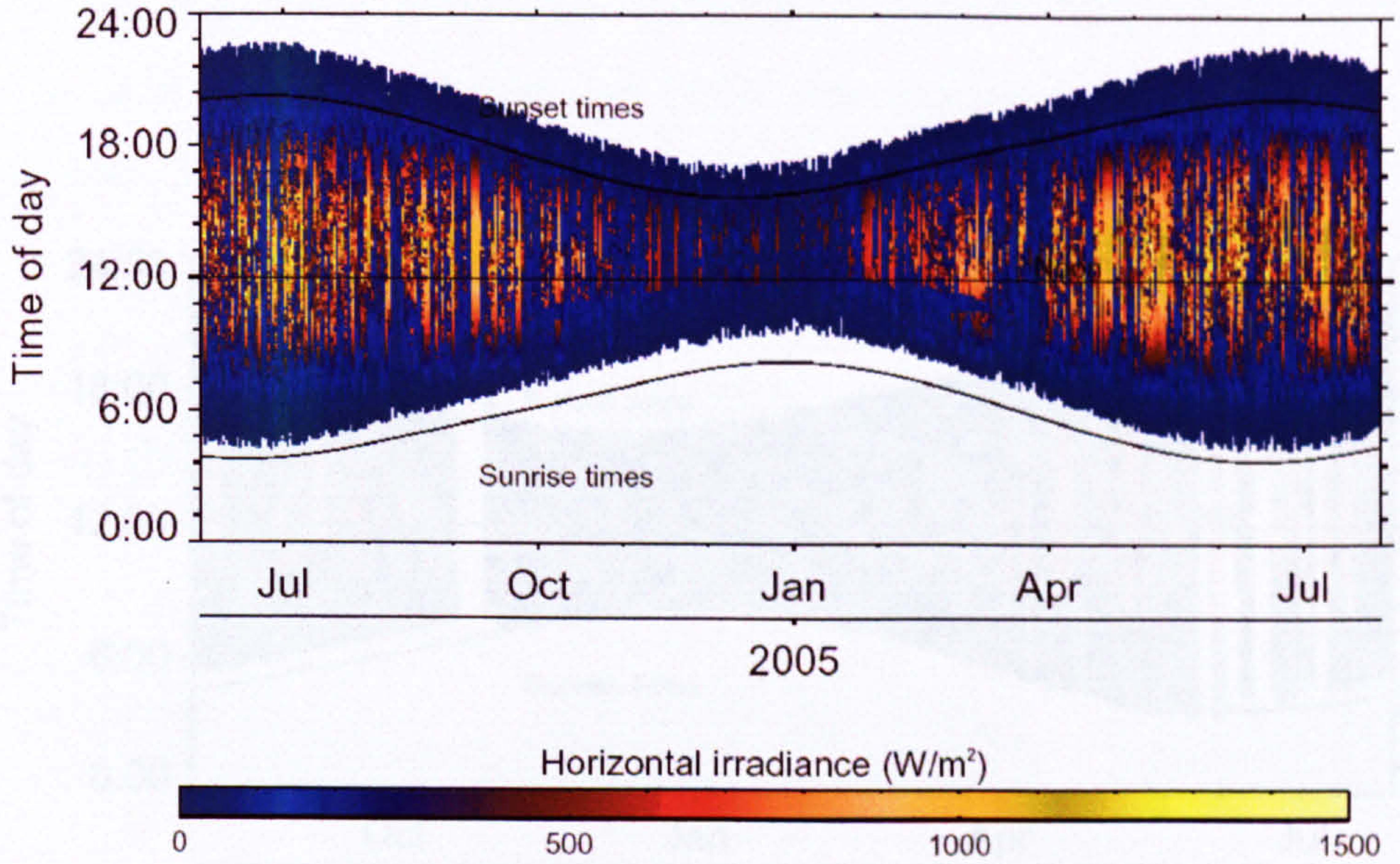

Figure B-2: Horizontal irradiance at Panmure Street plotted on date and time axes. White space represents zero or missing data values.

B.1.4 Newbiggin Hall

Data at Newbiggin Hall was recorded on a single PC clock. The data was recorded in a combination of GMT and BST, possibly due to the PC clock altering itself. BST recording was 1st August 2004 to 31st October 2005 and 14th May 2005 to 31st July 2005. The data recorded for all parameters in these time periods was converted to GMT.

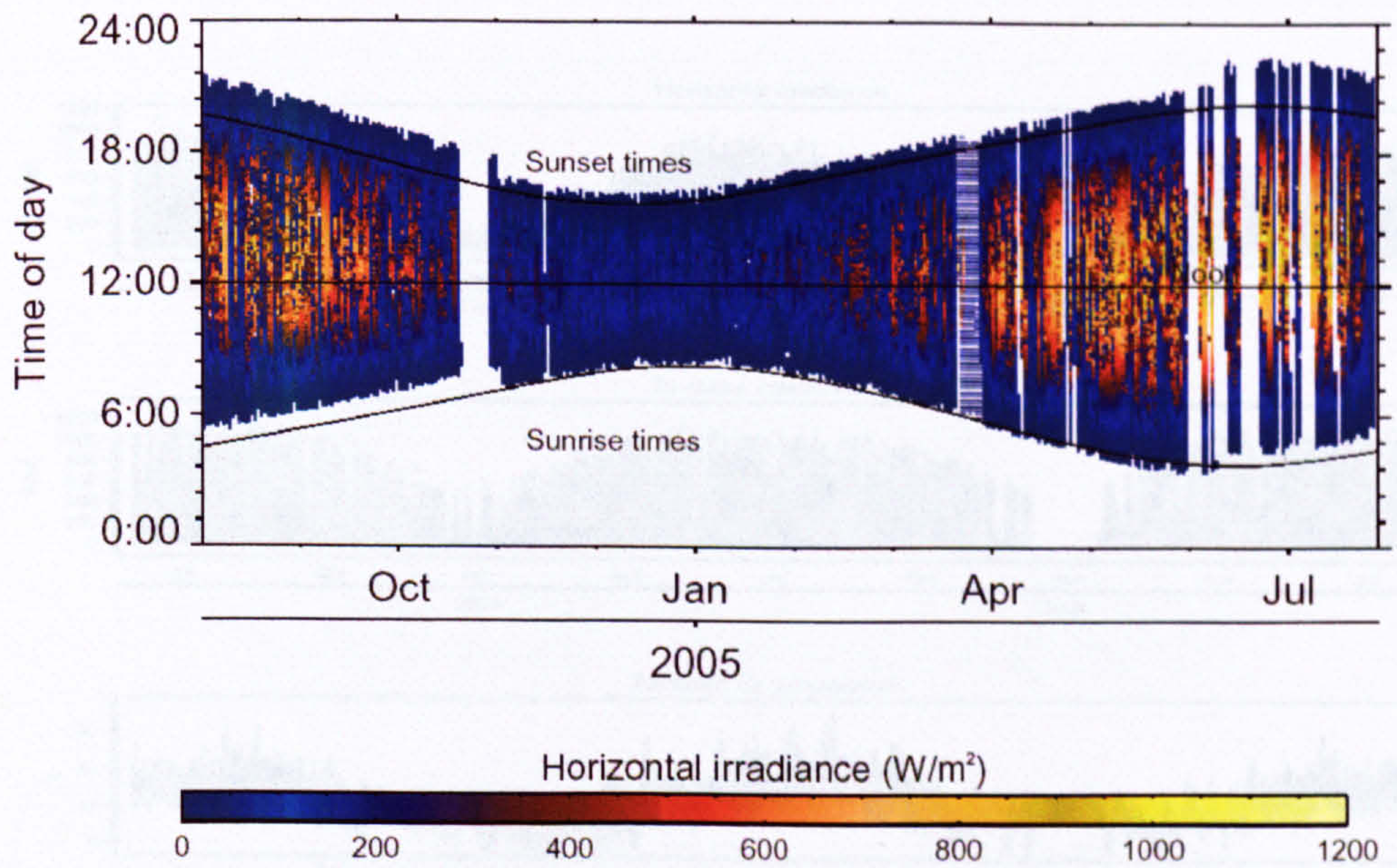

Figure B-3: Horizontal irradiance at Newbiggin Hall plotted on date and time axes. White space represents zero or missing data values.

B.2. Data screening

B.2.1 Corncroft

A plot of the meteorological parameters at Corncroft versus date and time showed no error values (Figure B-4). There were no high, improbable values or no negative values in the irradiance data. The sustained constant zeros that occurred in the irradiance data in Dec 2003 and Jan 2004 represented only the night time values. In the daytime in this time period, the irradiance data was missing.

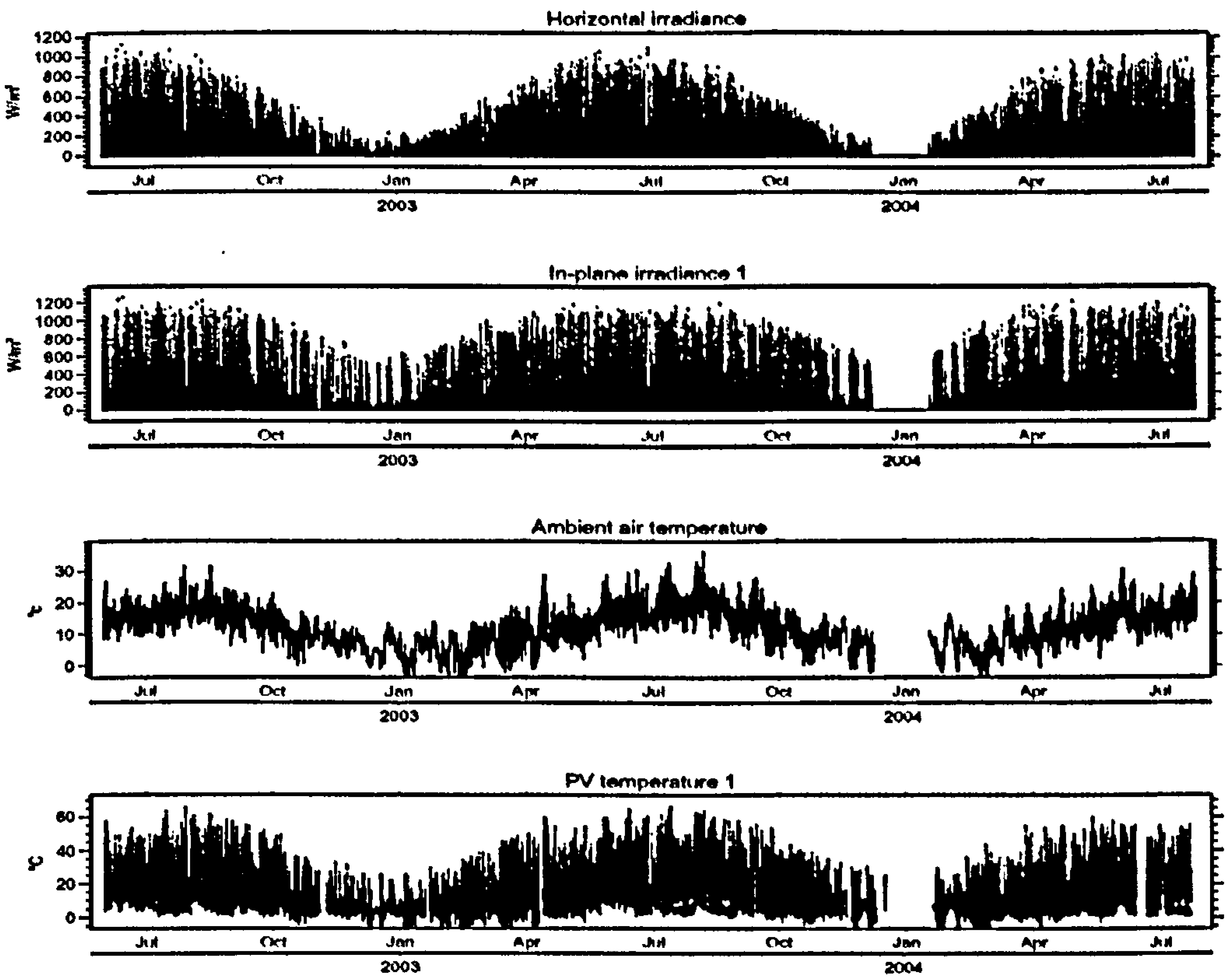

Figure B-4: Corncroft meteorological data plotted on date and time axes

B.2.2 Heron Close

A plot of the meteorological parameters at Heron Close shows that there were some sections of sustained zero values in the ambient air and second set of PV module temperature measurements (Figure B-5). These occurred in July and October 2004 in the ambient air data and in April and July 2004 in the second set of PV temperature data. The measurements were considered to be errors and the values were converted to missing data. There were also some periods of sustained zero measurements in the second set of irradiance data (in March, April and July 2004 and April 2005). This represented missing data where the night time values had been replaced with zeros.

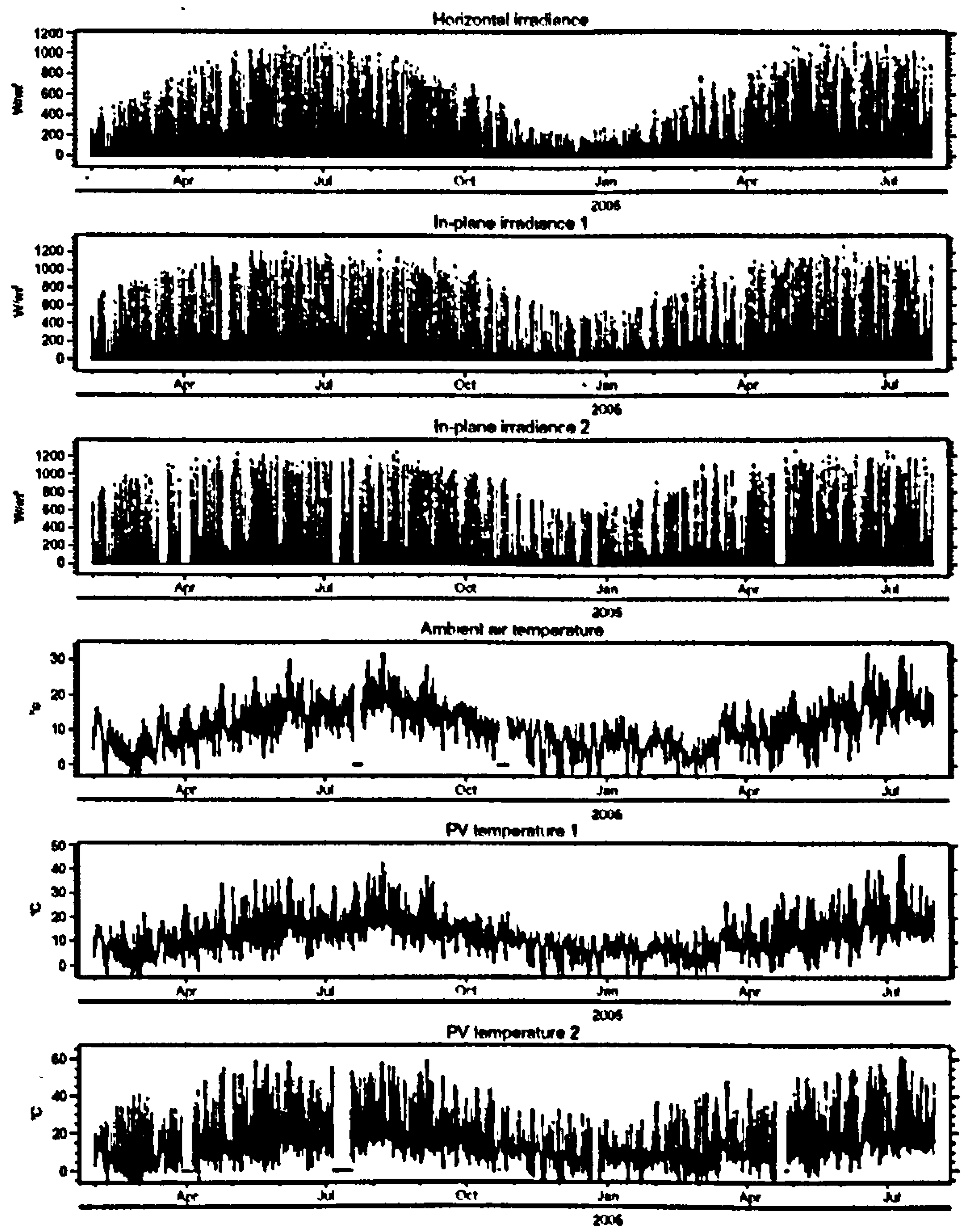

Figure B-5: Heron Close meteorological data plotted on date and time axes

B.2.3 Panmure Street

Plots of the Panmure Street meteorological data shows no sign of outliers or other error values (Figure B-6).

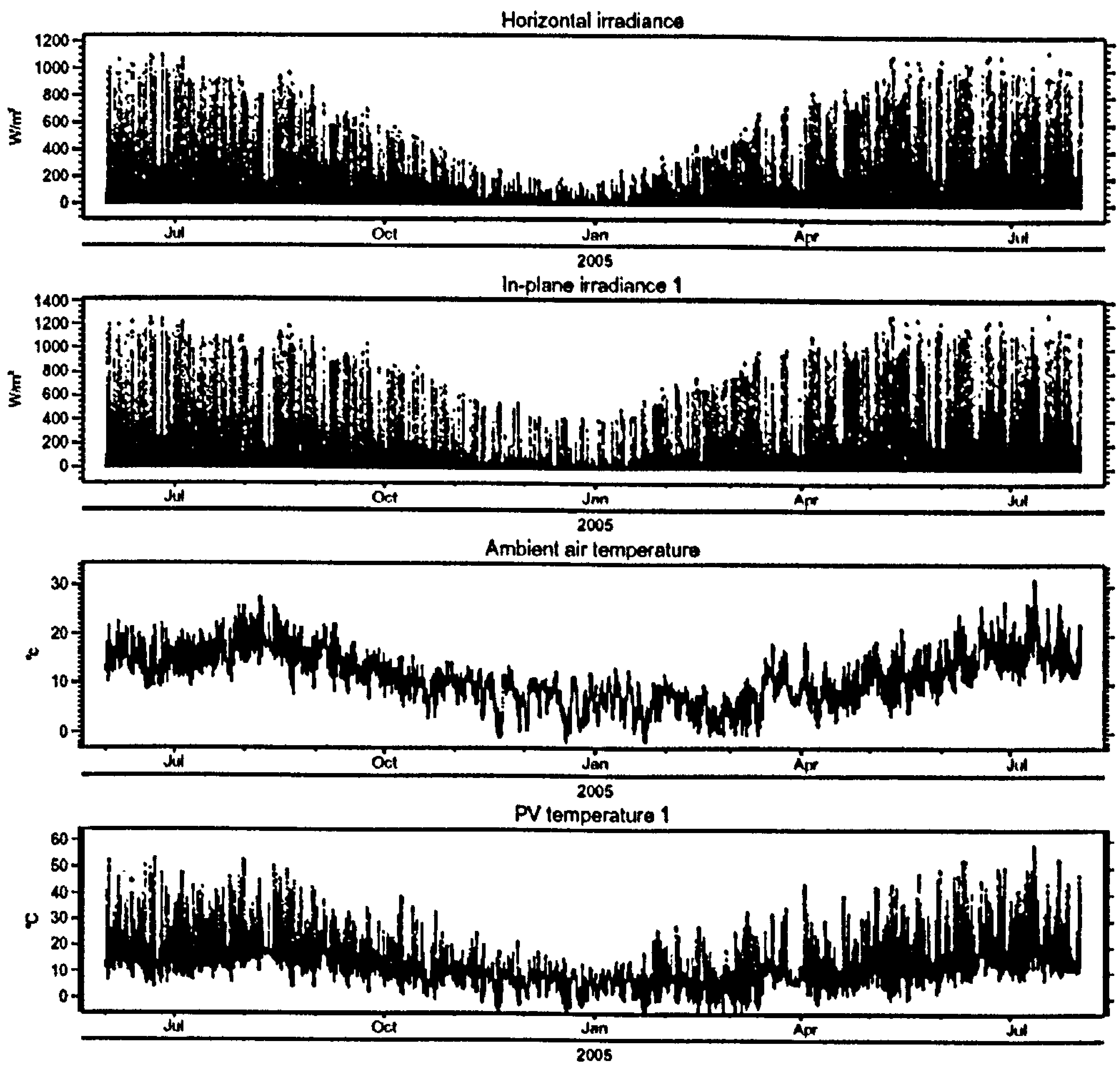

Figure B-6: Panmure Street meteorological data plotted on date and time axes

B.2.4 Newbiggin Hall

The Newbiggin Hall meteorological data shows a number of unexpected zero values in the ambient air temperature parameter (Figure B-7). These zero values occur sporadically after March 2005 (circled in red in the figure) and are removed as error values. The PV temperature 3 data showed unexpected readings and the plausibility of this data is discussed in Section B.4.2.

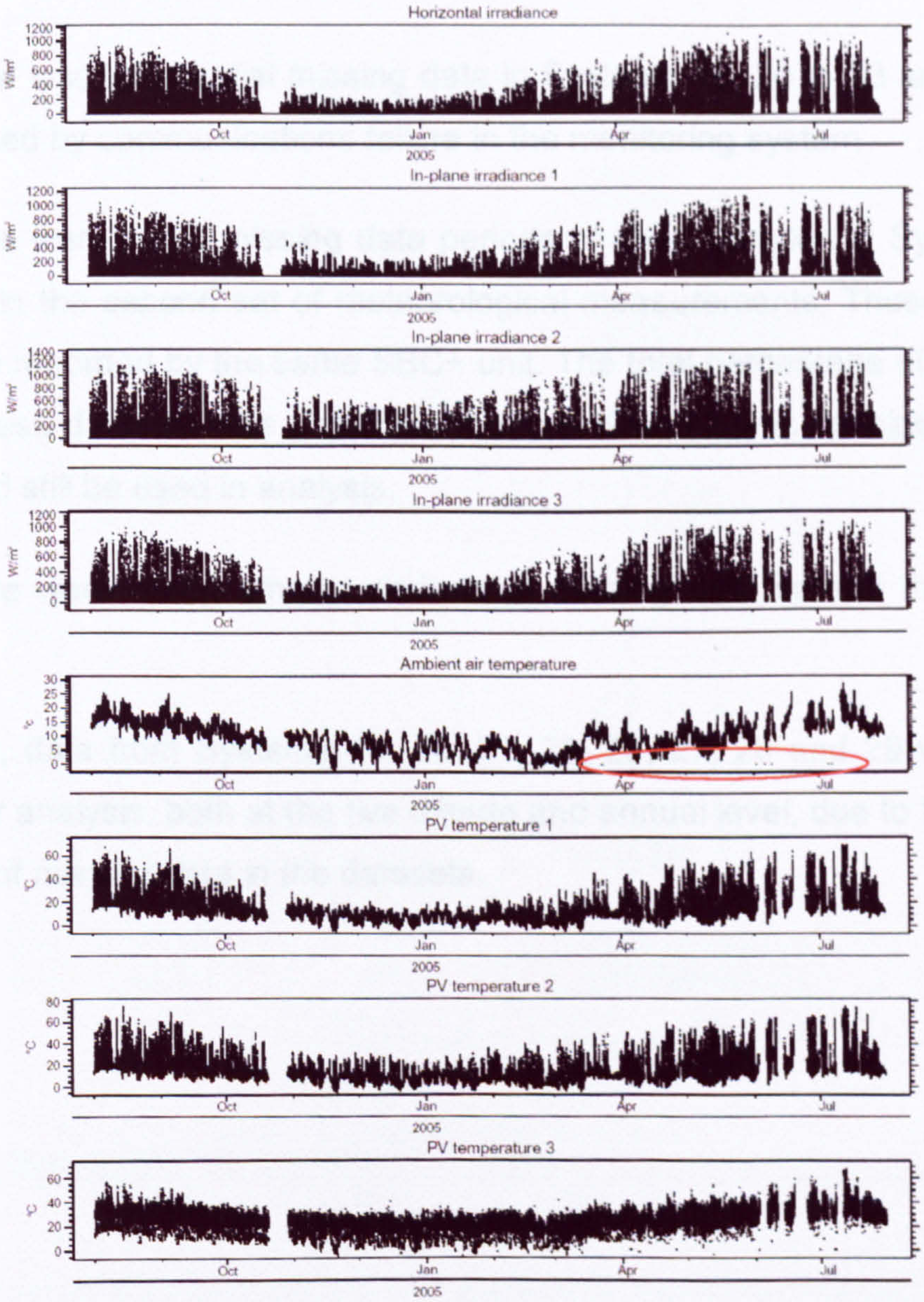

Figure B-7: Newbiggin Hall meteorological data plotted on date and time axes

B.3. Missing Data

B.3.1 Corncroft

The Corncroft missing data was discussed in Section 4.1.5.

B.3.2 Heron Close

The plot of the daily percentage missing data at Heron Close (Figure B-8) shows number of issues:

- There was substantial missing data in Systems 18, 20 to 23 and 27 to 29 – caused by communications failure in the monitoring system

- There were many missing data periods of short duration in Systems 4 to 7 and in the second set of meteorological measurements. These parameters were recorded by the same SBC+ unit. The total percentage of missing data in these datasets was a maximum of 3.5 % and it was considered that they could still be used in analysis.

- There were other, smaller periods of missing data spread throughout the data

As a result, data from Systems 18, 20, 21, 22, 23, 27, 28 and 29 was excluded from further analysis, both at the five minute and annual level, due to the significant proportion of missing data in the datasets.

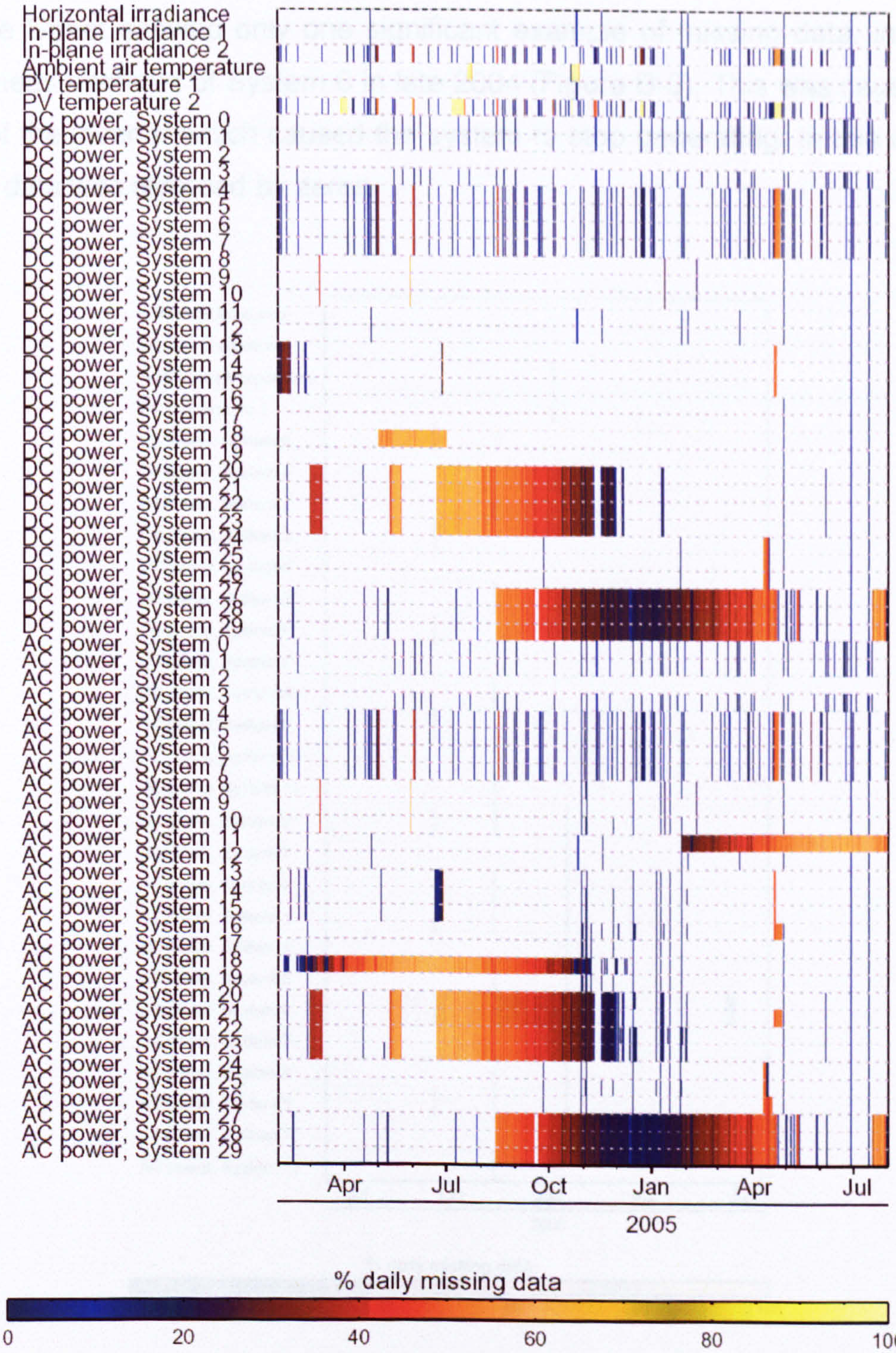

Figure B-8: Daily percentage of missing data at Heron Close. The percentage of missing data on each day is indicated by the colour scale in the legend. White space indicates that no missing data was present.

B.3.3 Panmure Street

Panmure Street showed only one significant example of missing data, in the AC power measurements of System 6 in late 2004 (Figure B-9). This was caused by a failure of the inverter which caused the system to stop generating. In this case the missing data was replaced by zeros.

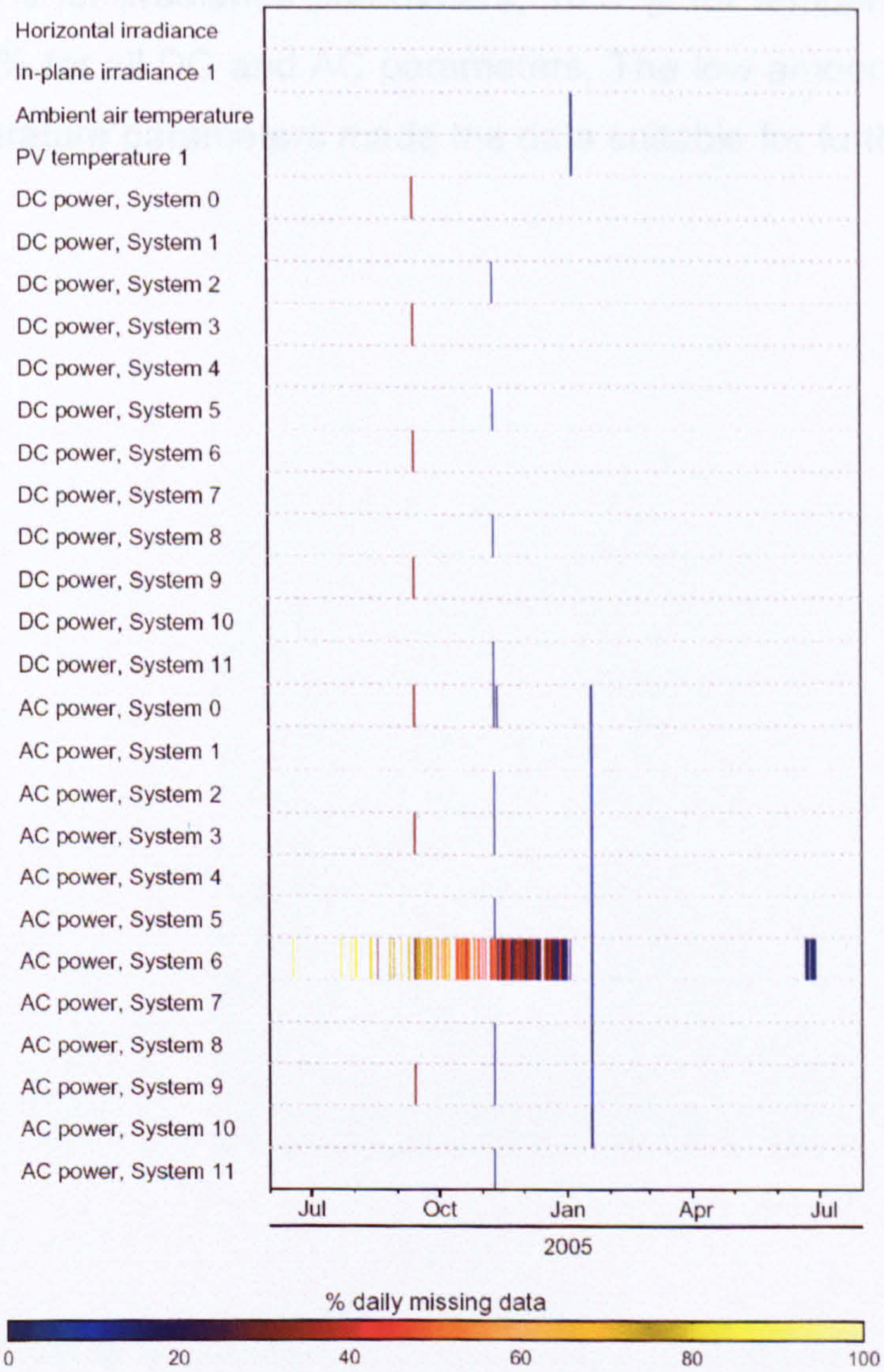

Figure B-9: Daily percentage of missing data at Panmure Street. The percentage of missing data on each day is indicated by the colour scale in the legend. White space indicates that no missing data was present.

B.3.4 Newbiggin Hall

Data at Newbiggin Hall was recorded by a single PC and, if the PC failed, then data was not recorded for all the parameters. The effect can be seen in periods of missing data which extend through all parameters (Figure B-10). There was also extensive low levels of missing data in the DC and AC datasets due to the removal of error values (described in Section 4.1.5).The total percentage of missing data was around 6.0 % for irradiance parameters, 10.3 % for temperature parameters and from 2 to 5 % for all DC and AC parameters. The low amount of missing data in the non-temperature parameters made the data suitable for further analysis.

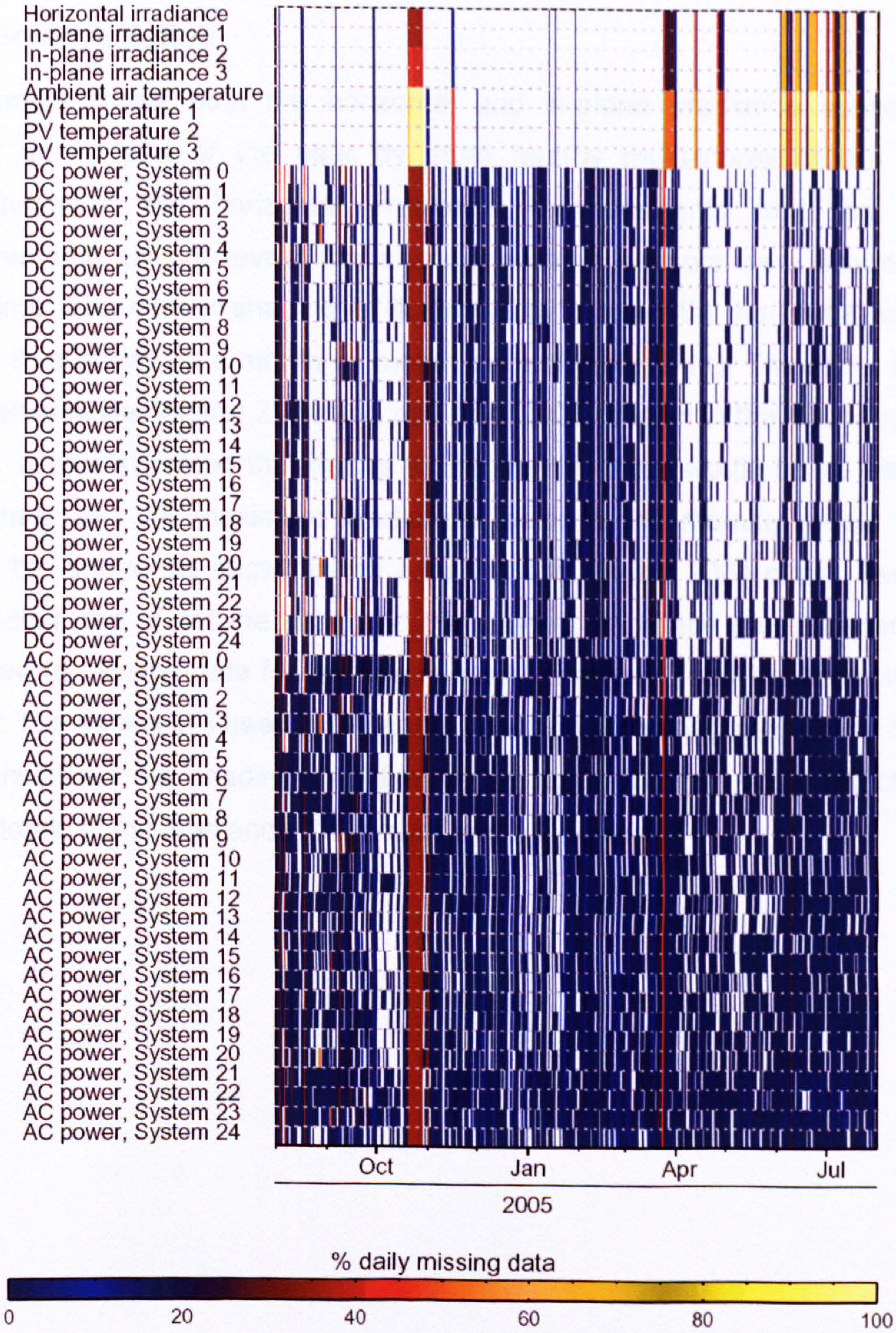

Figure B-10: Daily percentage of missing data at Newbiggin Hall. The percentage of missing data on each day is indicated by the colour scale in the legend. White space indicates that no missing data was present.

B.4. Plausibility checks

B.4.1 Solar radiation

At Panmure Street both the horizontal and in-plane irradiance sensors were shaded during part of the year by three nearby multi-storey blocks of flats. Comparison of the horizontal irradiance measurements and the in-plane measurements did not reveal this shading as both sensors were shaded at the same time. The sensor shading is illustrated by plotting the horizontal irradiance against time of day on a month by month basis (Figure B-11). The effect is clearly seen between September 2004 and mid April 2005 (shown in the figure by the red circles). It was expected that during these months there would be at least some bright days and the maximum irradiances seen in the morning would follow a smooth bell shape (as shown in the June 2004 to August 2004 plots). Because of the shading, this is not the case and the shaded irradiance measurements were converted to missing data for the five minutely analysis. The PV arrays were also shaded. The data is still used in the annual performance analysis (Section 5.1) as it was considered the shading would have an approximately equal effect on the annual totals of the irradiance, DC power and AC power.

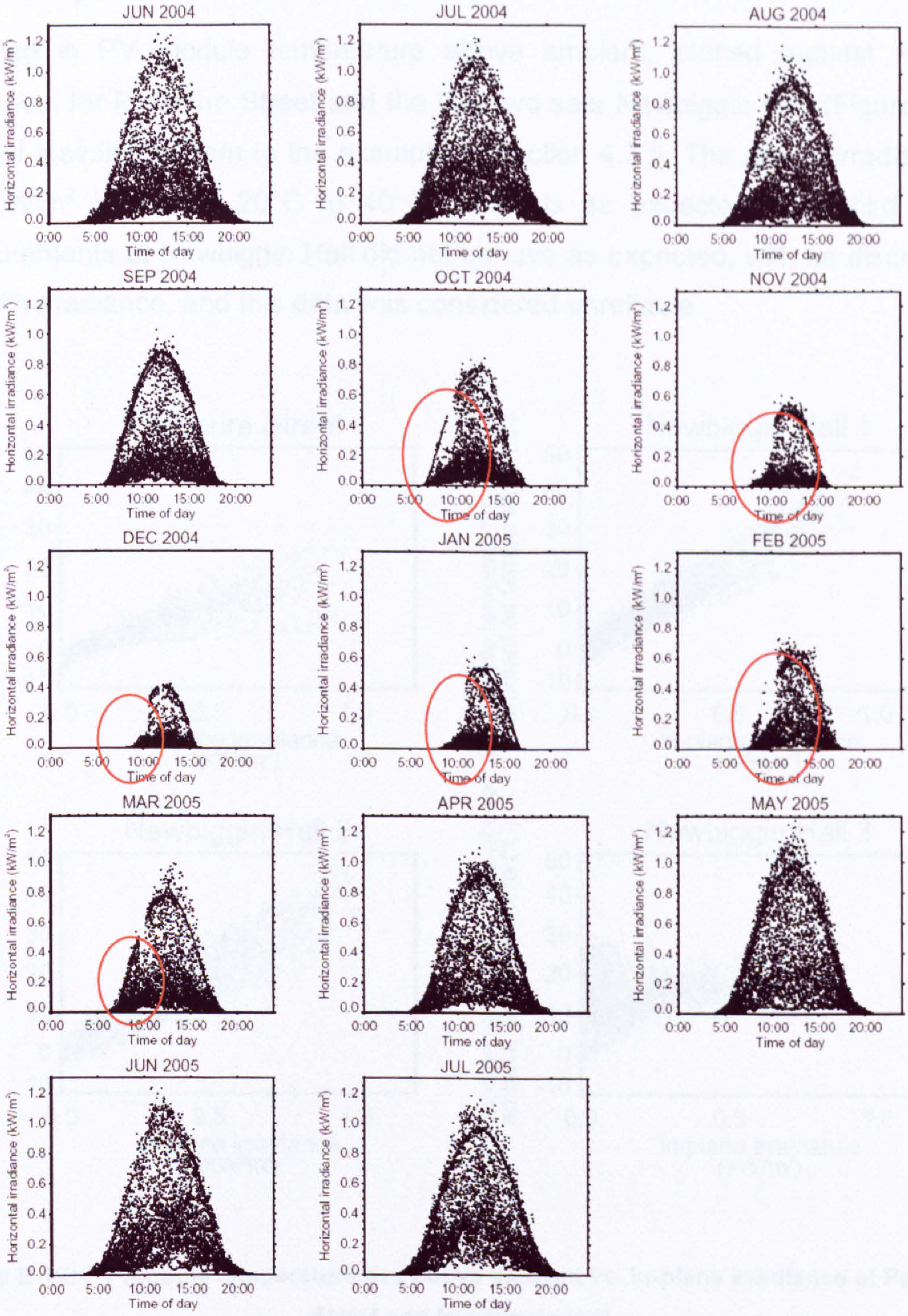

Figure B-11: Time of day vs. horizontal irradiance at Panmure Street. Separate plots for each month. The red circles show the effects of shading.

B.4.2 Temperature

The rise in PV module temperature above ambient, plotted against in-plane irradiance, for Panmure Street and the first two sets Newbiggin Hall (Figure B-12) showed a similar pattern to the example in Section 4.3.5. The rise at irradiance of 1000 W/m^2 is around 20°C to 40°C, which is as expected. The third set of measurements at Newbiggin Hall did not behave as expected, with no discernable rise with irradiance, and this data was considered unreliable.

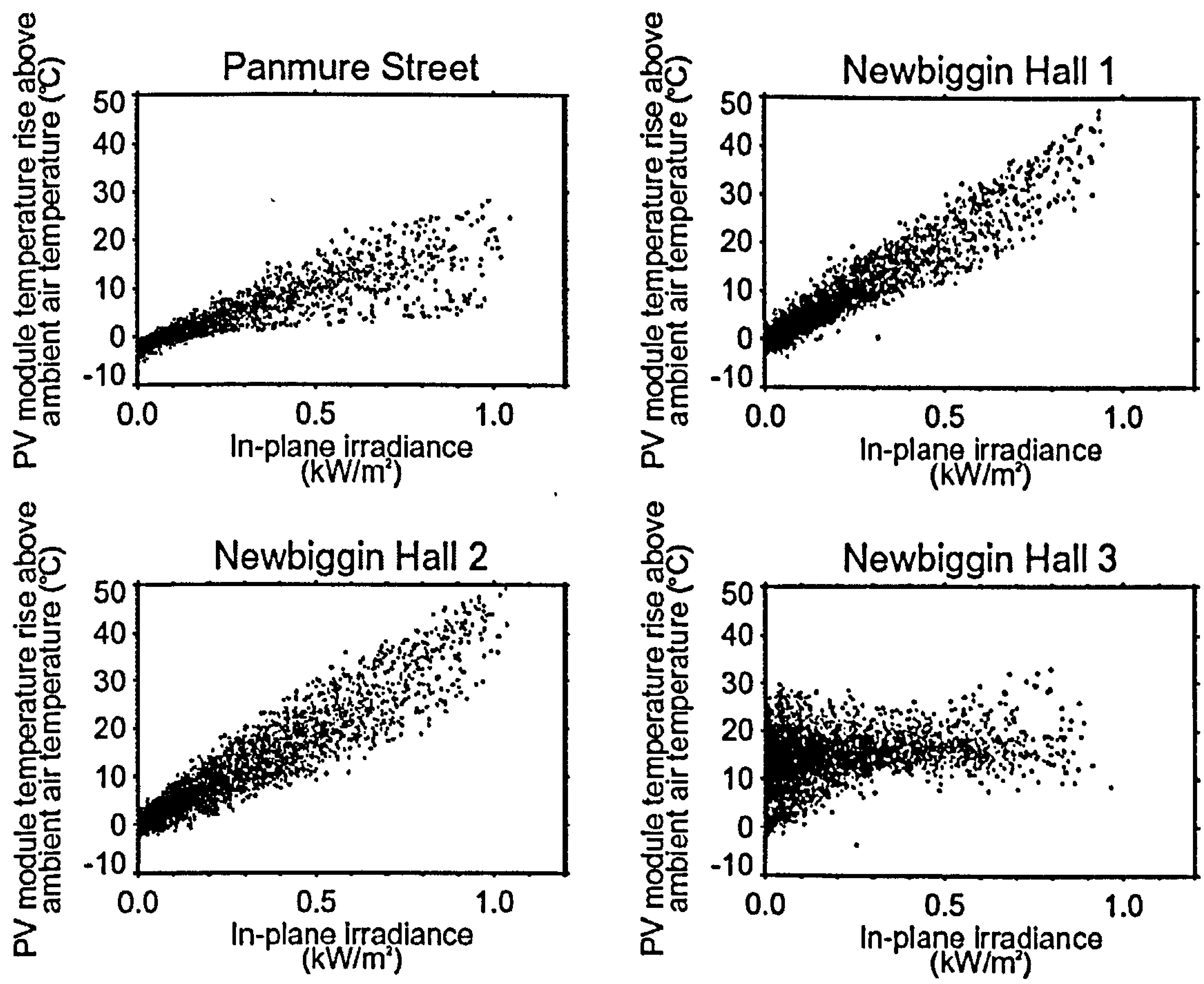

Figure B-12: PV module temperature rise above ambient vs. in-plane irradiance at Panmure Street and Newbiggin Hall

Appendix C. Annual results and Five Minutely Analysis

C.1. Annual results

C.1.1 Corncroft Year 1

Table C-1: Annual monitoring results at Corncroft in the first year of operation

System	Horizontal solar irradiation (kWh/m^2)	In-plane solar irradiation (kWh/m^2)	DC energy output from array (kWh)	AC energy output from inverter (kWh)	Final yield (kWh/kWp)	Performance ratio (%)	System efficiency	Inverter efficiency (%)
1	858	1024	1324	1095	716	69.9	0.094	82.7
2	858	1024	1488	1237	808	79.0	0.106	83.1
3	858	1024	965	766	501	48.9	0.066	79.4
4	858	1024	1352	1106	723	70.6	0.095	81.8
5	858	1024	1449	1203	787	76.8	0.103	83.0
6	858	1024	1393	1141	746	72.9	0.098	81.9
7	858	1024	1489	1247	815	79.6	0.107	83.7
8	858	1024	1431	1181	772	75.4	0.101	82.6
9	858	1024	1275	1082	707	69.1	0.093	84.9
10	858	1024	1571	1317	775	75.7	0.101	83.8
11	858	1024	1487	1232	805	78.7	0.105	82.9
12	858	1024	1527	1280	836	81.7	0.109	83.8
13	858	1024	1440	1204	787	76.9	0.103	83.6
14	858	1024	1469	1216	795	77.6	0.104	82.7
15	858	1024	1605	1356	797	77.9	0.104	84.5
16	858	1024	1504	1256	821	80.2	0.107	83.5
17	858	1024	1486	1234	806	78.8	0.106	83.0
18	858	1024	1504	1252	818	79.9	0.107	83.2
19	858	1024	1525	1278	836	81.6	0.109	83.9
20	858	1024	1487	1237	809	79.0	0.106	83.2
21	858	1024	1507	1261	824	80.5	0.108	83.7
22	858	1024	1409	1185	774	75.7	0.101	84.1

C.1.2 Corncroft Year 2

Table C-2: Annual monitoring results at Corncroft in the first year of operation

System	Horizontal solar irradiation (kWh/m^2)	In-plane solar irradiation (kWh/m^2)	DC energy output from array (kWh)	AC energy output from inverter (kWh)	Final yield (kWh/kWp)	Performance ratio (%)	System efficiency	Inverter efficiency (%)
1	854	1027	1190	996	651	63.4	0.085	83.7
2	854	1027	1461	1230	804	78.3	0.105	84.2
3	854	1027	597	482	315	30.7	0.041	80.7
4	854	1027	1306	1085	709	69.0	0.092	83.0
5	854	1027	1407	1181	772	75.2	0.101	83.9
6	854	1027	1341	1110	725	70.6	0.095	82.7
7	854	1027	1457	1234	806	78.5	0.105	84.7
8	854	1027	1402	1171	766	74.5	0.100	83.5
9	854	1027	1288	1099	718	69.9	0.094	85.3
10	854	1027	1544	1309	770	74.9	0.100	84.8
11	854	1027	1463	1230	804	78.2	0.105	84.0
12	854	1027	1505	1275	834	81.1	0.109	84.7
13	854	1027	1407	1190	778	75.7	0.101	84.6
14	854	1027	1429	1198	783	76.2	0.102	83.8
15	854	1027	1571	1343	790	76.9	0.103	85.5
16	854	1027	1436	1219	797	77.5	0.104	84.8
17	854	1027	1431	1206	789	76.8	0.103	84.3
18	854	1027	1092	913	597	58.1	0.078	83.6
19	854	1027	1494	1266	828	80.6	0.108	84.7
20	854	1027	1401	1186	775	75.5	0.101	84.6
21	854	1027	1469	1242	812	79.0	0.106	84.5
22	854	1027	1385	1178	770	75.0	0.100	85.1

C.1.3 Heron Close

Table C-3: Annual monitoring results at Heron Close

System	Horizontal solar irradiation (kWh/m^2)	In-plane solar irradiation (kWh/m^2)	DC energy output from array (kWh)	AC energy output from inverter (kWh)	Final yield (kWh/kWp)	Performance ratio (%)	System efficiency	Inverter efficiency (%)
1	858	895	1074	968	672	75.1	0.093	90.1
2	858	895	872	782	502	56.0	0.069	89.7
3	858	895	0	0	0	0.0	0.000	0.0
4	858	895	1055	951	660	73.8	0.091	90.1
5	858	895	942	848	589	65.8	0.081	90.1
6	858	895	417	368	256	28.6	0.035	88.3
7	858	895	960	878	610	68.1	0.084	91.5
8	858	895	898	818	487	54.4	0.067	91.1
9	858	940	901	810	562	59.8	0.074	89.9
10	858	940	1134	1022	608	64.7	0.080	90.1
11	858	940	976	878	610	64.9	0.080	90.0
12	858	940	16	0	0	0.0	0.000	0.0
13	858	940	816	733	555	59.1	0.073	89.9
14	858	895	931	850	506	56.5	0.070	91.4
15	858	895	804	735	510	57.0	0.070	91.3
16	858	895	807	737	511	57.1	0.070	91.2
17	858	940	512	456	475	50.5	0.062	89.1
18	858	940	684	610	636	67.6	0.083	89.3
19	858	940	56	48	50	5.3	0.007	85.2
20	858	940	529	472	492	52.4	0.064	89.2
25	858	895	1196	1071	558	62.3	0.077	89.5
26	858	895	521	466	529	59.1	0.063	89.3
27	858	895	889	799	558	62.4	0.067	89.8

C.1.4 Panmure Street

Table C-4: Annual monitoring results at Panmure Street

System	Horizontal solar irradiation (kWh/m^2)	In-plane solar irradiation (kWh/m^2)	DC energy output from array (kWh)	AC energy output from inverter (kWh)	Final yield (kWh/kWp)	Performance ratio (%)	System efficiency	Inverter efficiency (%)
1	919	790	657	589	545	69.0	0.085	89.5
2	919	790	703	631	584	74.0	0.091	89.8
3	919	790	705	634	587	74.3	0.092	89.8
4	919	790	660	591	547	69.3	0.085	89.6
5	919	790	540	479	444	56.2	0.069	88.7
6	919	790	685	615	569	72.1	0.089	89.8
7	919	790	343	304	281	35.6	0.044	88.7
8	919	790	622	556	515	65.2	0.080	89.5
9	919	790	701	630	583	73.8	0.091	89.8
10	919	790	710	636	589	74.6	0.092	89.6
11	919	790	603	537	497	63.0	0.078	89.2
12	919	790	718	645	597	75.7	0.093	89.8

C.1.5 Newbiggin Hall

Table C-5: Annual monitoring results at Newbiggin Hall

System	Horizontal solar irradiation (kWh/m^2)	In-plane solar irradiation (kWh/m^2)	DC energy output from array (kWh)	AC energy output from inverter (kWh)	Final yield (kWh/kWp)	Performance ratio (%)	System efficiency	Inverter efficiency (%)
1	720	714	1766	1587	622	87.2	0.117	89.9
2	720	714	1730	1554	609	85.3	0.114	89.8
3	720	904	929	823	605	67.0	0.090	88.6
4	720	904	867	768	565	62.5	0.084	88.6
5	720	714	1769	1591	624	87.3	0.117	89.9
6	720	904	1056	935	687	76.1	0.102	88.6
7	720	904	1085	961	707	78.2	0.105	88.5
8	720	904	1057	935	687	76.0	0.102	88.4
9	720	683	453	392	512	75.0	0.100	86.4
10	720	904	1019	903	664	73.4	0.098	88.5
11	720	904	1048	928	682	75.5	0.101	88.5
12	720	904	1073	947	697	77.1	0.103	88.3
13	720	904	1072	949	698	77.2	0.103	88.5
14	720	904	957	847	623	68.9	0.092	88.5
15	720	904	1072	946	696	77.0	0.103	88.3
16	720	904	1067	940	692	76.5	0.103	88.1
17	720	904	875	775	570	63.1	0.085	88.6
18	720	904	994	878	646	71.5	0.096	88.4
19	720	904	1111	982	722	79.9	0.107	88.4
20	720	904	1008	890	654	72.4	0.097	88.3
21	720	904	1070	947	697	77.1	0.103	88.6
22	720	714	1207	1065	626	87.7	0.118	88.2
23	720	714	1183	1042	613	85.8	0.115	88.1
24	720	714	1175	1034	608	85.2	0.114	88.0
25	720	904	1062	938	690	76.3	0.102	88.4

C.2. In-plane irradiance vs. system efficiency plots

C.2.1 Corncroft

The in-plane irradiance to system efficiency relationships for the five minute data at Corncroft display the anticipated skewed boomerang-shaped cloud of points (Figure C-1). Systems 0, 1, 10 to 12 and 15 to 21 had few efficiency values falling below the cloud of points which indicates that few faults occurred. System 2 to 9 and 13 had a larger proportion of low efficiency values (i.e. values below the main cloud of points) and this suggests that these systems had a higher occurrence of faults.

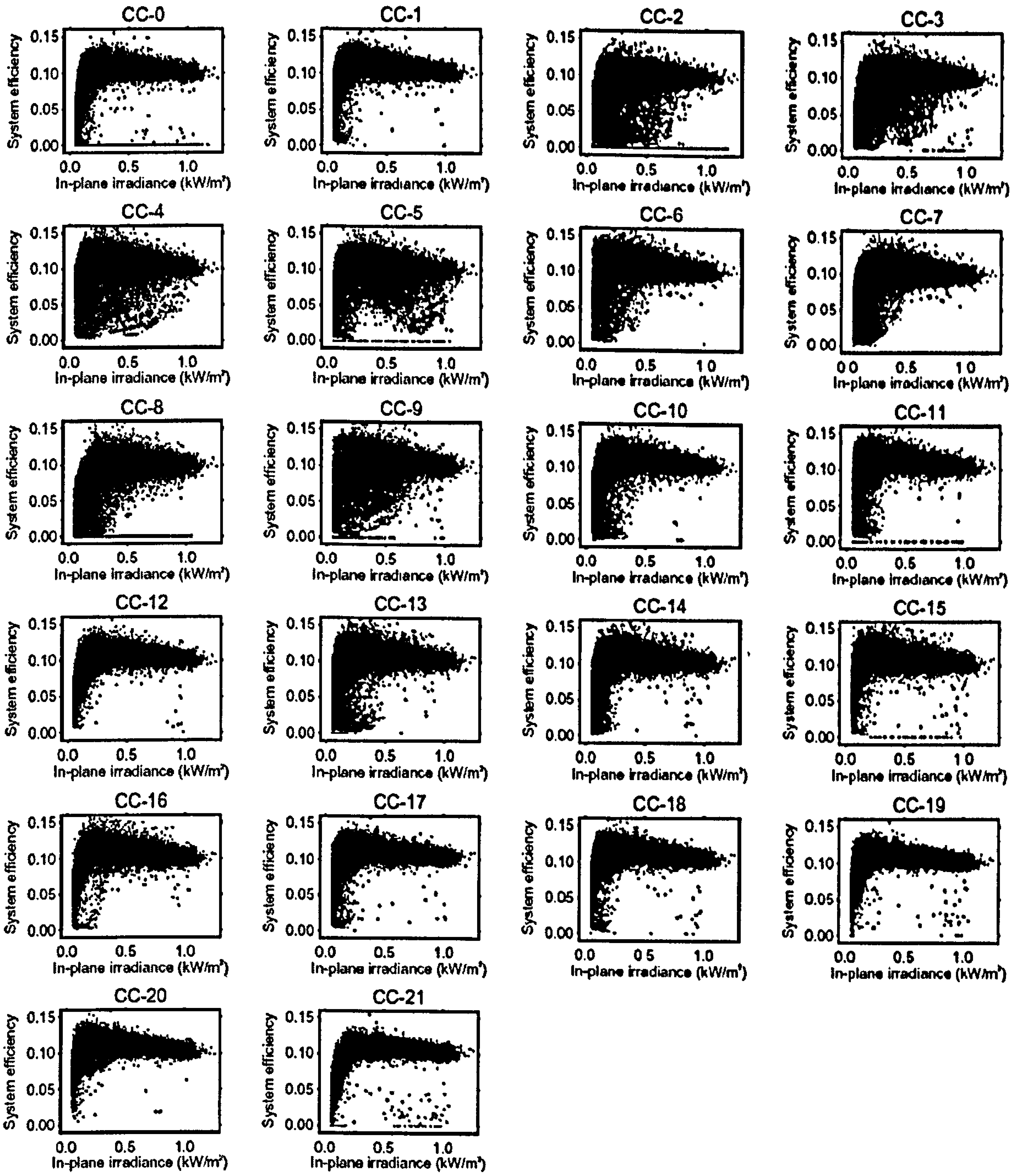

Figure C-1: Five minute values of In-plane irradiance vs. system efficiency at Corncroft

C.2.2 Heron Close

The five minute irradiance versus system efficiency plots for Heron Close show many values below the main cloud of points (Figure C-2). Systems 6 and 7 contained a higher proportion of low efficiencies suggesting these systems suffered from many faults. In systems 6, 7 and 12 a decrease in the maximum efficiency at high irradiance was noticeable and was caused by inverter power derating (see Section 6.2.1). At this level of irradiance the PV arrays generated power that was above the power rating of the inverters. The inverters could not convert all the generated power and the efficiency of the system was reduced.

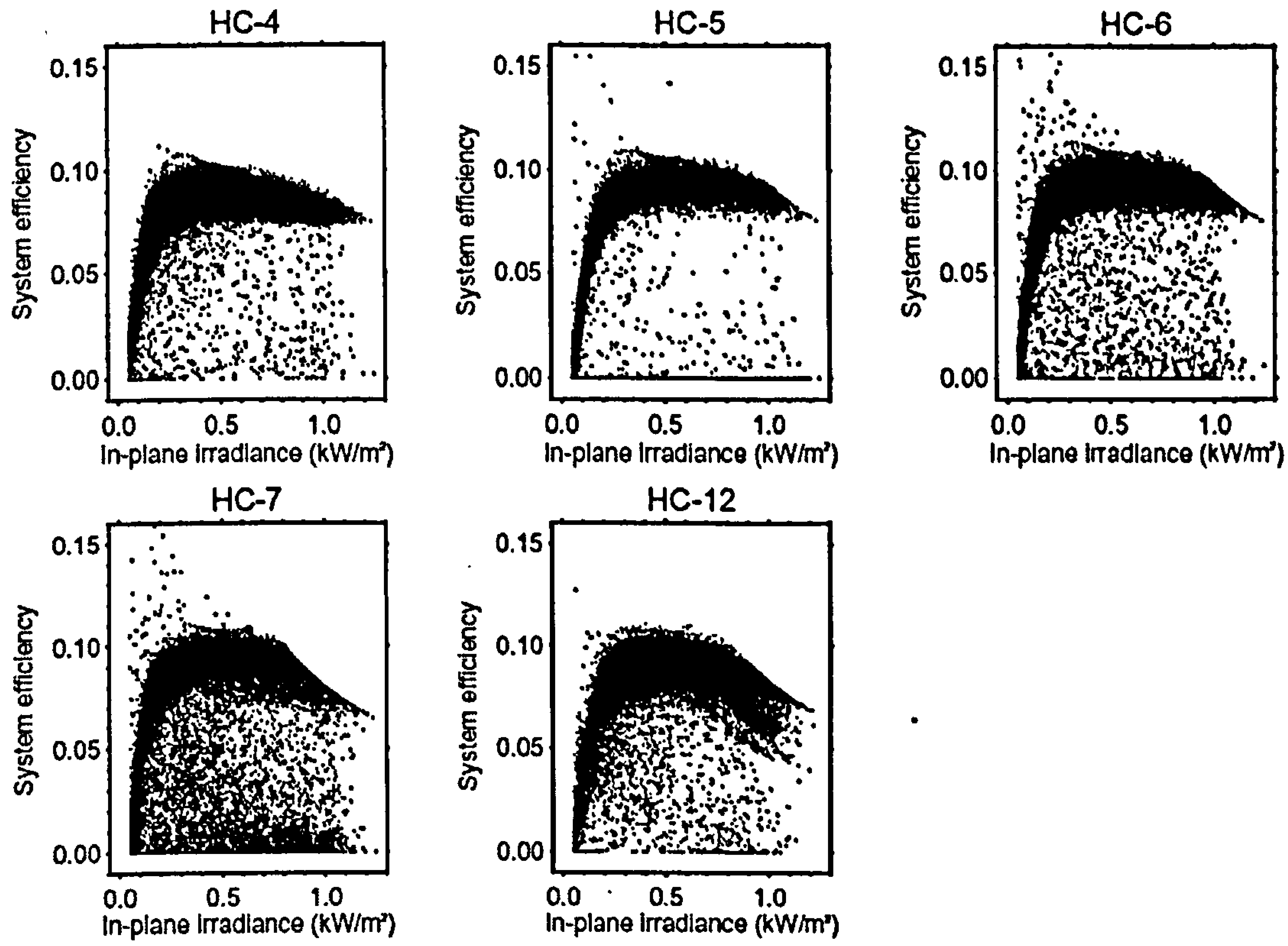

Figure C-2: Five minute values of In-plane irradiance vs. system efficiency at Heron Close

C.2.3 Panmure Street

The relationship of irradiance to system efficiency at Panmure Street was based on the five minute data which was not affected by the winter shading described in Appendix B.4.1 (Figure C-3). In particular system 4 produced many values below the main cloud of points, which suggests that many faults occurred.

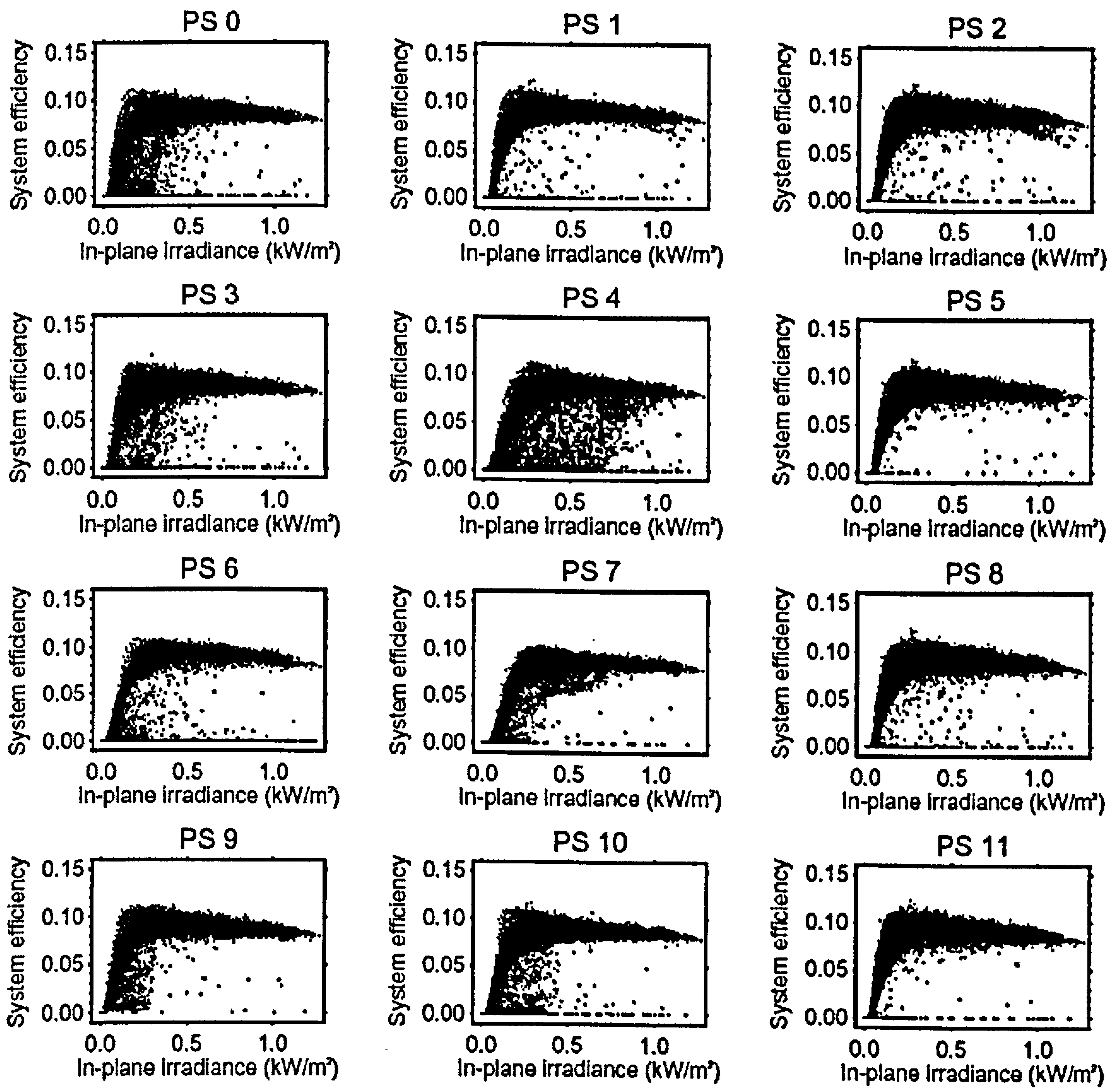

Figure C-3: Five minute values of In-plane irradiance vs. system efficiency at Panmure Street

C.2.4 Newbiggin Hall

The Newbiggin Hall irradiance to efficiency relationships did not follow the expected pattern (Figure C-4). For the reasons discussed in Section 5.2.1 this data was excluded from the five minute analysis.

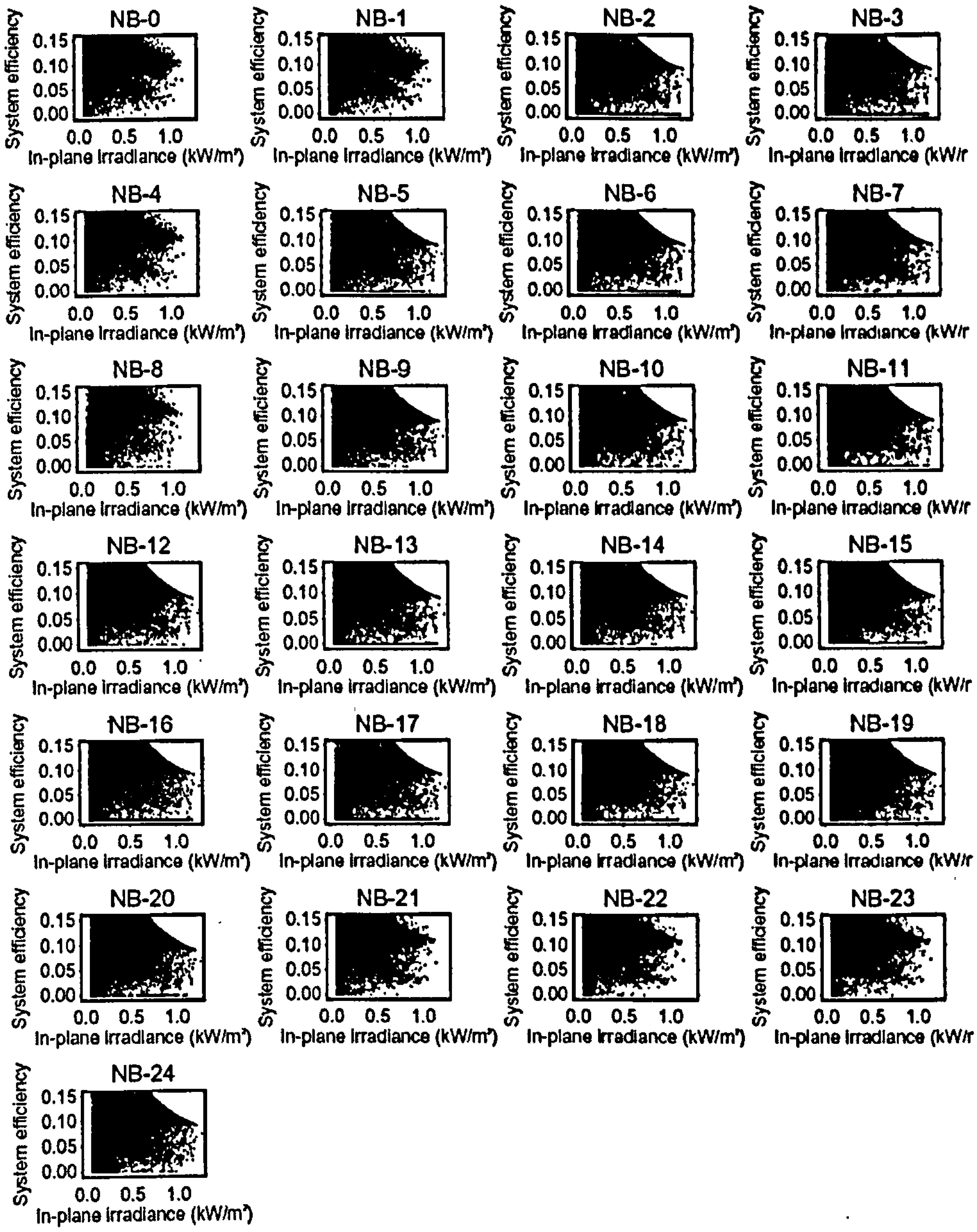

Figure C-4: Five minute values of In-plane irradiance vs. system efficiency at Newbiggin Hall

C.3. Efficiency frequency distribution curves

C.3.1 Corncroft

The frequency distributions of system efficiency within the variable irradiance bins at Corncroft, taking CC 21 as an example, shows they have roughly Gaussian distribution (Figure C-5). The spread of values within each bin was similar for all levels of irradiance.

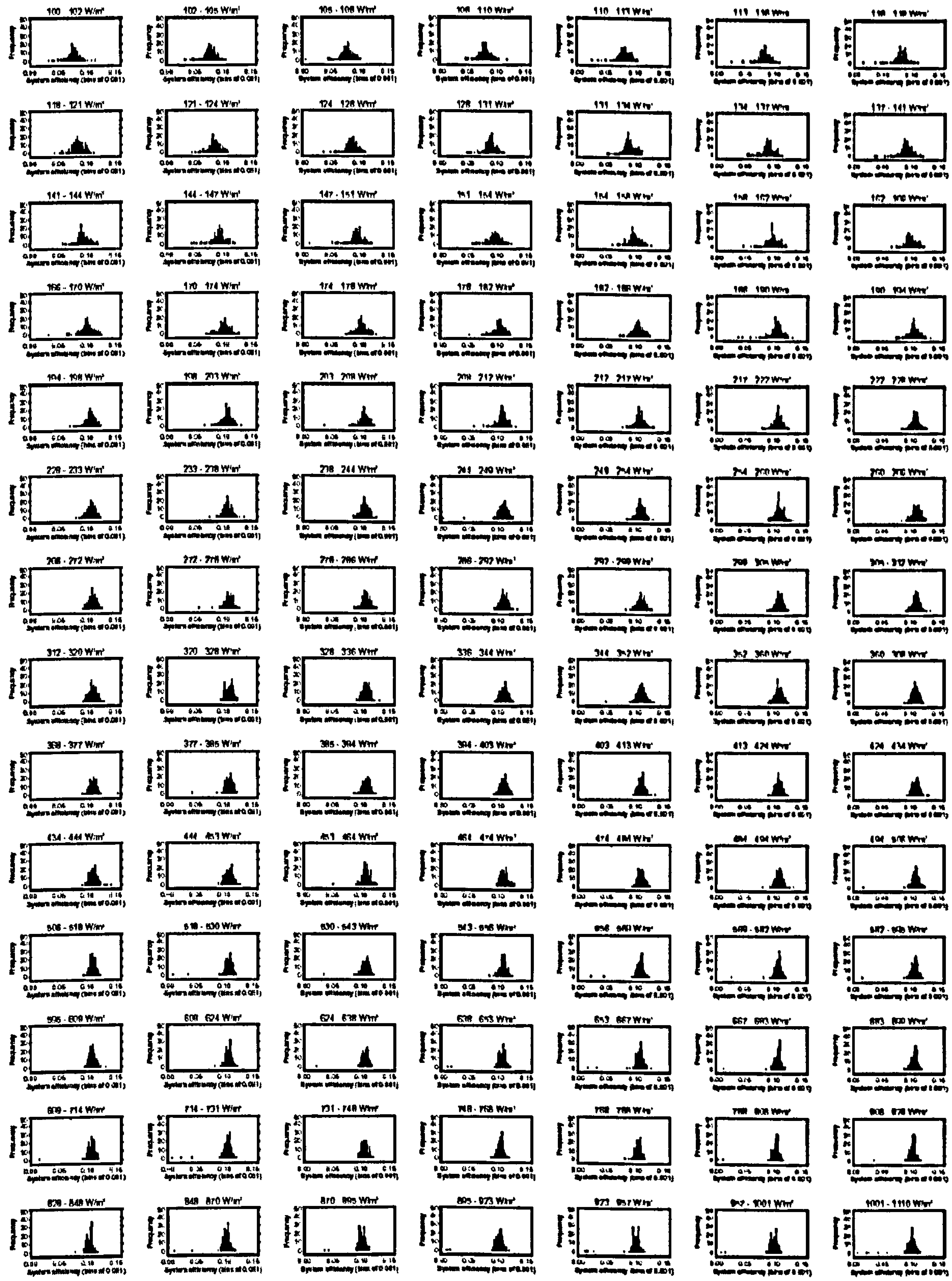

Figure C-5: System efficiency distribution curves for each irradiance bin at CC 21

C.3.2 Heron Close

The frequency distributions of system efficiency within the variable irradiance bins for all the bins at HC 4 showed Gaussian shaped distributions (Figure C-6).

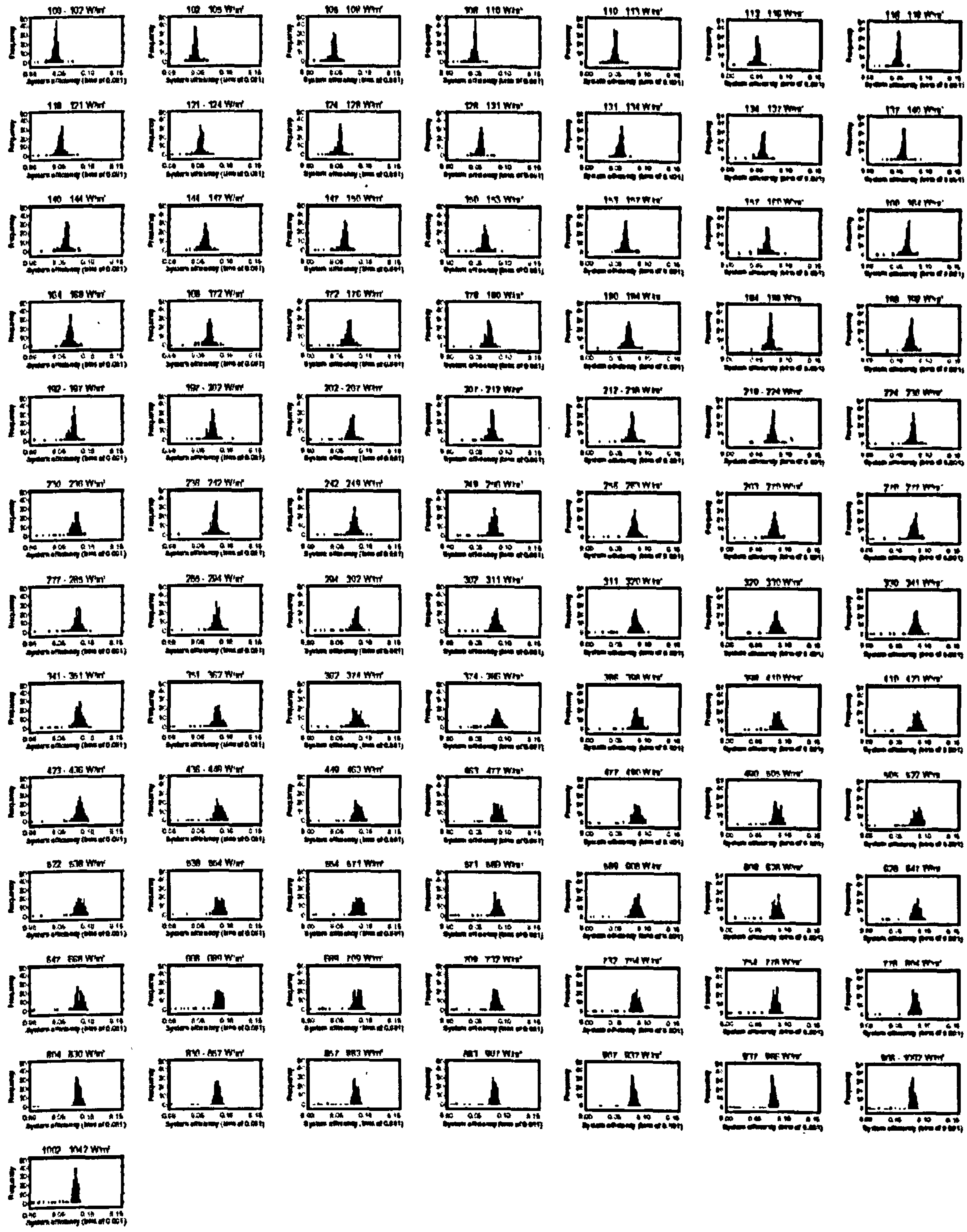

Figure C-6: System efficiency distribution curves for each irradiance bin at HC 4

C.3.3 Panmure Street

The frequency distributions of system efficiency within the variable irradiance bins at Panmure Street, taking PS 0 as an example, also demonstrated the suitability of using the Gaussian distribution to model the distributions (Figure C-7).

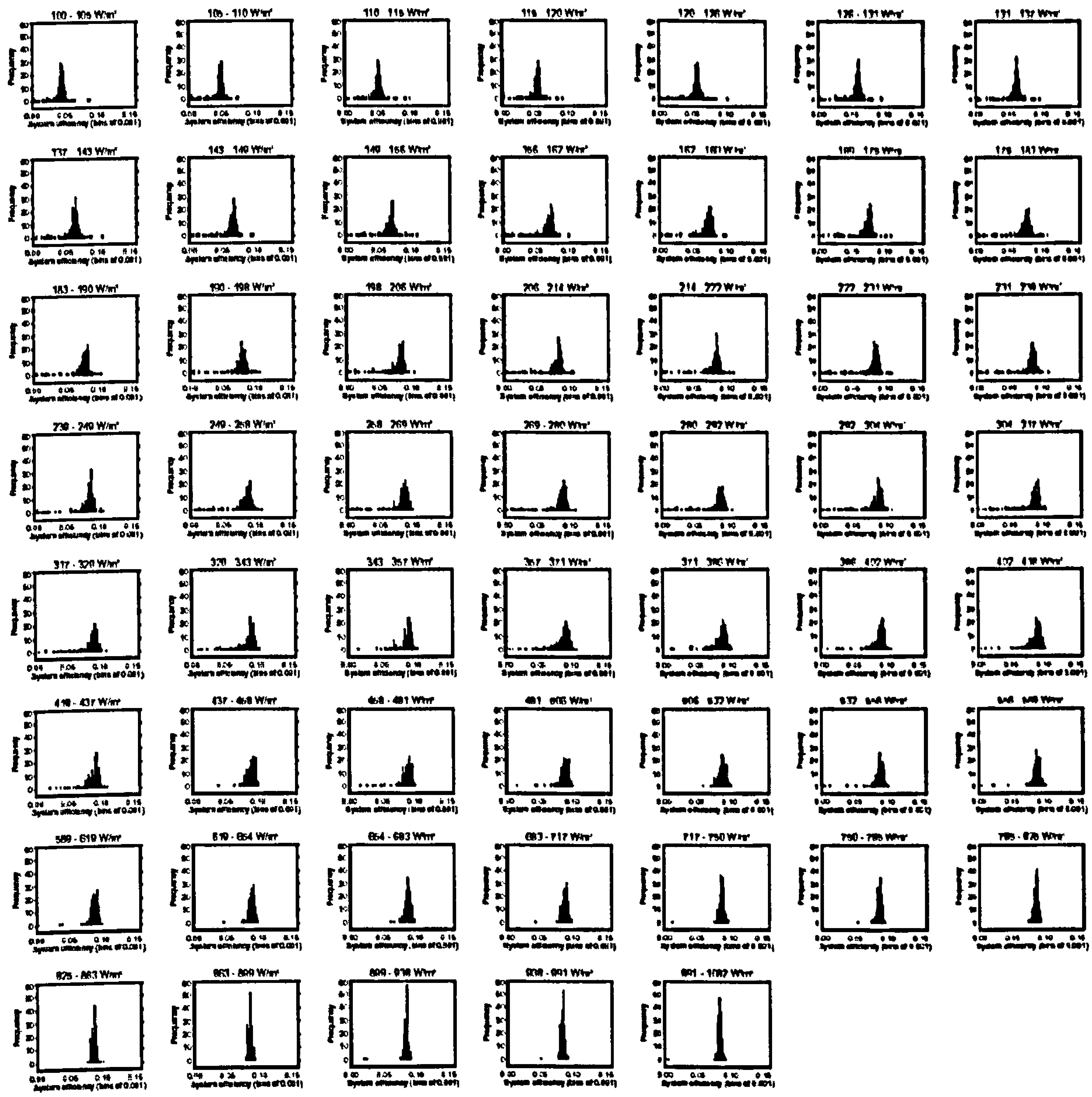

Figure C-7: System efficiency distribution curves for each irradiance bin at PS 0

C.4. Gaussian distribution fits

C.4.1 Corncroft

Gaussian distributions were fitted to the system efficiency frequency distributions within irradiance bins to describe the normal operation of the PV systems. At Corncroft, taking six irradiance bins of CC 21 as an example, Gaussian distributions were fitted and compare well with the efficiency distributions (Figure C-8). Similar plots were seen for the other irradiance bins and the other systems at Corncroft.

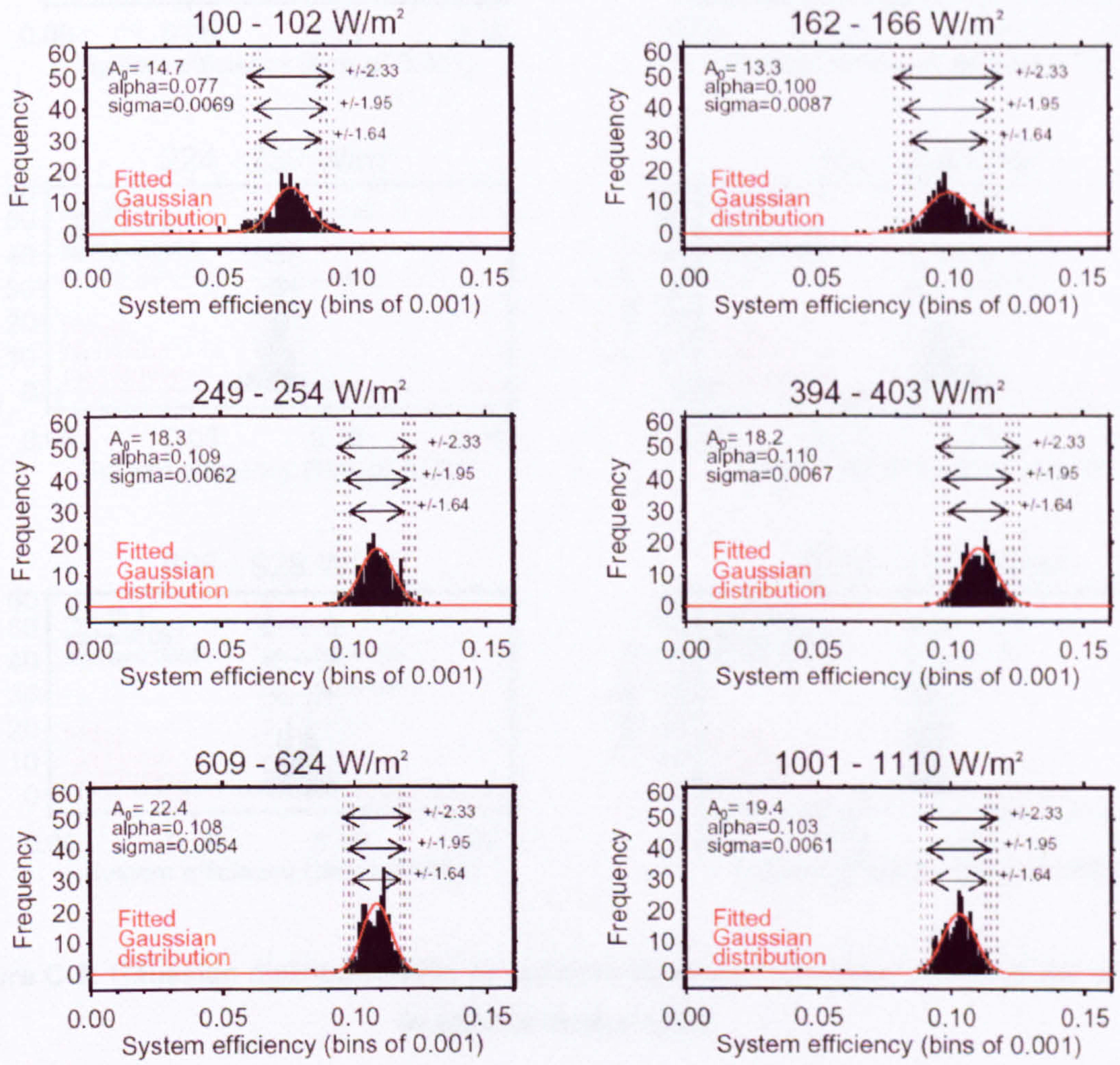

Figure C-8: Gaussian distribution fits to system efficiency frequency distributions of six irradiance bins at CC 21

C.4.2 Heron Close

To demonstrate the Gaussian distribution fits at Heron Close, six irradiance bins at HC 4 are shown (Figure C-9). Similar plots can be seen for the other irradiance bins and other systems on the site.

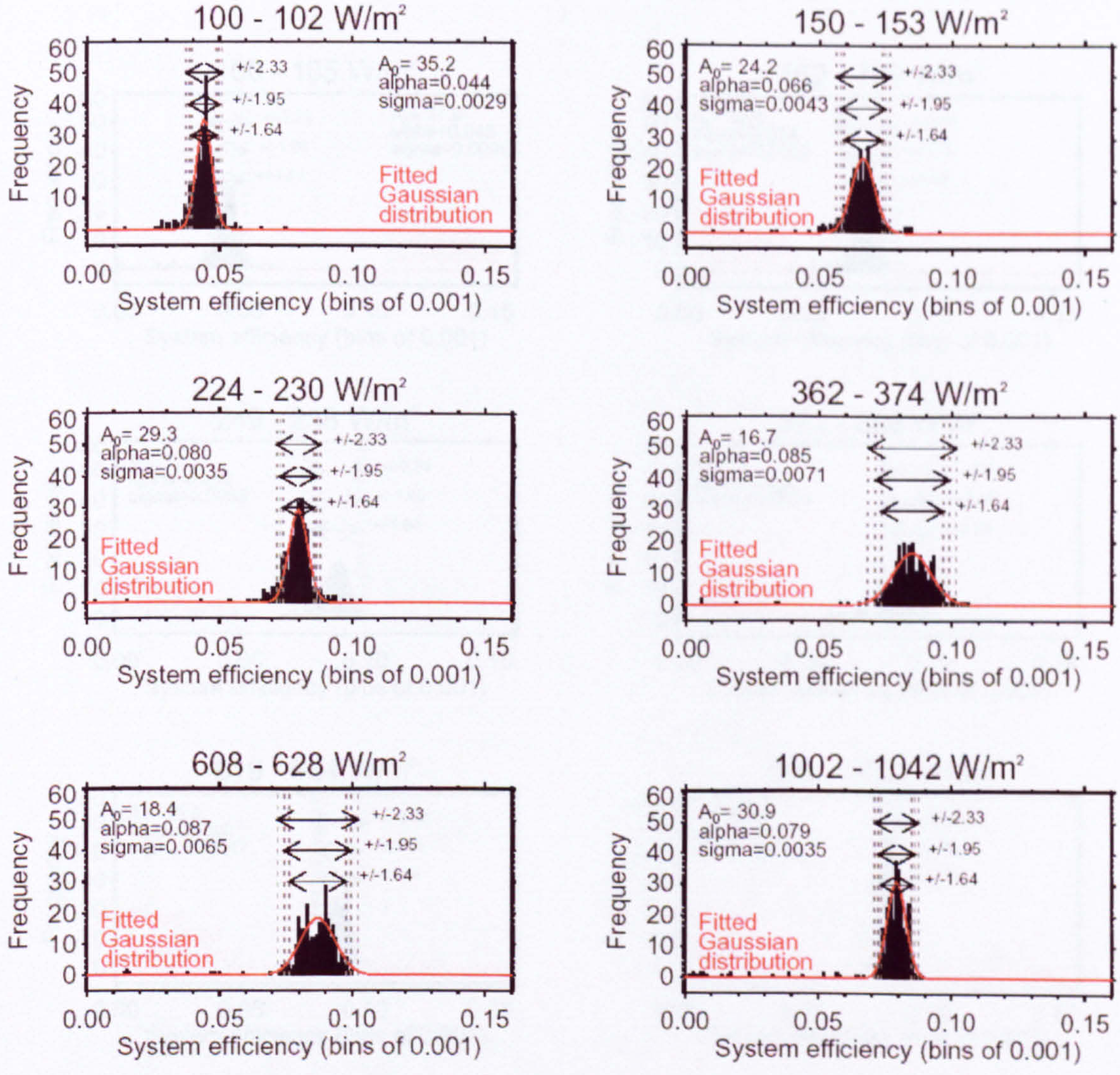

Figure C-9: Gaussian distribution fits to system efficiency frequency distributions of six irradiance bins at HC 4

C.4.3 Panmure Street

The Gaussian distributions could also be used to describe the efficiency values in each irradiance bin at Panmure Street, as shown for six example irradiance bins at System 0 (Figure C-10). Similar plots can be seen for the other irradiance bins and other systems on the site.

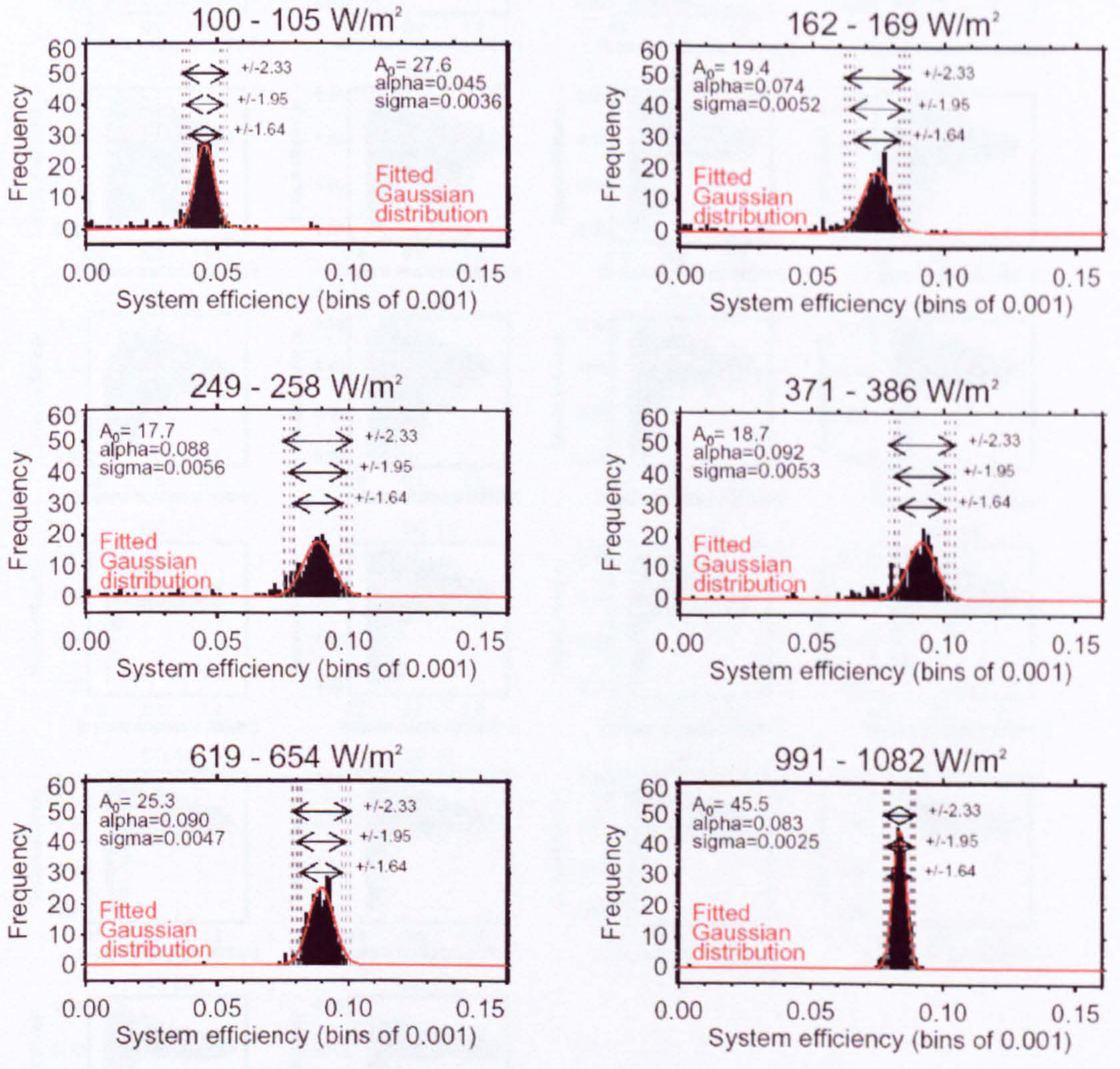

Figure C-10: Gaussian distribution fits to system efficiency frequency distributions of six irradiance bins at PS 0

C.5. System efficiency curves

C.5.1 Corncroft Year 1

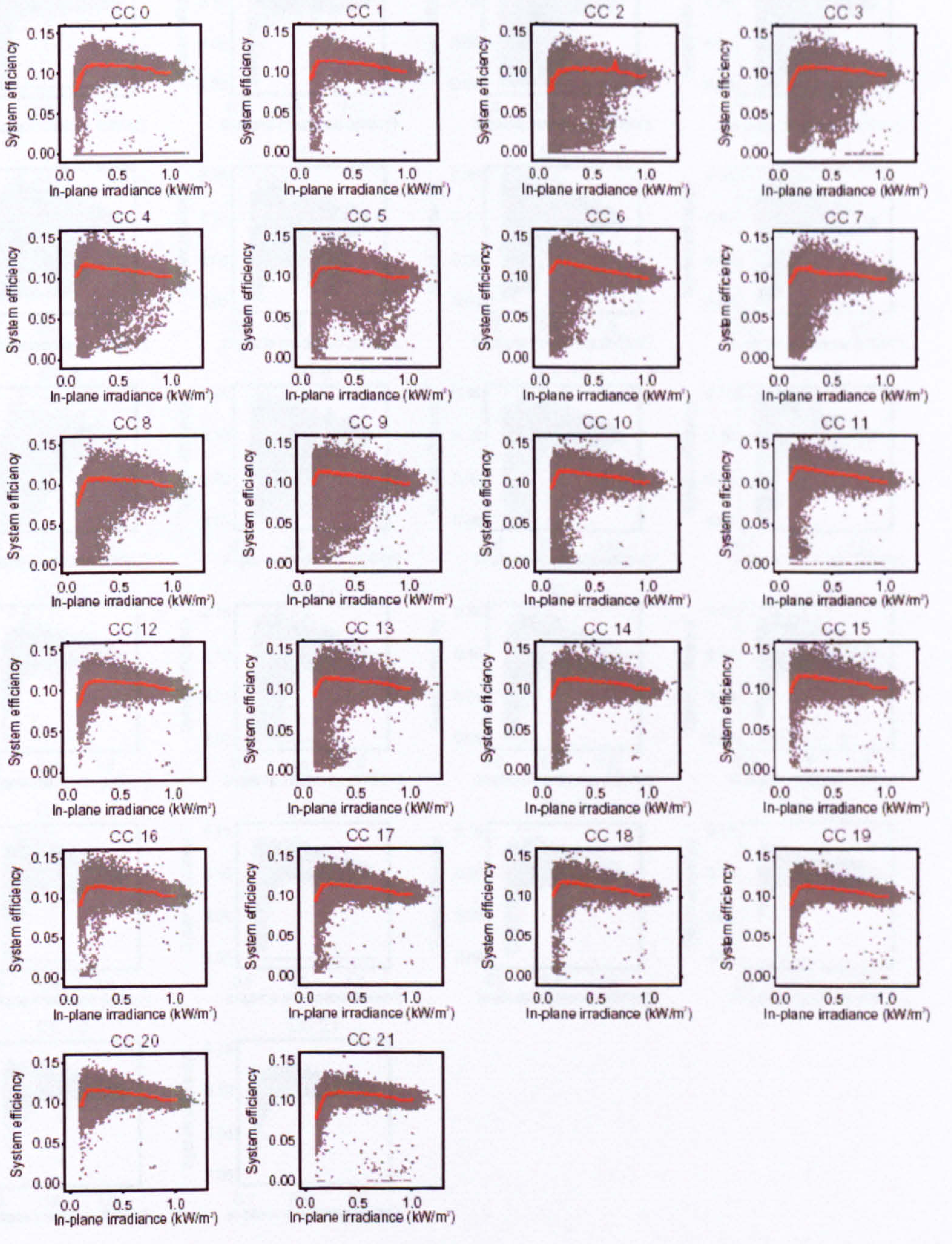

Figure C-11: System efficiency curves at Corncroft in the second year of operation

C.5.2 Corncroft Year 2

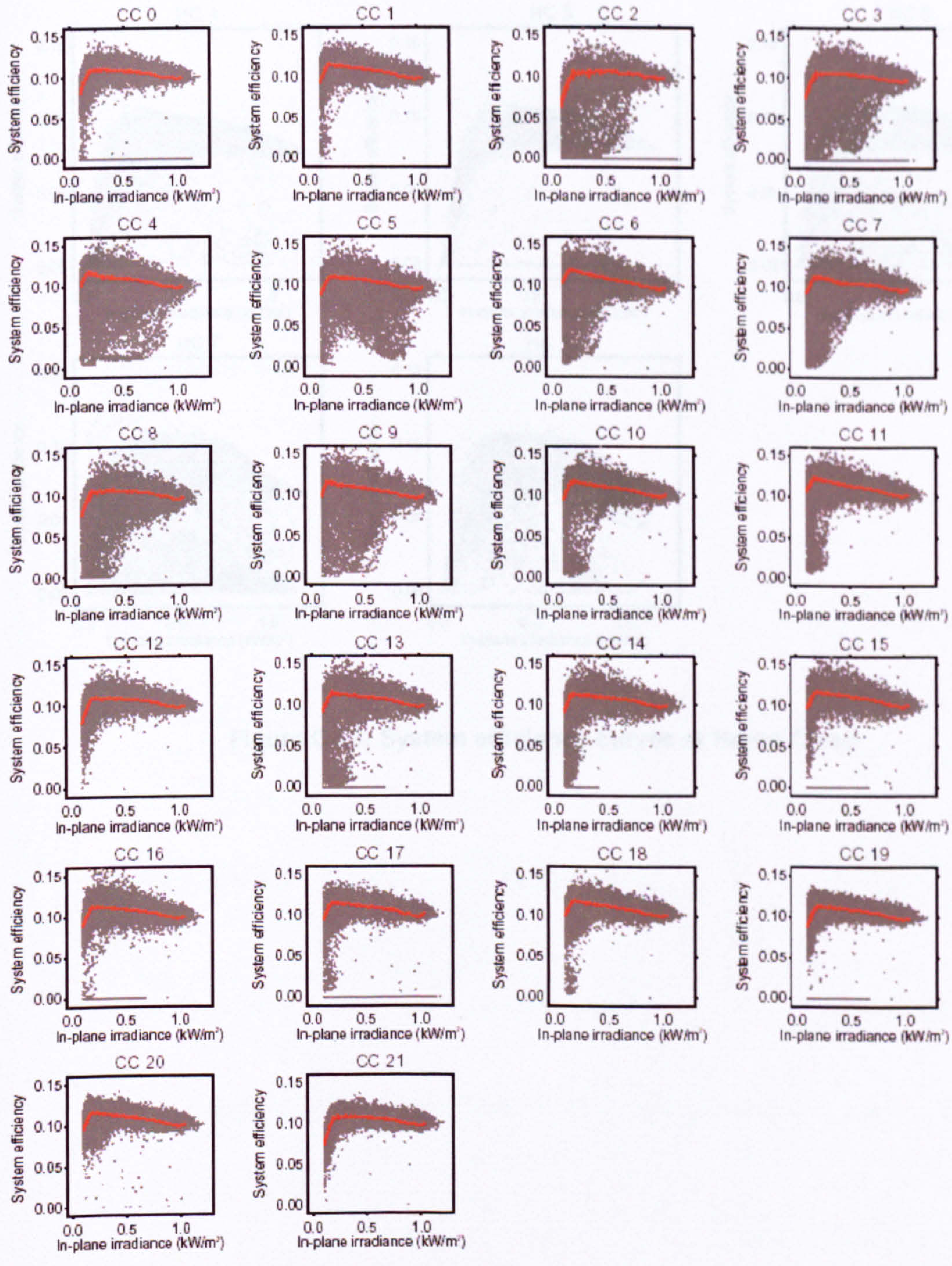

Figure C-12: System efficiency curves at Corncroft in the second year of operation

C.5.3 Heron Close

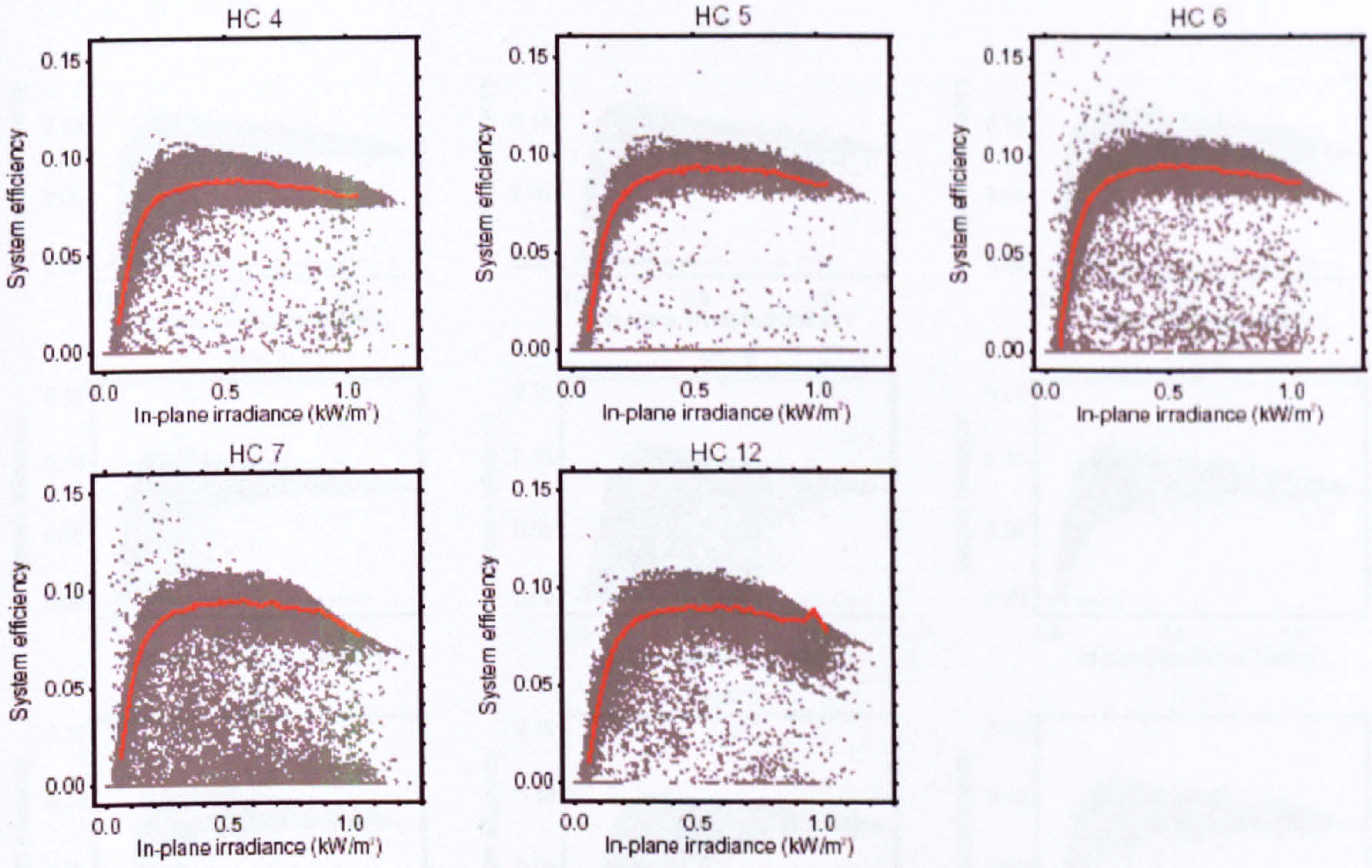

Figure C-13: System efficiency curves at Heron Close

C.5.4 Panmure Street

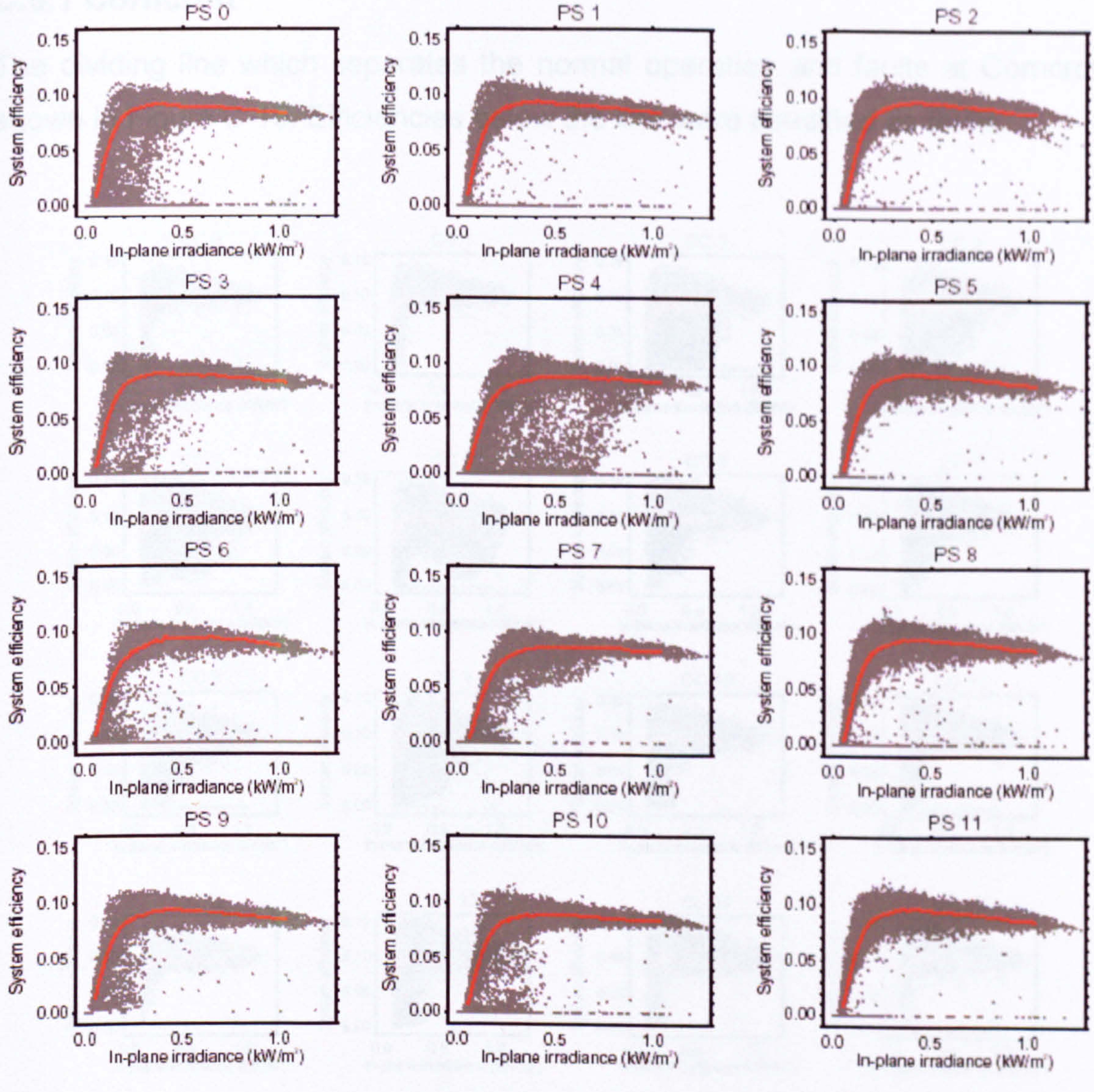

Figure C-14: System efficiency curves at Panmure Street

C.6. Fault efficiency curves

C.6.1 Corncroft

The dividing line which separates the normal operation and faults at Corncroft is shown in Figure C-15. Efficiencies below the line were identified as faults.

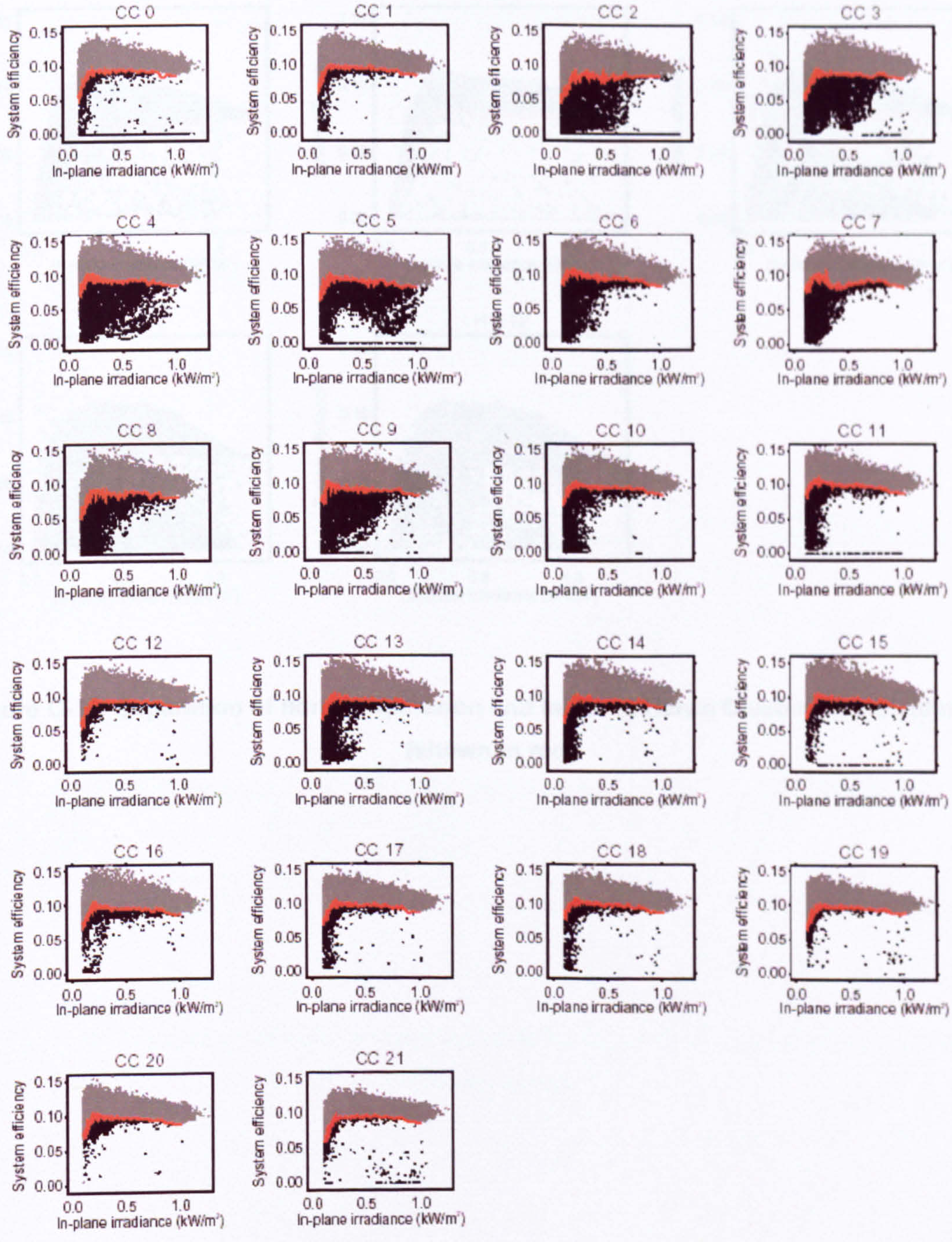

Figure C-15: Separation of normal operation and faults at Corncroft with a dividing line (shown in red)

C.6.2 Heron Close

The dividing line which separates the normal operation and faults at Heron Close is shown in Figure C-16. The inverter derating in systems 7 and 12 caused unexpected results in the shape of dividing line.

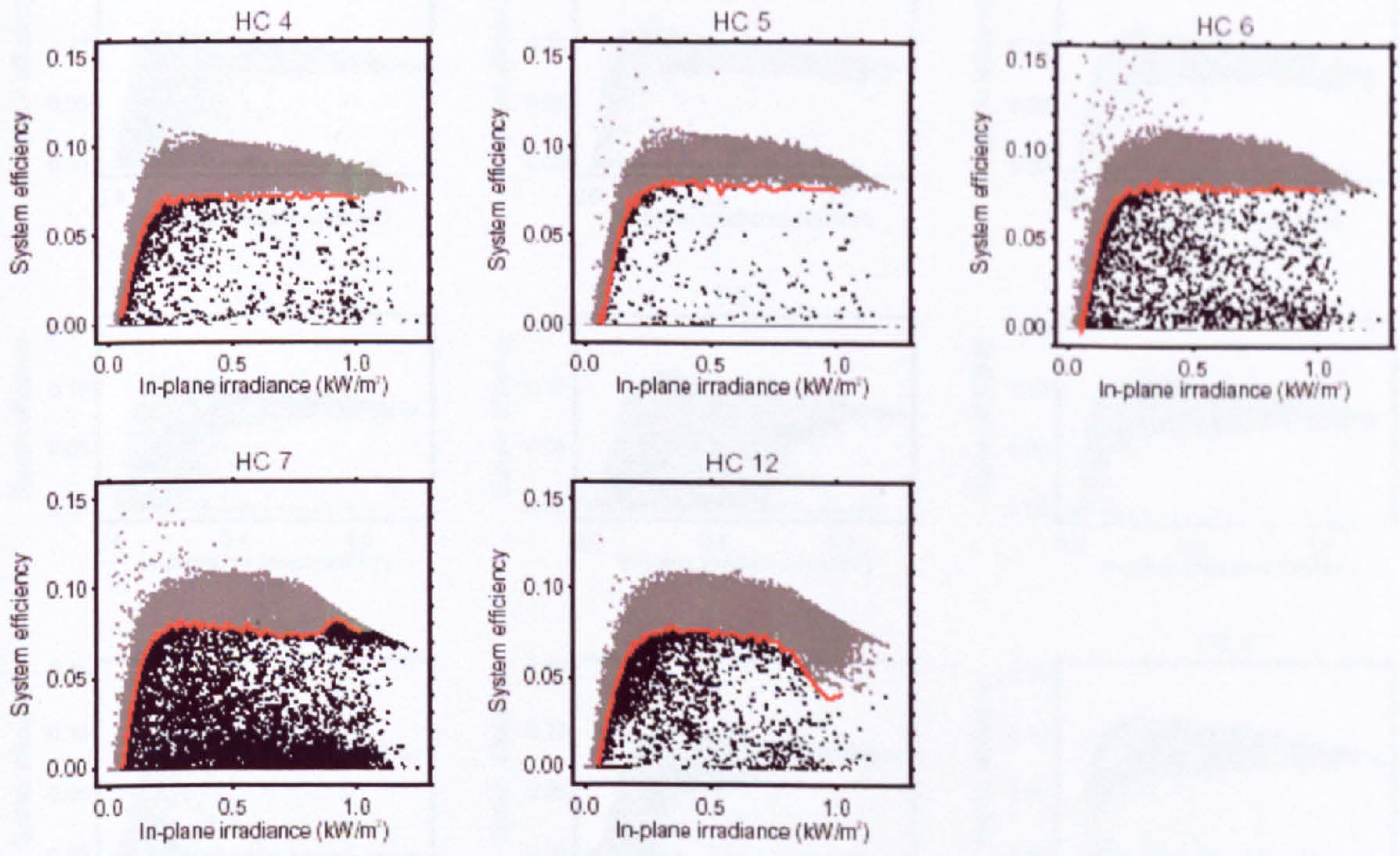

Figure C-16: Separation of normal operation and faults at Heron Close with a dividing line (shown in red)

C.6.3 Panmure Street

The dividing line which separates the normal operation and faults at Panmure is shown in Figure C-17.

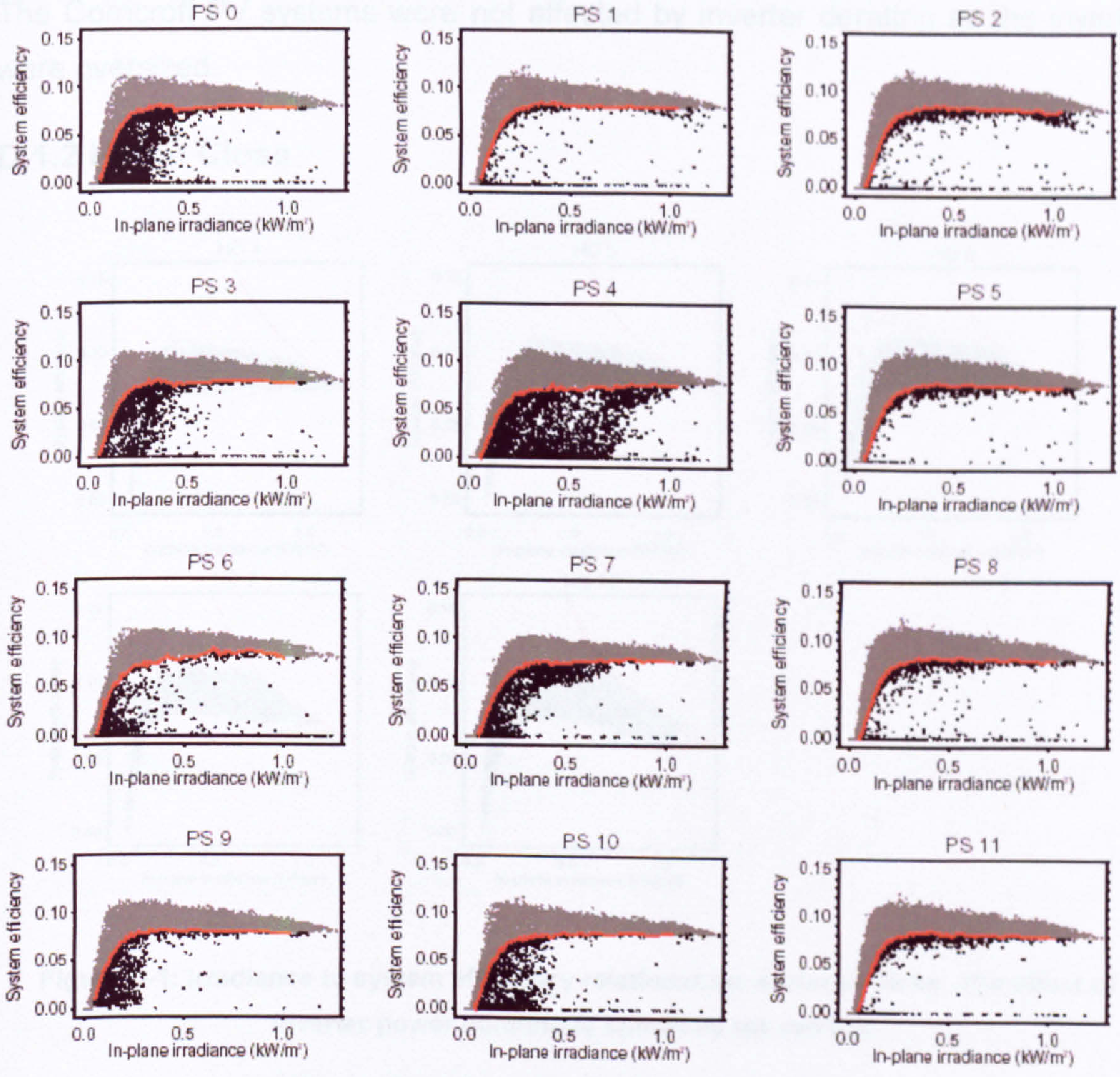

Figure C-17: Separation of normal operation and faults at Heron Close with a dividing line (shown in red)

Appendix D. Normal Operation Analysis

D.1. Inverter power derating

D.1.1 Corncroft

The Corncroft PV systems were not affected by inverter derating as the inverters were oversized.

D.1.2 Heron Close

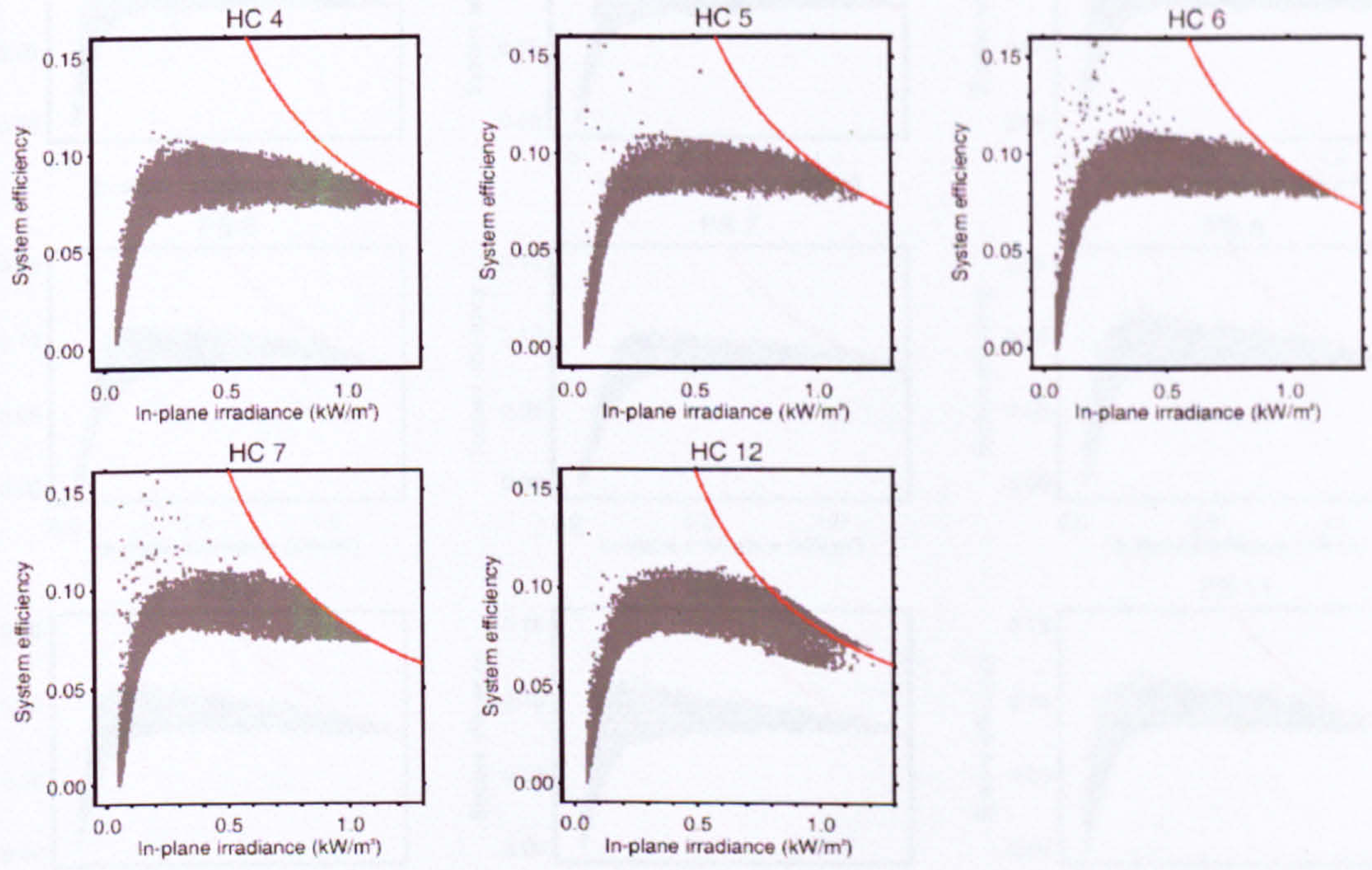

Figure D-1: Irradiance to system efficiency relationships at Heron Close. The effect of inverter power derating is shown by the red line.

D.1.3 Panmure Street

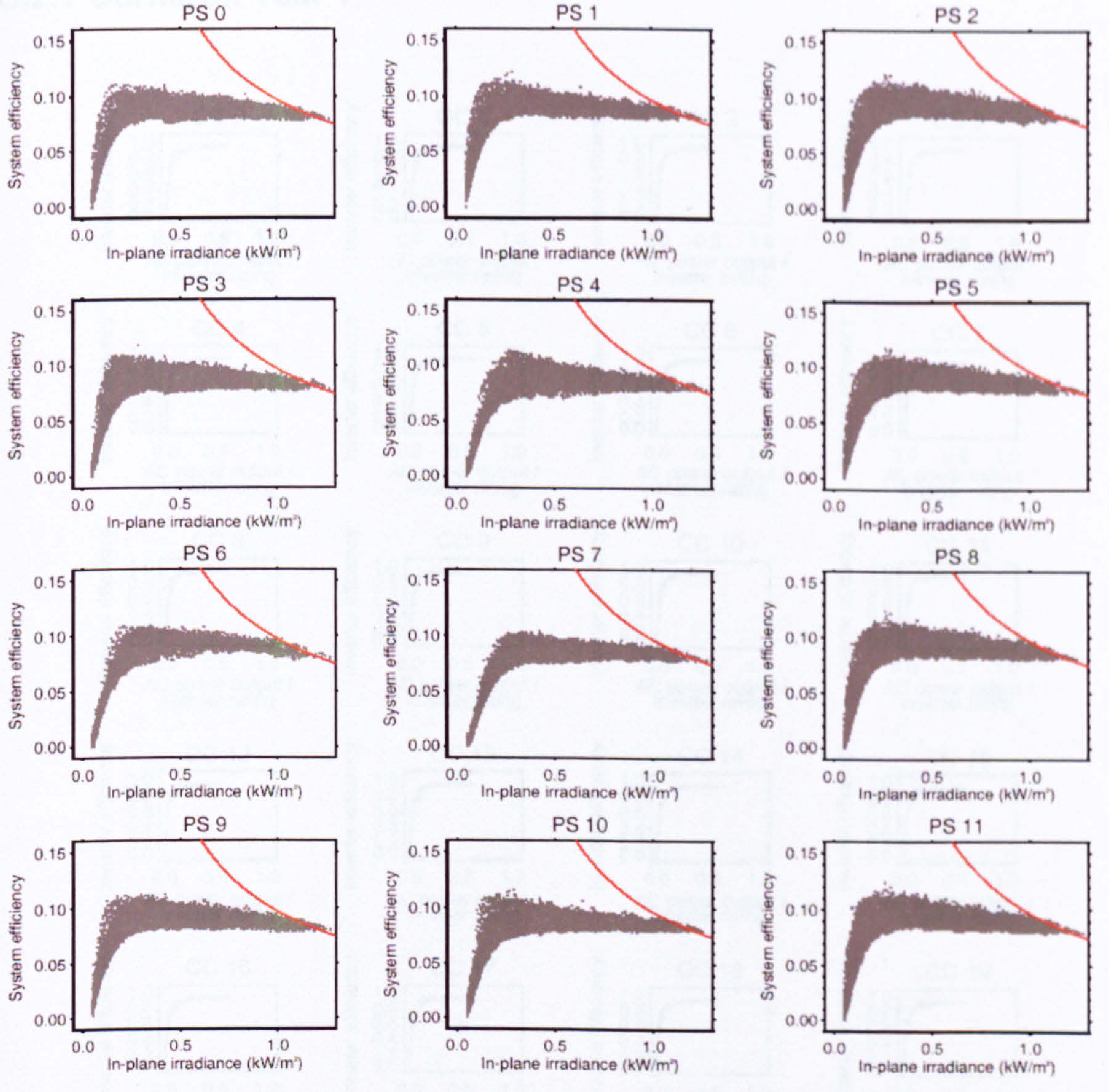

Figure D-2: Irradiance to system efficiency relationships at Panmure Street. The effect of inverter power derating is shown by the red line.

D.2. Inverter efficiency curves

D.2.1 Corncroft Year 1

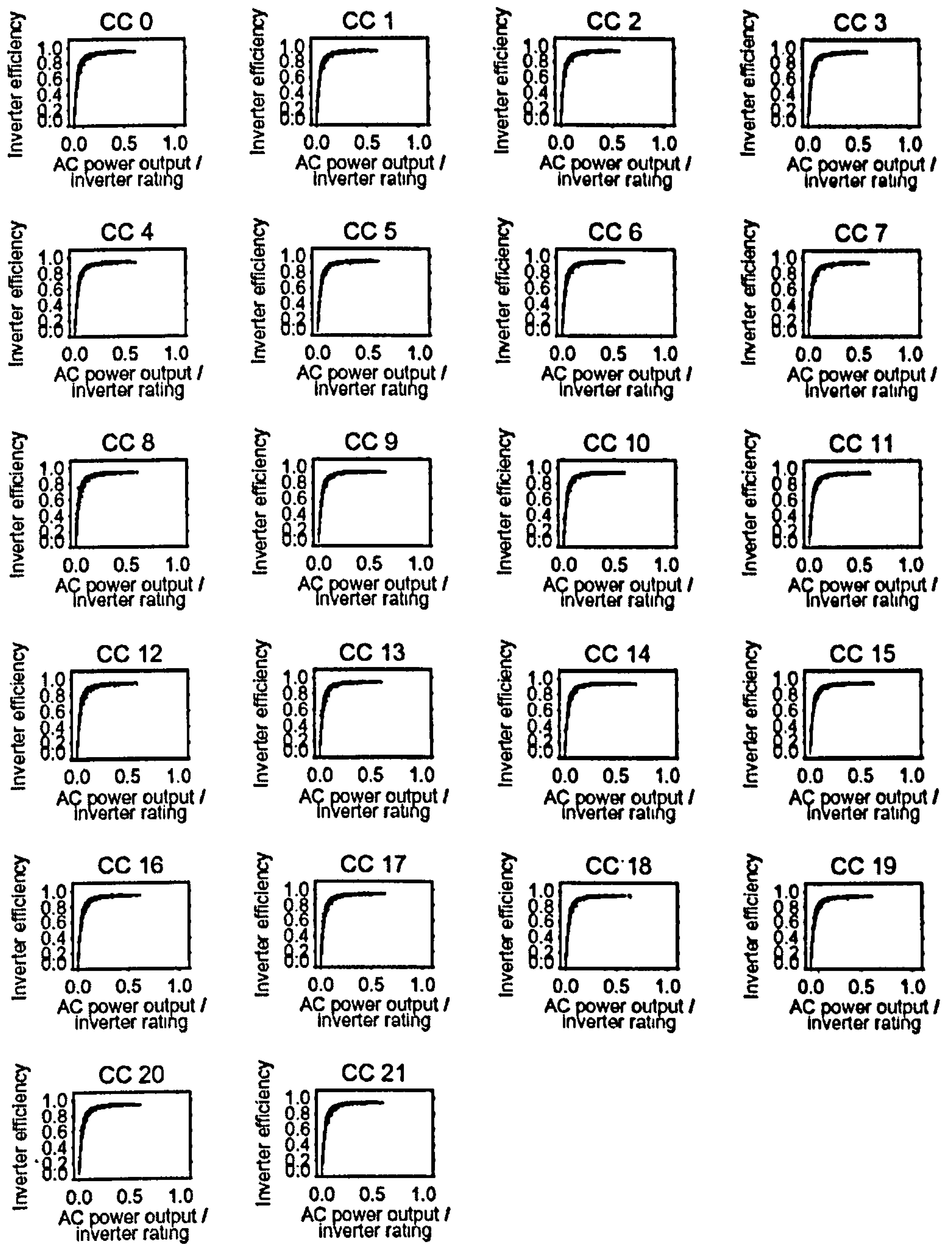

Figure D-3: Inverter efficiency curves for the Corncroft systems in the first year of operation

D.2.2 Corncroft Year 2

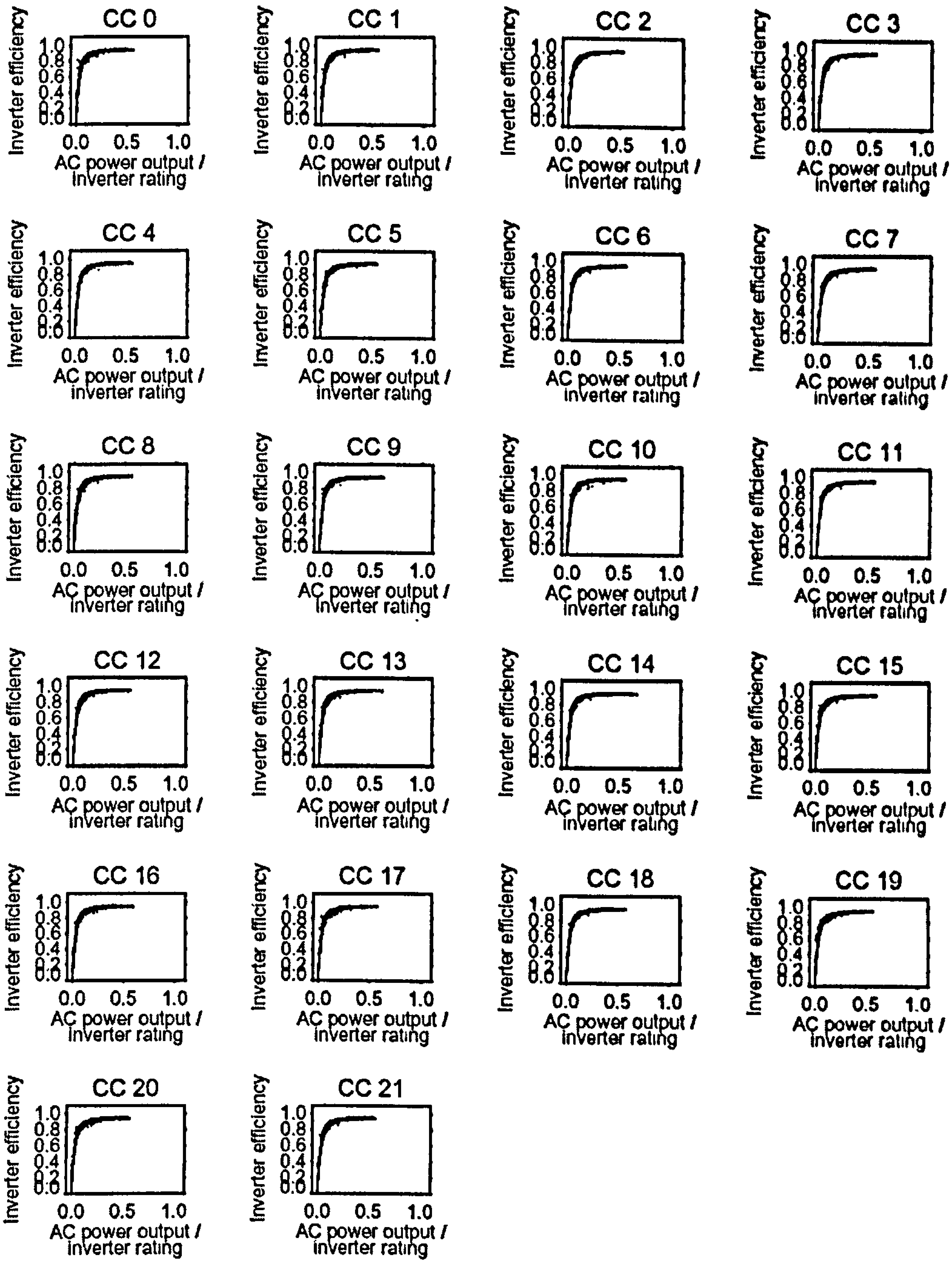

Figure D-4: Inverter efficiency curves for the Corncroft systems in the second year of operation

D.2.3 Heron Close

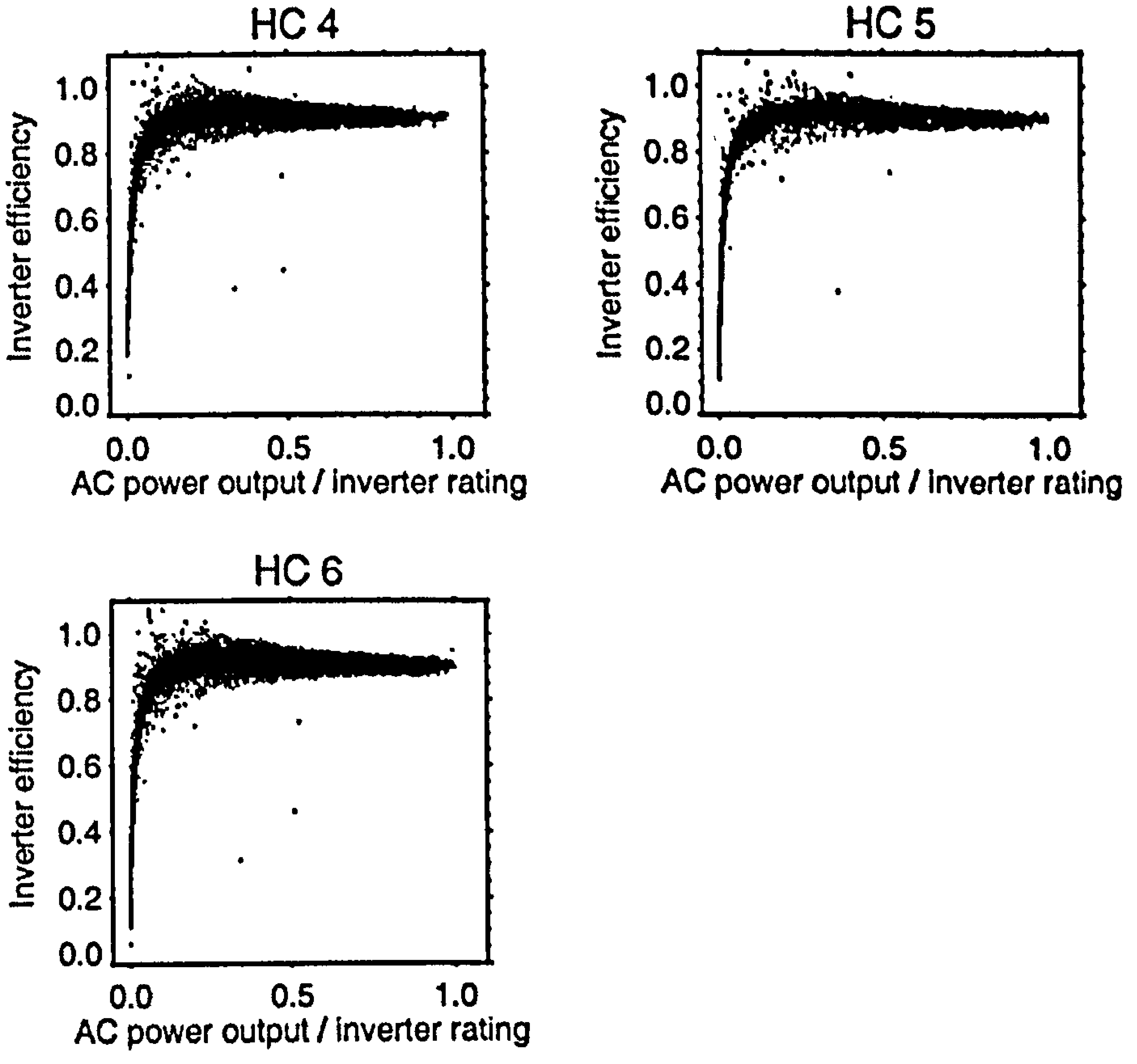

Figure D-5: Inverter efficiency curves for the Heron Close systems

D.2.4 Panmure Street

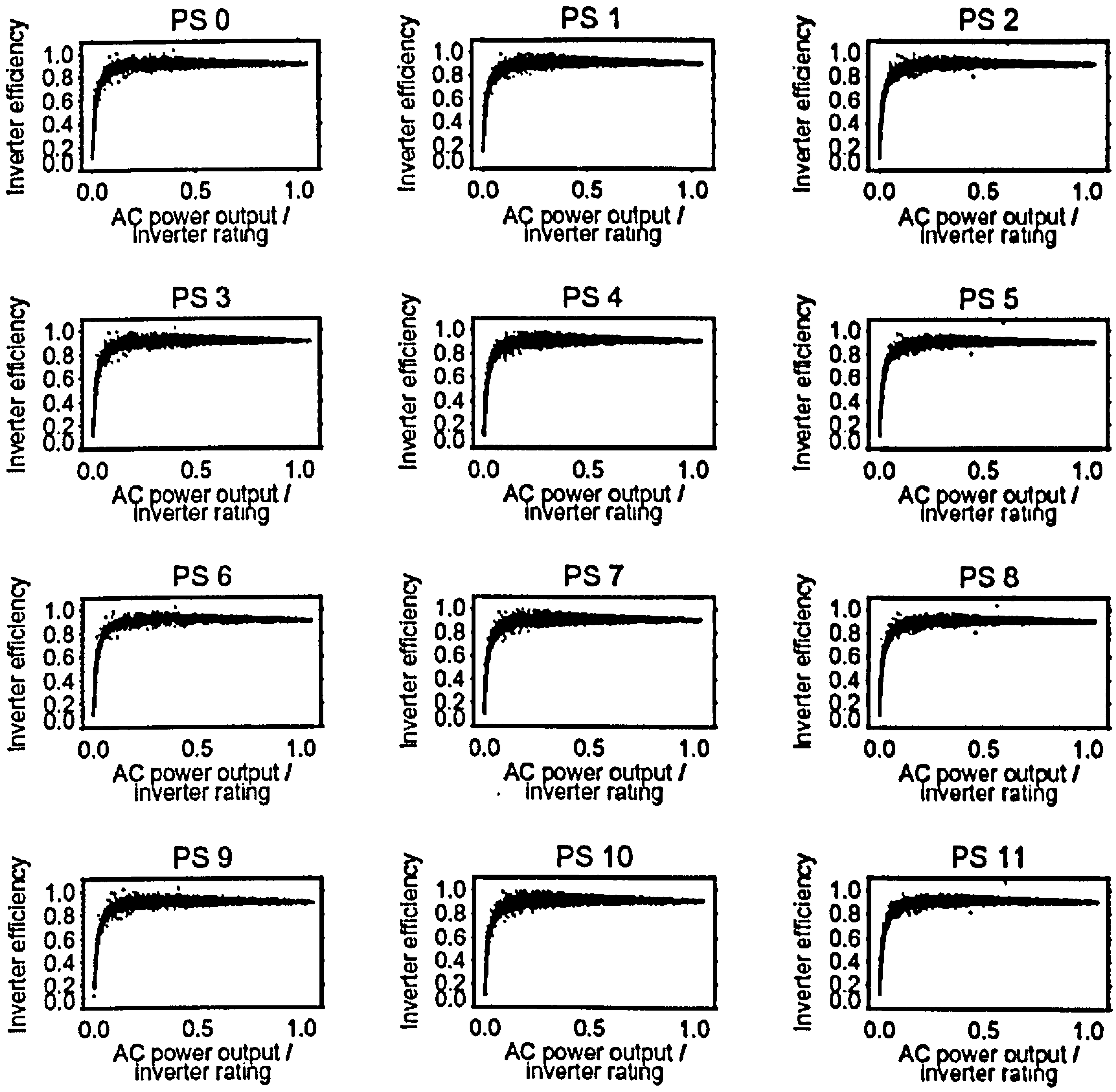

Figure D-6: Inverter efficiency curves for the Panmure Street systems

D.3. Array efficiency curves

D.3.1 Corncroft Year 1

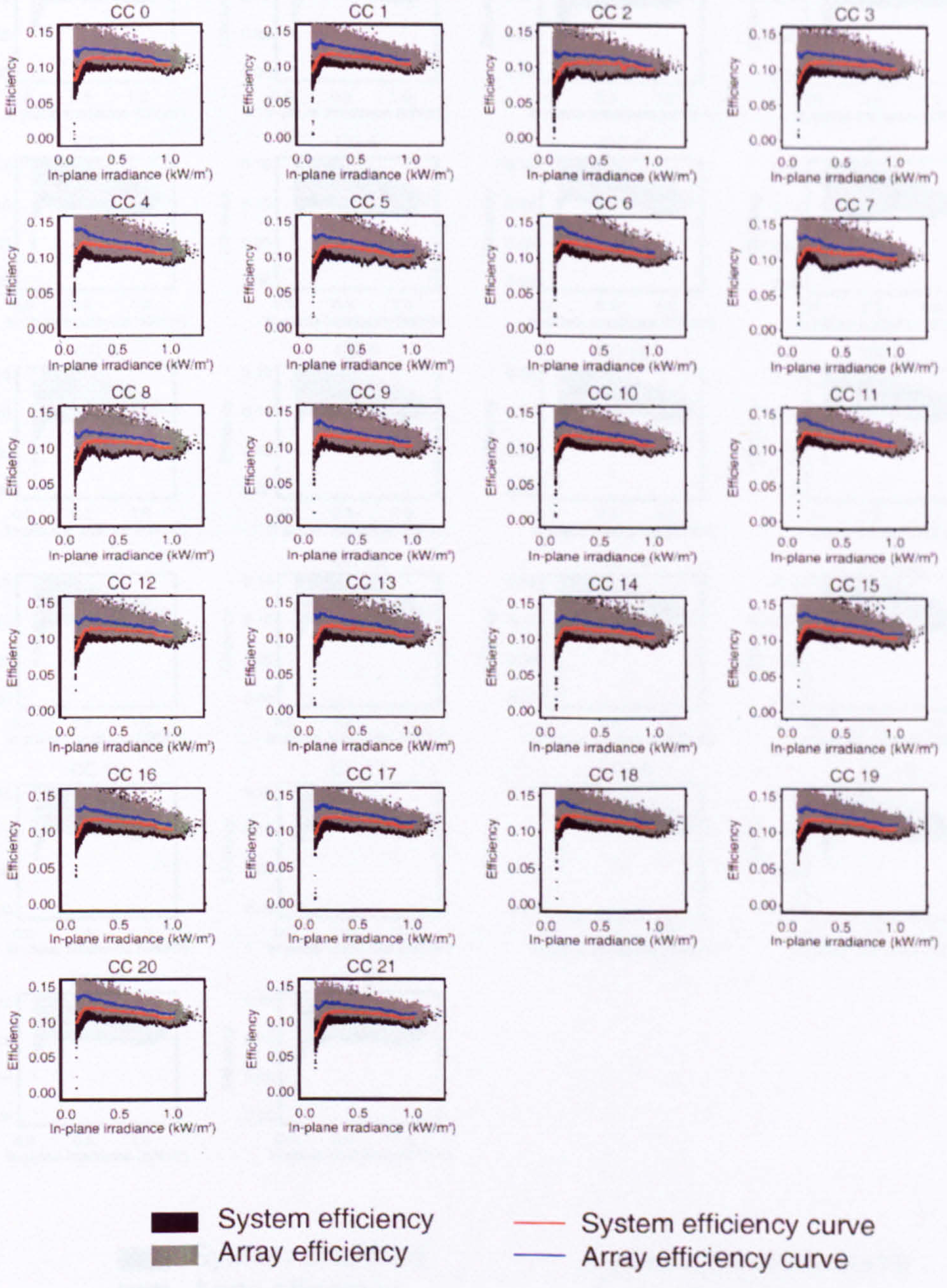

Figure D-7: System and array efficiency curves for Corncroft in the first year of operation

D.3.2 Corncroft Year 2

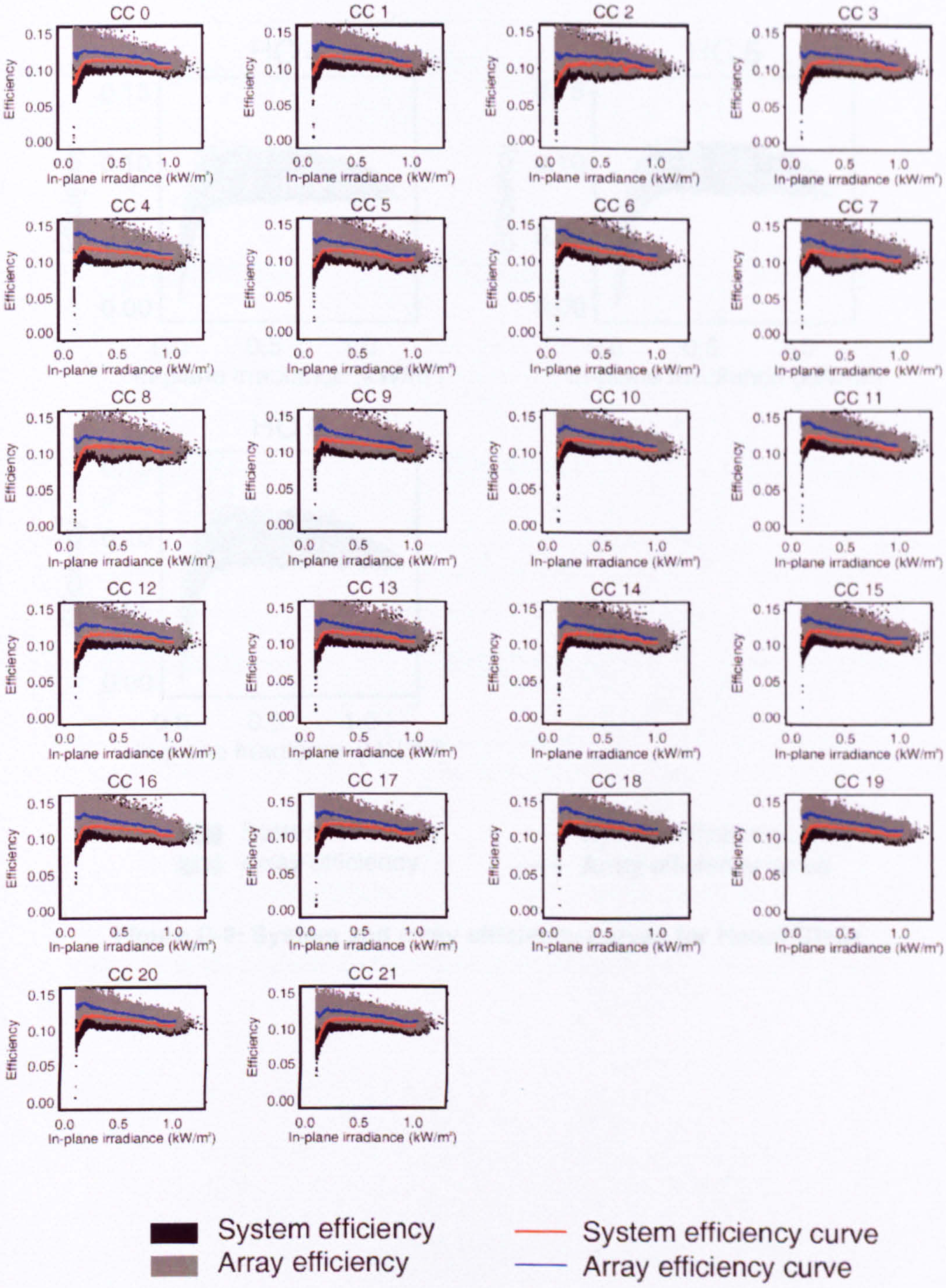

Figure D-8: System and array efficiency curves for Corncroft in the second year of operation

D.3.3 Heron Close

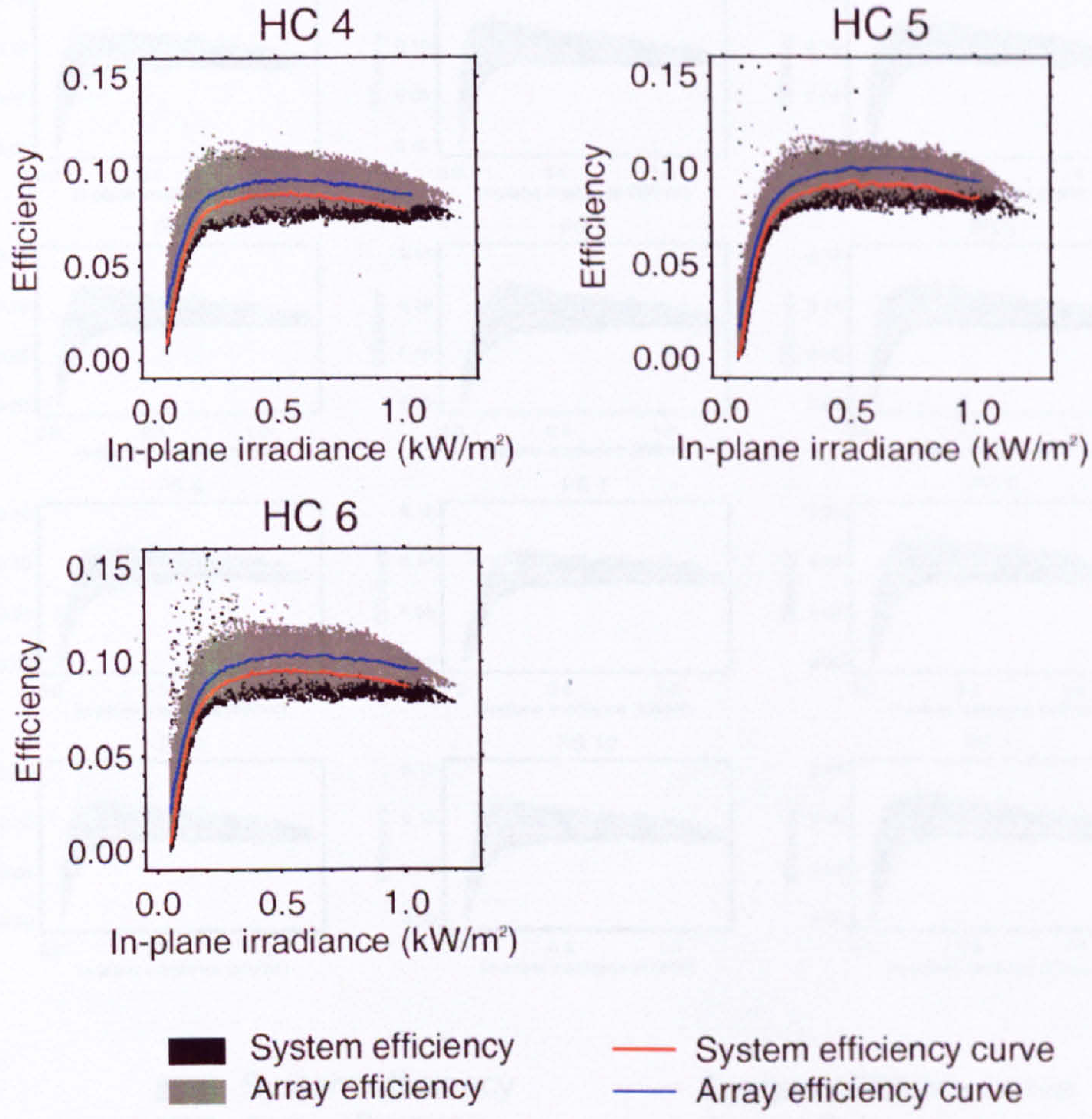

Figure D-9: System and array efficiency curves for Heron Close

D.3.4 Panmure Street

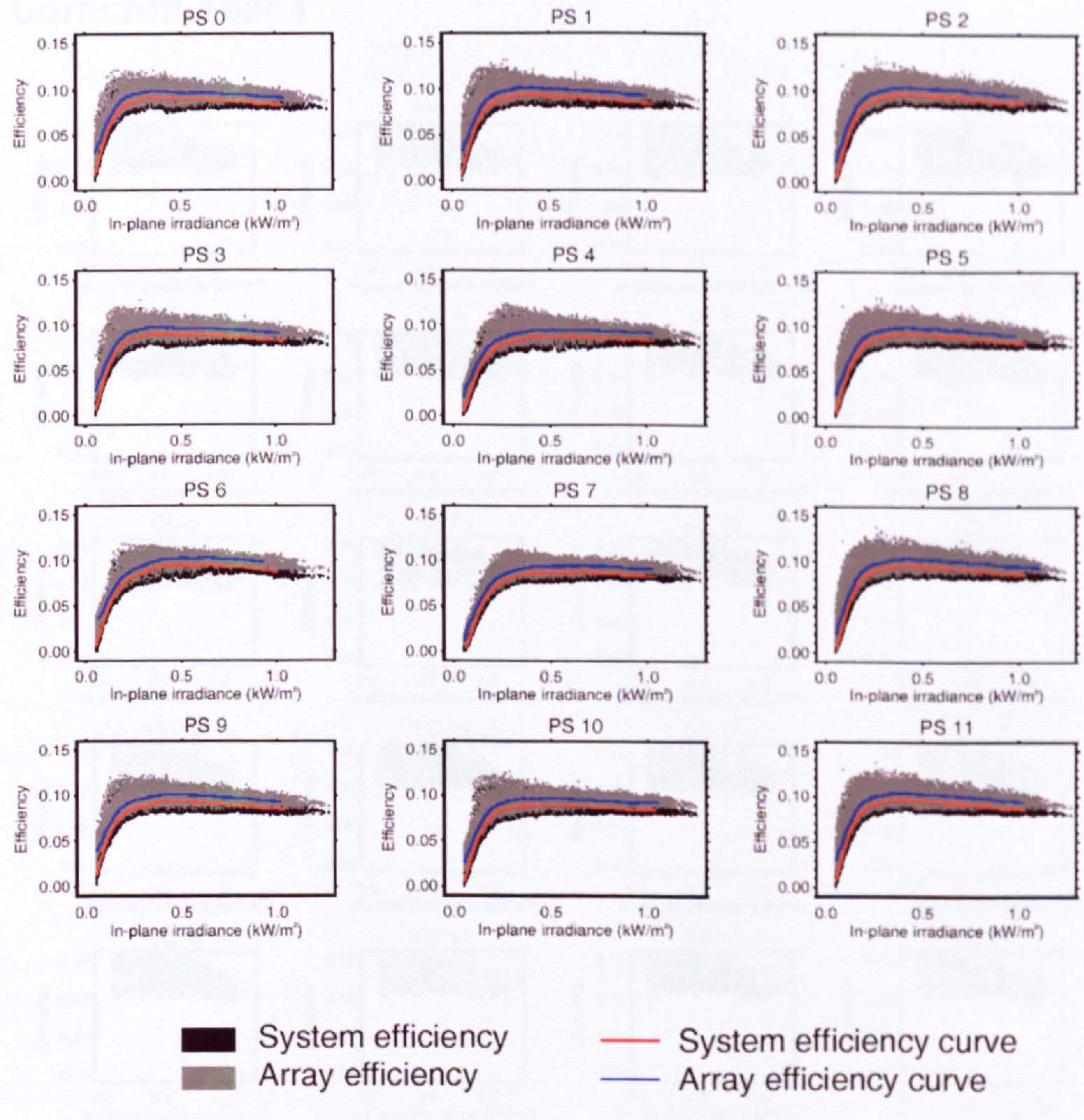

Figure D-10: System and array efficiency curves for Panmure Street

D.4. Temperature correction

D.4.1 Corncroft Year 1

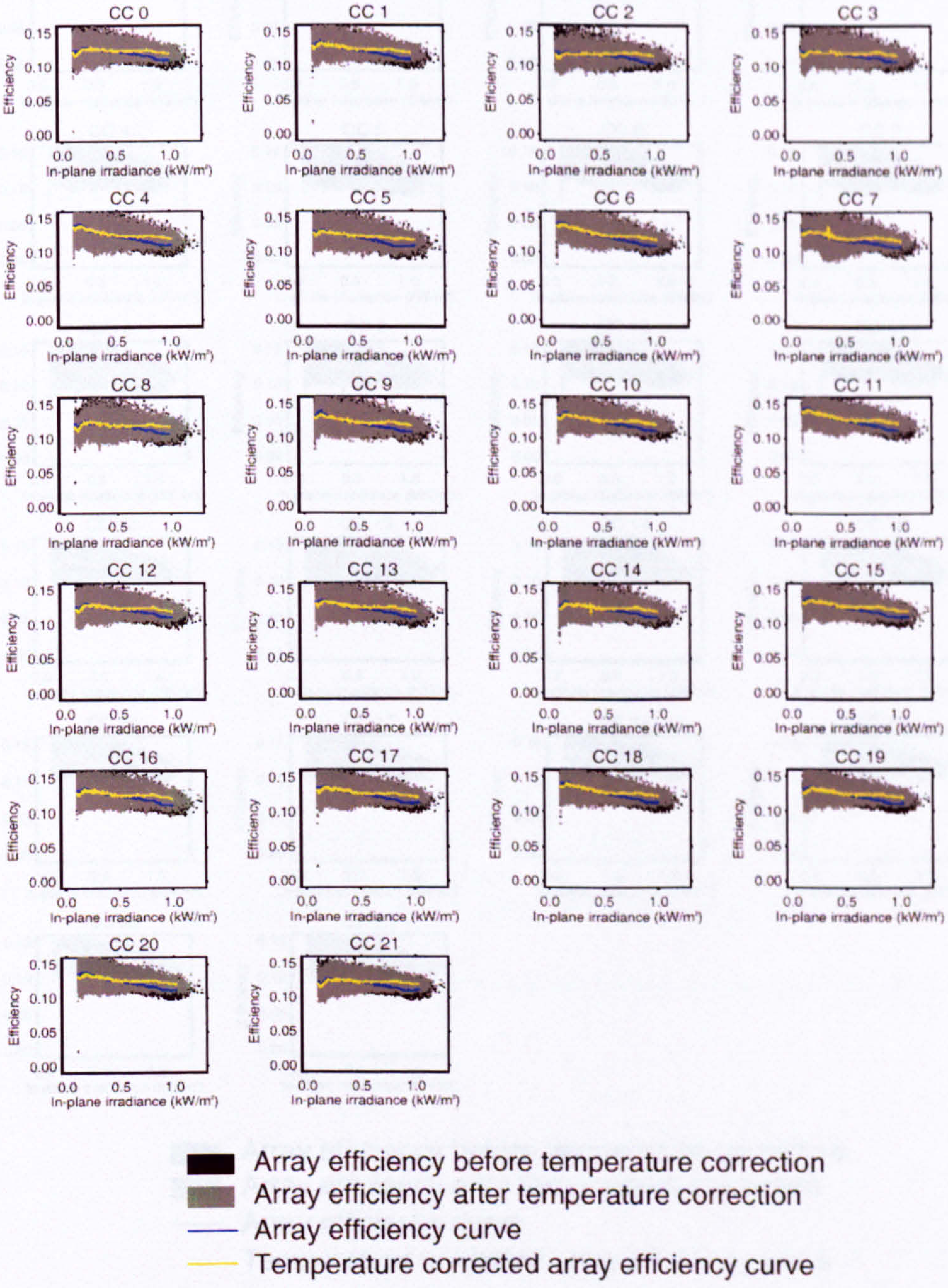

Figure D-11: Irradiance to temperature corrected array efficiency at Corncroft in first year of operation

D.4.2 Corncroft Year 2

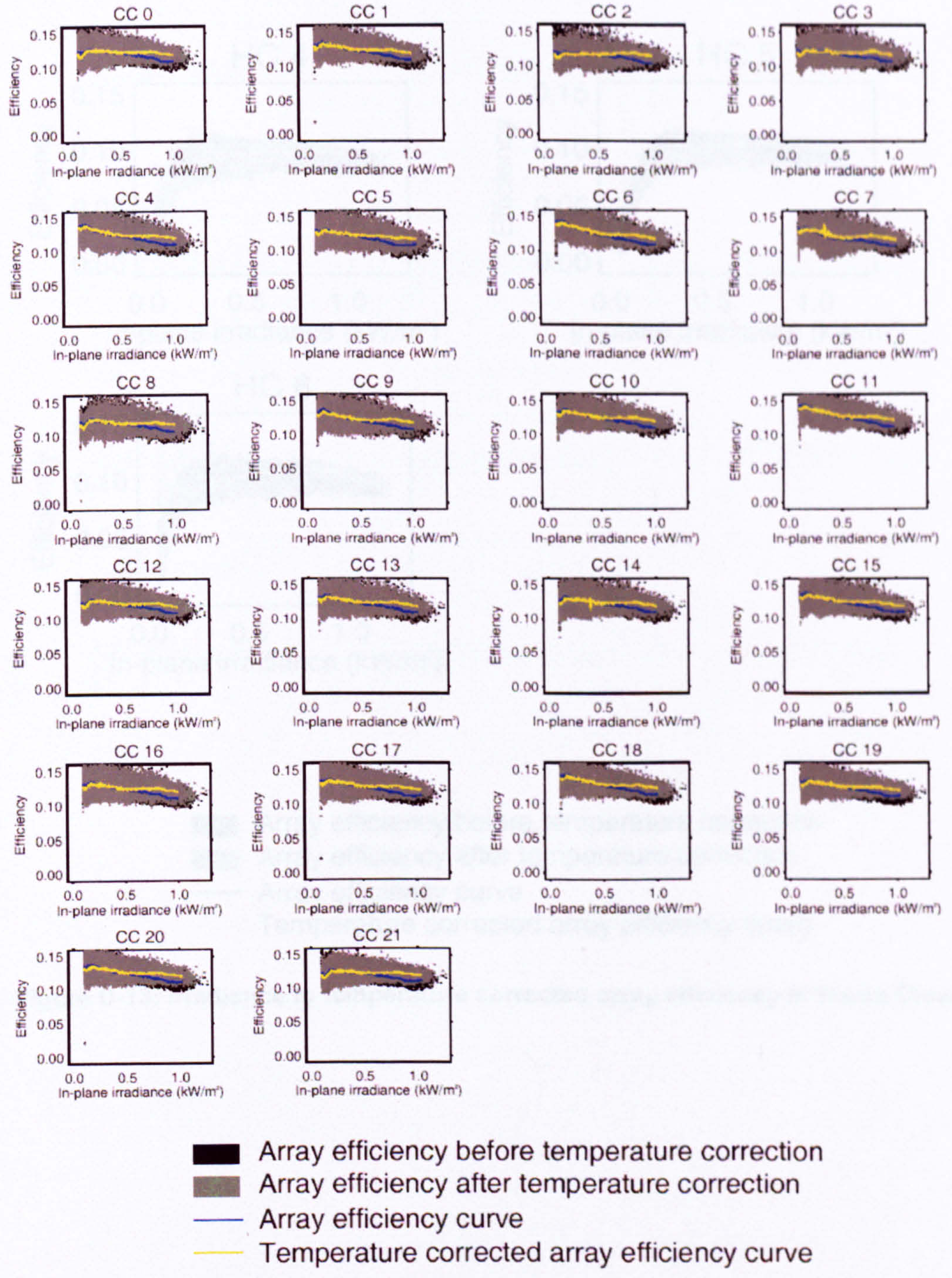

Figure D-12: Irradiance to temperature corrected array efficiency at Corncroft in the second year of operation

D.4.3 Heron Close

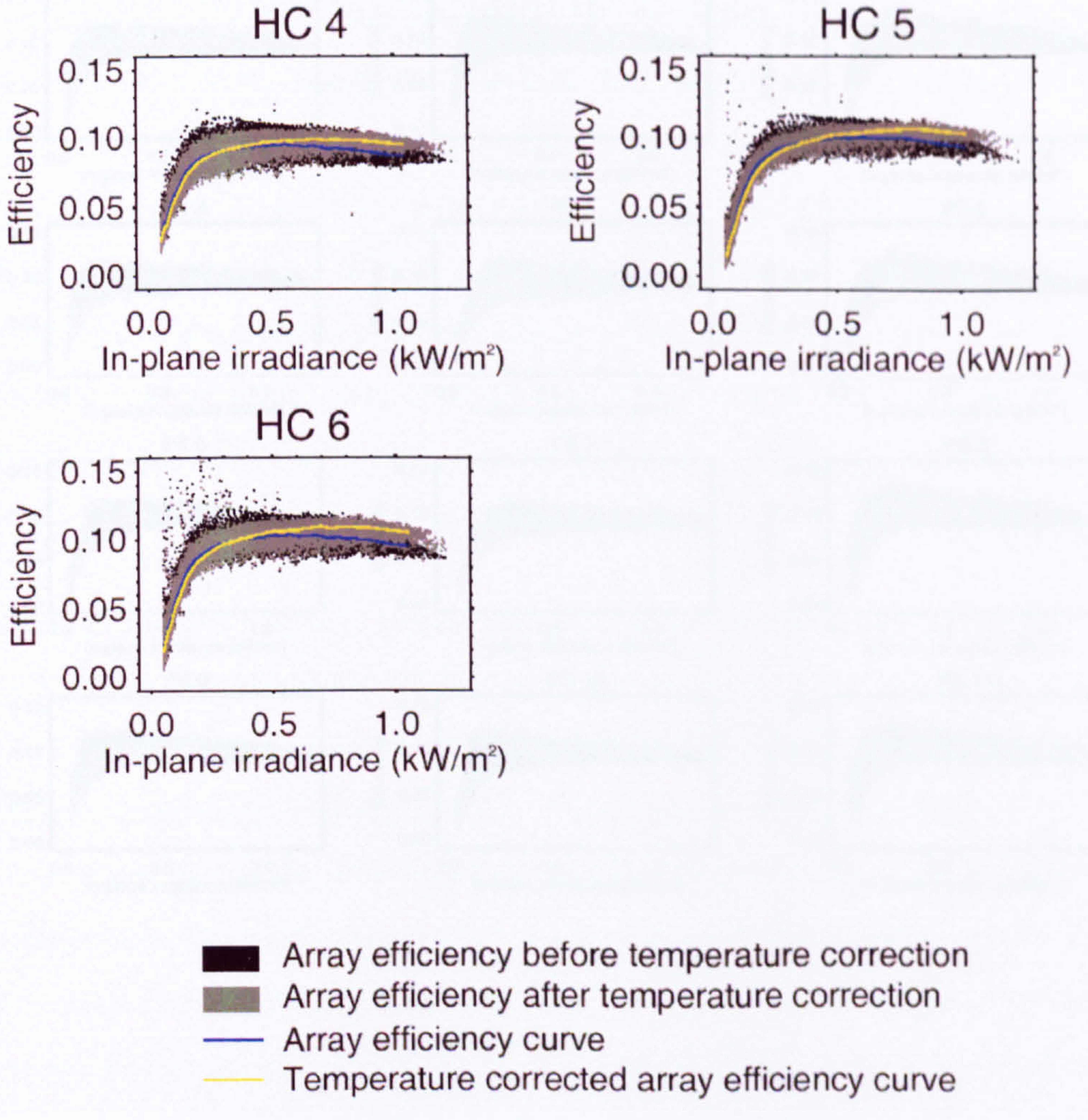

Figure D-13: Irradiance to temperature corrected array efficiency at Heron Close

D.4.4 Panmure Street

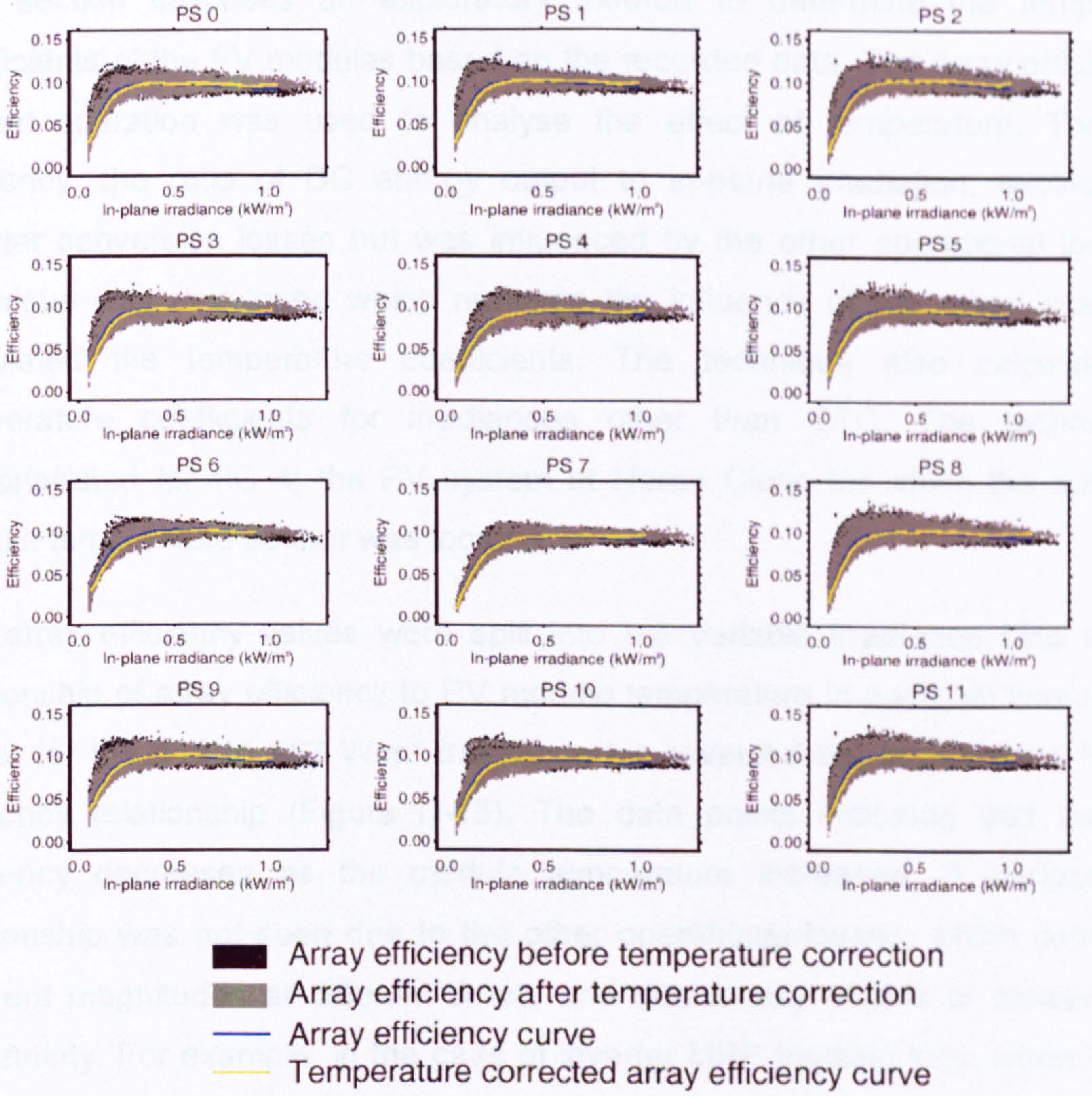

Figure D-14: Irradiance to temperature corrected array efficiency at Panmure Street

D.5. Determining temperature coefficients

This section describes an exploratory method to determine the temperature coefficients of the PV modules based on the recorded data. The array efficiency at normal operation was used to analyse the effect of temperature. The array efficiency, the ratio of DC energy output to in-plane irradiation, excluded the inverter conversion losses but was influenced by the other operational losses. A technique was developed which removed the influence of the other losses and calculated the temperature coefficients. The technique also calculates the temperature coefficients for irradiances other than STC. The technique is demonstrated for HC 4; the PV system at Heron Close for which the actual PV module temperature sensor was located.

The array efficiency values were split into the variable irradiance bins and the relationship of array efficiency to PV module temperature in each bin was studied. A plot for the 449 to 463 W/m^2 irradiance bin revealed the temperature to array efficiency relationship (Figure D-15). The data points indicated that the array efficiency decreased as the module temperature increased. A perfect linear relationship was not seen due to the other operational losses, which could have different magnitudes at different times, and due to any effects of measurement uncertainty. For example, in the case of inverter MPP tracking loss, when inverter MPP loss was at a minimum this would result in an efficiency value close to the top of the cloud of points. A high MPP tracking loss would result in a value close to the bottom of the cloud. To exclude this and other losses in the temperature coefficient analysis, the efficiency to temperature relationship of the top of the cloud of points was investigated.

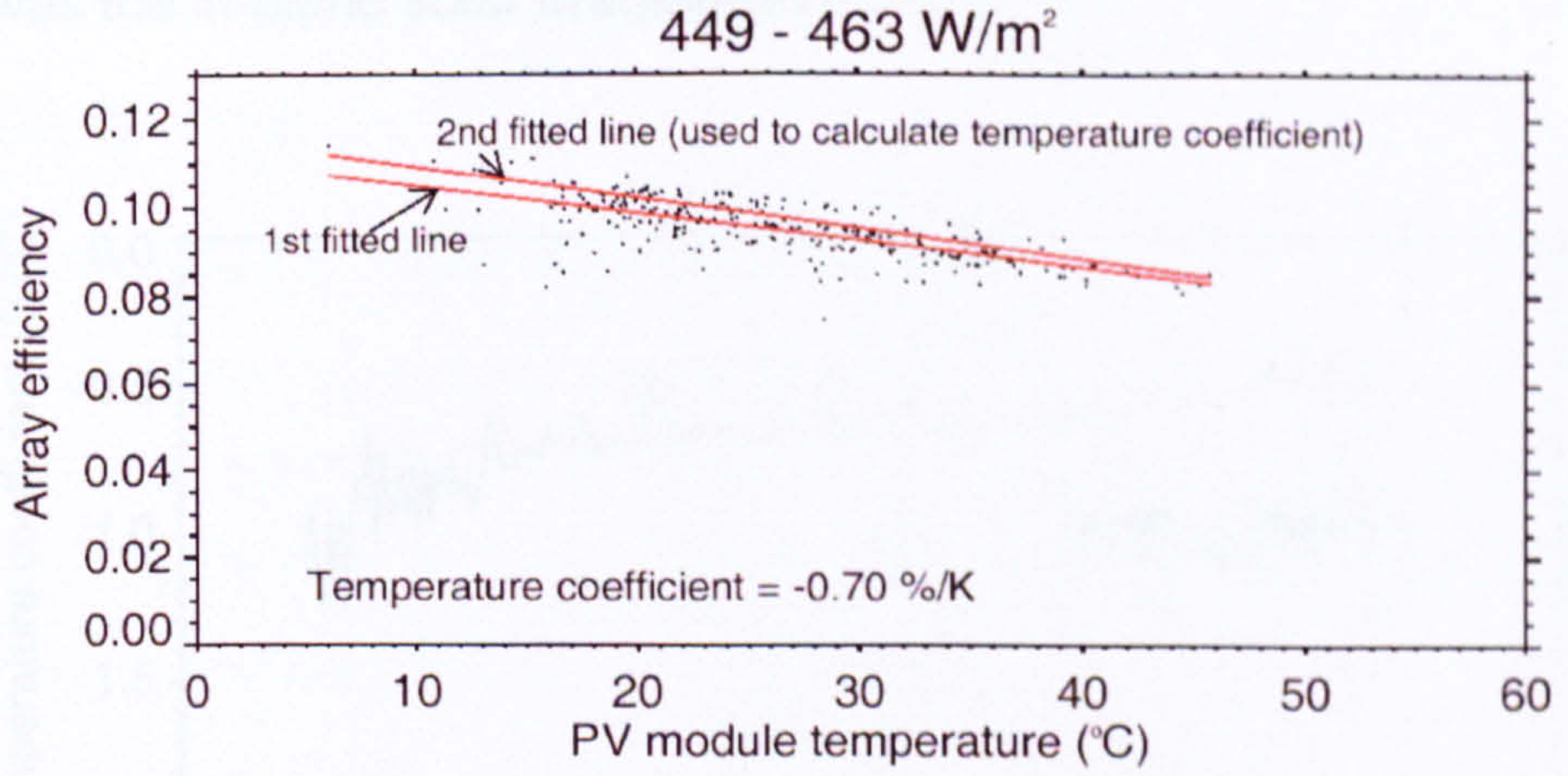

Figure D-15: Module temperature to array efficiency of normal operation at HC 4 in the 449 to 463 W/m^2 irradiance bin

A straight line was fitted using a least squares fit to the efficiency values in each bin and the values below the fitted line were excluded. A second straight line was fitted to the remaining efficiency values above the first line. This line was used to represent the temperature to efficiency relationship of the top of the cloud of points. The gradient of the second fitted line and its value at 25°C were used to calculate the temperature coefficients of power with the following equation:

$$\alpha_t = \frac{A}{B} \times 100$$

where α_t is the temperature coefficient of power (%/K); A is the gradient of the second fitted line; and B is the value of the second fitted line at a temperature of 25°C

The temperature coefficient for the 449 to 463 W/m^2 irradiance bin of HC 4 was calculated as -0.70%/K. This process was repeated for all the irradiance bins of HC 4 and the relationship of irradiance to temperature coefficient was established (Figure D-16). A straight line was fitted using a least squares method to the calculated temperature coefficients based on irradiances above 300 W/m^2. For simplicity the low irradiance values were ignored. The equation of this fitted line described the variation of the temperature coefficients with irradiance at HC 4 as:

$$\alpha_t = -0.78 + 0.29 \times H_i$$

where H_i was the in-plane solar irradiance (kW/m^2)

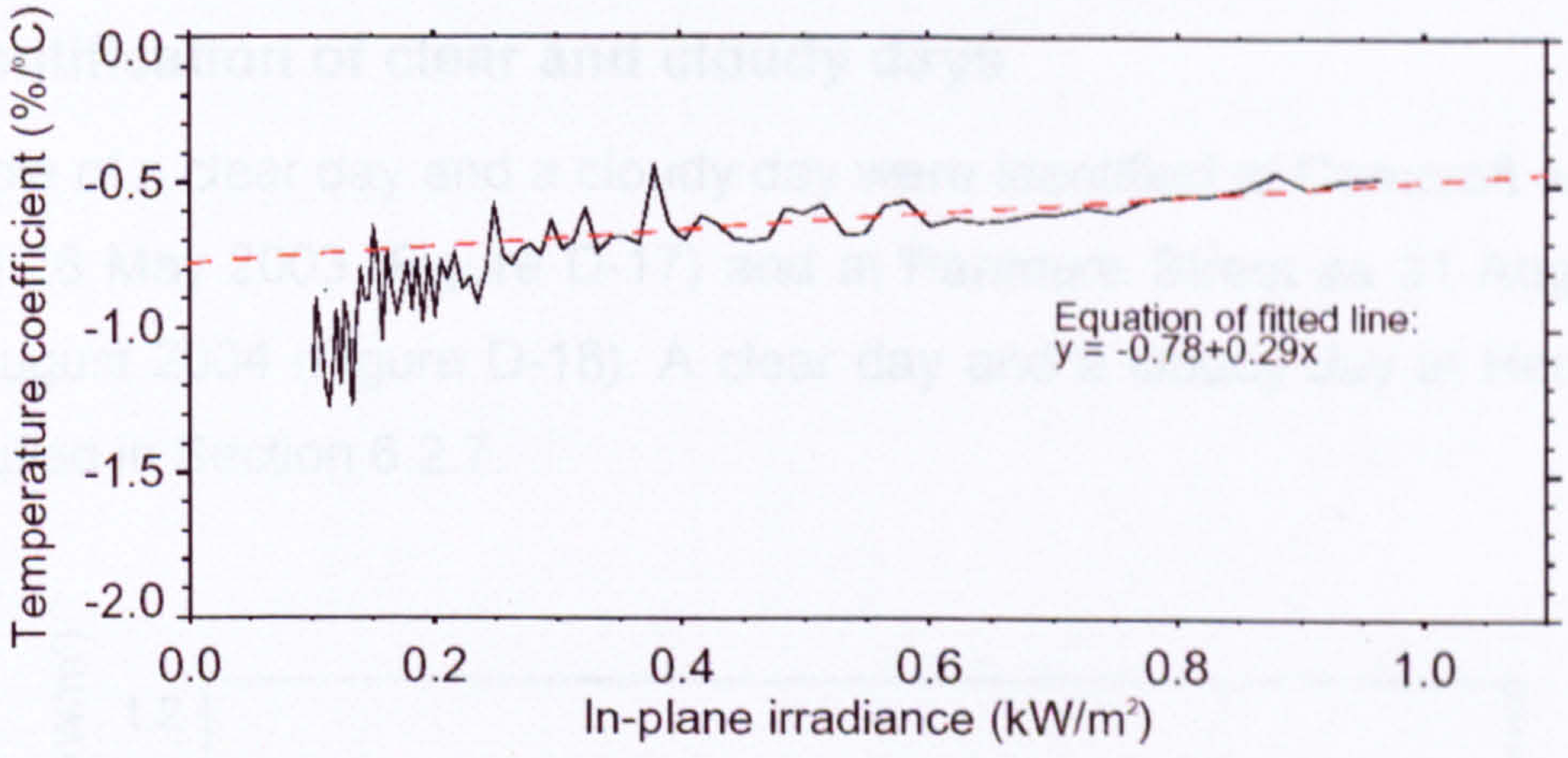

Figure D-16: In-plane irradiance to temperature coefficient relationship for HC 4

Based on this relationship, the temperature coefficient at the STC irradiance of 1000 W/m^2 was calculated as -0.49%/°C. This compares well with the manufacturer's STC value of -0.473%/°C (Astropower, 2004); a satisfying result.

The temperature coefficient appeared to decrease with decreasing irradiance (Figure D-16). No reference was found in the literature to either confirm or refute this result. For this reason this analysis has been presented as an experimental study of possible techniques to determine the temperature coefficients from monitored data and to investigate the variation of the temperature coefficients with irradiance. In the normal operation analysis of Chapter 6 it was decided to use constant temperature coefficients, based on the manufacturer's specifications, for the temperature correction process.

D.6. Assessment of inverter MPP tracking loss on clear and cloudy days

D.6.1 Identification of clear and cloudy days

An example of a clear day and a cloudy day were identified at Corncroft as 30 May 2003 and 26 May 2003 (Figure D-17) and at Panmure Street as 31 August 2004 and 27 August 2004 (Figure D-18). A clear day and a cloudy day at Heron Close was identified in Section 6.2.7.

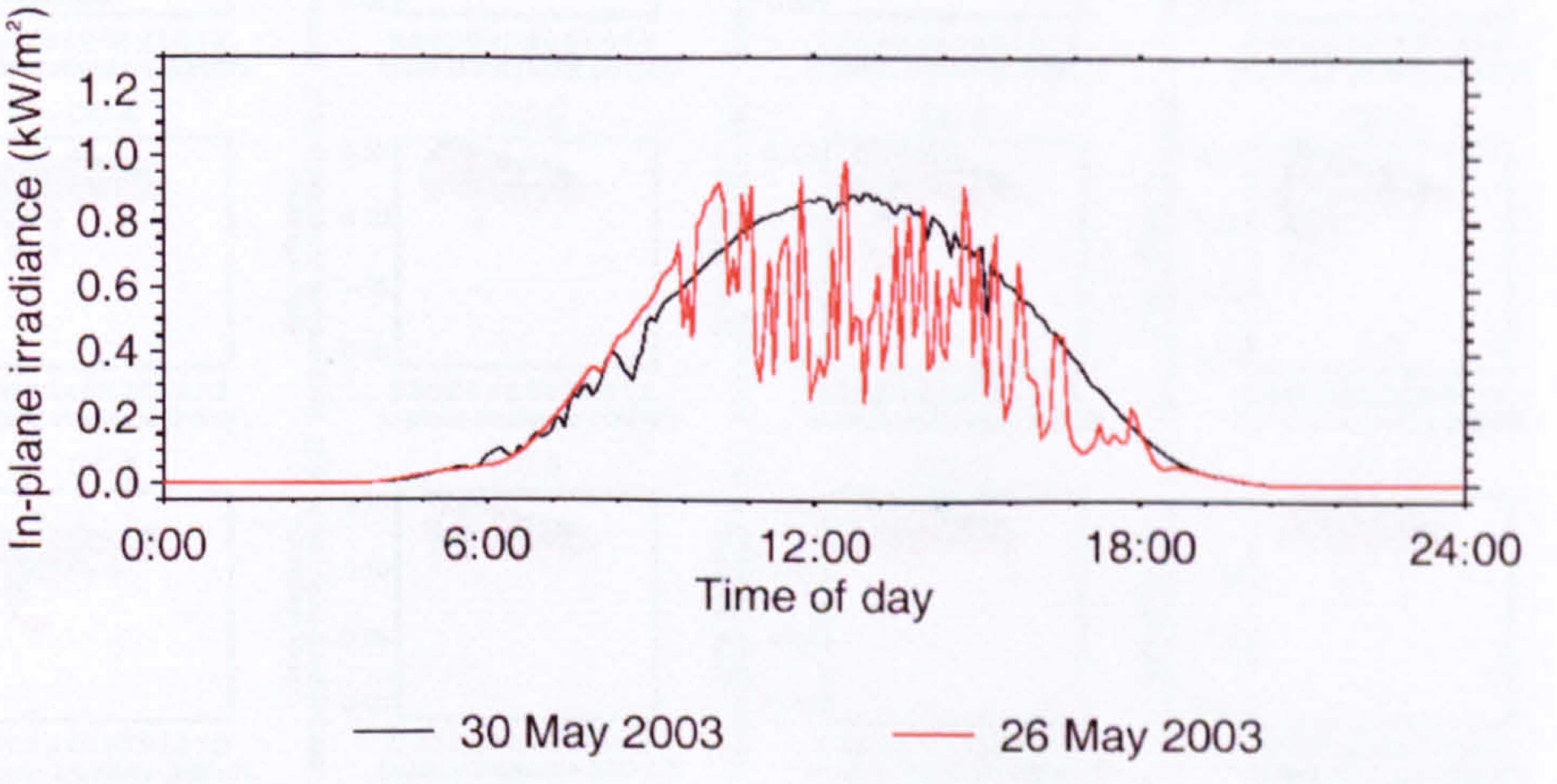

Figure D-17: Time of day against in-plane irradiance for Corncroft on a clear day and a cloudy day

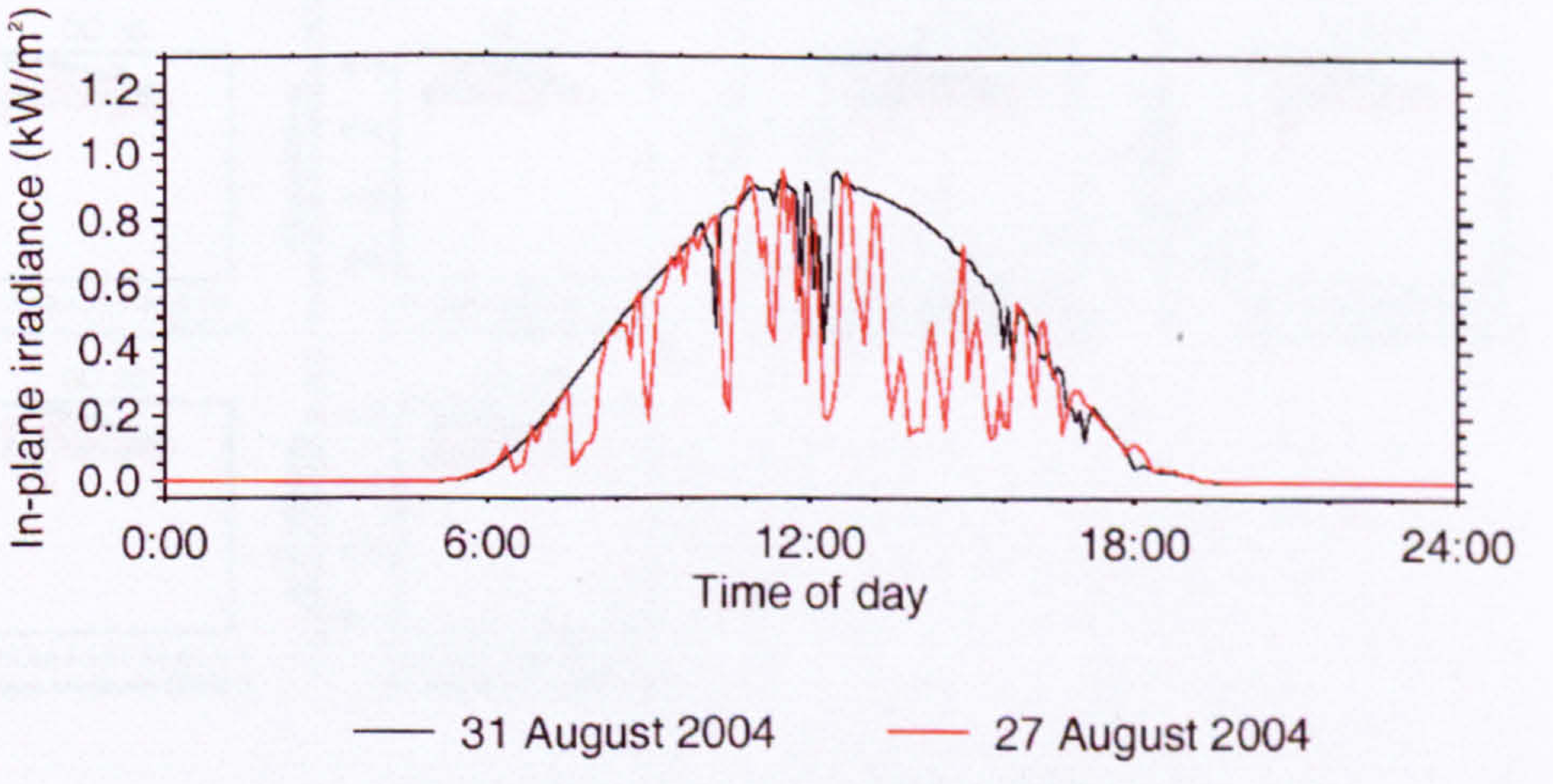

Figure D-18: Time of day against in-plane irradiance for Panmure Street on a clear day and a cloudy day

D.6.2 Corncroft

Irradiance to efficiency plots for a clear day and a cloudy day at Corncroft show more efficiency variation occurs on the cloudy day (Figure D-19). At CC0 there appears to be inverter fault during the clear day and at CC2 the PV system was not operational on either of the days.

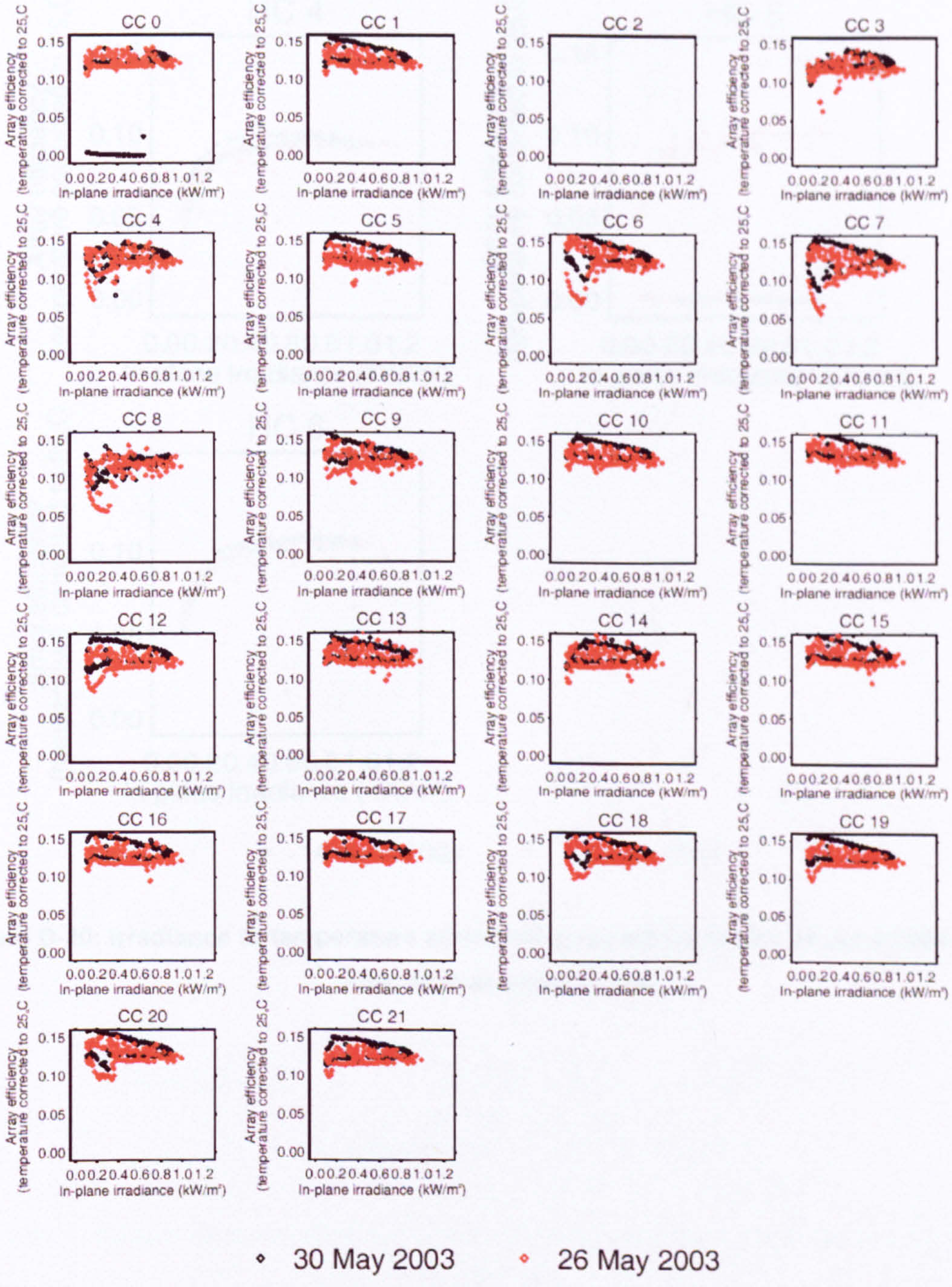

Figure D-19: Irradiance to temperature corrected array efficiency for 30 May 2003 and 26 May 2003 at Corncroft

D.6.3 Heron Close

Irradiance to efficiency plots for a clear day and a cloudy day at Heron Close show more efficiency variation occurs on the cloudy day (Figure D-20). Here it appears that HC 5 did not operate at all on the clear day.

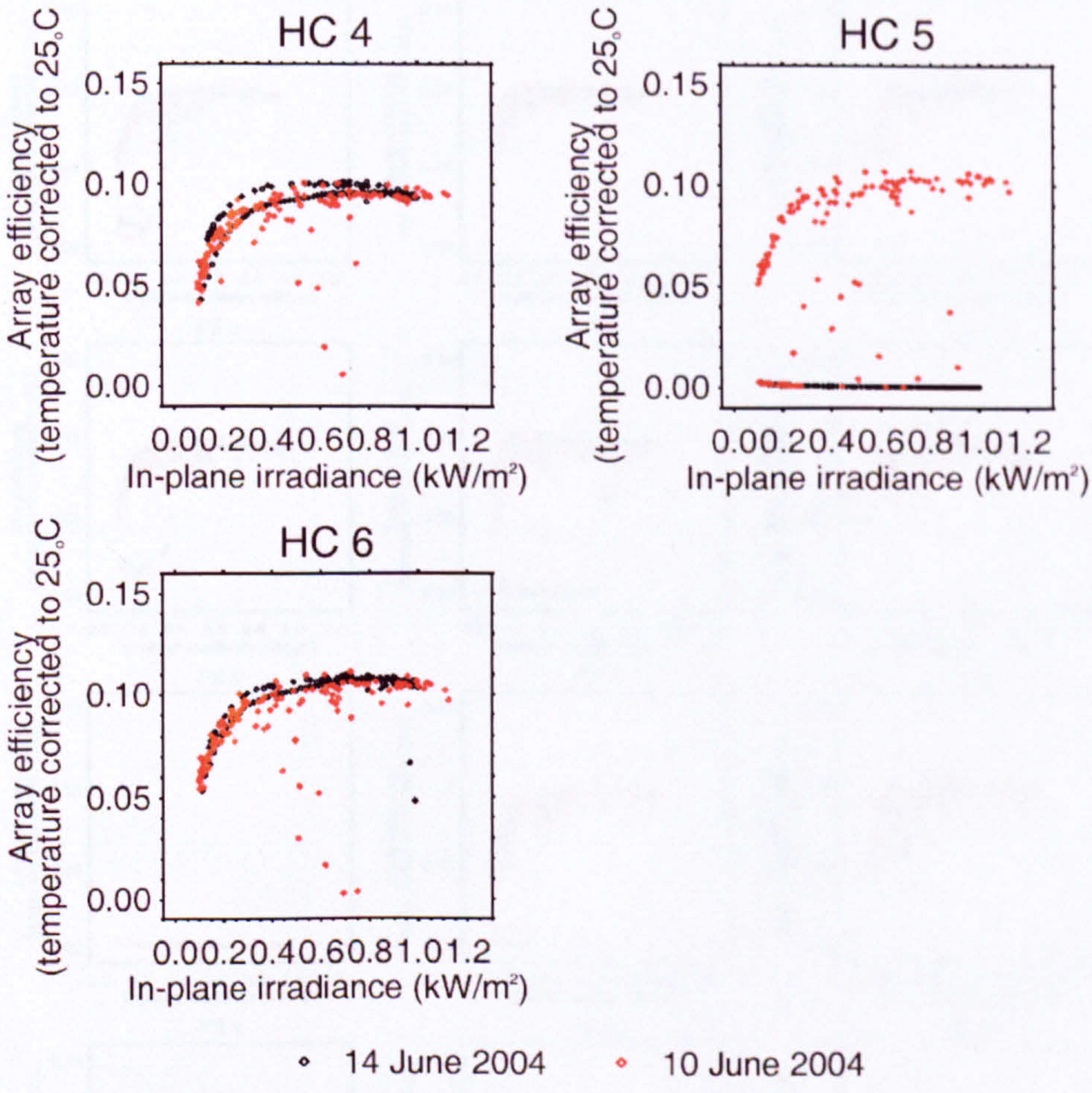

Figure D-20: Irradiance to temperature corrected array efficiency for 14 June 2004 and 10 June 2004 at Heron Close

D.6.4 Panmure Street

Irradiance to efficiency plots for a clear day and a cloudy day at Panmure Street show more efficiency variation occurs on the cloudy day (Figure D-21). At this site, PS 6 did not generate on either day.

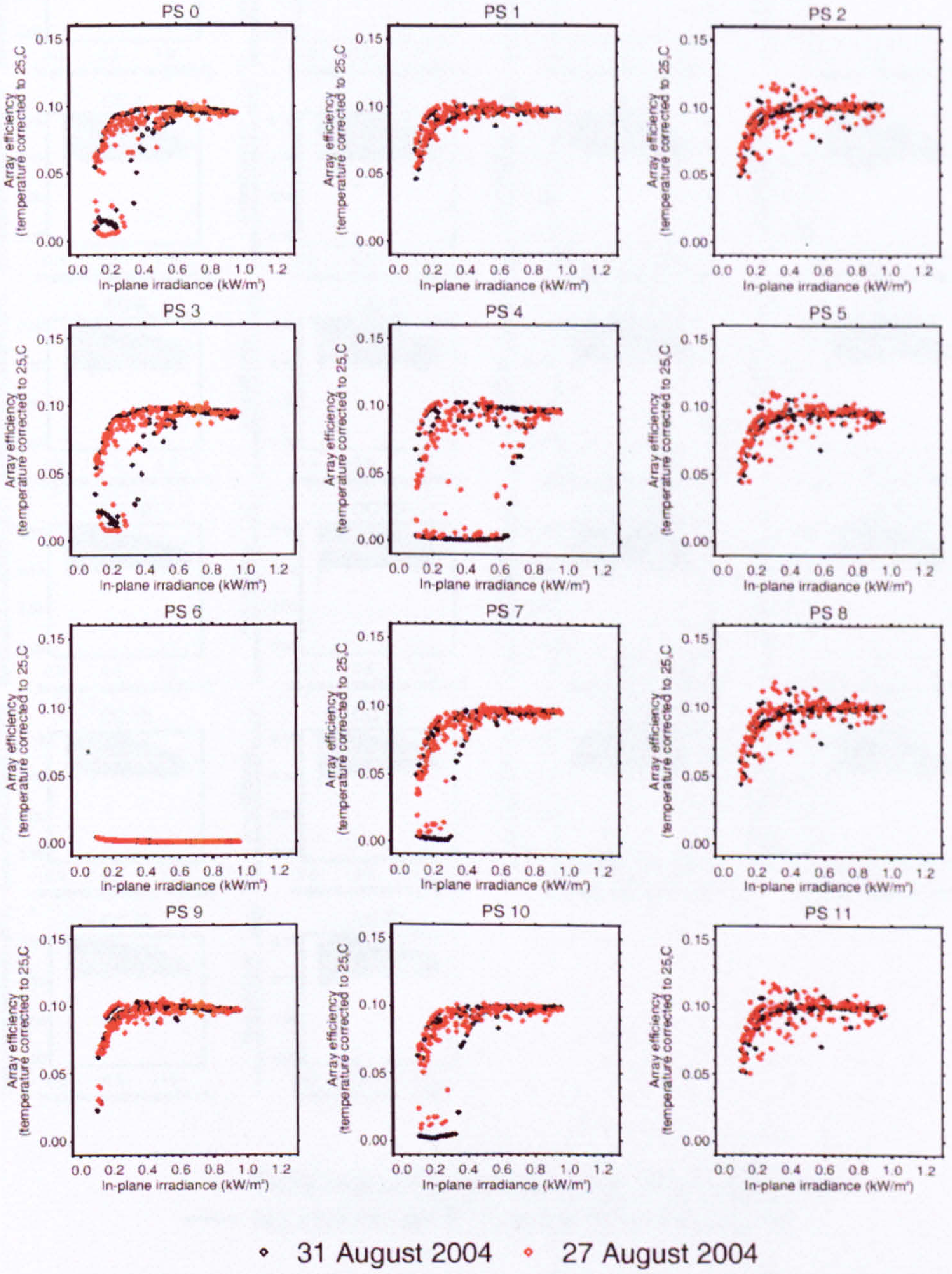

Figure D-21: Irradiance to temperature corrected array efficiency for 31 August 2004 and 27 August 2004 at Panmure Street

D.7. No MPPT curves

D.7.1 Corncroft Year 1

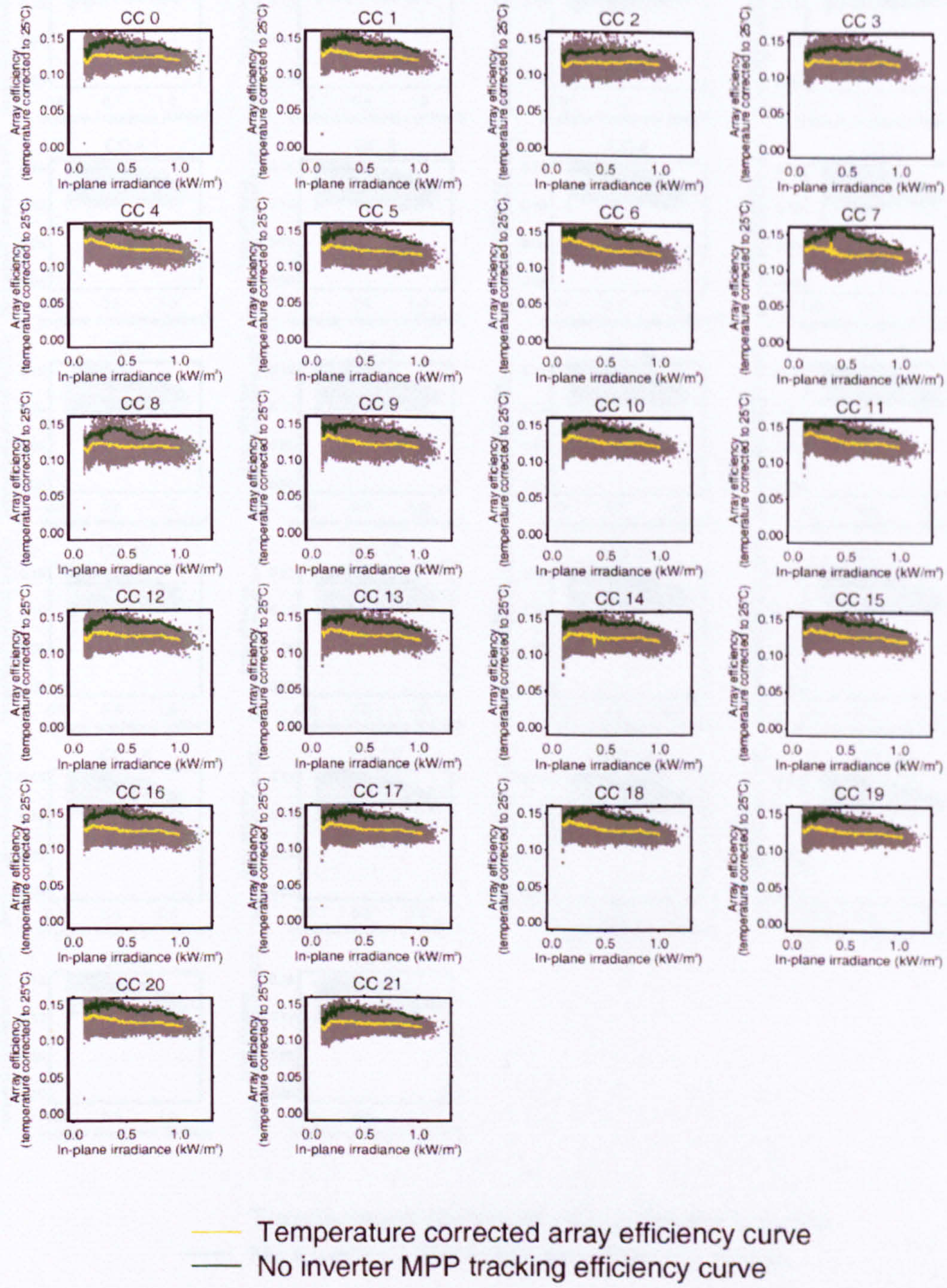

Figure D-22: No MPPT curves and temperature corrected array efficiency curves at Corncroft in the first year of operation

D.7.2 Corncroft Year 2

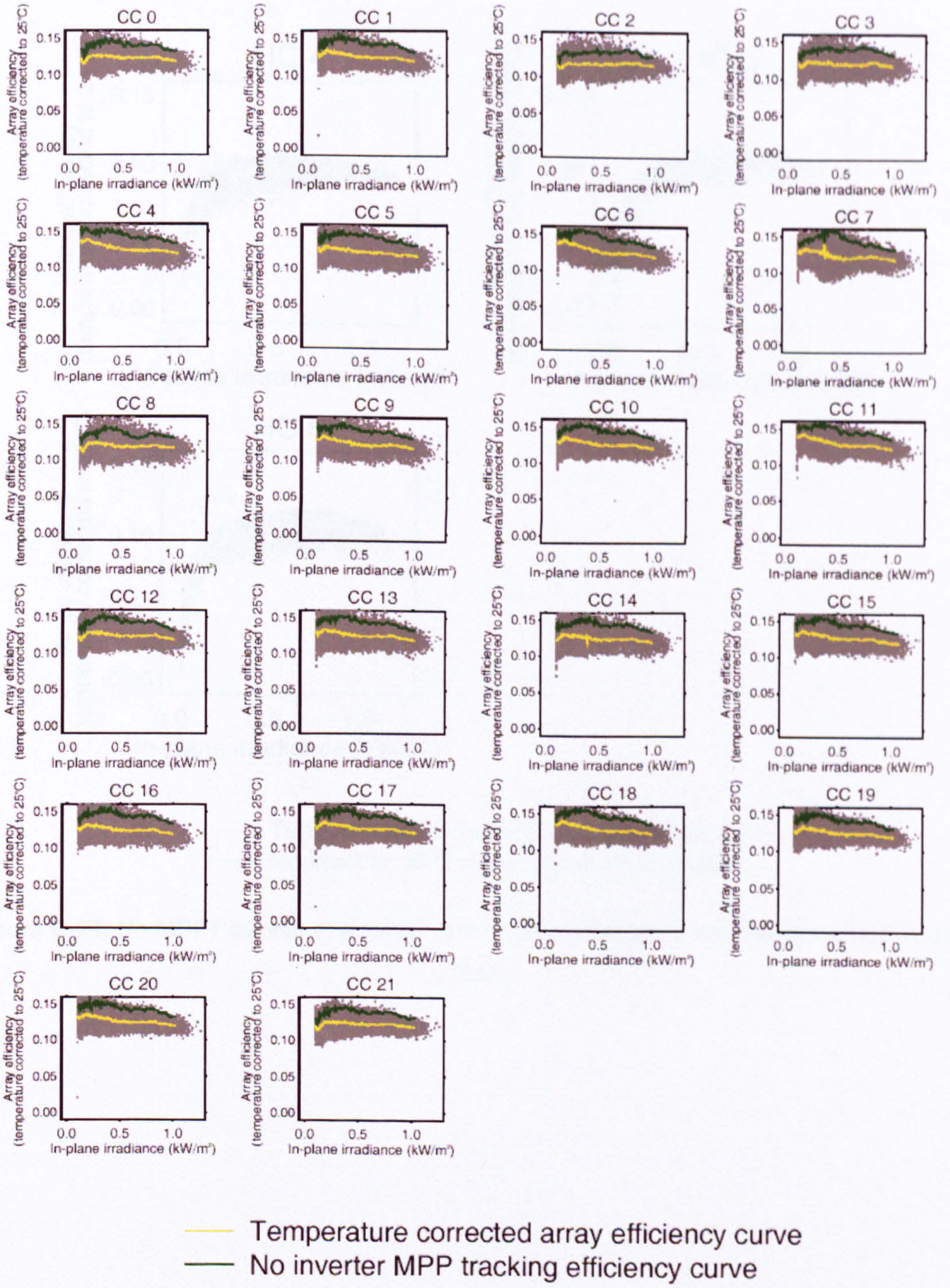

Figure D-23: No MPPT curves and temperature corrected array efficiency curves at Corncroft in the second year of operation

D.7.3 Heron Close

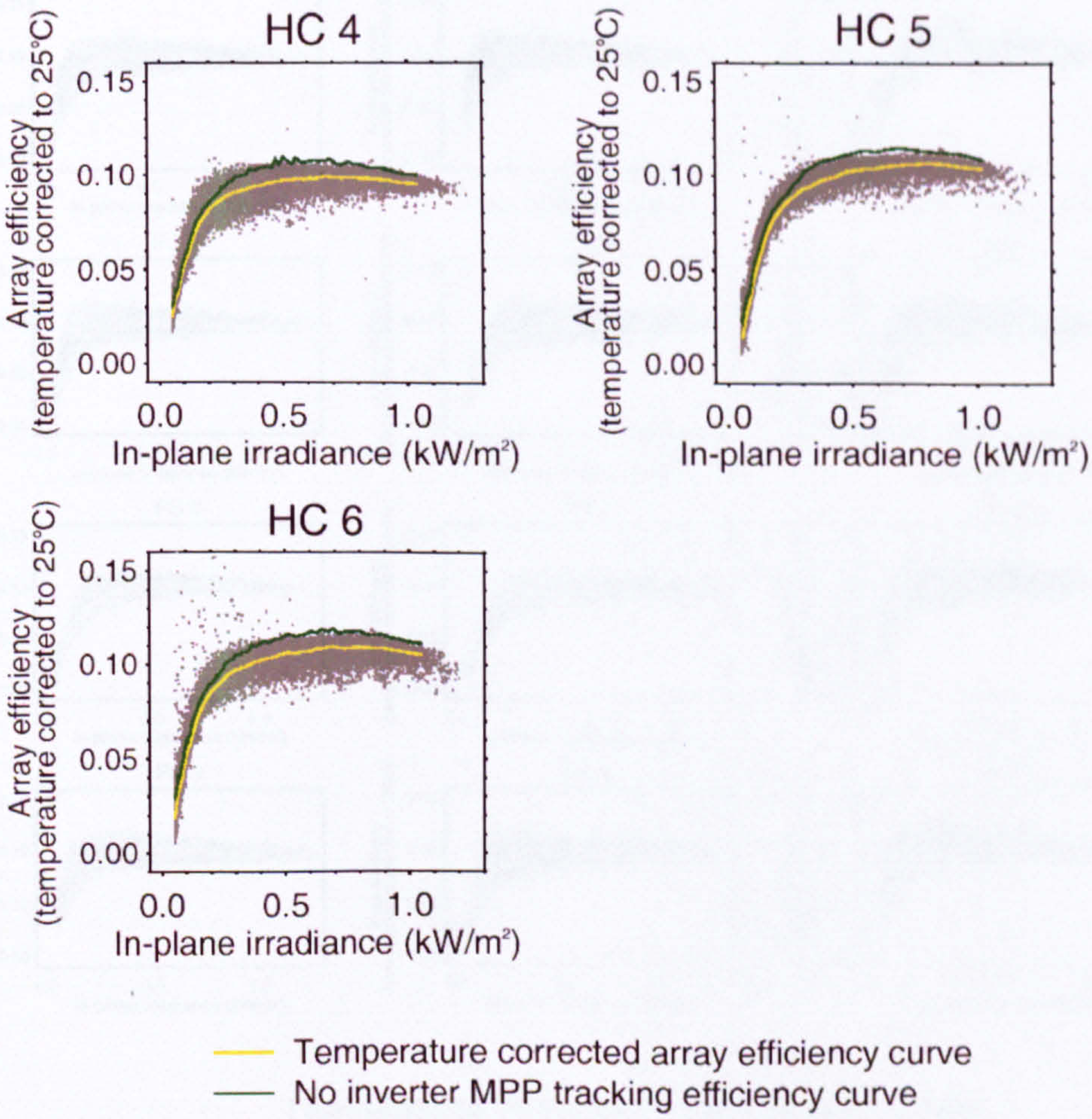

Figure D-24: No MPPT curves and temperature corrected array efficiency curves at Heron Close

D.7.4 Panmure Street

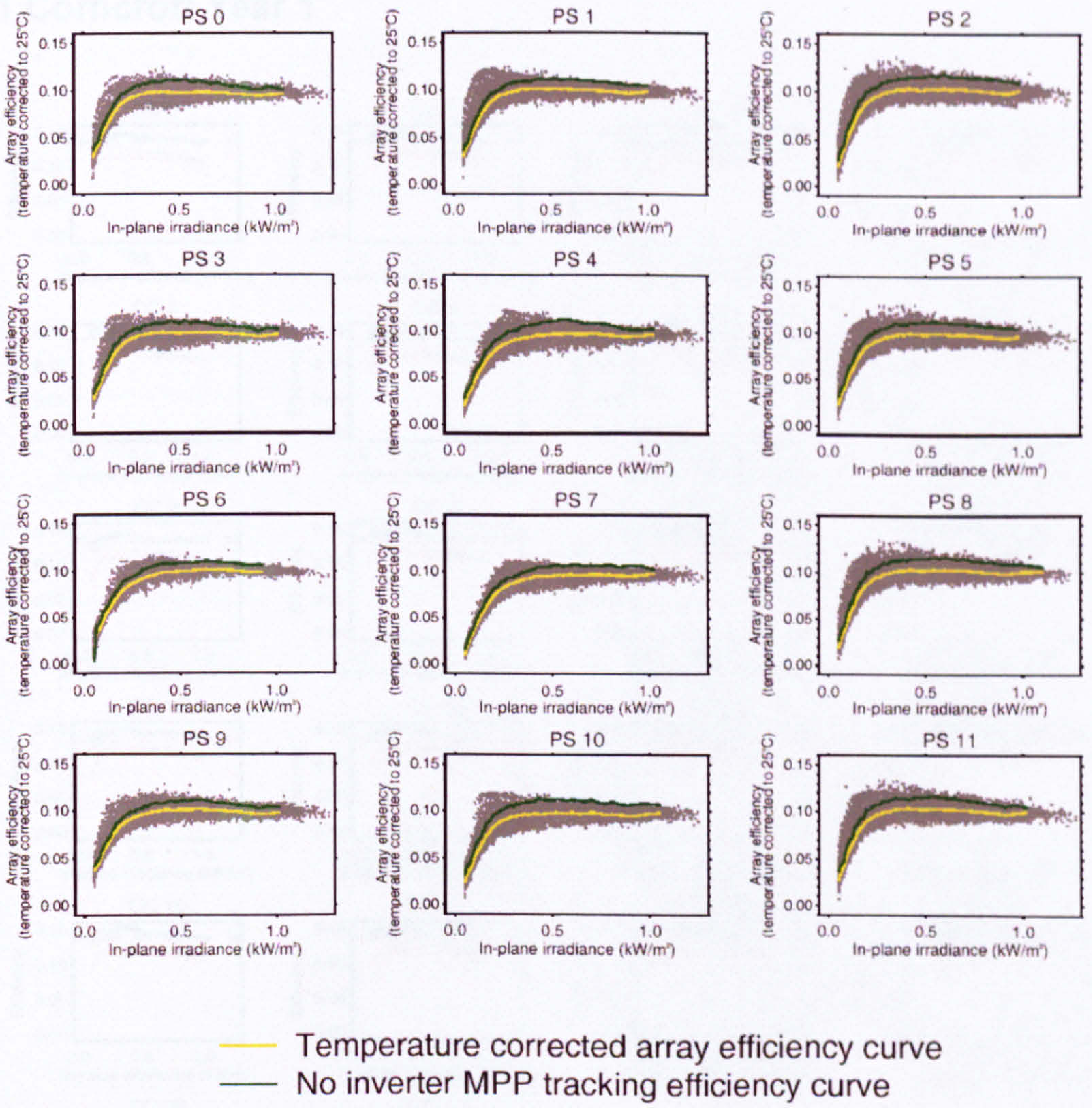

Figure D-25: No MPPT curves and temperature corrected array efficiency curves at Panmure Street

D.8. Efficiency curves

D.8.1 Corncroft Year 1

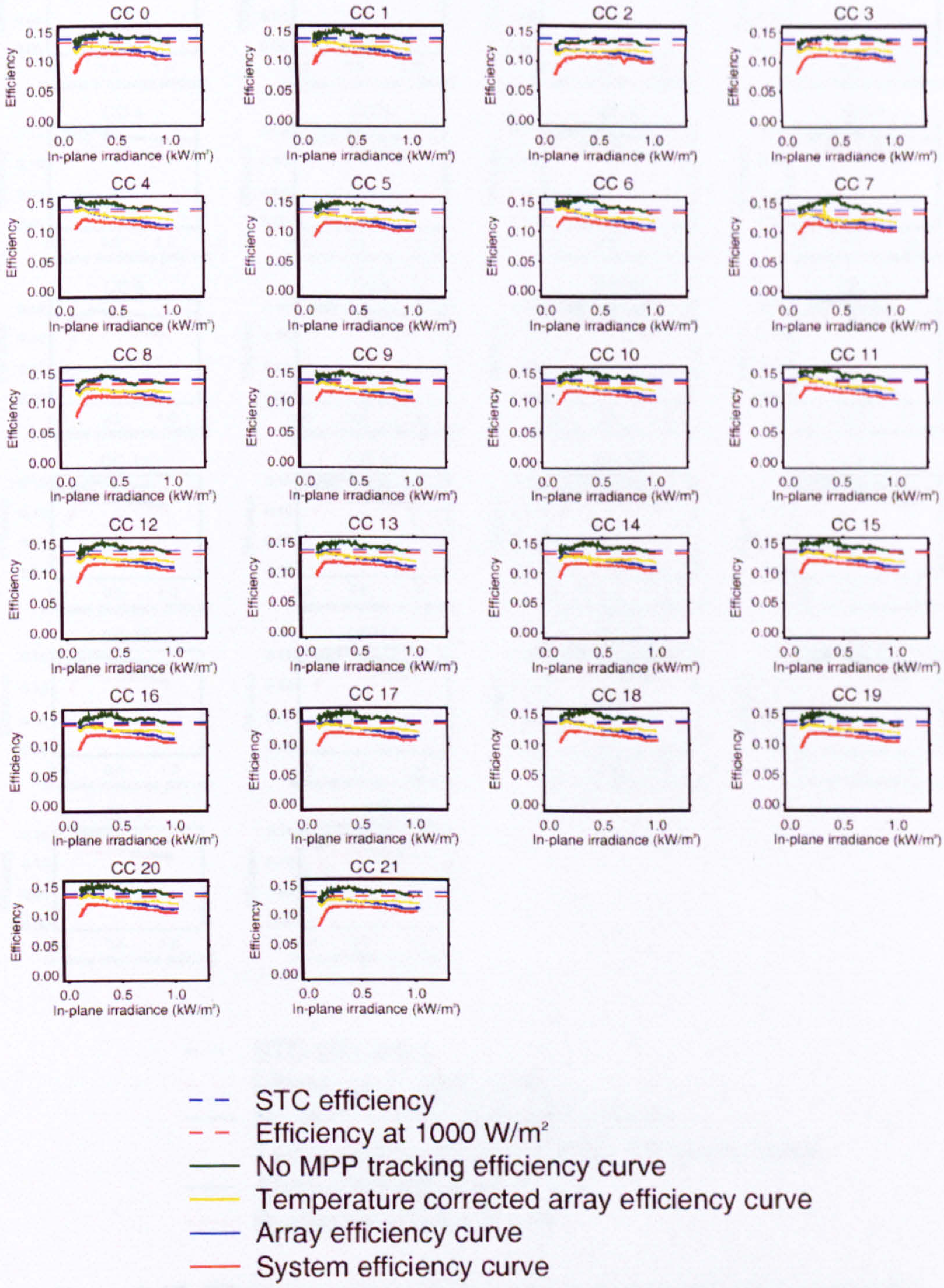

Figure D-26: Efficiency curves at Corncroft in the first year of operation

D.8.2 Corncroft Year 2

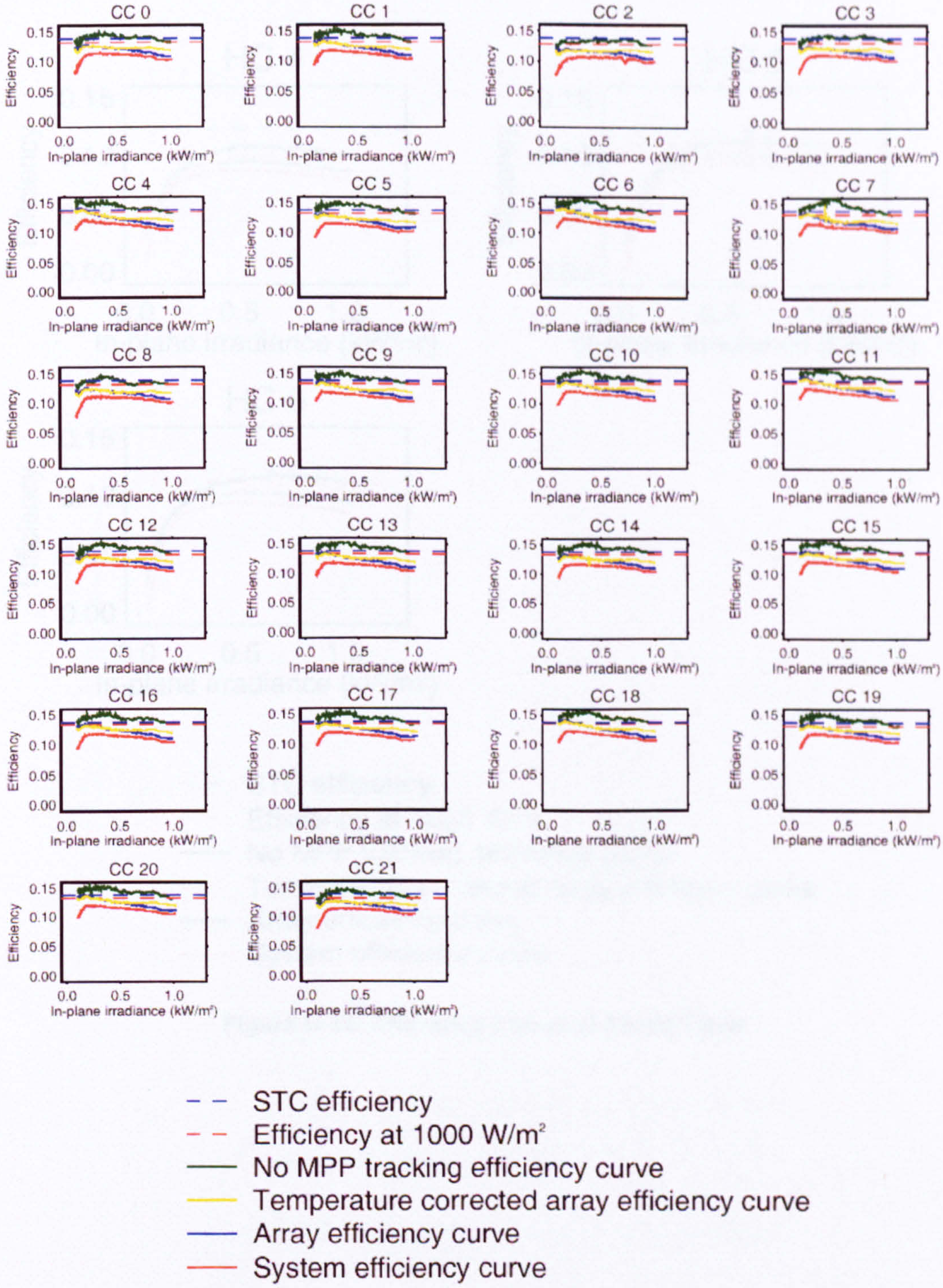

Figure D-27: Efficiency curves at Corncroft in the second year of operation

D.8.3 Heron Close

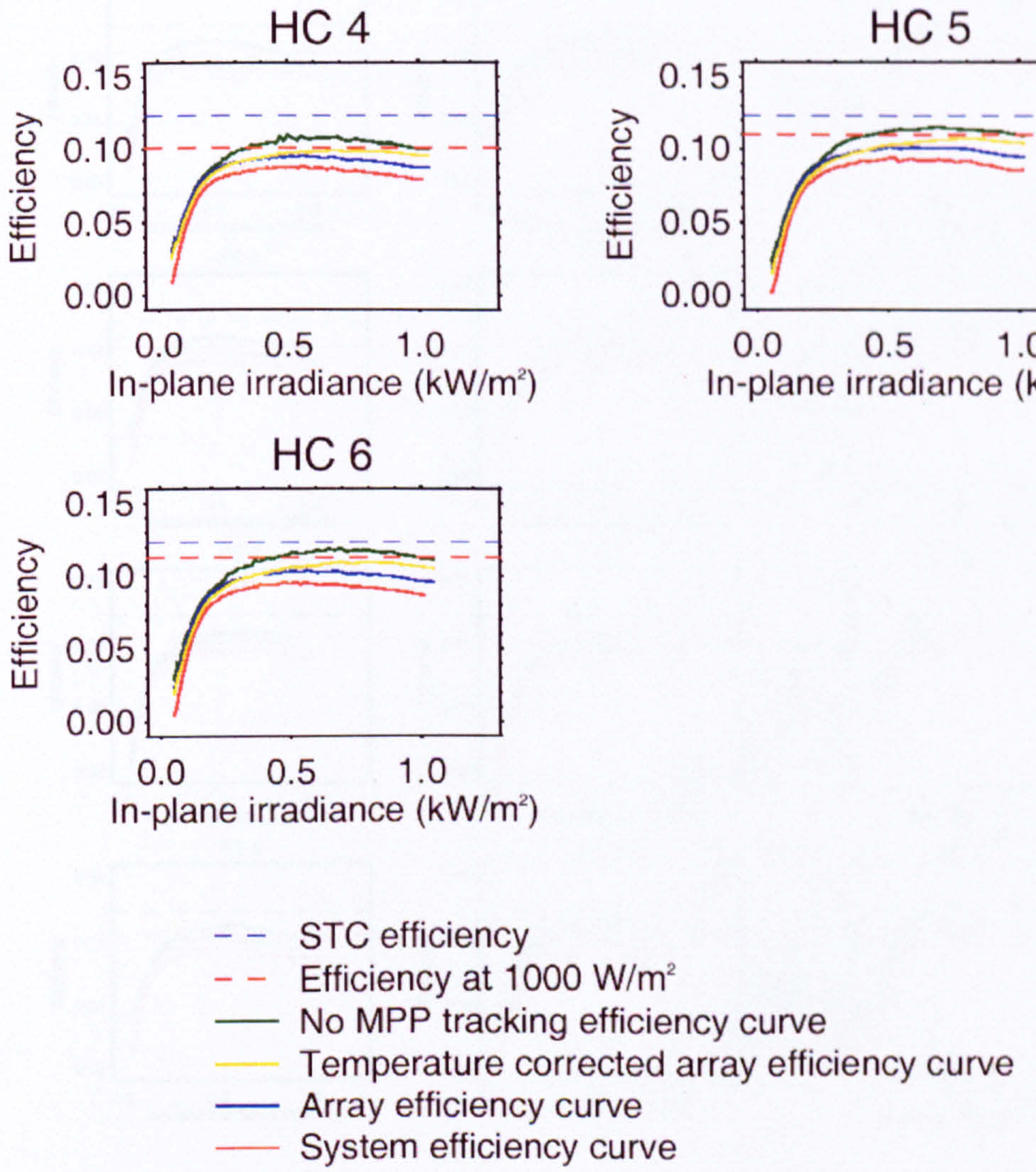

Figure D-28: Efficiency curves at Heron Close

D.8.4 Panmure Street

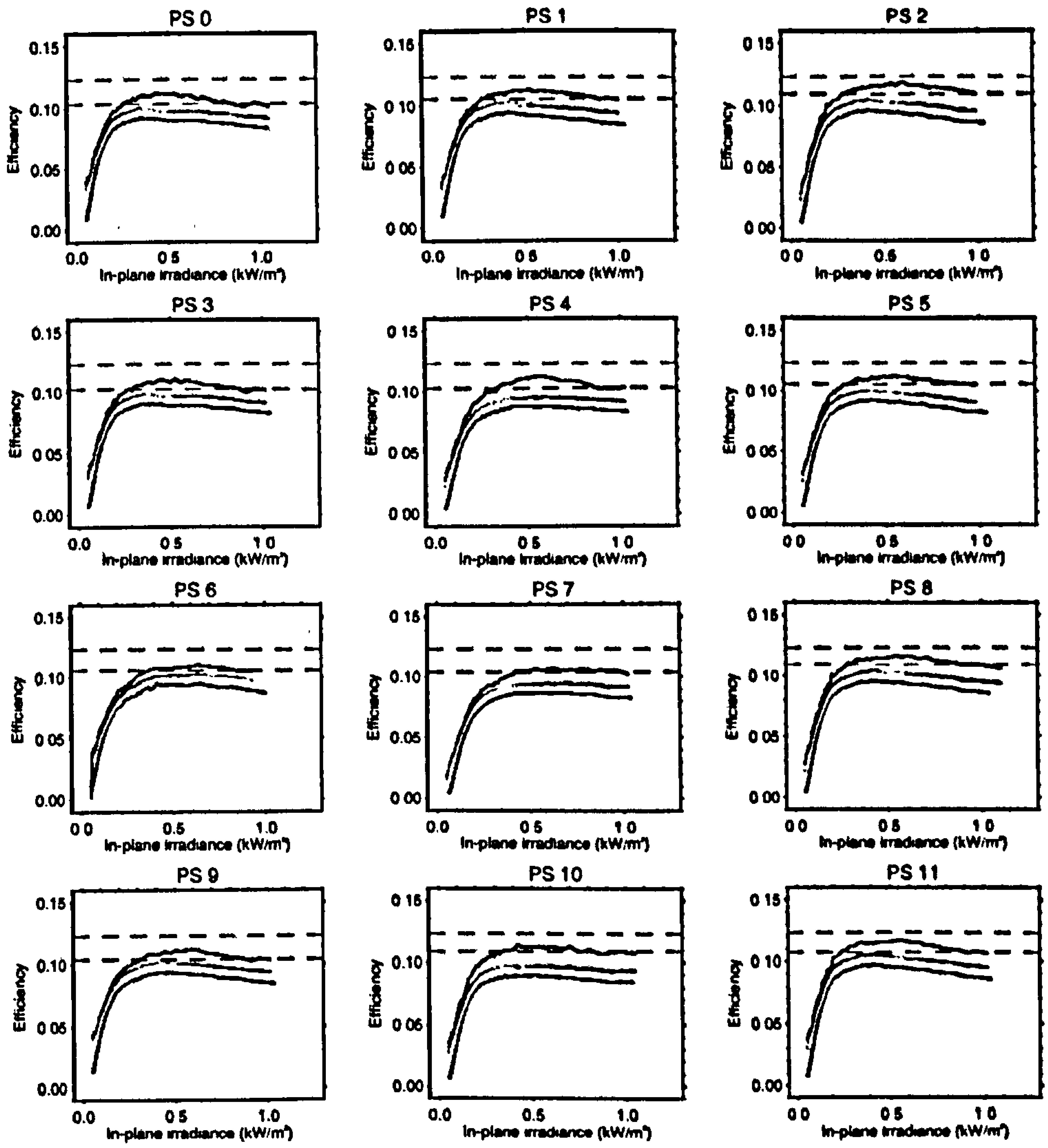

-- STC efficiency
-- Efficiency at 1000 W/m²
—— No MPP tracking efficiency curve
······ Temperature corrected array efficiency curve
—— Array efficiency curve
—— System efficiency curve

Figure D-29: Efficiency curves at Panmure Street

D.9. Reduction in annual performance ratios

D.9.1 Corncroft Year 1

Table D-1: Annual performance ratio and losses in normal operation at Corncroft in the first year of operation

System	Mismatch and deviation from STC loss	Irradiance effect	Inverter MPP tracking loss	Temperature loss	DC wiring loss	Inverter DC to AC conversion loss	Annual perfor-mance ratio of normal operation
	loss in annual perfomance ratio (in performance ratio %)						(%)
0	4.2	-2.5	12.2	2.0	0.1	8.4	75.6
1	4.5	-5.4	12.6	1.9	0.1	8.2	78.1
2	7.2	-0.3	10.7	1.9	0.1	8.6	71.8
3	5.0	-2.6	13.0	2.1	0.1	8.3	74.1
4	2.5	-4.2	12.4	2.2	0.1	8.1	79.0
5	3.6	-4.1	13.7	2.2	0.1	8.2	76.3
6	3.0	-5.4	12.4	2.0	0.1	8.1	79.8
7	4.3	-6.1	14.6	2.5	0.1	8.1	76.5
8	5.0	-0.5	11.8	1.6	0.1	8.4	73.5
9	3.7	-3.7	12.5	2.0	0.1	7.5	77.9
10	3.5	-5.1	12.4	2.0	0.1	8.2	78.9
11	2.6	-6.4	12.2	2.0	0.1	8.1	81.5
12	4.7	-5.0	13.2	2.0	0.1	8.3	76.6
13	3.1	-4.5	13.0	2.0	0.1	8.2	78.0
14	3.1	-3.9	13.4	1.9	0.1	7.5	77.9
15	1.8	-4.5	13.1	1.8	0.1	8.2	79.5
16	3.2	-4.7	13.0	1.9	0.1	8.2	78.2
17	3.0	-4.7	12.2	1.9	0.1	8.2	79.2
18	1.3	-4.7	12.2	2.0	0.1	8.1	80.9
19	4.6	-5.0	12.1	1.8	0.1	8.2	78.2
20	3.6	-5.3	12.3	1.8	0.1	8.2	79.3
21	4.6	-2.1	11.5	1.8	0.1	8.4	75.7

D.9.2 Corncroft Year 2

Table D-2: Annual performance ratio and losses in normal operation at Corncroft in the second year of operation

System	Mismatch and deviation from STC loss	Irradiance effect	Inverter MPP tracking loss	Temperature loss	DC wiring loss	Inverter DC to AC conversion loss	Annual performance ratio of normal operation
	loss in annual performance ratio (in performance ratio %)						(%)
0	4.1	-1.3	11.5	1.7	0.1	8.0	75.8
1	5.2	-4.8	12.0	2.2	0.1	7.9	77.5
2	7.2	1.7	9.6	-0.5	0.1	8.4	73.5
3	5.9	-1.9	12.7	2.1	0.1	8.1	72.9
4	6.0	-5.6	11.4	2.0	0.1	7.9	78.3
5	5.5	-5.7	14.0	2.7	0.1	7.9	75.4
6	5.7	-6.7	12.0	2.3	0.1	7.8	78.8
7	7.2	-8.1	14.6	2.5	0.1	7.9	75.8
8	6.8	-1.8	11.7	1.4	0.1	8.2	73.7
9	5.9	-5.0	12.3	2.2	0.1	7.2	77.2
10	4.4	-4.8	11.8	2.2	0.1	7.9	78.3
11	3.9	-6.4	11.5	2.2	0.1	7.9	80.8
12	4.1	-2.9	12.9	2.4	0.1	8.1	75.3
13	5.8	-5.4	12.3	2.2	0.1	7.9	77.1
14	5.8	-5.1	12.5	2.3	0.1	7.3	77.1
15	5.1	-6.4	12.4	2.3	0.1	7.9	78.7
16	5.2	-5.2	12.6	2.3	0.1	8.0	77.0
17	4.5	-4.9	11.4	2.1	0.1	7.7	79.1
18	2.7	-4.8	12.0	2.1	0.1	7.9	80.0
19	6.7	-5.5	11.9	2.1	0.1	8.0	76.7
20	4.6	-4.6	11.8	2.1	0.1	7.9	78.2
21	6.3	-2.6	11.2	2.1	0.1	8.2	74.7

D.9.3 Heron Close

Table D-3: Annual performance ratio and losses in normal operation at Heron Close

System	Mismatch and deviation from STC loss	Irradiance effect	Inverter MPP tracking loss	Temperature loss	DC wiring loss	Inverter DC to AC conversion loss	Annual perfor-mance ratio of normal operation
	loss in annual performance ratio (in performance ratio %)						(%)
4	18.1	5.8	5.6	2.0	0.1	6.7	61.7
5	10.5	9.9	6.2	1.8	0.1	7.0	64.4
6	8.5	9.0	6.3	2.3	0.1	7.3	66.5

D.9.4 Panmure Street

Table D-4: Annual performance ratio and losses in normal operation at Panmure Street

System	Mismatch and deviation from STC loss	Irradiance effect	Inverter MPP tracking loss	Temperature loss	DC wiring loss	Inverter DC to AC conversion loss	Annual perfor-mance ratio of normal operation
	loss in annual performance ratio (in performance ratio %)						(%)
0	16.1	5.0	7.7	-0.3	0.1	7.1	64.3
1	14.3	5.5	7.0	-0.1	0.1	7.3	65.8
2	11.0	5.9	9.5	-0.3	0.2	7.3	66.4
3	16.8	5.7	7.3	-0.2	0.1	7.0	63.3
4	16.3	7.0	8.7	0.3	0.1	6.9	60.6
5	14.4	6.1	8.8	-0.4	0.1	7.1	63.8
6	15.0	8.9	5.9	-1.9	0.1	7.3	64.6
7	15.7	11.2	6.8	0.4	0.1	6.6	59.2
8	11.4	6.8	9.0	-0.4	0.1	7.3	65.8
9	15.2	5.8	6.2	-0.3	0.1	7.4	65.5
10	11.7	8.1	10.0	0.2	0.1	7.1	62.8
11	13.3	3.9	8.6	-0.6	0.1	7.4	67.1

D.10. Investigation of DC power measurements at Corncroft

As discussed in Section 6.3.4, the DC power measurements at Corncroft were thought to be inaccurate because of the negative irradiance loss that was calculated in the annual performance ratio losses. The main cause of the negative irradiance losses was the high temperature corrected array efficiencies seen at Corncroft. These efficiency values are calculated directly from the DC power measurements.

The DC power measurements at Corncroft were shown to have a step change in readings at low irradiance (Section 4.2.3). At irradiances below 50 W/m^2 the DC power was recorded at discrete intervals up to a maximum of 100 W (Figure D-30). Further inspection of this error shows that the DC values at Corncroft above 100 W are similar to the DC values seen at Heron Close above 0 W. One explanation of this finding is that all of the DC power measurements are recorded at 100 W above their true value and it is this increase in the DC power measurements which causes the negative irradiance losses seen in the annual performance ratio results.

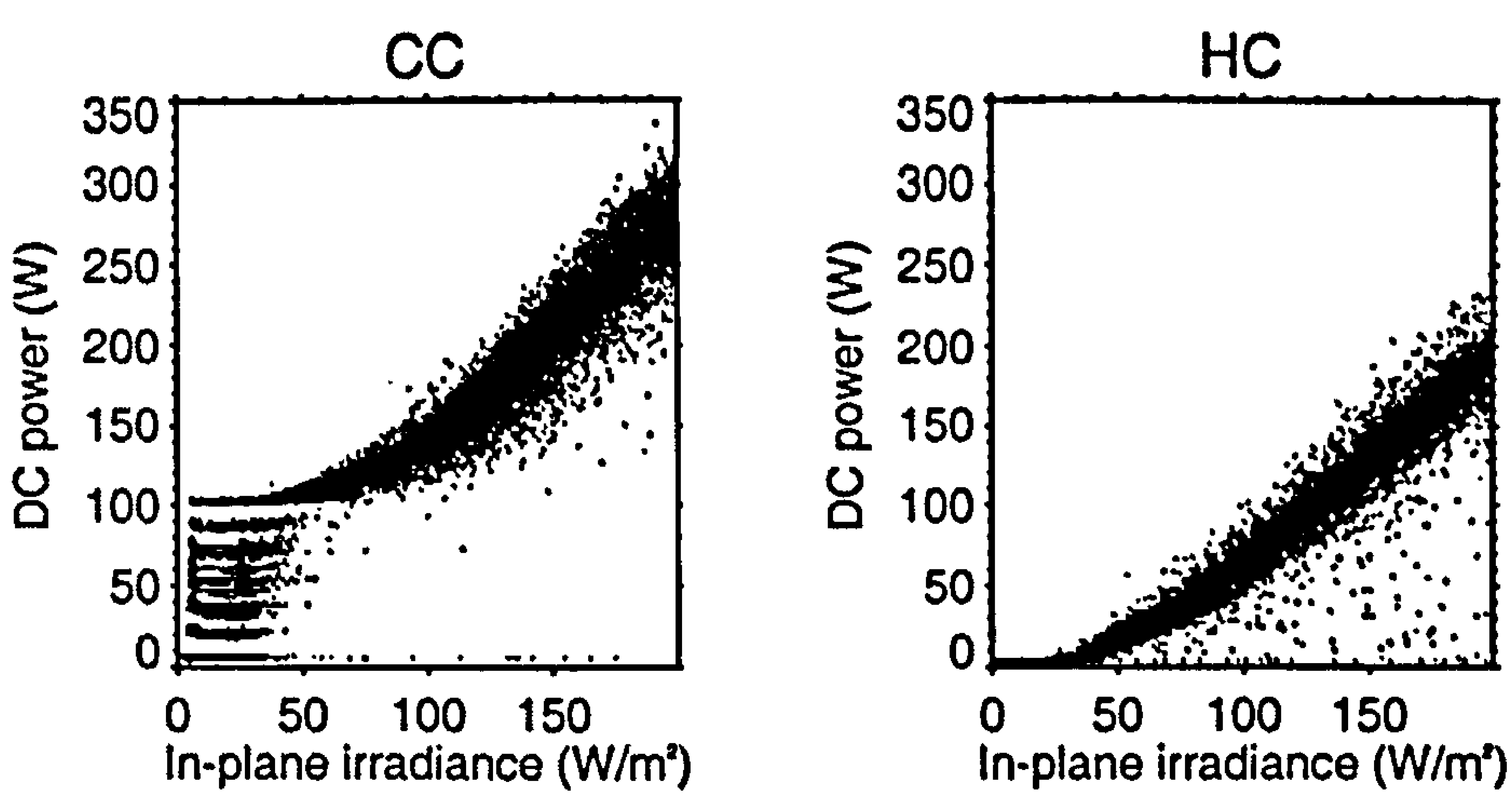

Figure D-30: DC power measurements at low irradiance levels for a Corncroft and Heron Close PV system.

The possibility of the over-measurement of DC power is investigated by considering the effects on the results if the DC power measurements are corrected by lowered all the measurements by 100W. Any negative values that result through this correction are converted to missing data values. The corrected DC power measurements at low irradiance compare well to the Heron Close DC measurements at low irradiance (Figure D-31).

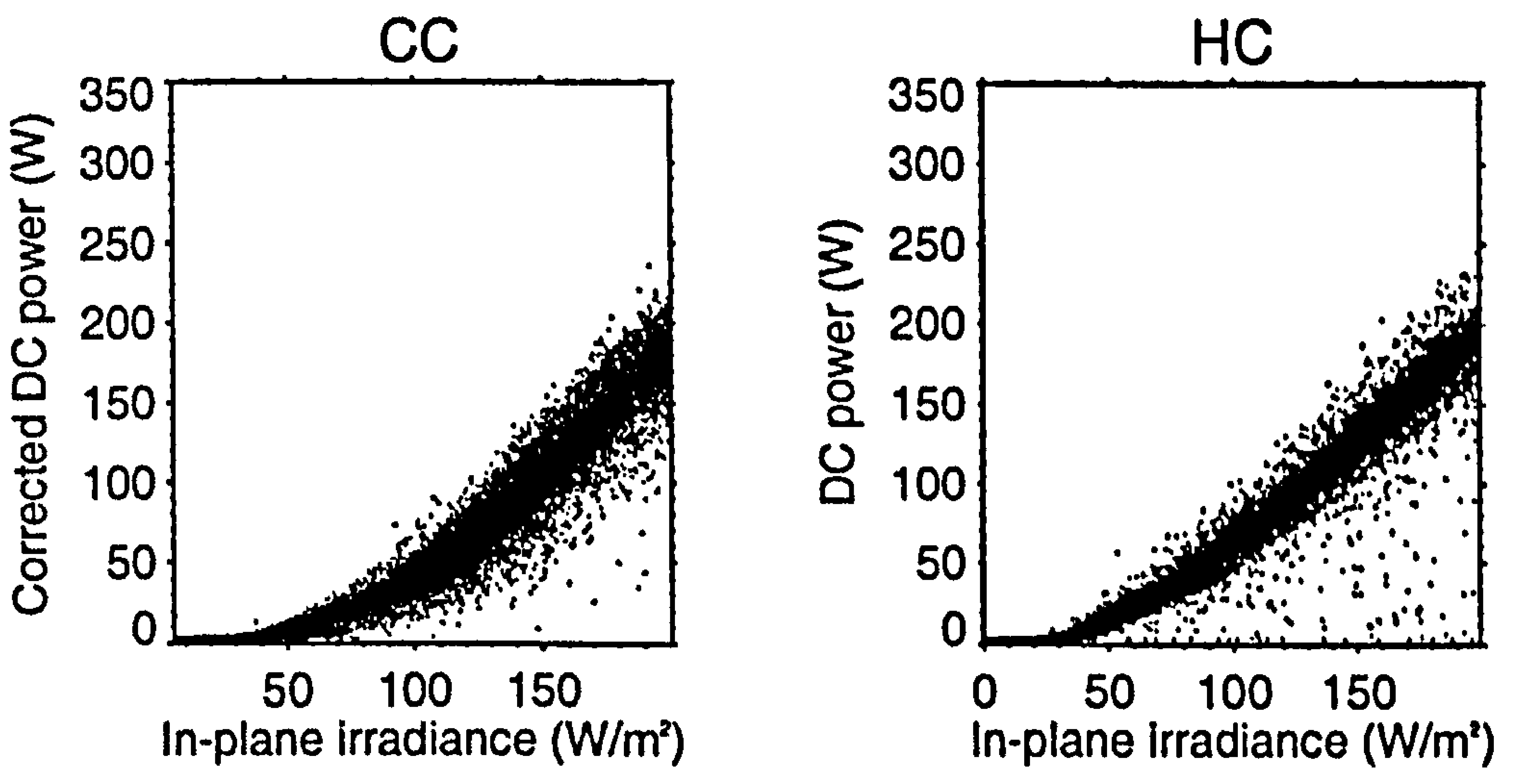

Figure D-31: Corrected DC power measurements at low irradiance levels for a Corncroft and Heron Close PV system.

However, lowering the DC power measurements at Corncroft by 100 W meant that the DC power measurements no longer correspond well with the AC power measurements. The inverter efficiency curve for CC 21 with corrected DC power shows that the majority of the AC power readings are recorded as higher than the DC powers (Figure D-32; an unrealistic result.

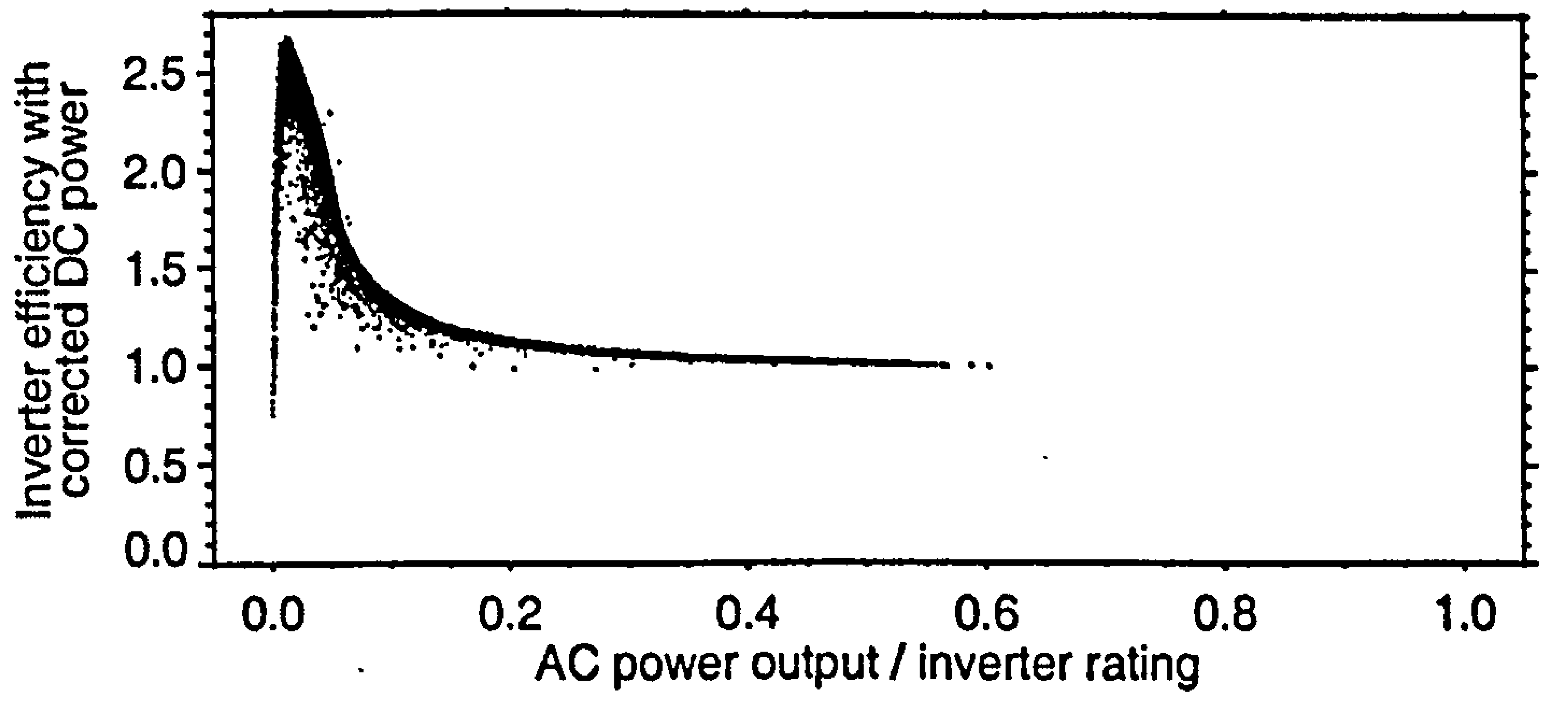

Figure D-32: Corrected inverter efficiency curve at CC 21.

This suggested that if the DC power was corrected by lowering the measurements by 100 W then the AC power also had to be corrected. However it is not clear whether the AC values should be lowered by the same amount as the DC values (100 W) or a different value. A comparison between the Corncroft and Heron Close AC power measurements at low irradiance shows that there is no step change in the AC power measurements at the Corncroft site (Figure D-33). If all the AC power measurements at Corncroft were lowered by 100 W then this would result in negative AC power measurements at irradiance less than 100 W/m^2.

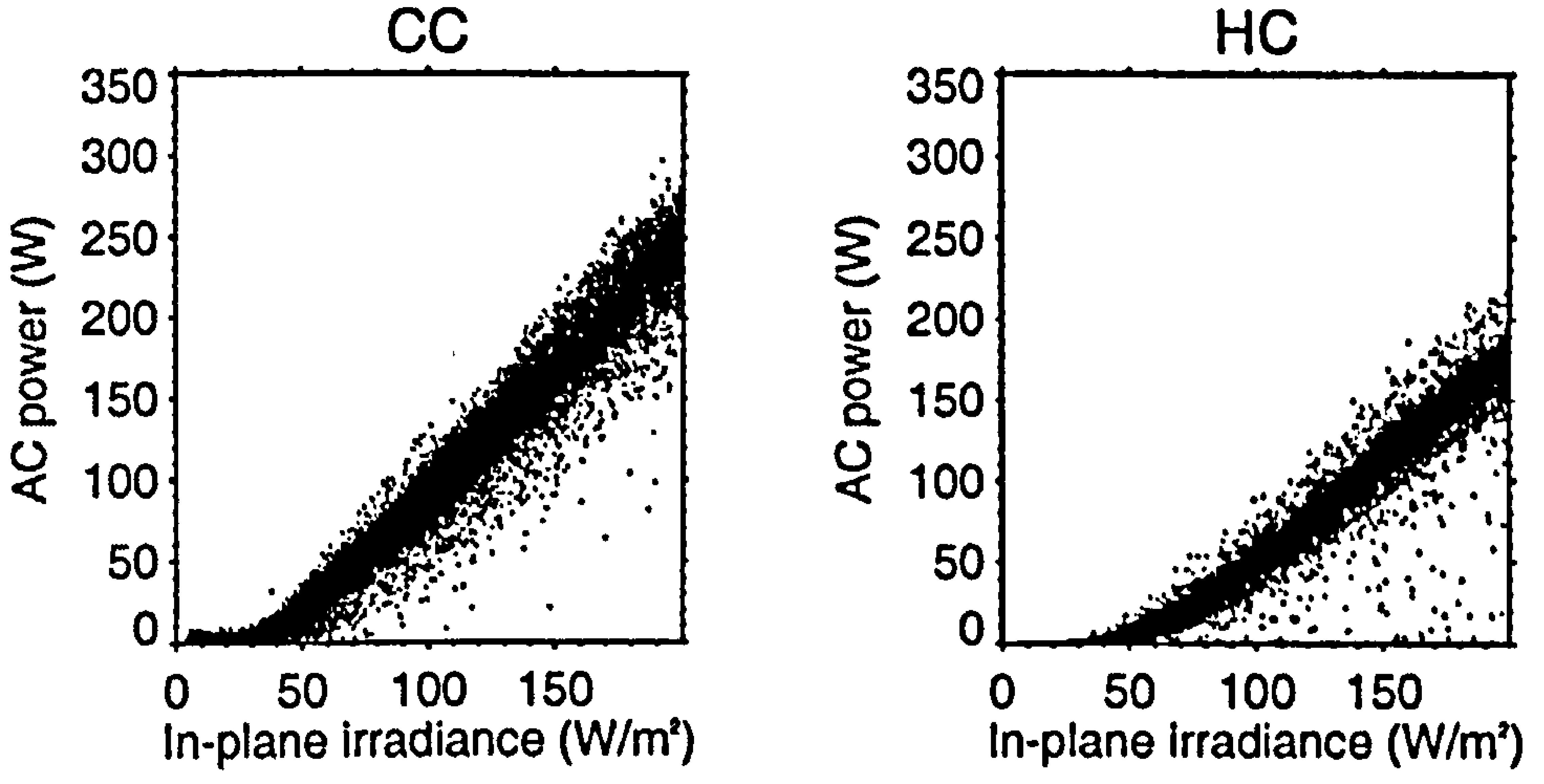

Figure D-33: Comparison of AC power measurements at low irradiance for a Corncroft and Heron Close PV system

This exploratory analysis illustrates the difficulties in investigating measurement errors from the recorded five minutely data and highlights the need for accuracy in the measurements. This leads to the suggestion that an on-site check and calibration of the DC and AC power measurements at the Corncroft site is required.

Appendix E. Fault Analysis

E.1. Fault detection

E.1.1 Corncroft Year 1

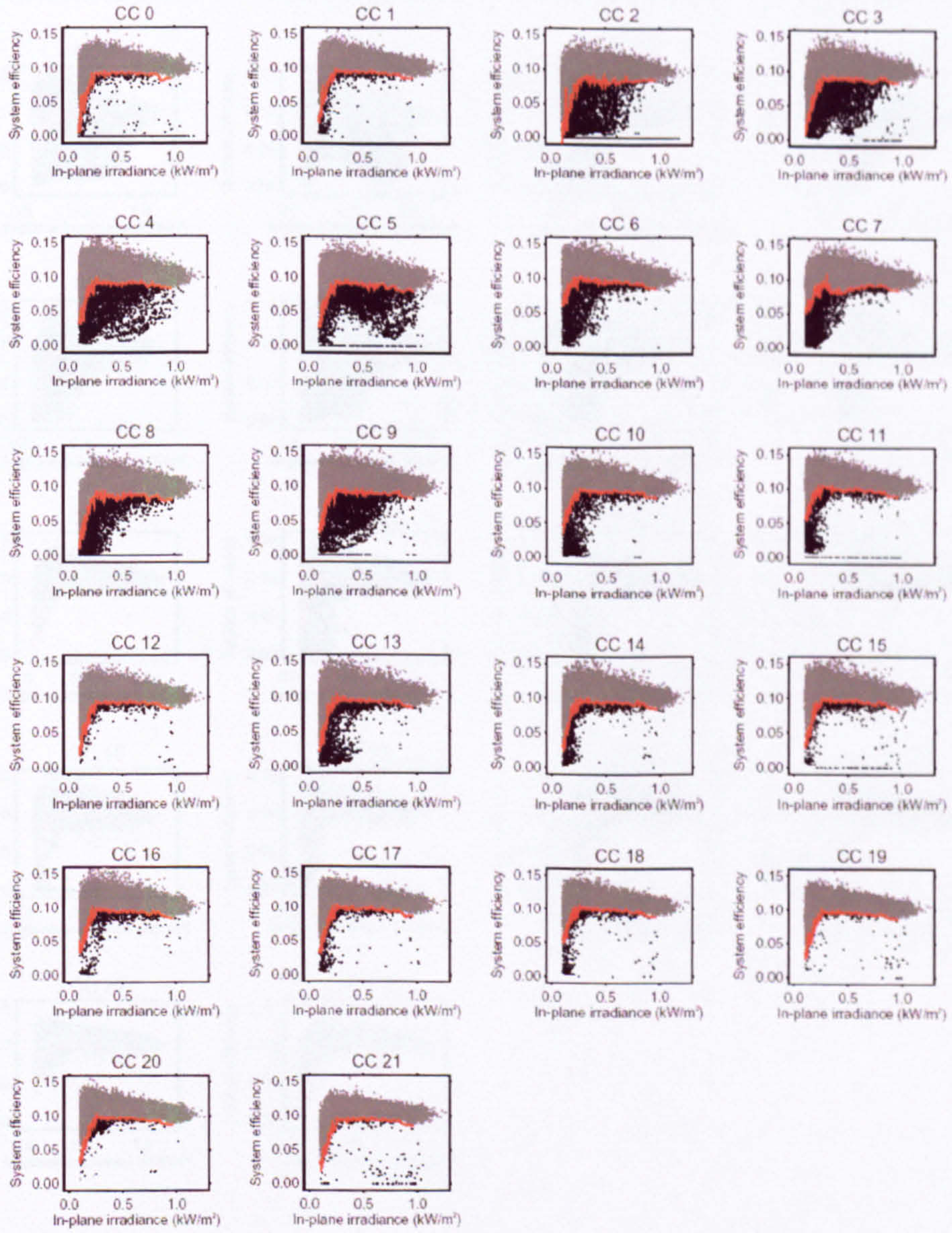

Figure E-1: Detection of faults at Corncroft in first year of operation. Faults are shown by black points and the fault efficiency curve in red.

E.1.2 Corncroft Year 2

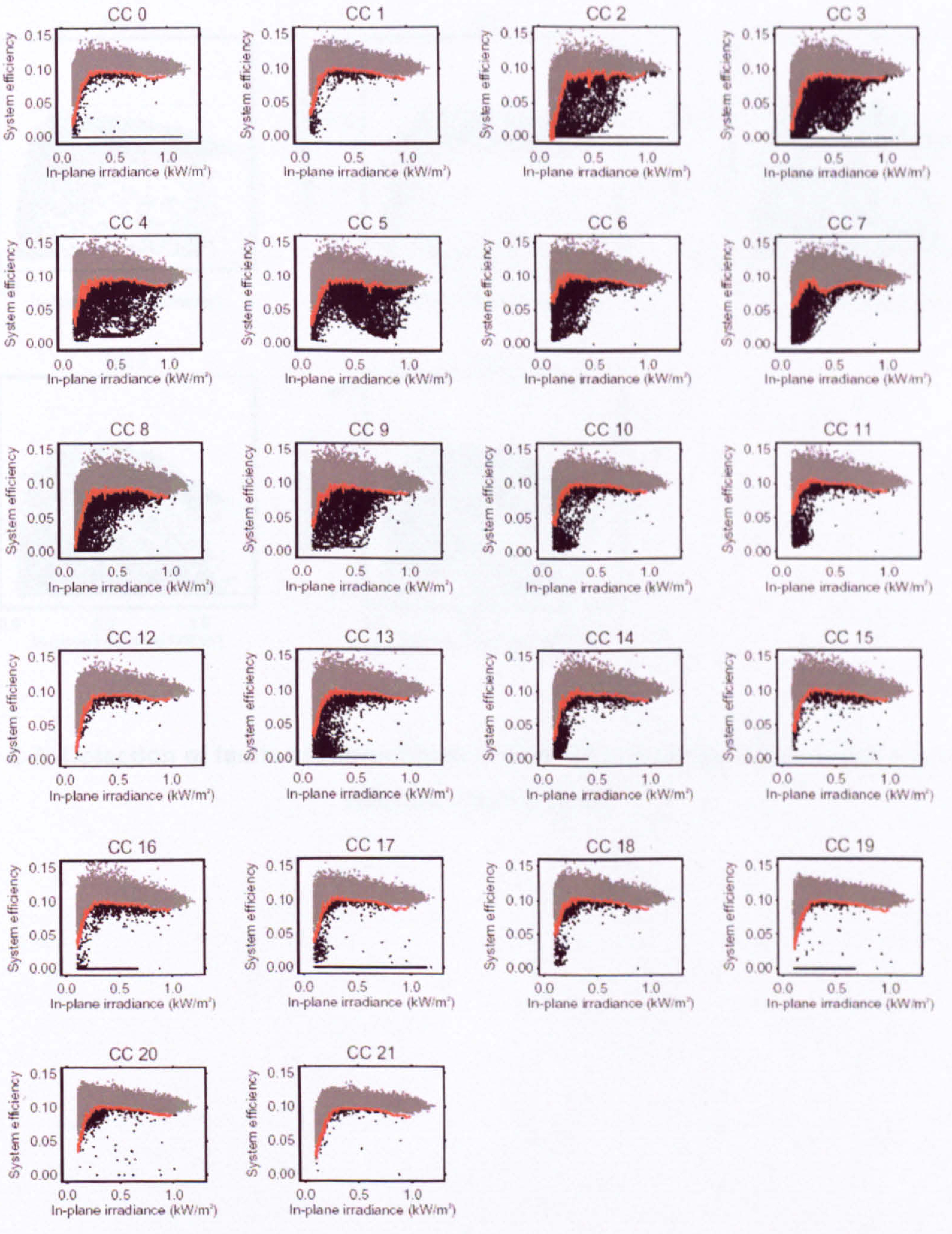

Figure E-2: Detection of faults at Corncroft in second year of operation. Faults are shown by black points and the fault efficiency curve in red.

E.1.3 Heron Close

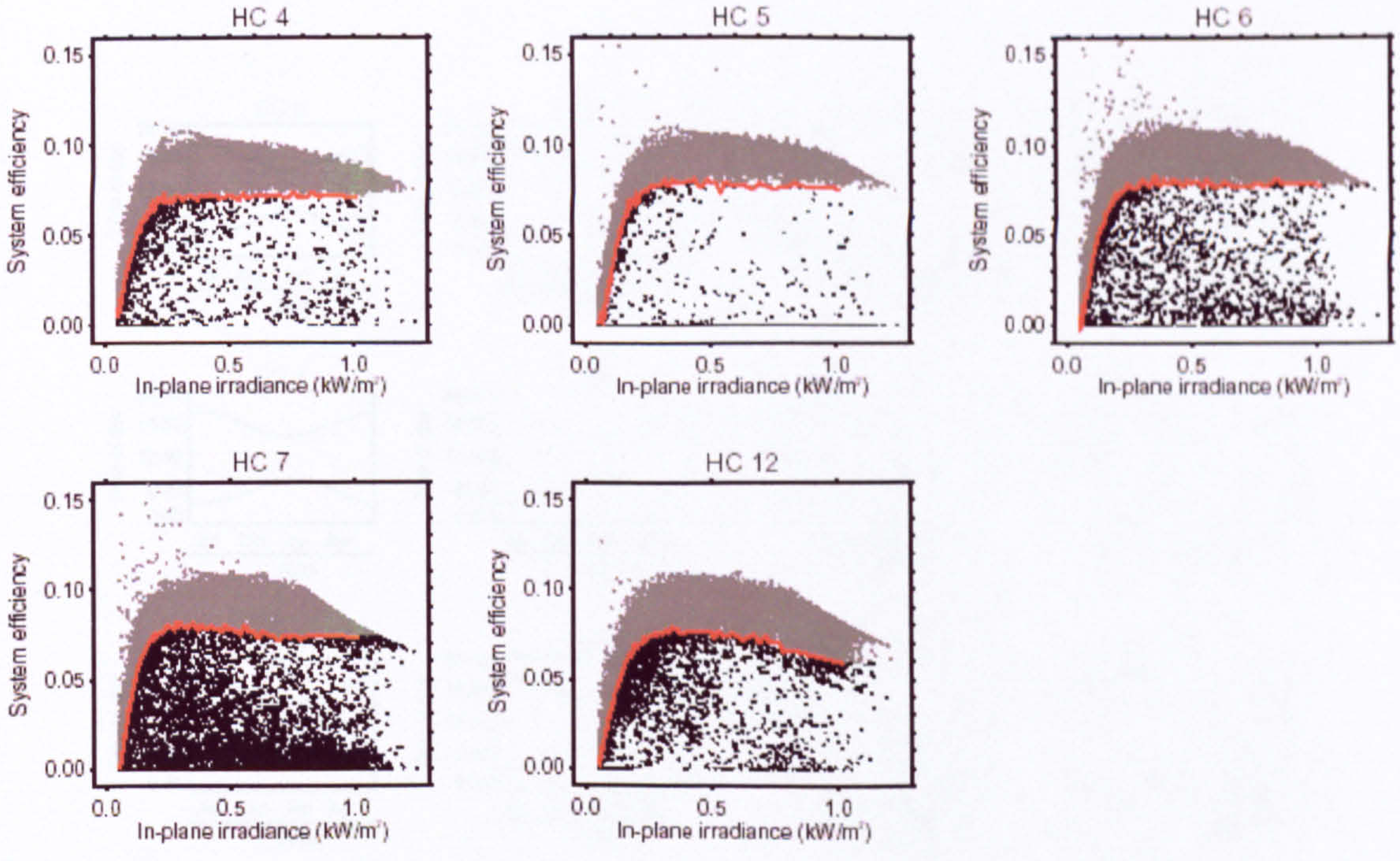

Figure E-3: Detection of faults at Heron Close. Faults are shown by black points and the fault efficiency curve in red.

E.2. Zero efficiency faults

E.2.1 Corncroft Year 1

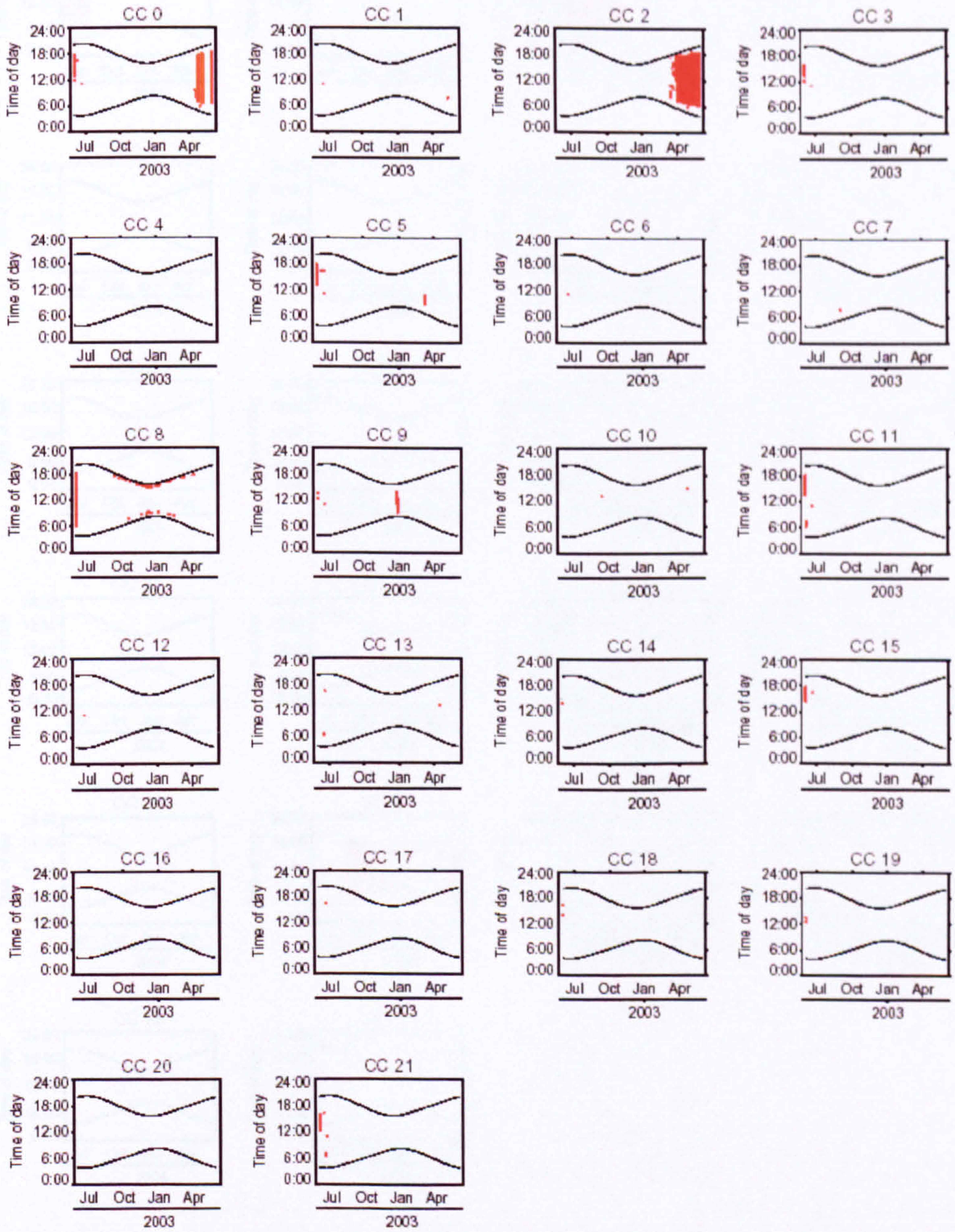

Figure E-4: System failure plotted on time and date axes at Corncroft for the first year of operation. Sunrise and sunset times are shown by black lines.

E.2.2 Corncroft Year 2

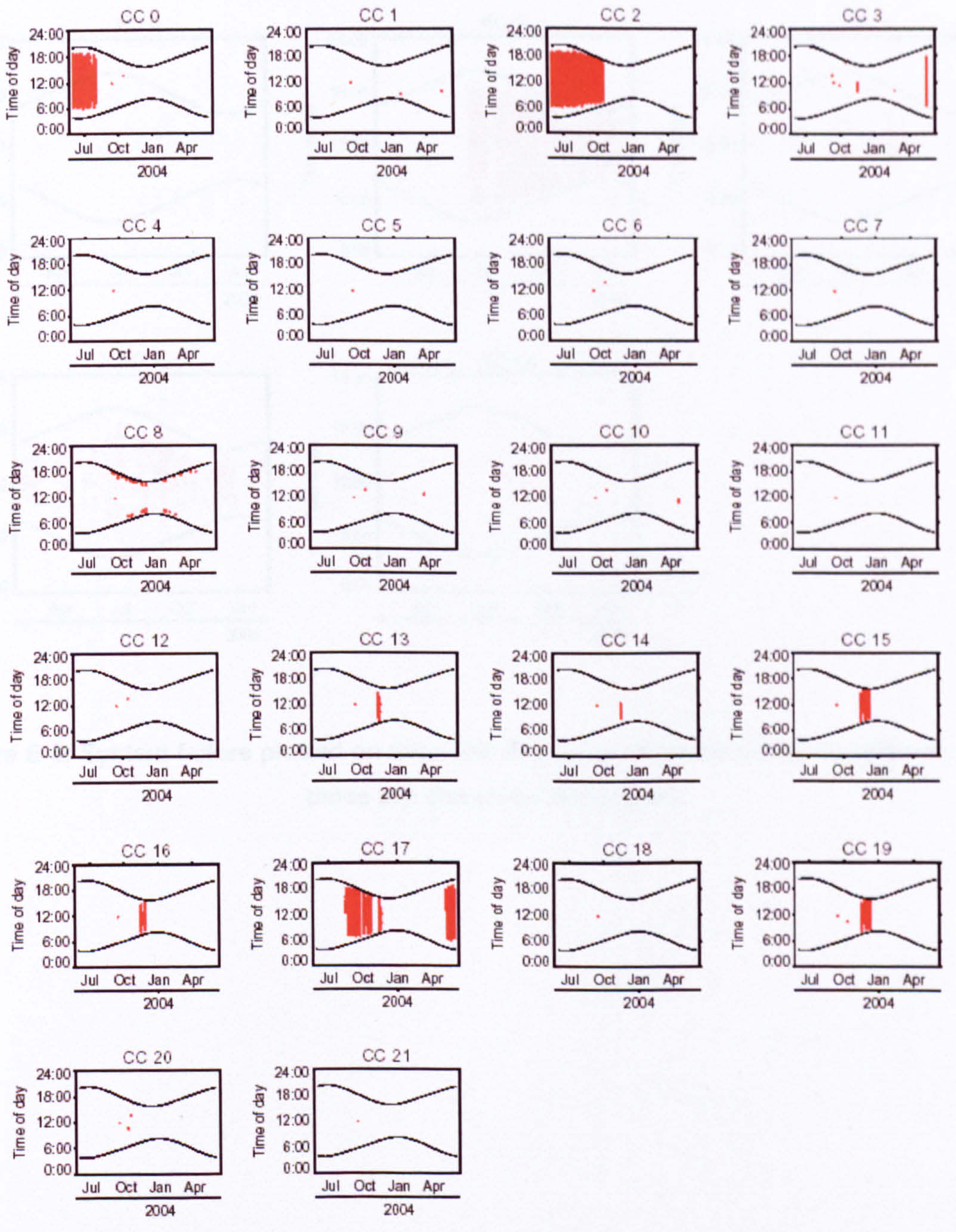

Figure E-5: System failure plotted on time and date axes at Corncroft for the second year of operation. Sunrise and sunset times are shown by black lines.

E.2.3 Heron Close

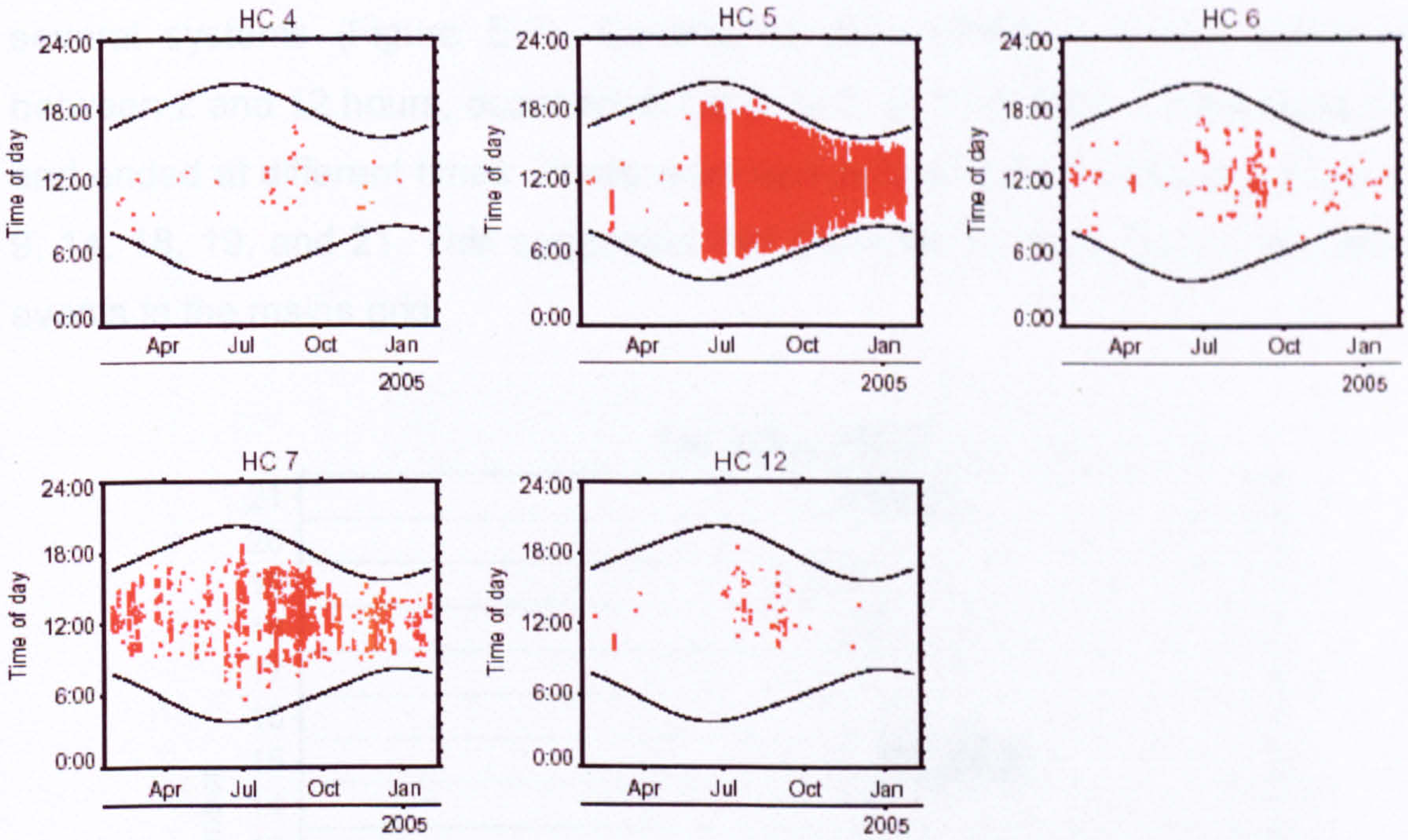

Figure E-6: System failure plotted on time and date axes at Heron Close. Sunrise and sunset times are shown by black lines.

E.2.4 Simultaneous faults

Zero efficiency faults at Corncroft on 1st June 2002 occurred simultaneously in several systems (Figure E-7). Continuous zero efficiency faults, which lasted between 2 and 12 hours, occurred at CC 0, 3, 5, 8, 11 and 15. These faults started and ended at different times. There were also sporadic zero efficiency faults at CC 9, 14, 18, 19, and 21. This suggested that these faults were caused by abnormal events in the mains grid.

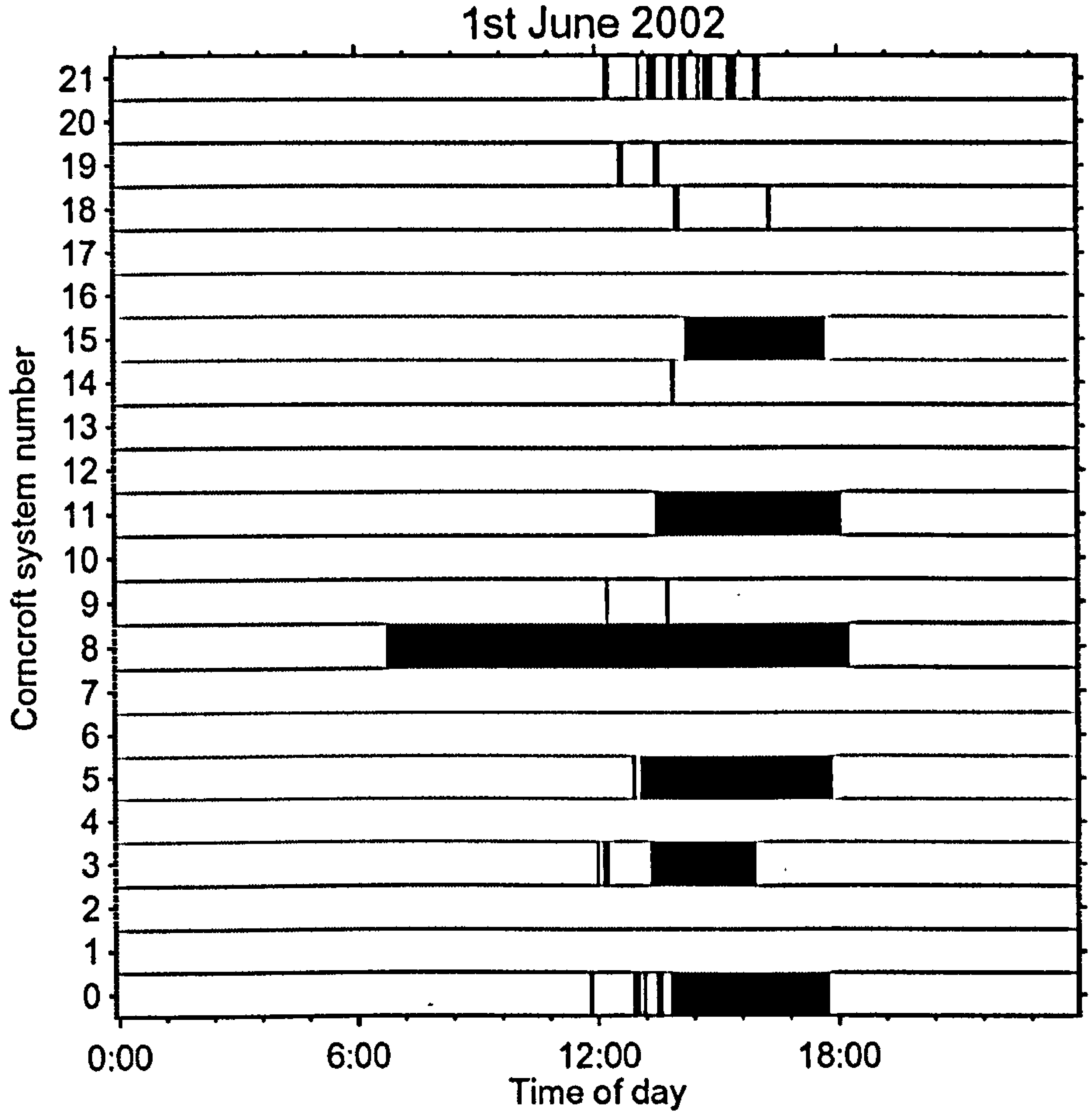

Figure E-7: Zero efficiency faults at Corncroft on 1st June 2002

Many brief zero efficiency faults also occurred at Heron Close and there were occasions of simultaneous faults in the systems. As an example, in a two day period beginning 1st July 2004, HC 5 had sustained zero efficiency faults throughout the daytime due to its faulty inverter (Figure E-8). HC 7 had the most brief zero efficiency faults and HC 6 had faults which occurred at the same time as some of the HC 7 Faults. HC 12 also had two faults which occurred at times similar to HC 7 faults.

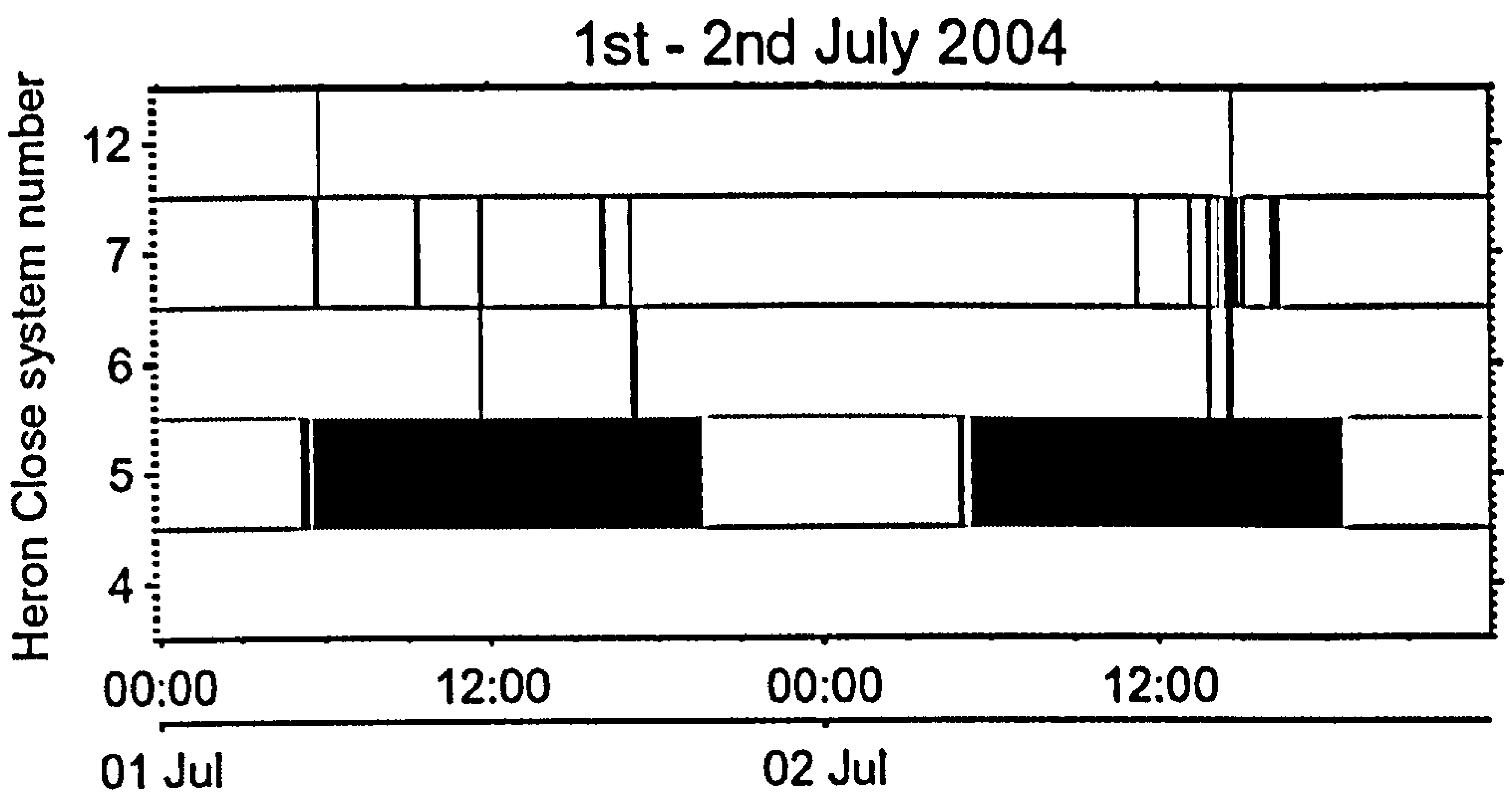

Figure E-8: Zero efficiency faults at Heron Close on 1st and 2nd July 2004

E.3. Sun position of faults

E.3.1 Exclusion of high solar incidence angle fault values

It was observed in the datasets that in each PV system there were a large number of faults at the beginning and end of each day. These faults occurred in systems whose arrays were known to be free of shade and therefore could not be attributed to shading. However if these faults were included in the shading analysis then their high concentration about particular sun positions would mean that they would be falsely identified as shading.

At Corncroft many faults occurred at the beginning of each day and at Heron Close many faults occurred at the end of each day. Sun position fault plots of CC 21 and HC 4 provide examples of these faults (Figure E-9 and Figure E-10). Site visits had showed that CC 21 and HC 4 should be free of shading effects. The main difference between the two systems was their orientation and this suggested that the early morning or late evening faults could be caused by the solar incidence angle. Solar incidence angle is defined as the angle between a line drawn from the PV array to the sun and a line normal to the PV array. It was concluded that at high solar incidence angles many faults were observed. These faults could be caused the solar radiation reflecting off the glass cover of the PV array (and lowering the efficiency) or inverter MPP tracking failure at low solar irradiances.

To continue with the shading analysis the high solar incidence angle faults needed to be ignored. Through inspection of the datasets, it was decided that faults with solar incidence angles greater than 80° would be ignored in the shading fault analysis.

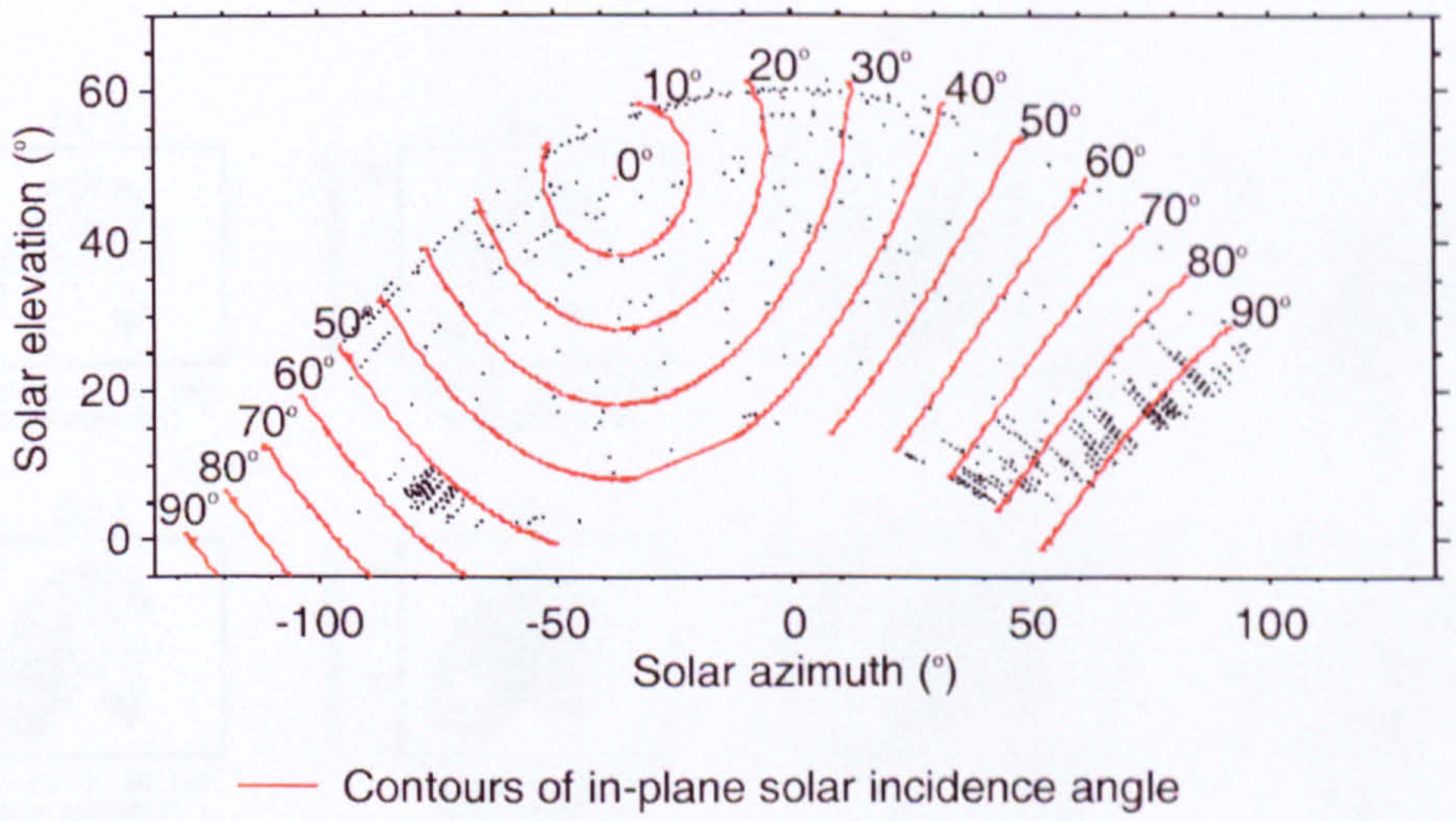

Figure E-9: Sun position of faults at CC 21 with levels of solar incidence angle shown in red

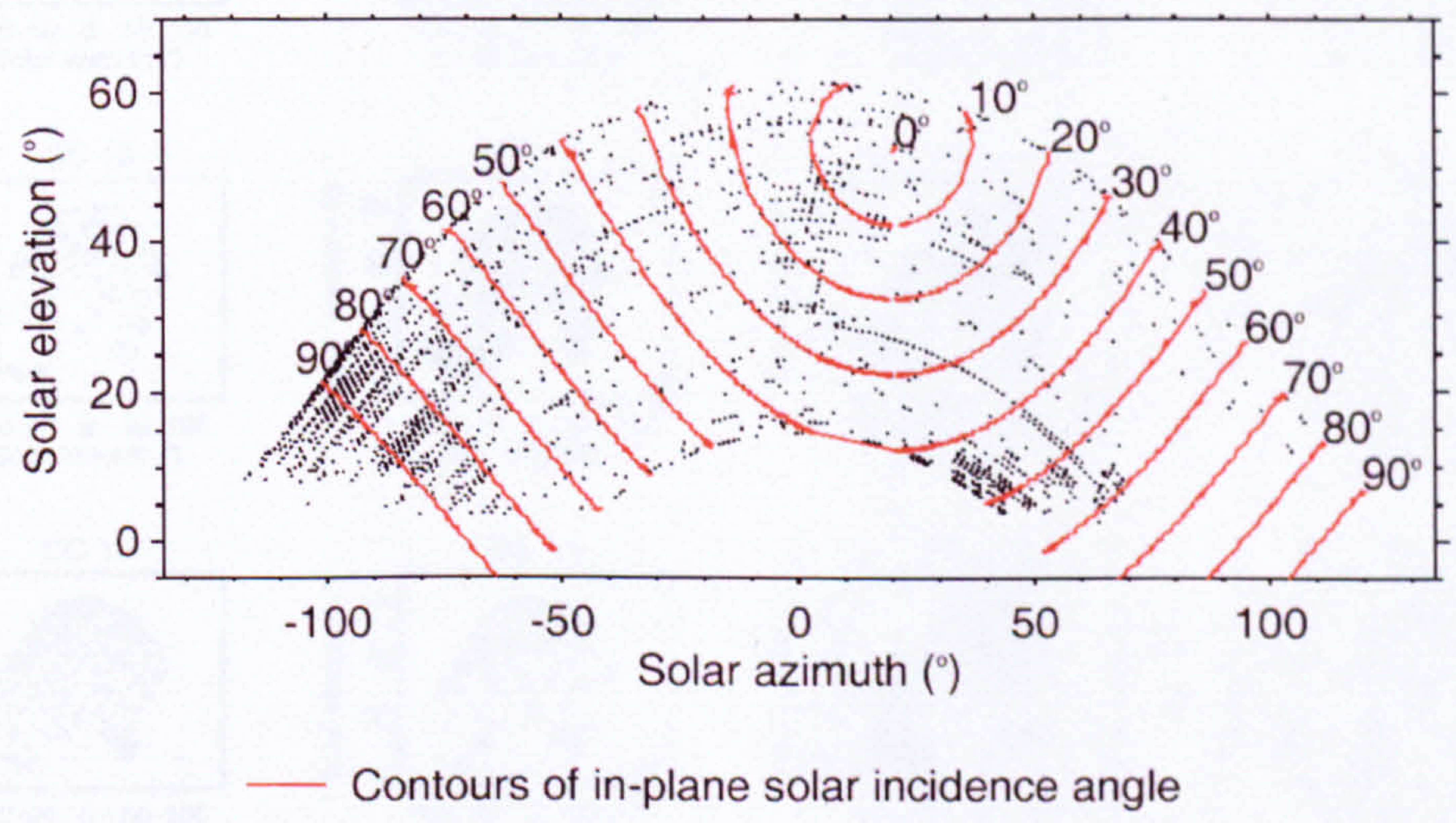

Figure E-10: Sun position of faults at HC 4 with levels of solar incidence angle shown in red

E.3.2 Corncroft Year 1

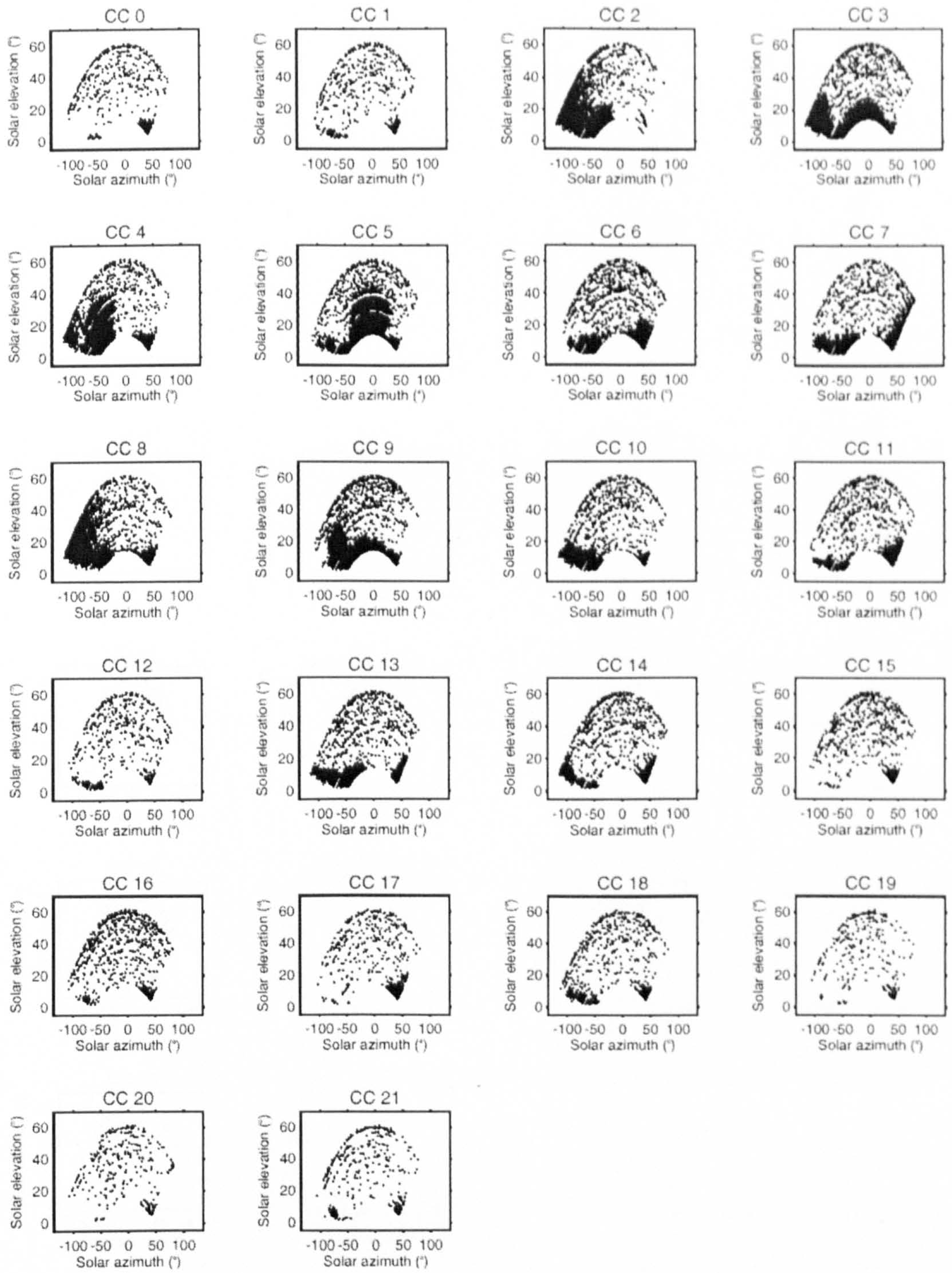

Figure E-11: Sun position of faults at Corncroft in the first year of operation

E.3.3 Corncroft Year 2

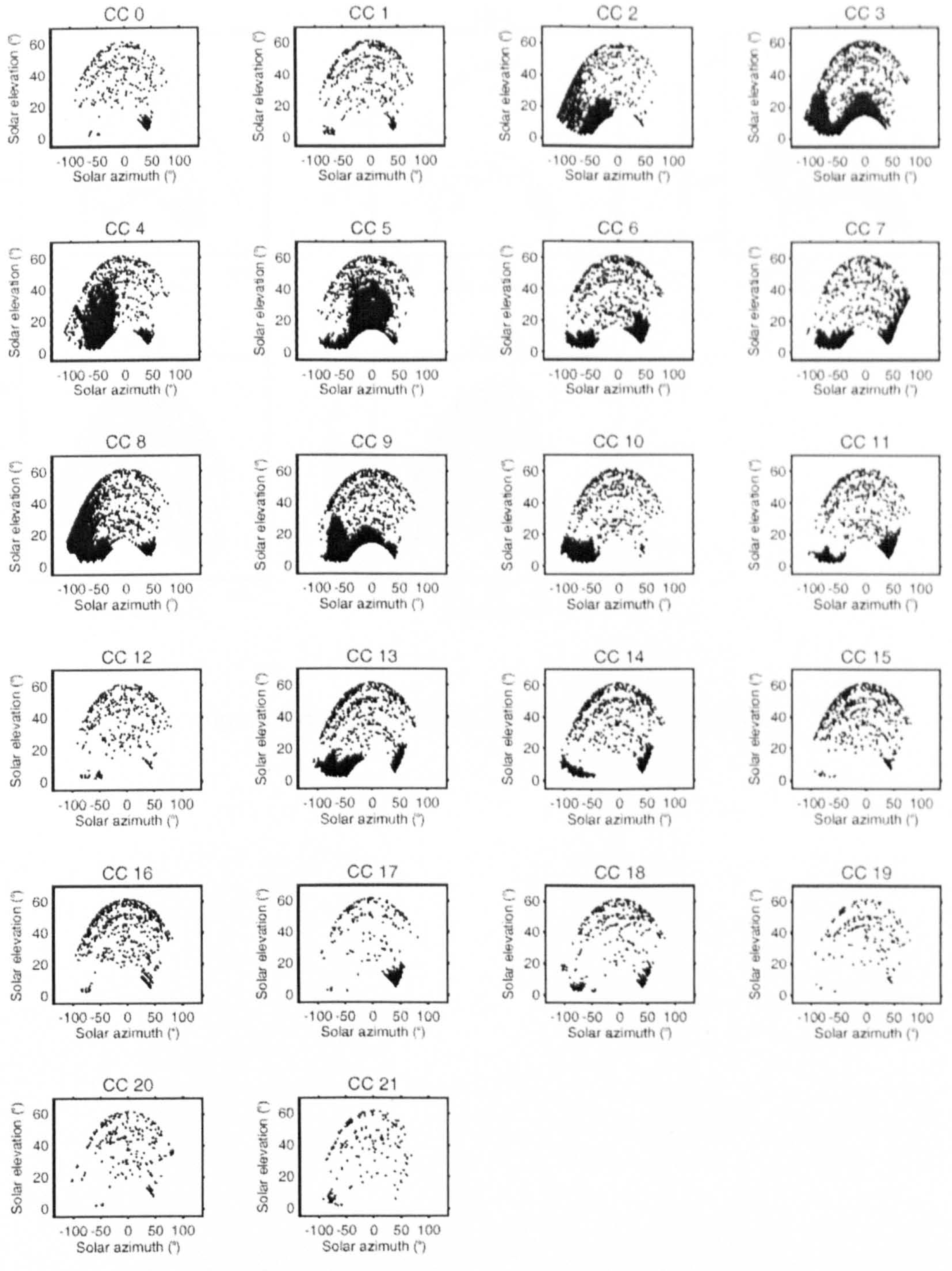

Figure E-12: Sun position of faults at Corncroft in the second year of operation

E.3.4 Heron Close

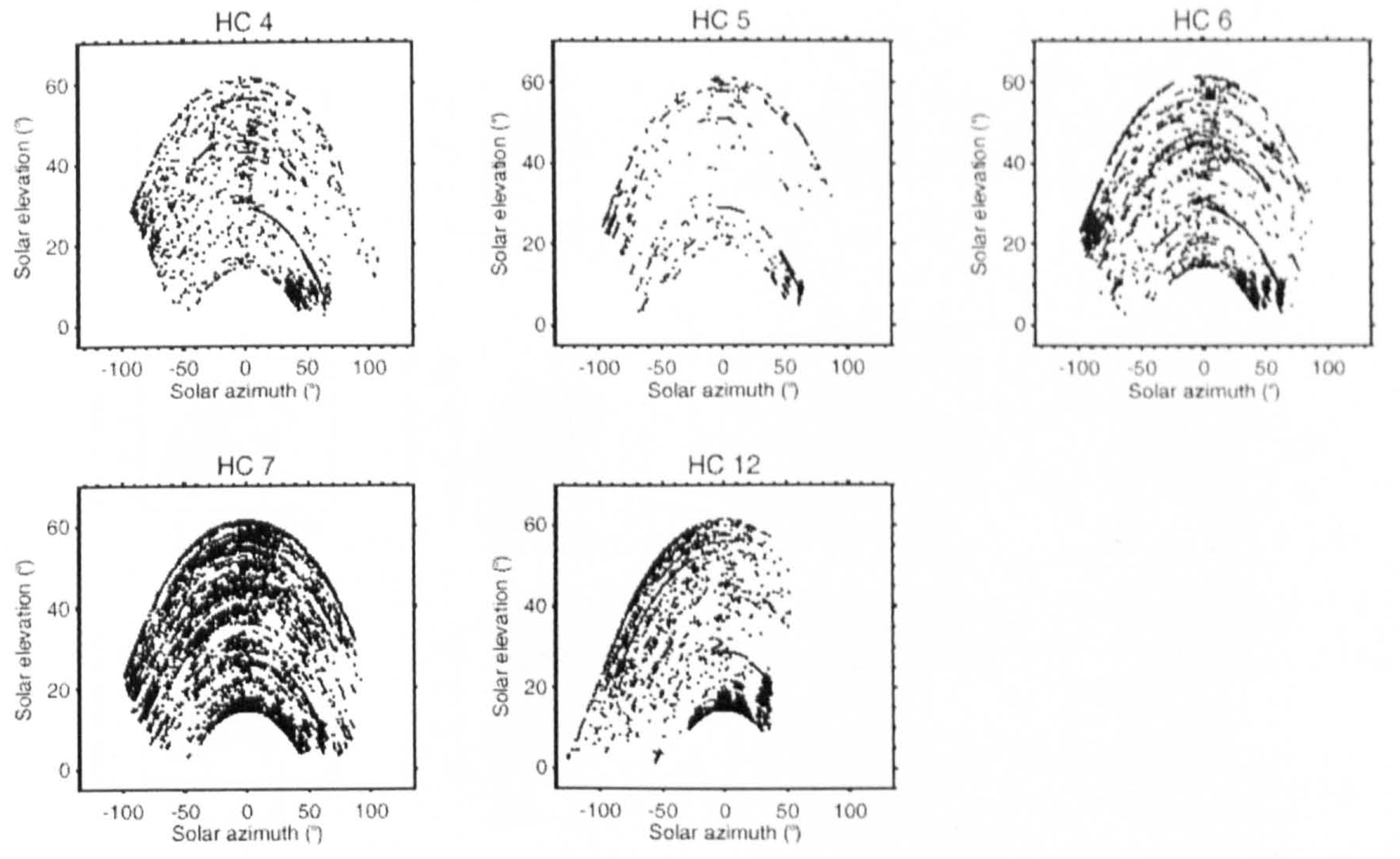

Figure E-13: Sun position of faults at Heron Close

E.4. Fault concentrations

E.4.1 Corncroft Year 1

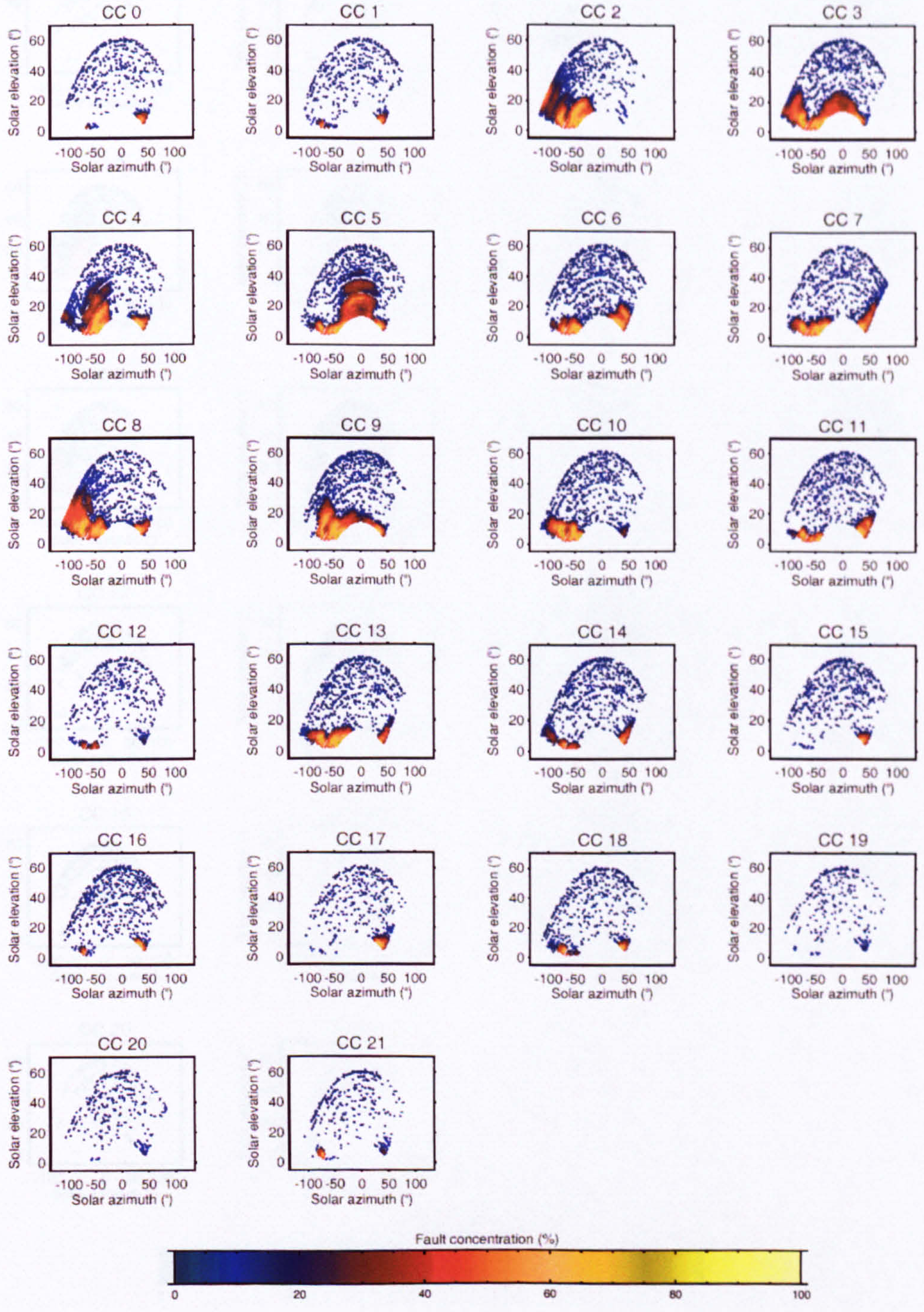

Figure E-14: Sun when faults detected at Corncroft in the first year of operation. The fault concentration of each fault is shown in colour.

E.4.2 Corncroft Year 2

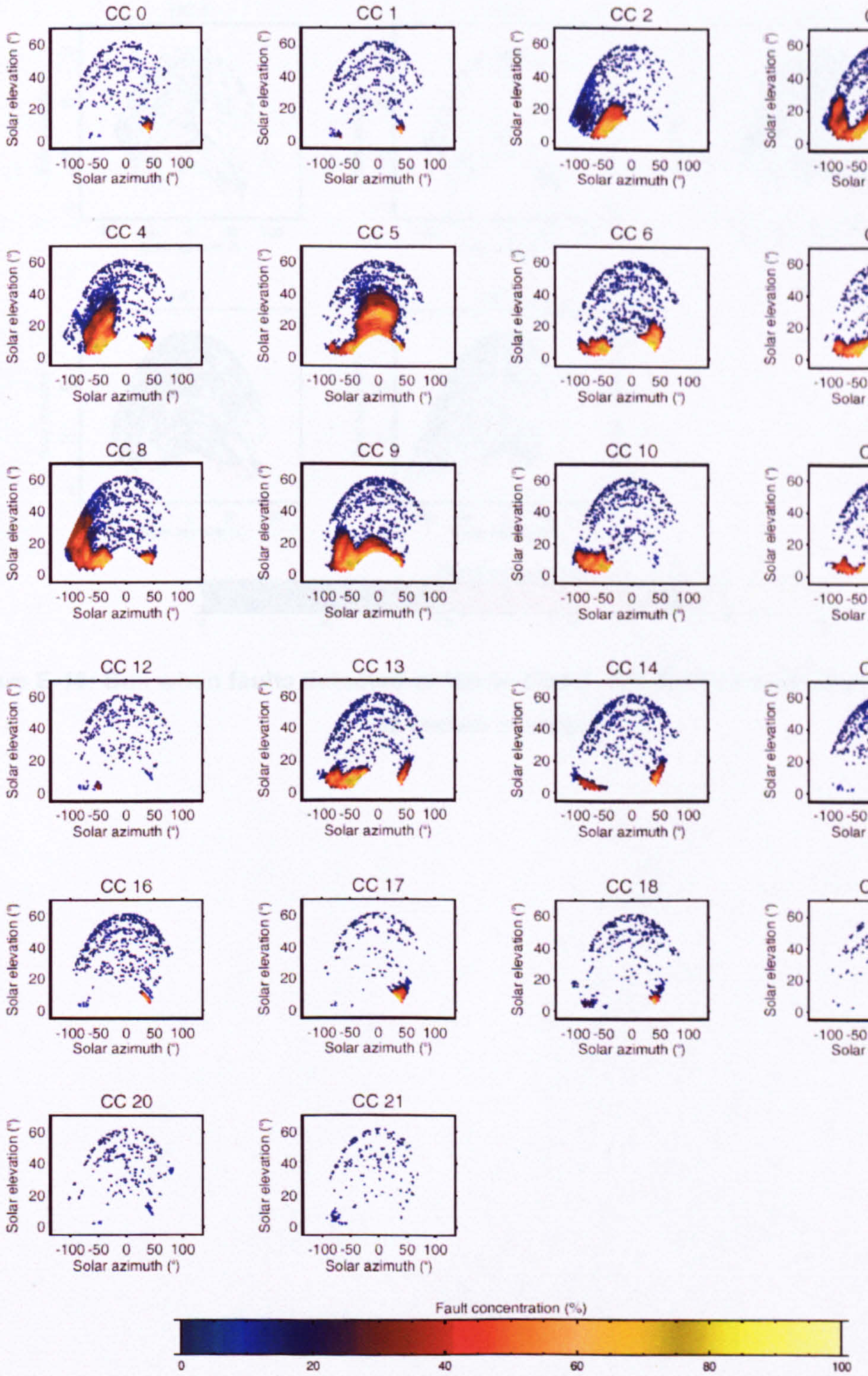

Figure E-15: Sun position when faults detected at Corncroft in the second year of operation. The fault concentration of each fault is shown in colour.

E.4.3 Heron Close

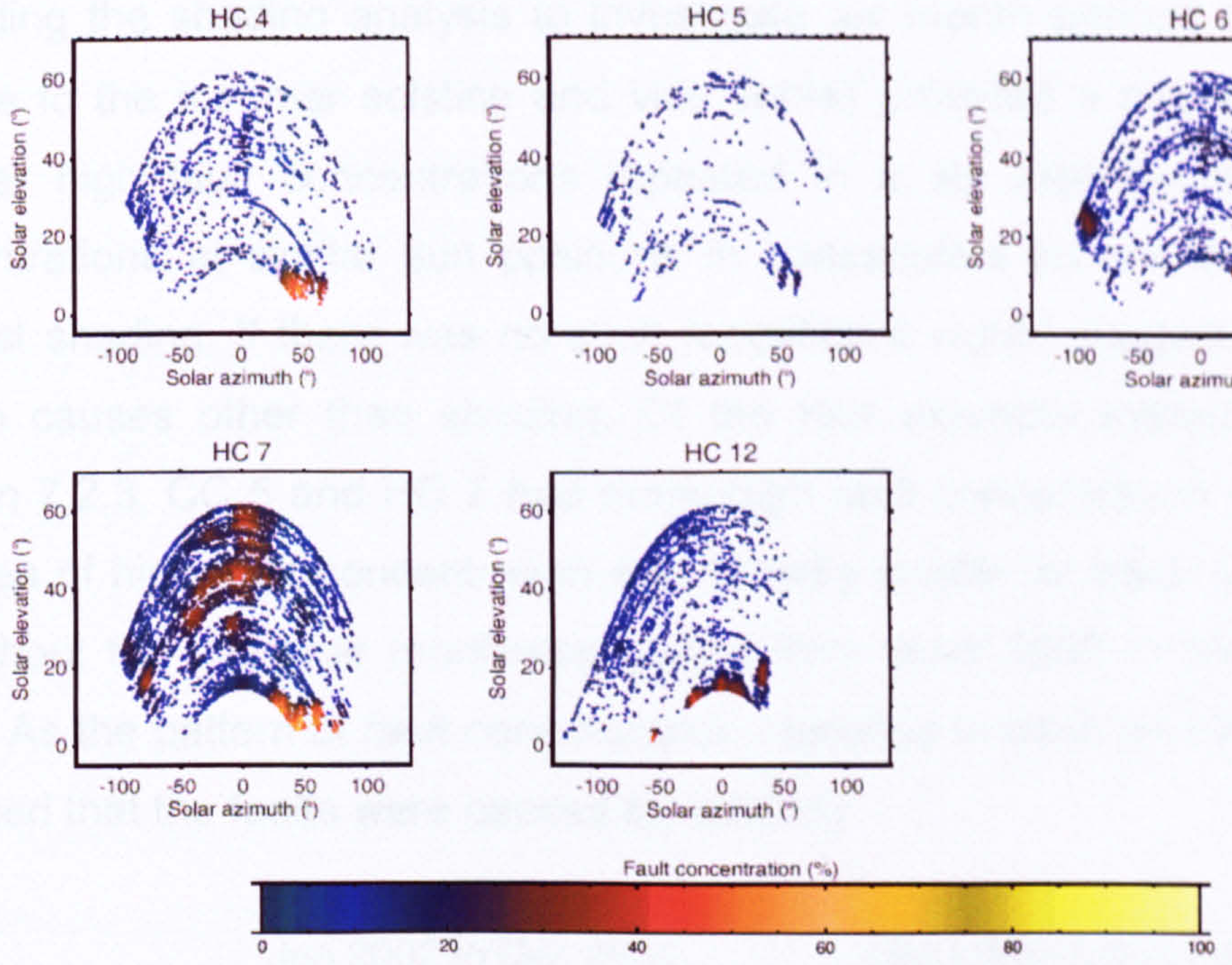

Figure E-16: Sun when faults detected at Heron Close. The fault concentration of each fault is shown in colour.

E.4.4 Shading analysis per six month period

Extending the shading analysis to investigate six month periods (from the winter solstice to the summer solstice and vice versa) provided a method of assessing whether high fault concentrations repeated in a six monthly cycle. High fault concentrations at similar sun positions in consecutive six month periods would suggest shading. If there was no such repetition it would suggest the faults were due to causes other than shading. Of the four example systems discussed in Section 7.2.3, CC 5 and HC 7 had many high fault concentration values. At CC 5 the area of high fault concentration was broadly similar for each six month period throughout the two year monitoring period from June 2002 to May 2004 (Figure E-17). As the pattern of fault concentration repeated in each six month period, this indicated that the faults were caused by shading.

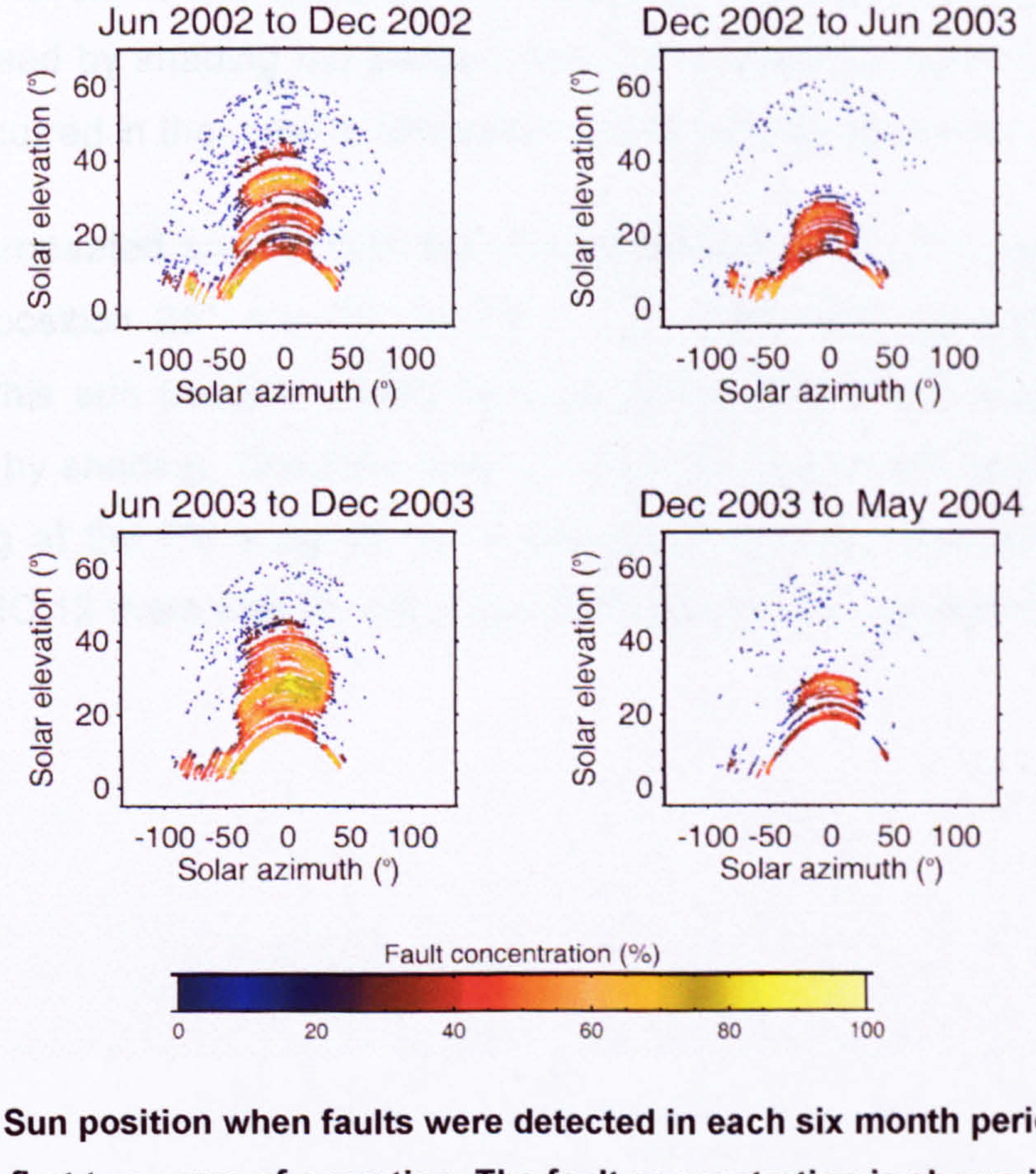

Figure E-17: Sun position when faults were detected in each six month period for CC 5 during the first two years of operation. The fault concentration is shown in colour.

The area of high concentration values was greatest in the autumn months (June 2002 to December 2002 and June 2003 to December 2003). In the spring months this area was reduced in size and the shading effect was less. A site visit had determined that the PV array of CC 5 was shaded by a deciduous tree. The leaves of deciduous trees start growing in spring and become larger as the year progresses before dropping in late autumn. Therefore the tree presented a larger shading object in autumn than in spring and this accounts for the difference in the amount of high fault concentration values in the spring and autumn months.

High fault concentration values were observed at HC 7 in the first year of operation from February 2004 to January 2005. Analysis of the fault concentration values for each six month period shows that many areas of high fault concentrations did not repeat (Figure E-18). In June to December 2004 there was a large number of high fault concentrations in the sun position region $-50° < \alpha$ $25°$ and $25° < \beta < 60°$. However, in the preceding six month period from February 2004 to June 2004, there were fewer faults in this region of sun position and loverall ower fault concentration levels. It was therefore concluded that the high concentration values were not caused by shading but instead due to the large numbers of non-shading faults that occurred in the June to December 2004 monitoring period.

There was a repeated area of high fault concentration at HC 7 in winter mornings around sun position $25° < \alpha$ $70°$ and $\beta < 15°$. High fault concentrations were observed in this sun position region throughout the year which suggested these were caused by shading. The PV arrays of HC 4, 5, and 6 were positioned on the same building at the PV array of HC 7 and similar results were found for these systems. At HC 12 there was an indication of shading at sun positions $\beta < 30°$.

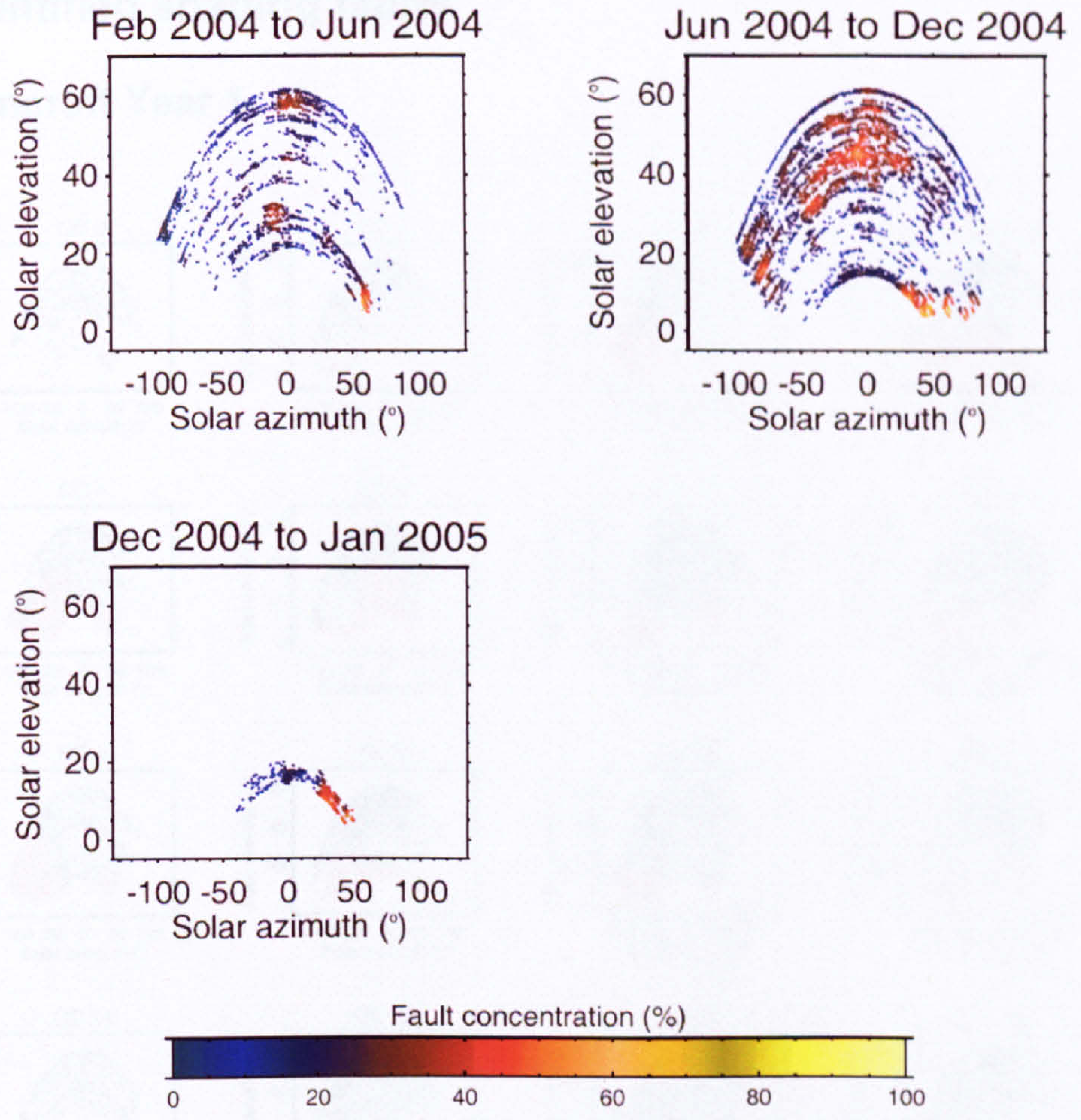

Figure E-18: Sun position when faults were detected in each six month period for HC 7 during the first year of operation. The fault concentration is shown in colour.

E.5. Identified shading faults

E.5.1 Corncroft Year 1

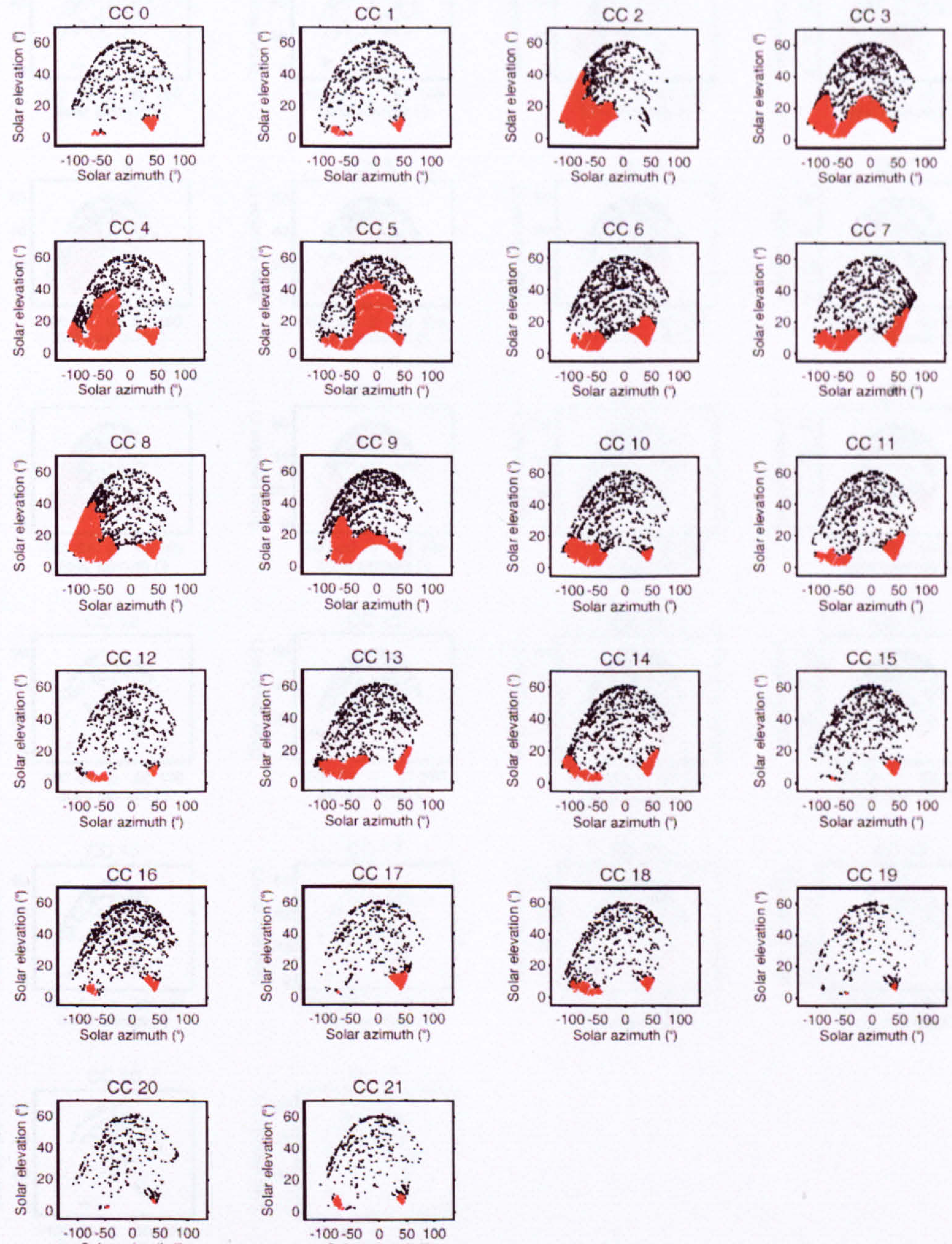

Figure E-19: Sun position when faults detected at Corncroft in the first year of operation. Identified shading is shown in red.

E.5.2 Corncroft Year 2

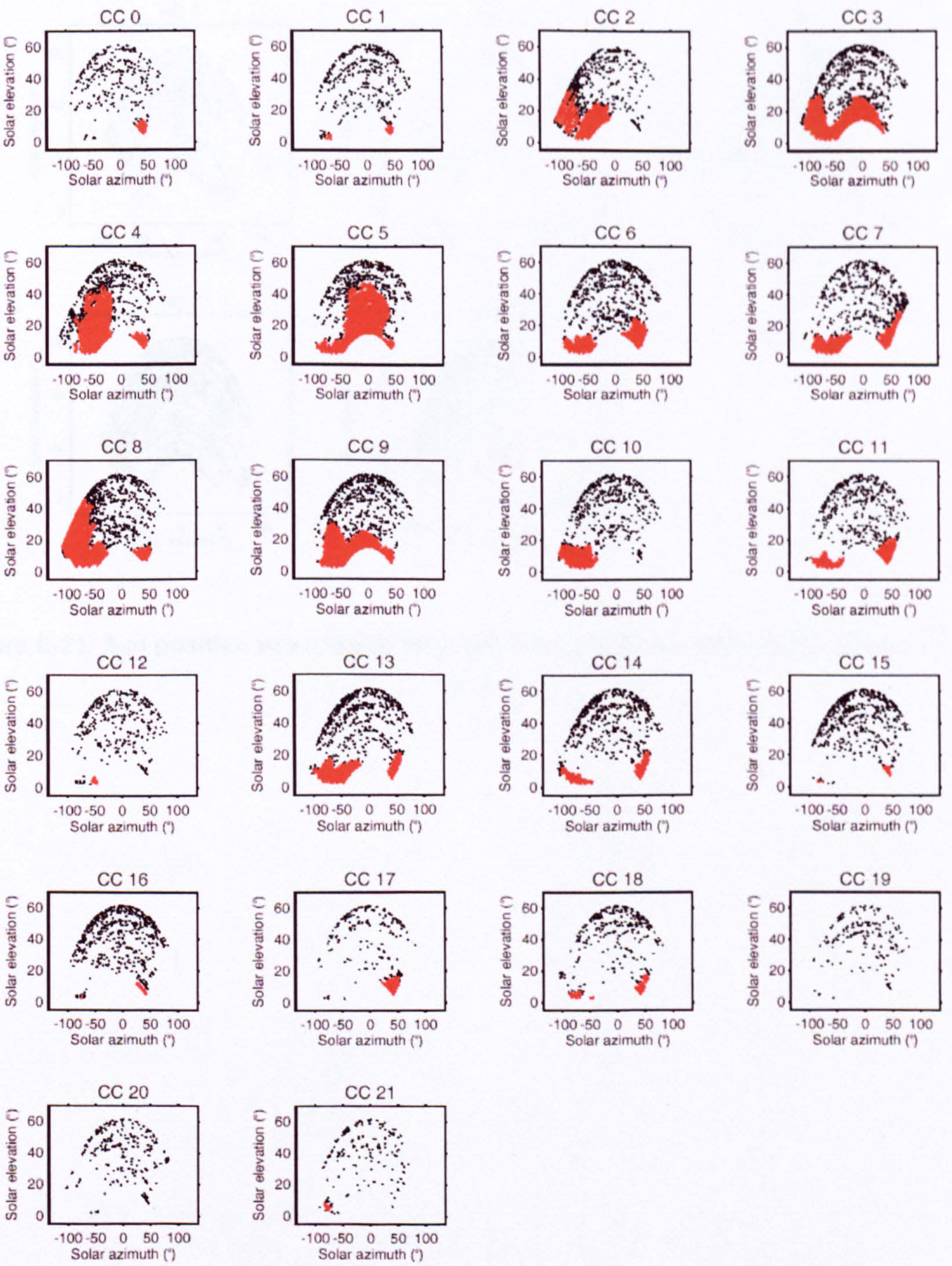

Figure E-20: Sun position when faults detected at Corncroft in the second year of operation. Identified shading is shown in red.

E.5.3 Heron Close

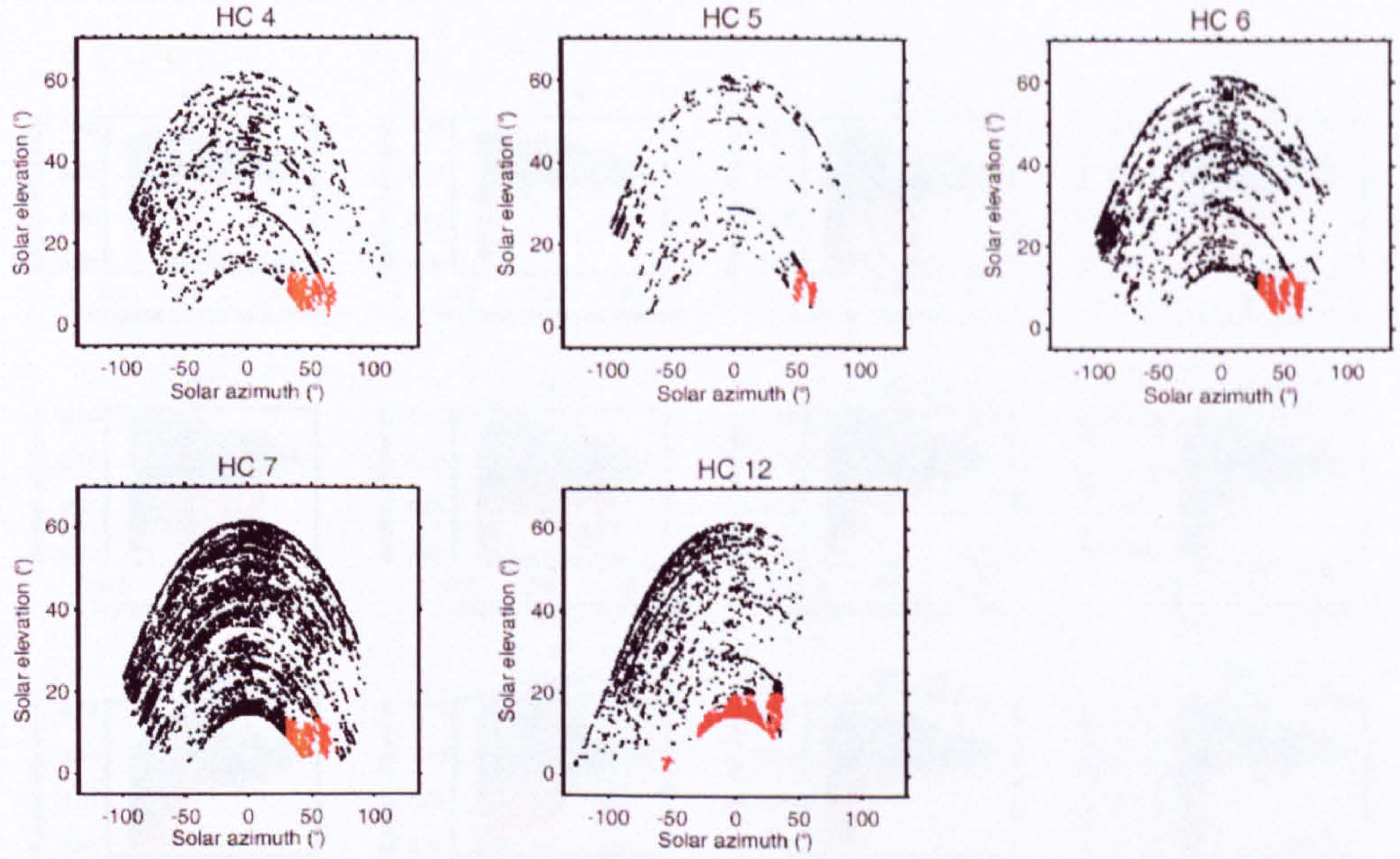

Figure E-21: Sun position when faults detected at Heron Close. Identified shading is shown in red.

E.6. Inverter MPP tracking faults

E.6.1 Corncroft Year 1

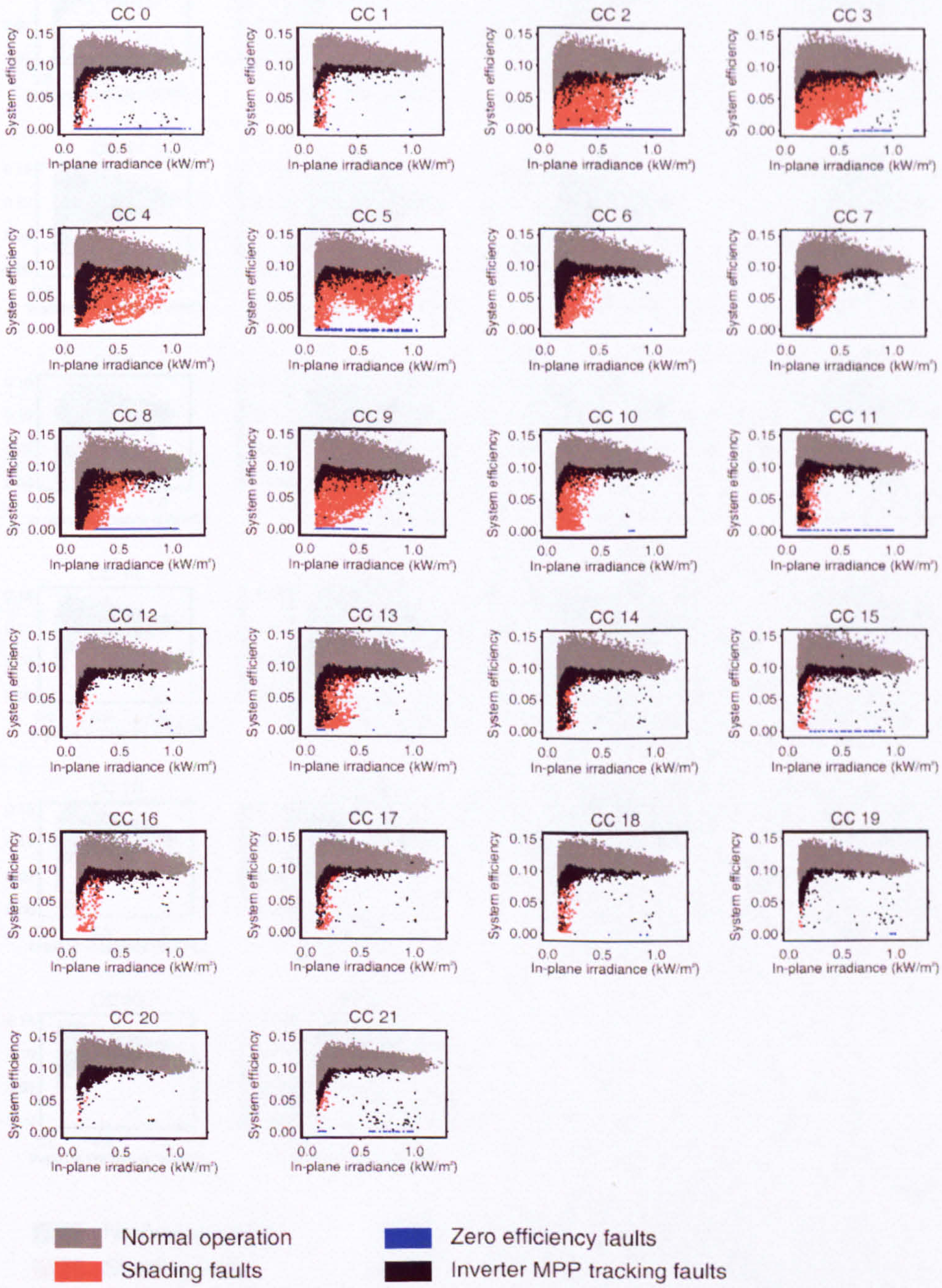

Figure E-22: Irradiance to system efficiency relationships at Corncroft in the first year of operation. Normal operation is shown in grey, zero efficiency faults in blue, shading faults in red and inverter MPP tracking faults in black.

E.6.2 Corncroft Year 2

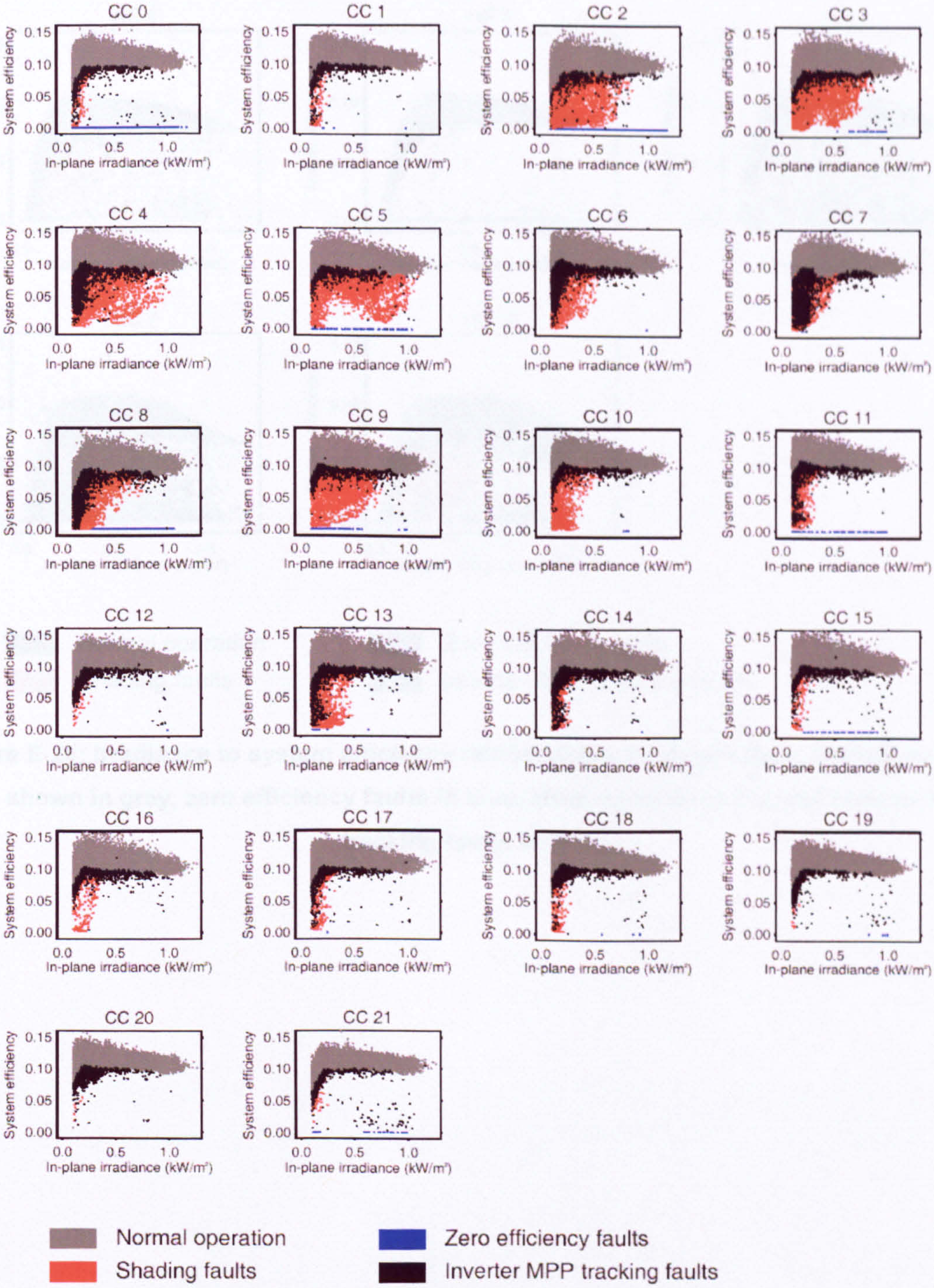

Figure E-23: Irradiance to system efficiency relationships at Corncroft in the second year of operation. Normal operation is shown in grey, zero efficiency faults in blue, shading faults in red and inverter MPP tracking faults in black.

E.6.3 Heron Close

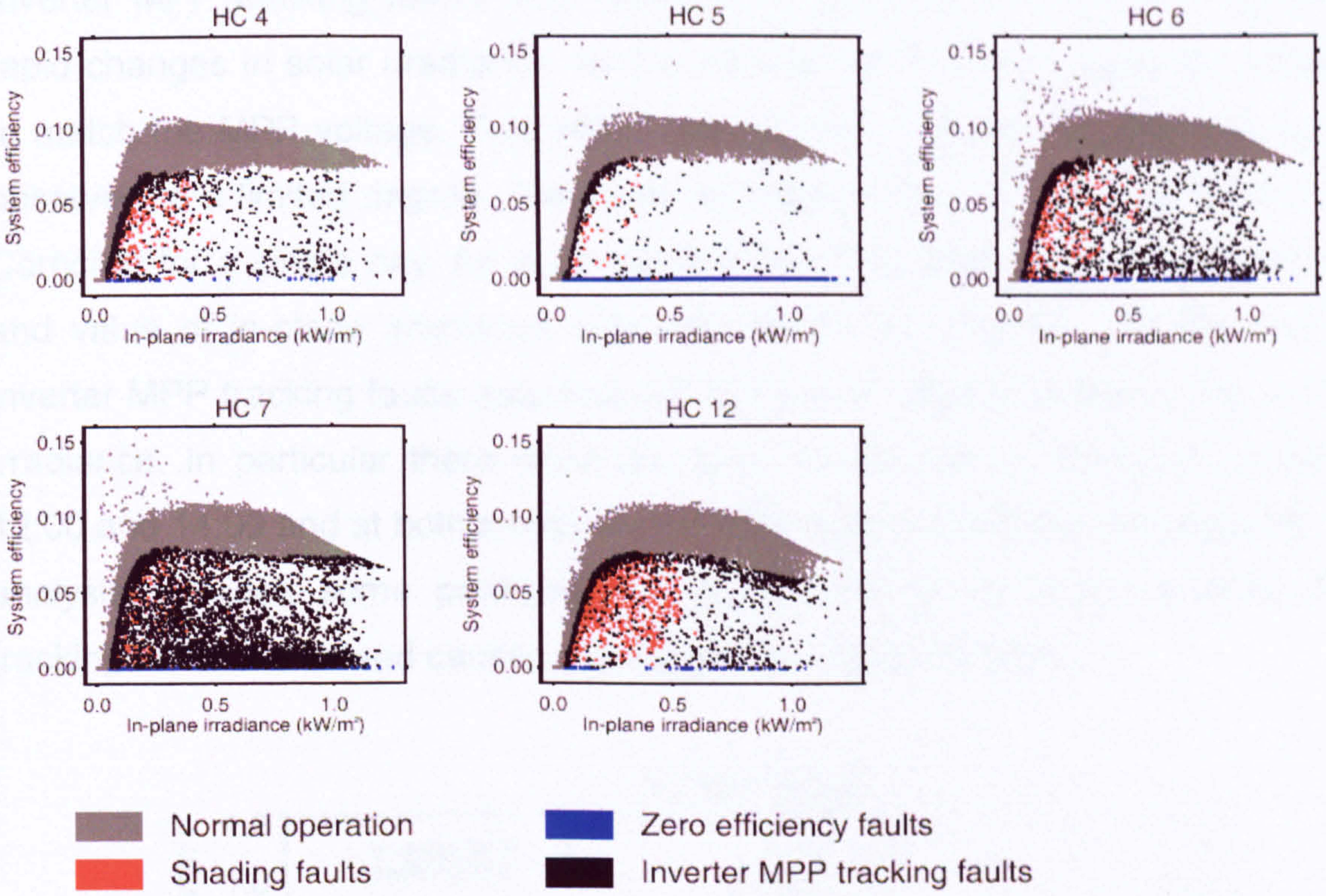

Figure E-24: Irradiance to system efficiency relationships at Heron Close. Normal operation is shown in grey, zero efficiency faults in blue, shading faults in red and inverter MPP tracking faults in black.

E.6.4 Fluctuation in solar irradiance levels

Inverter MPP tracking failure was expected to occur during times of significant rapid changes in solar irradiance, as the inverter MPP tracking routines struggled to match the MPP voltage. This affect was studied briefly in the data and can be observed to a limited degree. Taking as an example the operation of system 5 at Corncroft for a single day, for each identified inverter MPP tracking fault the time and value of in-plane irradiance was calculated (Figure E-25). On this day the inverter MPP tracking faults occurred during times of large changes in the in-plane irradiance. In particular there were two large decreases in irradiance at around 12:00 and 14:00 and at both times inverter MPP tracking faults were detected. This analysis provides some preliminary evidence that some of the inverter MPP tracking faults are indeed caused by changes in irradiance levels.

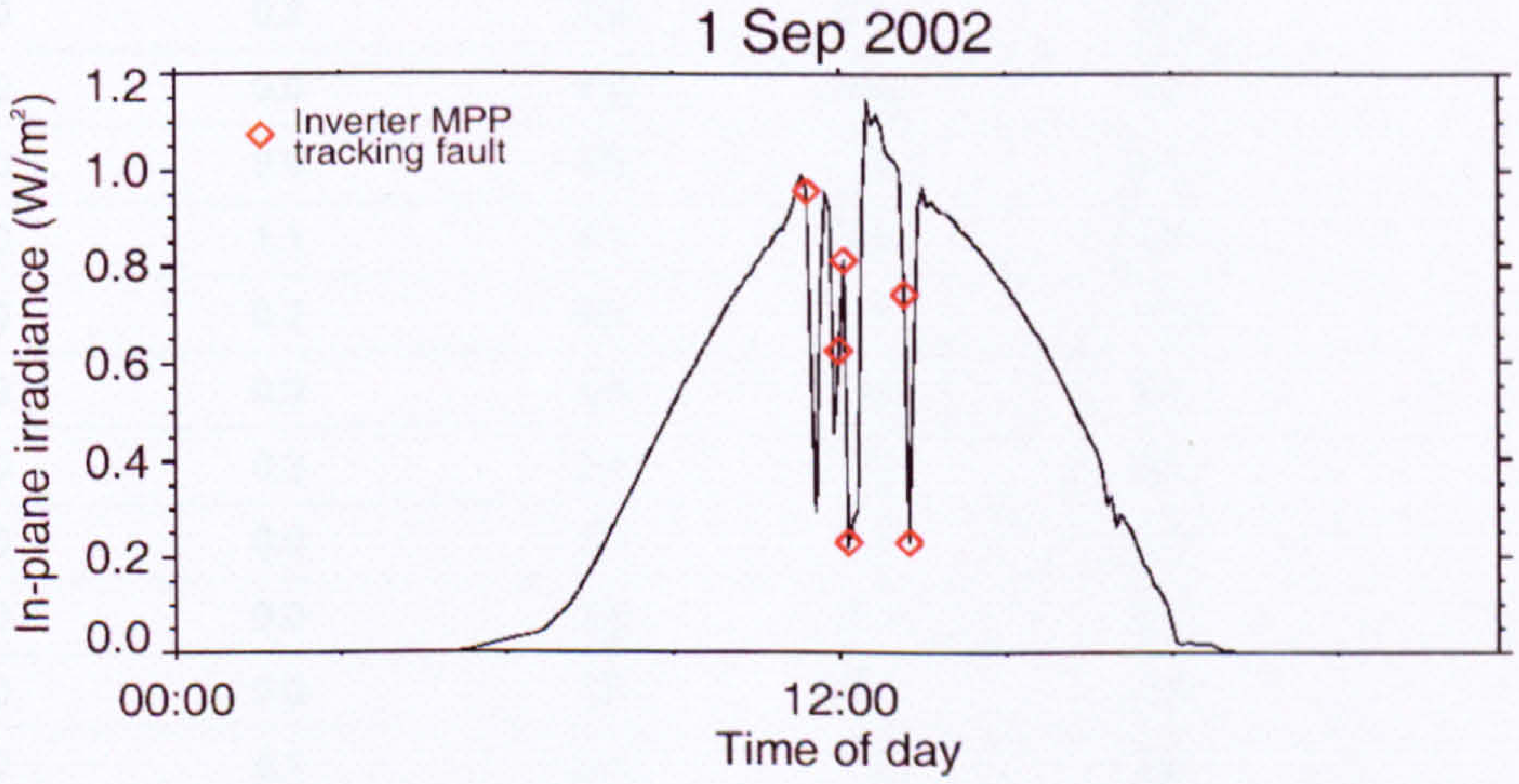

Figure E-25: Time of day vs. solar in-plane irradiance for CC 5 on 1st September 2002. The timings of identified inverter MPP tracking faults are shown by red diamonds.

E.7. Number of faults

E.7.1 Corncroft Year 1

Table E-1: Percentage of daylight operation during which faults occurred at Corncroft in the first year of operation

System	Sustained zero efficiency faults	Brief zero efficiency faults	Shading faults	Inverter MPP tracking faults	Total faults
			(%)		
0	5.8	0.2	0.3	1.9	8.2
1	0.0	0.0	0.3	1.9	2.3
2	18.0	0.0	7.0	2.9	27.9
3	0.0	0.1	7.6	3.6	11.2
4	0.0	0.0	7.1	3.6	10.7
5	0.0	0.2	7.8	2.9	10.9
6	0.0	0.0	4.2	4.0	8.2
7	0.0	0.0	5.6	3.5	9.1
8	0.0	1.1	8.1	4.5	13.7
9	0.0	0.2	6.3	3.9	10.4
10	0.0	0.0	2.3	3.2	5.5
11	0.0	0.2	2.3	2.9	5.4
12	0.0	0.0	0.1	3.0	3.1
13	0.0	0.0	3.5	3.1	6.7
14	0.0	0.0	1.4	3.4	4.8
15	0.0	0.1	0.4	2.4	2.8
16	0.0	0.0	0.4	2.6	3.1
17	0.0	0.0	0.8	1.9	2.7
18	0.0	0.0	0.8	3.1	3.9
19	0.0	0.0	0.0	1.8	1.8
20	0.0	0.0	0.6	2.0	2.5
21	0.0	0.1	0.1	1.7	1.9

E.7.2 Corncroft Year 2

Table E-2: Percentage of daylight operation during which faults occurred at Corncroft in the second year of operation

System	Sustained zero efficiency faults	Brief zero efficiency faults	Shading faults	Inverter MPP tracking faults	Total faults
	(%)				
0	12.8	0.1	0.3	0.8	13.9
1	0.0	0.0	0.3	1.0	1.3
2	41.6	0.0	4.4	1.4	47.5
3	0.0	0.5	7.5	1.7	9.7
4	0.0	0.0	7.4	1.7	9.1
5	0.0	0.0	9.6	1.3	10.9
6	0.0	0.0	5.2	1.7	6.9
7	0.0	0.0	6.2	1.4	7.5
8	0.0	0.3	8.6	1.8	10.7
9	0.0	0.0	6.4	1.5	7.9
10	0.0	0.0	2.2	1.3	3.5
11	0.0	0.0	2.7	1.4	4.1
12	0.0	0.0	0.1	1.0	1.1
13	0.0	0.5	3.6	1.6	5.7
14	0.0	0.1	1.7	1.7	3.6
15	0.0	2.1	0.2	1.5	3.9
16	0.0	1.0	0.2	1.5	2.7
17	21.0	0.0	0.8	0.7	22.4
18	0.0	0.0	0.9	1.3	2.2
19	0.0	2.2	0.0	0.5	2.7
20	0.0	0.0	0.8	0.9	1.8
21	0.0	0.0	0.0	0.5	0.5

E.7.3 Heron Close

Table E-3: Percentage of daylight operation during which faults occurred Heron Close

System	Sustained zero efficiency faults	Brief zero efficiency faults	Shading faults	Inverter MPP tracking faults	Total faults
	(%)				
0	0.0	0.1	0.3	5.5	6.0
1	58.6	0.4	0.1	1.6	60.7
2	0.0	0.9	0.6	5.5	7.0
3	0.0	4.9	0.7	12.9	18.5
4	0.0	0.3	1.5	5.4	7.2

E.8. Reduction in annual performance ratios

E.8.1 Corncroft Year 1

Table E-4: Annual performance ratios and losses due to faults at Corncroft in the first year of operation

System	Annual performance ratio of normal operation	Sustained zero efficiency loss	Brief zero efficiency loss	Shading loss	Other faults loss	Measured annual performance ratio
	(%)	loss in annual performance ratio (in performance ratio %)				(%)
0	75.6	5.6	0.2	0.1	0.3	69.9
1	78.1	0.0	0.0	0.1	0.3	79.0
2	71.8	16.2	0.0	3.0	0.5	48.9
3	74.1	0.0	0.2	3.2	0.6	70.6
4	79.0	0.0	0.0	3.0	0.6	76.8
5	76.3	0.0	0.3	3.8	0.4	72.9
6	79.8	0.0	0.0	1.2	0.6	79.6
7	76.5	0.0	0.0	1.5	0.5	75.4
8	73.5	0.0	1.1	2.3	0.7	69.1
9	77.9	0.0	0.1	2.5	0.6	75.7
10	78.9	0.0	0.0	0.7	0.5	78.7
11	81.5	0.0	0.2	0.6	0.4	81.7
12	76.6	0.0	0.0	0.0	0.4	76.9
13	78.0	0.0	0.0	1.1	0.5	77.6
14	77.9	0.0	0.0	0.3	0.5	77.9
15	79.5	0.0	0.2	0.1	0.5	80.2
16	78.2	0.0	0.0	0.1	0.4	78.8
17	79.2	0.0	0.0	0.2	0.3	79.9
18	80.9	0.0	0.0	0.2	0.4	81.6
19	78.2	0.0	0.0	0.0	0.3	79.0
20	79.3	0.0	0.0	0.1	0.3	80.5
21	75.7	0.0	0.1	0.0	0.3	75.7

E.8.2 Corncroft Year 2

Table E-5: Annual performance ratios and losses due to faults at Corncroft in the second year of operation

System	Annual performance ratio of normal operation	Sustained zero efficiency loss	Brief zero efficiency loss	Shading loss	Other faults loss	Measured annual performance ratio
	(%)	loss in annual performance ratio (in performance ratio %)				(%)
0	75.8	12.3	0.0	0.1	0.2	63.4
1	77.5	0.0	0.0	0.1	0.2	78.3
2	73.5	38.5	0.0	2.2	0.3	30.7
3	72.9	0.0	0.6	3.3	0.3	69.0
4	78.3	0.0	0.0	3.5	0.3	75.2
5	75.4	0.0	0.0	5.2	0.3	70.6
6	78.8	0.0	0.0	1.4	0.3	78.5
7	75.8	0.0	0.0	1.7	0.3	74.5
8	73.7	0.0	0.1	2.7	0.4	69.9
9	77.2	0.0	0.0	2.7	0.3	74.9
10	78.3	0.0	0.0	0.7	0.2	78.2
11	80.8	0.0	0.0	0.7	0.2	81.1
12	75.3	0.0	0.0	0.0	0.2	75.7
13	77.1	0.0	0.4	1.1	0.3	76.2
14	77.1	0.0	0.1	0.4	0.3	76.9
15	78.7	0.0	1.8	0.0	0.3	77.5
16	77.0	0.0	0.9	0.0	0.3	76.8
17	79.1	20.1	0.0	0.2	0.1	58.1
18	80.0	0.0	0.0	0.2	0.2	81.6
19	76.7	0.0	1.8	0.0	0.1	79.0
20	78.2	0.0	0.0	0.1	0.2	80.5
21	74.7	0.0	0.0	0.0	0.1	75.7

E.8.3 Heron Close

Table E-6: Annual performance ratios and losses due to faults at Heron Close

System	Annual performance ratio of normal operation	Sustained zero efficiency loss	Brief zero efficiency loss	Shading loss	Other faults loss	Measured annual performance ratio
	(%)	loss in annual performance ratio (in perfomance ratio %)				(%)
4	61.6	0.0	0.1	0.1	1.3	60.6
5	64.4	36.7	0.1	0.0	0.5	25.9
6	66.5	0.0	1.1	0.2	2.8	62.9
7	66.1	0.0	5.5	0.2	9.3	50.5
12	62.2	0.0	0.3	0.5	1.7	59.1